NOTICE

The quality of this microform is heavily dependent upon the quality of the original thesis submitted for microfilming. Every effort has been made to ensure the highest quality of reproduction possible.

If pages are missing, contact the university which granted the degree.

Some pages may have indistinct print especially if the original pages were typed with a poor typewriter ribbon or if the university sent us an inferior photocopy.

Reproduction in full or in part of this microform is governed by the Canadian Copyright Act, R.S.C. 1970, c. C-30, and subsequent amendments.

AVIS

La qualité de cette microforme dépend grandement de la qualité de la thèse soumise au microfilmage. Nous avons tout fait pour assurer une qualité supérieure de reproduction.

S'il manque des pages, veuillez communiquer avec l'université qui a conféré le grade.

La qualité d'impression de certaines pages peut laisser à désirer, surtout si les pages originales ont été dactylographiées à l'aide d'un ruban usé ou si l'université nous a fait parvenir une photocopie de qualité inférieure.

La reproduction, même partielle, de cette microforme est soumise à la Loi canadienne sur le droit d'auteur, SRC 1970, c. C-30, et ses amendements subséquents.

STRUCTURE, METAMORPHISM AND TECTONIC SETTING OF A GNEISSIC TERRANE, THE SAGAN AFELATA AREA, SOUTHERN ETHIOPIA.

by

Samuel Gichile

A thesis submitted to Ottawa - Carleton Geoscience centre and the University of Ottawa, as a partial fulfillment for the requirements of the degree of Master of Science.

ISBN 0-315-75099-5

UNIVERSITÉ D'OTTAWA
UNIVERSITY OF OTTAWA

Abstract

The Sagan-Afelata area, which extends east approximately 100 km from the Main Ethiopian Rift towards the Adola gold fields, is underlain by high-grade rocks, dominantly biotite and quartzofeldspathic gneiss. The gneissic rocks are characteristically of K-rich mineralogy and appear to form a Proterozoic supracrustal sequence rather than Archean basement as thought earlier. These rocks have a few intercalations of basic metavolcanic units and are at places intruded by granitic plutons and hypabyssal equivalents. All have been variably deformed and metamorphosed.

The bulk-chemistry of a low-K calc-alkaline tonalite (dated at about 760 Ma, U-Pb on zircon) and a basaltic arc-tholeiite of komatititic affinity outcropping east of the area suggest an island arc related magmatism of late Proterozoic age. It is suggested that the protolith of the amphibolite and the tonalite formed by Pan-African island arc magmatism over a west dipping late Proterozoic subduction zone. A later high-K megacrystic granite intruded west of the island arc-related rocks suggests that the later phases of this continental margin magmatism took place within a relatively thickened (cordilleran type) crust. The island arc terrane to the east was welded to the continental land masses on either side by subsequent continental collision probably at about 710 Ma (U-Pb date on zircon from a late syn kinematic granite). Two peralkaline to alkaline late to post tectonic granitic plutons (one of which is dated at about 530 Ma), farther west are interpreted as marking the stage of late to post-collisional (anorogenic magmatism) in this part of southern Ethiopia.

The gneissic rocks were subjected to at least three distinct phases of deformation. The first, D_1, to which probably several generations of structures are attributed, formed migmatitic layering then isoclinal folds that transposed the layers parallel to flat-lying regional foliation (S_1), during amphibolite to granulite facies metamorphism. The second, D_2, formed upright folds in S_1 and parallel layers with subhorizontal NNW to NNE trending axes, accompanied by amphibolite facies metamorphism that overprinted most rocks. D_3, resulted in local E-W trending, open, upright folds that are confined to the eastern part of the area. The sequence of structures (D_1 to D_3) resembles sequences that have been recognized in adjacent portions of the Mozambique belt in southern Ethiopia and Kenya.

High metamorphic pressure (approx. 9 kbar) under which granulites in the western part of the area formed indicates significant crustal thickening, which may be related to collision-induced major thrusting associated with the D_1 deformation. It is conjectured that the collision may be of a Himalayan type as in the rest of the Mozambique belt to the south. The northerly trending D_2 folds and the associated orogen-parallel lineations (L_2) indicate significant transpressional crustal shortening across the belt that appears to be due to the obliqueness of convergence.

ACKNOWLEDGMENTS

Professors W. K. Fyson and R. Kretz and Dr. A. E. Lalonde of the Department of Geology of the University of Ottawa are thanked for their patient reviews of the various parts of the manuscripts of this thesis. Parts of a manuscript of this thesis has benefited from critical comments by Professors J. M. Moore and J. A. Donaldson of the Department of Earth Sciences, Carleton University.

My colleagues Getahun Seyid, Alula H/Giorgis, Kiros Mehari, Solomon Birhane, Taddese Alemu, Wolde Gabriel Genzebu and Ashebir Wolde Giorgis, of the Ethiopian Institute of Geological Surveys are acknowledged for their assistance and contributions during the field work stages of this project and for making some relevant data available to me.

Due to the unusual conditions under which I had to take on this project I have been offered both friendly and professional encouragements and support from a number of kind people both in Ottawa and at distant places to all of whom (for they know) I have to extend my thanks in anonymity due to lack of space. However, special thanks are due Professors R. Kretz and A. D. Fowler of the Department of Geology, University of Ottawa and Dr. Gidey WoldaGabriel of the Los Alamos National Laboratory (New Mexico, U.S.A) for their patient and considerably kind encouragements during my depressive moments in Ottawa.

Field work and the first two years of this project in Canada were funded by the Ethiopian Institute of Geological Surveys through a World Bank/UNDP scholarship concerned EIGS authorities, Getahun Demissie, Alemu Shiferaw, Belay Desta and Amenti Abraham are thanked for their support at that stage. However, this project would not have come to completion with out the financial support in terms of research assistantships from my supervisor Prof. W. K. Fyson and a number of teaching assistantships and tuition waiver scholarships offered to me from the Department of Geology and the School of Graduate Studies and research of the University of Ottawa respectively all of which are gratefully acknowledged.

TABLE OF CONTENTS

Chapter 1 INTRODUCTION 1
Introduction 1
1:1 The project 1
1:2 Previous studies 2
1:2:1 Large scale studies 4
1:2:2 Studies on the Ethiopian Precambrian 4
1:2:3 Local studies 6
1:3 Thesis objectives and scope 6
1:4 Geography 7
1:4:1 Location and size 7
1:4:2 Accessibility 8
1:4:3 Physiography 8
1:4:4 Vegetation 9
1:4:5 Population 9

Chapter 2 REGIONAL GEOLOGY 10
Introduction 10
2:1 The Mozambique belt 11
2:2 The Red Sea fold belt 12
2:3 The Pan-African 17

Chapter 3 ROCK UNITS 19
Introduction 19
3:1 The Sagan domain (SD) 22
3:1:1 Mafic granulites (SD 1) 22
3:2 The Fincha domain (FD) 24
3:2:1 Granitic gneiss (FD 1) 27
3:2:2 Layered biotite gneiss (FD 2) 29
3:2:3 Paragneisses (FD 3) 34
3:2:4 Quartzofeldspathic gneiss (FD 4) 38
3:2:5 Meta-megacrystic granite (FD 5) 42
3:2:6 Small foliated granitoids (FD 6) 46
3:2:7 Foliated aegirine-bearing leucogranite (FD 7) 48
3:2:8 Meta-pyroxene-hornblende plutonic complex (FD 8) 50
3:2:9 Massive granite (FD 9) 52
3:3 Afelata domain (AD) 55
3:3:1 Meta-tonalite (AD 1) 55
3:3:2 Amphibolite (AD 2) 60
3:3:3 Meta-pyroxenite (AD 3) 64

Chapter 4 STRUCTURES 67
Introduction 67
4:1 Structural generations 69
4:1:1 D_1' structures 69
4:1:2 D_1 structures 69
4:1:2:1 S_1 foliation 71
4:1:2:2 L_1 lineations 74
4:1:2:3 F_1 folds 74
4:1:3 D_2 structures 76
4:1:3:1 S_2 foliation 77
4:1:3:2 L_2 lineations 77
4:1:3:3 F_2 minor folds 78
4:1:3:4 F_2 major folds 80
4:1:4 D_3 structures 82
4:1:4:1 L_3 Lineations 84
4:1:4:2 F_3 Minor folds 84
4:1:4:3 F_3 Major folds 84
4:2 Orientation data 85
4:2:1 Structural domains (sD) 85
4:2:1:1 The Sagan structural domain (SsD) 86
4:2:1:2 The Burji structural domain (BsD) 86
4:2:1:3 The Bokossa structural domain (BksD) 88
4:2:1:4 The Fincha structural domain (FsD) 88
4:2:1:5 The Afelata structural domain (AsD) 90
4:3 Summary and discussion 90
4:4 Correlation with other areas 95
4:5 Precambrian Lineaments 100
4:5:1 The Kolle-Altuntu lineament 100
4:5:2 The Doga-Didiga lineament 102

Chapter 5 METAMORPHISM 105
Introduction 105
5:1 Metamorphic mineral assemblages 106
5:1:1 The Sagan domain (SD) 106
5:1:2 The Fincha domain (FD) 110
5:1:2:1 Burji-Bokossa subdomain 110
5:1:2:2 Kinsho-Melu subdomain 113
5:1:3 The Afelata domain 115
5:2 Geothermometry and geobarometry 120
5:2:1 Two pyroxene geothermometry 123
5:2:1:1 Sagan domain (SD) 124
5:2:1:2 Fincha domain (FD) 127
5:2:2 Garnet-biotite geothermometry 129

5:2:2:1 Sagan domain (SD) 130
5:2:2:2 Fincha domain (FD) 131
5:2:3 Geobarometry 131
5:2:3:1 Sagan domain (SD) 134
5:3 Summary and discussions 135
5:3:1 Metamorphic P-T conditions 135
5:3:2 Metamorphic gradients 137
5:3:3 Structure and metamorphism 137
5:3:4 Crustal thickness and metamorphism 141
5:3:5 Metamorphic conditions in adjacent areas 144

Chapter 6 PETROCHEMISTRY AND TECTONIC SETTING OF SELECTED IGNEOUS ROCKS. 145
Introduction 145
6:1 Geologic setting, lithological and geochemical characteristics 147
6:1:1 The Sebbeto tonalite (AD 1) 147
6:1:2 The Altuntu granite (FD 5) 151
6:1:3 The Kinsho granite (FD 7) 152
6:1:4 The Bergudda plutonic complex (FD 8) 153
6:1:5 The Hiddi-Asasu amphibolite (AD 2) 155
6:2 Alteration and metamorphism 156
6:3 Comparative geochemistry of the granitoid units 157
6:4 Classification of the granitoid units 159
6:5 Tectonic setting of the granitoid units 164
6:6 Classification of the volcanic unit 172
6:7 Tectonic setting of the volcanic unit 177
6:8 Discussion and conclusions 180

Chapter 7 SUMMARY AND CONCLUSIONS 186
Introduction 186
7:1 Summary and discussion 186
7:1:1 On lithology and stratigraphy 187
7:1:2 On structure and metamorphism 189
7:1:3 On magmatism 190
7:2 A model for late Proterozoic crustal accretion 190
7:2:1 The model 190
7:2:2 Evaluation of the model and suggestions for further work 195
Refrences 198
Appendix I Petrographic tables (main units) 209
Appendix II Tables of geochemical analyses (magmatic rocks) 212

LIST OF FIGURES

Fig. 1 Geological map of the Sagan - Afelata area. encl.

Fig. 1.1 The Mozambique belt and the Red Sea fold belt in a pre-Red Sea Africa and Arabian peninsula. 3

Fig. 4.1 Simplified structural map of the Sagan-Afelata area. encl.

Fig. 4.2 Lower hemisphere equal area projection of poles to S_1 foliation in the Burji structural domain (BsD). 87

Fig. 4.3 Lower hemisphere equal area projection of poles to S_1 foliation in the Bokossa structural domain (BksD). 87

Fig. 4.4 Lower hemisphere equal area projection of poles to S_1 foliation in the Fincha structural domain (FsD). 89

Fig. 4.5 Lower hemisphere equal area projection of poles to S_1 foliation in the Afelata structural domain (AsD). 89

Fig. 4.6 Lower hemisphere equal area projection of poles to S_1 foliation in the northern half of the Afelata structural domain (AsD). 91

Fig. 4.7 Lower hemisphere equal area projection of poles to S_1 foliation in the southern half of the Afelata domain (AsD). 91

Fig. 4.8 Simplifed geological map of the Precambrian of southern Ethiopia. 93

Fig. 4.9 Lower hemisphere equal area projection of L_2 lineations from the Fincha domain. 94

Fig. 4.10 Map of major Precambrian lineaments in the Sagan-Afelata Area. encl.

Fig. 5.1 Simplified metamorphic map of the Sagan - Afelata area. 107

Fig. 5.2 Metamorphic T - P field for SD 1 mafic granulite 109

Fig. 5.3 Metamorphic T - P fields for the Kinsho - Melu subdomain and the Afelata domain. 109

Fig. 5.4 Equilibrium curves in the T - X_{CO2} field at 6 kb for reactions in

fluid saturated marbles and calc-silicate rocks. 116

Fig. 5.5 T - P curves for granite/melt and the reaction Ms + Qtz = Al_2SiO_5 + Kfs + H_2O at different X_{H2O} values. 116

Fig. 5.6 Compositional fields of pyroxenes analyzed from the mafic granulites (SD 1) and the charnockitic granite gneiss (FD 1) in the pyroxene quadrilateral. 128

Fig. 6.1 Areal distribution and map outlines of the magmatic units studied from the Sagan-Afelata area. 148

Fig. 6.2 Normative classification of the four granitoids studied from the Sagan-Afelata area. 161

Fig. 6.3 AFM diagram and tectonic fields of the four granitoids of the Sagan - Afelata area. 162

Fig. 6.4. A/NK vs A/CNK plot and tectonic fields for the granitoids studied from the Sagan-Afelata area. 163

Fig. 6.5. Classification of granitoids of the Sagan-Afelata area on the basis of the Na_2O vs Ka_2O plot of White and Chapell (1983). 165

Fig. 6.6 Tectonic settings of the granitoids of the Sagan-Afelata area on the basis of Rb vs (Nb + Y) discriminant diagram of Pearce et al. (1984). 165

Fig. 6.7a Tectonic setting discrimination plot of the granitoids of the Sagan-Afelata area according to the K_2O and Na_2O fields of Maniar and Picolli (1989). 167

Fig. 6.7b Discrimination of the granitoids of the Sagan Afelata area into orogenic and anorogenic granitoids on the basis of the Al_2O_3 Vs SiO_2 plot. 167

Fig. 6.7c Discrimination of the granitoids of the Sagan Afelata area into orogenic and anorogenic granitoids on the basis of FeO (total), MgO and SiO_2 values. 168

Fig. 6.7d Discrimination of the granitoids of the Sagan Afelata area into orogenic and anorogenic granitoids on the basis of FeO (total) Vs MgO, values recalculated from the AFM. 168

Fig. 6.7e Discrimination of the granitoids of the Sagan Afelata area into

orogenic and anorogenic granitoids on the basis of FeO (total) and MgO vs CaO values recalculated from the AFM. 170

Fig. 6.7f Specific tectonic settings of the anorogenic granitoids of the Sagan-Afelata area. 170

Fig. 6.8 Discrimination diagram used to distinguish the Altuntu granite from collisional granites (GP II). 171

Fig. 6.9 Chondrite normalized REE pattern for a sample of the Sebbeto tonalite. 171

Fig. 6.10 Classification of the Hiddi Asasu amphibolite on the basis of the total alkali and silica values. 174

Fig. 6.11 Classification of the Hiddi Asasu amphibolite on the basis of Zr/TiO_2 Vs SiO_2 binary diagram. 174

Fig. 6.12 The Jensen (1976) plot for the Hiddi Asasu amphibolites. 175

Fig. 6.13 AFM diagram for the Hiddi Asasu amphibolites. 175

Fig. 6.14 K_2O-TiO_2-P_2O_5 ternary plot for analyses from the Hiddi-Asasu amphibolite. 176

Fig. 6.15 Tectonic setting of the Hiddi Asasu amphibolite on the basis of the Ti-Zr-Y ternary diagram. 176

Fig. 6.16 Tectonic setting of the Hiddi Asasu amphibolite on the basis of TiO_2 vs Zr plot. 178

Fig. 6.17 Tectonic setting of the Hiddi Asasu amphibolite on the basis of the Sr-Zr-Ti ternary diagram. 178

Fig. 6.18 Tectonic setting of the Hiddi Asasu amphibolite on the basis of the K_2O - MnO - P_2O_5 ternary diagram. 179

Fig. 6.19 A comparison of the K_2O-SiO_2 fields defined by the analyses from the Altuntu granite and the Sebbeto tonalite with that of Phanerozoic arc-related granitoids. 179

Fig. 6.20 A comparison of the K_2O-SiO_2 fields of the calc-alkaline plutonic rocks of the Sagan-Afelata area with that of similar granitoids in the Pan African of the Arabian shield. 182

Fig. 7.1 A schematic diagrm depicting the Late - Precambrian tectonic evolution of the eastern part of the Sagan - Afelata area.

LIST OF PLATES

Plate 3.1 Compositional layering in an outcrop of SD 1 mafic granulite. 25

Plate 3.2 Thin section scale layering in mafic granulite (SD 1). 25

Plate 3.3 Quartz-plagioclase veining in SD 1 mafic granulite. 26

Plate 3.4 Relatively coarser lenticular quartz defining foliation in mafic granulites (SD 1). 26

Plate 3.5 Rim of aggregates of crystallites of hornblende around an orthopyroxene grain, SD 1 mafic granulite. 28

Plate 3.6 A hornblende crystal enclosing a calcium pyroxene crystal in SD 1 mafic granulite. 28

Plate 3.7 Layered outcrop of FD 1 granite gneiss. 30

Plate 3.8 Small scale layering in FD 1 granite gneiss. 30

Plate 3.9 Photomicrograph of a thin section from a mafic layer of FD 1 granite gneiss in the Bokossa area. 32

Plate 3.10 Metamorphic layering in an outcrop of FD 2 layered biotite gneiss (Burji gneiss). 32

Plate 3.11 Photomicrograph of a thin section of a felsic blastoporphyritic fine-grained rock in unit FD 2. 35

Plate 3.12 Photomicrograph of a specimen of FD 3b calc-silicate gneiss. 35

Plate 3.13 Fine layering in a garnet bearing amphibole schist of unit FD 3d. 39

Plate 3.14 Fine layering in an outcrop of the Fincha gneiss (FD 4a). 39

Plate 3.15 Closer view of layering in the Fincha gneiss (FD 4a). 41

Plate 3.16 Thin-section scale layering defined by layers of different grain sizes, in Fincha gneiss (FD 4a). 41

Plate 3.17 General textural features of the Fincha gneiss (FD 4a) in thin section. 43

Plate 3.18 The Altuntu megacrystic granite (FD 5), weakly deformed outcrop. 43

Plate 3.19 The Altuntu megacrystic granite (FD 5), moderately deformed. 45

Plate 3.20 Textural variation in a single outcrop of the Altuntu megacrystic granite (FD 5). 45

Plate 3.21 Photomicrograph of a megacryst of microcline in a thin section of the AD 5 Altuntu megacrystic granite. 47

Plate 3.22 Photomicrograph of a thin section of a specimen from the Kinsho granite (FD 7). 47

Plate 3.23 Solid state growth texture in the matrix of a specimen from the dark core of the Bergudda complex (FD 8). 53

Plate 3.24 Preferred alignment of mineral grains, in a thin section of a specimen of the dark core of the Bergudda complex (FD 8). 53

Plate 3.25 Example of perthitic intergrowth of feldspars in the dark core of the Bergudda complex (FD 8). 54

Plate 3.26 An orthopyroxene grain (centre) in a thin section of a specimen of the dark core of the Bergudda complex (FD 8). 54

Plate 3.27 Strongly developed foliation in the pink granite forming the outer rim of the Bergudda complex. 56

Plate 3.28 Weakly foliated outcrop of the pink pyroxene-hornblende granite, in the inner regions of the pink granite of the Bergudda complex (FD 8). 56

Plate 3.29 General texture of strongly deformed pink rim of the Bergudda complex. 58

Plate 3.30 A vein of the pink pyroxene - hornblende granite rim of the FD 8 Bergudda complex intruding an outcrop of the FD 1 granite gneiss. 58

Plate 3.31 Porphyrocryst of plagioclase in a thin section of a sample of the Sebbeto meta-tonalite (AD 1). 61

Plate 3.32 Quartzofeldspathic veins parallel to foliation/gneissosity in the Sebbeto meta-tonalite (AD 1). 61

Plate 3.33 General texture of the fine-grained amphibolite of AD 2 at the scale of a thin section. 63

Plate 3.34 General texture of the medium-grained amphibolite of AD 2 at the scale of a thin section. 63

Plate 3.35 Migmatitic veining in an outcrop of AD 2a amphibolite. 66

Plate 3.36 Layering in calc-silicate gneiss (AD 2d) of unit AD 2. 66

Plate 3.37 Photomicrograph of a sillimanite - kyanite - quartz schist of unit AD 2. 68

Plate 3.38 Cumulate texture of the Korolle pyroxenite (unit AD 3). 68

Plate 4.1 Rootless F_1 intrafolial fold in an earlier migmatitic layering (S_1'). 70

Plate 4.2 Preserved hinge zones of F_1 minor folds in the layered biotite gneiss of unit FD 2. 70

Plate 4.3 F_1 asymetric Z folds in pre-S_1 leucosome within layered biotite gneiss of FD 2. 72

Plate 4.4 A pre-S_1 leucosome (thick) forming the limb of an F_1 minor fold, at an oblique angle to S_1 foliation. 72

Plate 4.5 F_1 minor fold in quartzofeldspathic gneiss (FD 4a). 75

Plate 4.6 A weak second foliation defined by opaque mineral and biotite grains (dark) cross-cutting an earlier layering/gneissosity (S_1). 75

Plate 4.7 A lineation (L_2 ?) defined by quartz blades in

quartzofeldspathic gneiss (FD 4a). 79

Plate 4.8 A lineation (L_2 ?) defined by ridges in FD 4a quartzofeldspathic gneiss. 79

Plate 4.9 An F_2 minor antiform. 81

Plate 4.10 An F_2 minor synform. 81

Plate 4.11 Intrafolial folds (F_1/F_2 ?) in Sebbeto tonalite (AD 1). 83

Plate 4.12 A close view of one of the intrafolial (F_1/F_2 ?) folds in Sebbeto tonalite (AD 1). 83

LIST OF TABLES

Table 2.1	Pseudo-stratigraphy of the rock successions of the Red Sea fold belt in the Arabian shield.	14
Table 3.1	Tectonostratigraphic units of the Ethiopian Precambrian to which the rocks of the Sagan - Afelata area belong.	21
Table 4.1	Correlation of the structural sequence and elements in the Sagan-Afelata area to that of neighbouring regions.	96
Table 5.1	Mineralogy of specimens used for geothermometry and barometry from the Sagan-Afelata area.	122
Table 5.2	Analyses of orthopyroxenes	125
Table 5.3	Analyses of clinopyroxens	126
Table 5.4	Analyses of garnets	132
Table 5.5	Analyses of biotite	133
Table 5.6	Analyses of plagioclase	136
Table 5.7	P-T conditions of metamorphism in the different domains in the Sagan-Afelata area.	138
Table 6.1	Summary of the main lithologic and geochemical characteristics of magmatic rocks studied from the Sagan-Afelata area.	149.
Table 6.7	Tectonic setting of granitoids studied from the Sagan - Afelata area.	173

CHAPTER ONE

INTRODUCTION

This chapter describes how the project that led to this petrological, structural and tectonic study of Precambrian rocks in the Sagan - Afelata area of southern Ethiopia was initiated. It outlines previous work concerning the Precambrian of Ethiopia and of the Arabo - Nubian shield, and presents the principal objectives of the thesis. The chapter also briefly describes the geography of the Sagan - Afelata area.

1:1 The project

The project which led to this thesis was part of a reconnaissance mapping program (1:250.000 scale) undertaken by the regional mapping department of the Ethiopian Institute of Geological Surveys (EIGS). The project targeted an area of approximately 21,000 km^2 in southern Ethiopia. The major portion of the target (map sheet NB 37-10) was mapped by EIGS geologists (Gichile et al., 1986; Gabriel, 1987; Taddese, 1987; Getaun and Alula, 1987; Kiros and Kinetibeb, 1987). The Sagan - Afelata area considered in this thesis, was selected for a more detailed study of an E - W crossection of the project area (map sheet NB 37-10). A reconnaissance study of the eastern part of the thesis area was made by Gichile et al. (1986) and of the western part by Getahun and Alula (1987). More detailed work, was conducted during the 1987 and 1988 field seasons by the present author. This included more detailed mapping, collection of samples for

geochronological and geochemical studies, air - photo interpretation and a map compilation at 1:100,000 scale.

The Sagan - Afelata area was chosen because it represents a bridging zone between two relatively well studied regions of contrasting geology in the Precambrian of southern Ethiopia. These are to the west, the Omo project area (Davidson et al. 1973, 1976; Shiferaw, 1981; Davidson, 1983), underlain by predominantly high-grade gneissic rocks and granulites and to the east, the Adola area, underlain by lower grade metavolcanic - metasedimentary rocks, largely studied for its gold mineralisation (Kozyrev et al. 1985) but also for its tectonic significance (Chater and Gilboy, 1968; Gilboy, 1970; Chater, 1971; Kazmin, 1976).

These two areas are often considered as belonging to two independent orogenic belts (e.g. Kazmin et al. 1978; Hepworth, 1979): the relatively higher grade Mozambique belt (Holmes, 1951) and a lower grade volcano - plutonic and sedimentary belt (Fig. 1.1a). The latter belt has been referred to as the Red-Sea fold belt (Kazmin, 1971, 1975b and Kazmin et al., 1978), the Hijaz magmatic arc (Kroner, 1979), and Pan-African arc basins (Engel et al., 1980).

1:2 Previous studies

Previous studies relevant to the thesis are presented in three categories: (1) large scale works dealing with the tectonics of the Precambrian basement of East Africa and the Arabian shield, (2) studies on the Ethiopian Precambrian basement in general and (3) local works on the Precambrian rocks in or close to the Sagan - Afelata area.

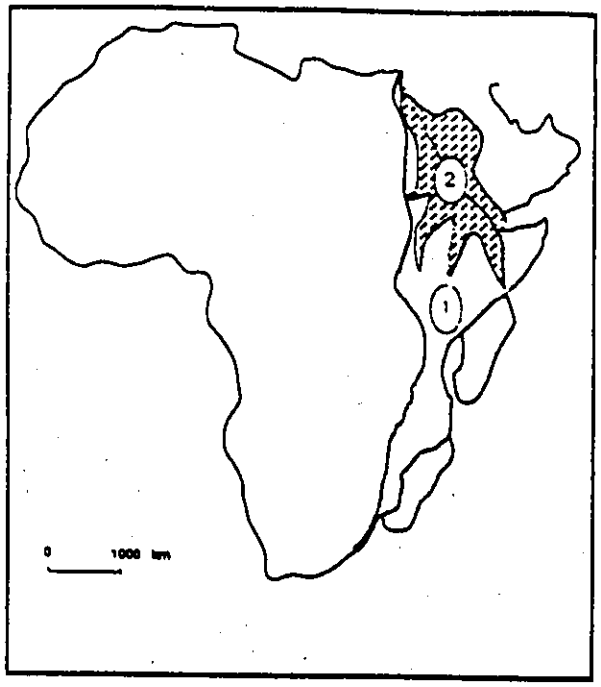

(a)

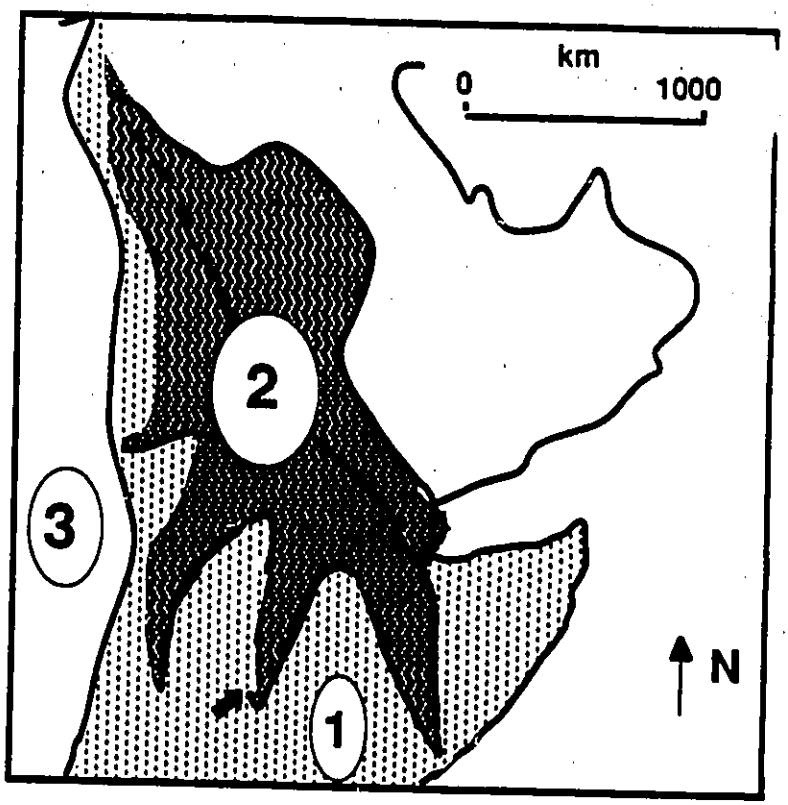

(b)

Fig. 1.1 (a) The Mozambique belt (1) and the Red Sea fold belt (2) in a pre-Red Sea Africa and Arabian peninsula. The island of Malagasy is shown in its two possible pre-Phanerozoic positions. (b) The Precambrian of northeastern Africa and the Arabian shield, (1) and (2) as in Fig. 1.1a, (3) Archean shield undifferentiated; black arrow points to approximate location of the Sagan - Afelata area (modified from Kroner, 1979).

1:2:1 Large scale studies: Much knowledge about the origin and evolution of the lower grade Red Sea Fold belt are largely based on studies of the Precambrian basement of regions north of Ethiopia. It is in these regions that volcanic, sedimentary and plutonic rocks of the belt are more voluminous (Fig. 1.1b), notably in the Arabian shield (e.g. Greenwood et al., 1976; Al Shanti and Mitchell, 1976), the eastern desert of Egypt (e.g. Garson and Shalaby, 1976; Church, 1982) and to a lesser extent the basement of eastern Sudan (e.g. Fitches et al., 1983; Embleton et al., 1982). As a result of these and other studies, it is acknowledged that the rocks of this lower grade belt originated in arc related settings and were accreted to the Arabo - Nubian shield in Upper Proterozoic time (see summaries by Gass, 1977, 1979, 1981, 1982; Vail, 1983; Fleck et al., 1980 and also chapter 2).

Increasingly more information, on ophiolitic rocks regarded as tectonically related to those in the Arabian shield is also coming from the East African basement south of Ethiopia (e.g. Vernacombe, 1981; Shackleton, 1977; Berhe, 1989). However, the small size and the dismembered nature of the belts formed by these rocks, in the polycyclic Mozambique belt south of Ethiopia, has rendered hypotheses about their origin and their relationships to the high - grade rocks (e.g. Hepworth, 1979; Shackleton, 1977, 1986) very tenuous (Vail, 1983).

1:2:2 Studies on the Ethiopian Precambrian: All the knowledge of the Precambrian basement of Ethiopia were obtained through the efforts of the EIGS and its affiliated projects. These mainly regional studies show that in Ethiopia the lower grade volcano - plutonic and sedimentary belt (the Red Sea fold belt) forms two or perhaps three N - S trending and south tapering branches (Kazmin, 1971, 1973, 1978; Kazmin et al. 1978).

The more extensive of these branches extends N - S in the western part of the country (Fig. 1.1b) and has been studied at reconnaissance levels (de Wit, 1977; Kazmin et al. 1979; Davidson, 1983; Mengesha and Berhe, 1988; Amenti, in progress) and at relatively more detailed scales by the Gore - Gambella - Geotraverse team (Moore et al., 1987) in a small area in southwestern Ethiopia. The results of this last project (Mengist, 1986; Ayalew and Moore, 1989; Ayalew, 1988 and Ayalew et al., 1990), indicate that the metavolcanic and plutonic rocks developed in Upper Proterozoic volcanic arc settings and the present low and high grade assemblage was perhaps brought about by a continental collision confirming an earlier regional geological interpretation (Kazmin et al., 1979).

The central branch, which outcrops in the Adola area and bounds the Sagan - Afelata area to the east (Fig. 1.1b), has been the subject of numerous works oriented towards mineral exploration, the most important of which is by Kozyrev et al. (1985). Also included are two tectono - stratigraphic studies (Gilboy, 1970 and Chater, 1971). The Bulbul - Agere Mariam mineral exploration project of the EIGS is presently underway, along the western margin and also on a southern extension of this belt.

Apart from these studies, which involved considerable data accumulation, some largely interpretative papers (Bogliotti, 1989; Beraki et al. 1989) have been published recently. Unlike for the western belt, none of these studies has given rise to a satisfactory plate tectonic model based on petrochemical data for the evolution of the central branch and its relationships to high-grade gneissic blocks bounding it on either side.

In general, lack of geochemical and geochronological data limits tectonic interpretation of the Ethiopian Precambrian rocks. In a few cases for example Kozyrev et al., (1985) geochemical

work has been carried out but no attempt has been made to use these data in making tectonic interpretations. Thus, except for the Gore - Gambella Geotraverse, and this thesis, no combined geological, geochemical and geochronological work focused on the tectonic settings and the relationships between the high - grade gneisses and the lower grade volcano - sedimentary belts has been conducted.

1:2:3 Local studies: No previous geological work covers specifically the Sagan - Afelata area. However, a regional study of the Yabello district based largely on air photo interpretation (Kazmin, 1970) includes the Sagan - Afelata area. Warden (1976) described most of the assumed tectono-stratigraphic units (Kazmin, 1973) in his unpublished catalogue of Precambrian rock units of Ethiopia. Two more recent studies on parts of map sheet NB 37-10, Getahun and Alula (1987) and Gichile et al. (1986) have been modified and incorporated in the accompanying geological map (Fig. 1).

1:3 Thesis objectives and scope

As mentioned above, the Sagan - Afelata area, is bound on the east by the Adola belt (Kozyrev et al. 1985) belonging to the central branch of the Red Sea fold belt and on the west by the Omo - project area (Davidson, 1983) regarded as a part of the high-grade Mozambique belt. Rocks akin to both of these belts are present in this area and from previous work their relationships and tectonic settings are unknown. Thus, a principal objective of this thesis is to establish the tectonic setting of the central branch of the Red Sea fold belt of Kazmin (1971) and understand its relationships with the contrasting higher grade Mozambique belt of Holmes (1951) in southern

Ethiopia.

Another related objective is to study variations in metamorphic conditions and structural styles from east to west across the area and fill in the gap of geological knowledge between the two relatively well studied Omo project (Davidson, 1983) and Adola (Kozyrev et al., 1985) areas. Accordingly, the thesis analyzes structural, metamorphic and petrochemical data of selected magmatic units and suggests the probable late Proterozoic plate tectonic setting for the area.

An important conclusion reached earlier in this thesis project based on petrochemical data (Gichile, 1990a) and preliminary U-Pb (zircon) dating (EIGS, unpublished data) is that a gneissose plutonic unit, previously assumed to be part of the high - grade gneissic terrain, of Archean age (Kazmin, 1973; Warden and Horkel, 1984) is a product of volcanic arc related plutonism related to the lower grade Proterozoic (Adola) belt. In a later report (Gichile, 1990b) it has been suggested that rocks of both the high and lower grade terranes within the Sagan-Afelata area are of Proterozoic than Archean age. Possible plate - tectonic models for the late Proterozoic evolution of rocks in the area and the adjacent Adola area forwarded subsequently (Gichile et al., 1991a and b) are outlined in this thesis.

1:4 Geography

1:4:1 Location and size

The Sagan - Afelata area covers approximately 3600 sq. km. It is elongated E - W about 110 km and straddles the Sagan half graben at the southern termination of the main Ethiopian rift segment of the east African rift system (Mohr, 1967), to the west, and the western margin of the Adola gold fields (Kozyrev et al., 1985) to the east. It is bound by latitudes 5° 15' N and 5° 30'

N and longitudes 37° 30' E and 38° 30' E (Fig. 1). The name Sagan - Afelata area is given to this thesis area from the name of two relatively big rivers, Sagan and Afelata that drain the southwestern and northeastern corners of the area respectively (Fig. 1).

1:4:2 Accessibility

The main access to the area is the Addis Ababa - Moyale highway which runs N - S along the western margin of the eastern quarter of the area. Other motorable tracks in the Sagan - Afelata area can only be travelled by 4-wheel drive vehicles, particularly during the rainy seasons.

1:4:3 Physiography

The Sagan - Afelata area has a high relief (about 1500 m) from less than 900 m above sea level at the floor of the Sagan half graben in the southwestern corner of the area, to 2350 m above sea level on top of the Bergudda block in the central part. Mountain ridges generally run N - S, while main streams drain southeast in the eastern half of the area and southwest in the western half. An exception to this is the northerly drainage in the Lula graben, east of the spectacular Amaro horst, a Tertiary tectonic edifice in the southernmost part of the main Ethiopian rift system (Levitte et al., 1974; Wolde Gabriel et al., in press) in the west central part of the area.

The divergent drainage system appears to have been controlled by Tertiary uplift, plateau volcanism and later, rift - related, sub - longitudinal, block faulting and perhaps rotation (away from the rift axis). However, it is obvious that the Tertiary movements and structures were controlled by, the regional, N - S trending, Mozambiquian metamorphic grain (see Gichile et al.

1986) and major Precambrian structural discontinuities.

1:4:4 Vegetation

The Sagan - Afelata area is fairly vegetated. Dense, equatorial forest is limited to an eastern highland area (the Megadda forest). In most other parts of the area, bushy vegetation dominated by thorny trees is common. The latter is particularly scenic in the Sagan graben in the west and in the Hiddi Asasu valley in the east.

1:4:5 Population

Population density is variable and is the highest in the west central part of the Sagan - Afelata area, where dense villages inhabited by the Burji people are interspersed in well cultivated farm lands. In contrast, the rest of the area is inhabited by Oromos (Borenas and Gujis) and fewer Gebra people who live in widely spaced settlements, in the midst of vast bushy grazing land. Relatively urbanized villages with permanent market places number only four in the entire area and the total population of these villages is small.

CHAPTER TWO

REGIONAL GEOLOGY

Introduction

As in all other Precambrian shields (Hoffman, 1988, 1989, Windley, 1984) the Precambrian of Africa consists of Archean cratons welded together by Proterozoic mobile belts of different ages. The cratons, can be regarded as microplates and the mobile belts, as intervening collisional belts. The collisional belts may have been initiated as continental rifts (Porada, 1989), and may have passed through the stage of oceanic rifts before closure and eventual collision.

The Precambrian of north east Africa is composed of two Archean cratons and two genetically related Proterozoic mobile belts (Fig. 1.1b). The Archean cratons are the Tanzanian shield (Clifford, 1970, Bell and Dodson, 1981) and the largely unexposed Nile shield (Cahen et al., 1984). Lying to the east of these shields are the two mobile belts, the Mozambique belt (Holmes, 1951) and the Red Sea fold belt (Kazmin, 1971).

The Sagan-Afelata area is situated far from the cratonic areas and stretches across a boundary between the two mobile belts. Thus, the following review will be limited to these two belts.

2:1 The Mozambique belt

The Mozambique belt of Holmes (1951) is a Proterozoic collisional belt (Shackleton, 1977, 1979) that extends along and underlies the eastern margin of much of the African continent (Fig. 1.1a). It is shorter than Phanerozoic orogenic belts such as the Alpine and Himalayan chains or the Proterozoic Grenville belt. However, it is wider than most Phanerozoic belts.

This belt although known for long is vaguely defined, geochronologically (Muhongo et al., 1987) and also structurally (Hepworth, 1979). It bears the records of a wide range of metamorphic ages (Cahen et al. 1984) and is believed to be poly-cyclic. One of the better known features of this belt is its western front, which although at most places obscured by Cenozoic volcanism and tectonism related to the development of the East African rift system, is relatively well defined south of Ethiopia (McConnell, 1980; Hepworth, 1972). In Kenya, close to southern Ethiopia the front is represented by relatively narrow zones of mylonites along the Nandi escarpment (Sanders, 1965) and also a belt of dismembered ophiolitic rocks interpreted to mark the suture zone between the belt and the cratonic foreland (Vearncombe, 1981, 1983a and b).

In contrast, in Ethiopia and areas to the north this boundary is uncertain (Vail, 1976; Vail and Hughes, 1987; Kroner et al., 1987). In Sudan the front is commonly taken to be at about the longitude of the river Nile (Vail, 1979, 1983; Hepworth, 1979; Ries et al., 1983). However, more recent work (Ries and Shackleton, 1985) shows that the true boundary must lie further to the west. This observation suggests that the front is perhaps to the west of the Ethio - Sudanese border at the latitude of the Sagan - Afelata area.

Internally, the belt is characterized by major and minor folds and metamorphic fabrics that predominantly and consistently trend between NNE and NNW, and consists of high-grade (amphibolite to granulite facies) gneissic rocks. Gneissic units form two broad tectonic sequences termed "geosynclinal" and "vestigeosynclinal" or "vestigial" facets (Clifford, 1970). These terms although they have almost lost their original genetic meanings (Shackleton, 1977, 1986; Burke and Sengor, 1986) are being used (Hepworth, 1979; Bell and Dodson, 1981) in order to distinguish between what are believed to be, older tectonically reworked basement (vestigial) and relatively younger and heterogenous cover (geosynclinal) sequences.

The geosynclinal facet, extends northwards (Hepworth, 1979) to include the lower grade volcano-plutonic and sedimentary rocks of the Red Sea fold belt of Kazmin (1971). Following this line of interpretation the extension of the Mozambique belt into the Arabian shield as a basement core underlying the rocks of the Red Sea fold belt has been a point of debate for some time (Hepworth, 1979). However, although the relation between the two belts is being accounted for differently, rather than by the classical basement-cover relationship (Burke and Sengor, 1986, Key et al., 1989) the presence of the rocks of the Mozambique belt in the Arabian shield as a rifted basement is being acknowledged (Stacey and Hedge, 1984, Stoeser and Camp, 1984).

2:1:2 The Red Sea Fold belt

This belt of lower grade rocks (Fig. 1.1a) is composed of calc-alkaline volcanic and plutonic rocks with associated marine, predominantly volcanogenic, sediments. The grade

of metamorphism, is commonly in the green schist facies (Kazmin, 1971, 1973; Kazmin et al. 1978; Hepworth, 1979). However, data from the Sagan - Afelata area (Gichile et al., 1986 and this work) and the adjacent Megaddo region (Chater, 1971, Kozyrev et al., 1985) indicate that at least a part (probably lower structural levels), of these rocks have been subjected to regional amphibolite facies metamorphism (see Chapters 5 and 7).

The metavolcanic and metaplutonic rocks of the Red Sea fold belt as pointed out in chapter 1 were accreted to the Arabo-Nubian shield by Pan-African (late Proterozoic) plate margin magmatism (see summaries in Gass, 1977, 1979, 1981, 1982). A "pseudo-stratigraphic" three fold classification, spanning the Pan-African time (1200 - 500 Ma), was proposed for these rocks by Gass (1981). This scheme, based on observations in the evolutionary trend of magmatic products in the Arabian shield, is presented in Table 2.1. The scheme shows that, the Lower Pan-African is dominated by dioritic plutonism and attendant low K-tholeiitic volcanism, while the subsequent events Middle and Upper Pan-African become increasingly dominated by more felsic products. The youngest episode is dominated by granites, granodiorites, rhyolites, and rhyodacites (Gass, 1979, 1981; Roobol et al. 1983; Stoeser, 1986).

Although rigorous chronostratigraphic correlation, of the rocks in different parts of this belt, on the basis of this subdivision is unsound, the scheme reflects the general evolutionary trend of the magmatic products of Pan-African plate-margin magmatism in the belt in time (Jackson, 1986, Stoeser, 1986). Thus, it may be used to access qualitatively the probable evolutionary stage at which a rock association or a specific segment of an "arc-basin" (Engel et al. 1980) evolved at least in the Arabian shield

Table 2.1 Pseudo-stratigraphy of the rock successions of the Red Sea fold belt in the Arabian shield (extracted from Gass, 1981).

Age (Ma)	Rock types: Plutonic	Volcanic	Sedimentary	Inferred tectonic setting
Post-Pan African	Peralkaline and alkaline granites	peralkaline and alkaline trachytes and rhyolites	Terriginous arkoses and shallow water shales	Continetal
500 - 600 Ma	DIACHRONOUS END OF DESTRUCTIVE MARGIN PROCESS			
Upper Pan-African	Calk-alkaline granites and granodiorites	Rhyolites, dacites, trachytes and andesites	Conglomeratic and arenaceous units with granitic and rhyolitic clasts. Stromatolitic limestones.	Continetal with Andean type of continetal margins.
600 - 700	MAJOR BREAK, REGIONAL UNCONFORMITY, CHANGE IN COMPOSITION AND MAGMATISM			
Middle Pan-African	Calk-alkaline diorites and granodiorites	Calc-alkaline andesites and basaltic andesites with subordinate rhyolitic and dacitic units	Greywackes and minor arkoses. Stromatolitic limestones and shallow water shales.	Numerous mature intra oceanic island arcs. Major breaks (stratigraphic and regional) suggest several arcs.
c. 1000	STRUCTURAL, COMPOSTIONAL AND METAMORPHIC BREAK; ARC COLLISION (OROGENESIS AT c. 960 Ma)			
Lower Pan-African	Gabbros, diorites granodiorites	Low-K basalts, and baslatic andesites	Immature greywackes, cherts, shales, occasional limestones	Numerous immature intra oceanic island arcs
1200 ?				

(Roobol et al., 1983).

These, juvenile Late Precambrian magmatic rocks, of the Red Sea fold belt developed in subduction related environments, which vary from oceanic (island arc) to continental arc types. In the Arabian shield, where these rocks are relatively extensive and have been studied more thoroughly, rocks occurring in the west i.e. west of the Nabitah orogen (Al Shanti and Mitchell, 1976) are known to have been evolved in more of oceanic settings, while terrains to the east have more continental characteristics (Stacey and Hedge, 1984; Stoeser and Camp, 1985; Stoeser, 1986; Jackson, 1986; Ramsay et al. 1986).

In the adjacent regions of northeast Africa, magmatism took place, in a probably cordilleran setting in northeastern Egypt (Abdel-Rahman, 1986, Abdel-Rahman and Martin, 1987, 1990) and in varied environments related to more oceanic arc settings, of probably different maturity, in southeastern Egypt (Engels et al. 1980; Ries et al. 1985) and the northeastern Sudan (El-Nadi, 1990, 1989; Fitches et al. 1983; Vail, 1979, 1983, 1985; Almond et al. 1989; Kroner et al., 1987).

In Ethiopia, on the basis of limited geochemical data and the relative proportions of felsic to mafic magmatic products, probably diachronous accretion of juvenile crust appears to have taken place at at least two different type of arc settings and/or arcs of different maturity.

The western and bigger branch (Fig. 1.1a and 1.1b) extends from Eritrea (Mohr, 1979) in the north, to the Akobo basin (Davidson, 1983) to the south, and is disposed far to the west of the Sagan-Afelata area. In western Ethiopia, this belt which perhaps consists of a number of arc-basins (de Wit and Chewaka, 1981) is dominated by intermediate

plutonic rocks of dioritic and granodioritic compositions (Amenti, in preparation, Kazmin et al. 1979; Mengesha and Berehe, 1988). These plutonic rocks are associated with coeval compositionally equivalent calc-alkaline arc lavas and pyroclastic rocks of basaltic-andesite, andesitic, and rhyolitic compositions, of which andesites are the predominant in southwestern Ethiopia (Mengist, 1986) and also in Tigrai to the north (Beyth, 1971, Morton, 1981, Garland, 1980). It is in this later area (Tigrai) that the volcanics appear to be the most extensively developed (the Tsalit metavolcanics of Kazmin, 1973).

The geochemistry of the magmatic products of the central branch has not been studied as of yet even to the extent of that of the western branch. In the relatively well exposed southern segment of this central branch, i.e the Megaddo region (Chater, 1971) of the Adola area and the Afelata domain of the thesis area, the intrusive phases are gabbroic to monzogranitic, with quartzdiorites and tonalites as the predominant rock types (Chater, 1971; Kozyrev et al., 1985; Gichile et al., 1986). The associated volcanic rocks are predominantly basaltic rather than andesitic (Chater, 1971; Kozyrev et al. 1985 and also this work).

In the eastern part of the Sagan - Afeleta area as shown in chapter 6 the plutonic association is represented by a tonalite and a monzogranite, while the volcanic unit(s) is a low K tholeiite of an apparently komatitic-basalt affinity. These magmatic rocks are interpreted in here (Chapter 6) as indicative of an immature island arc setting, for the Afeleta domain of this work and the Adjacent Megaddo region. Thus, these rocks and the tectonic setting they indicate is much similar to that of the lower Pan-African (Gass, 1981, Table 2.1) magmatic rocks of the Arabian shield (Roobol et al., 1983, Gass, 1979,

1981). The type of volcanic products also appear to be similar to that of the Late Precambrian of the Moyale area about 200 kms to the south (Berhe, 1989).

The central volcano - plutonic branch is therefore contrasting to that of the western branch, which probably represents a more evolved relatively mature arc setting. The western branch magmatic rocks appear to have more of the characteristics of the Middle Pan-African terranes (Gass, 1981) of the Arabian shield (Table 2.1). However, some of the early mafic (gabbroic) associations perhaps represent early immature island arc environments in the tectono-magmatic evolution of this bigger branch.

2:1:3 The Pan-African

This term was originally utilized (Kennedy, 1964) to refer to what was believed to be a thermo-tectonic episode responsible for the widespread radiometric dates at about 500 Ma from the Precambrian of most of Africa. In contemporary literature, the Pan-African is used to refer to time, orogeny and also orogenic belts. In its time connotation, it is very commonly used to denote the time span from 1200 - 500 Ma (Gass, 1981, Stoeser and Camp, 1985, Schmidt et al., 1979). This time is the time from initial continental rifting through oceanic accretional stage to the orogenic stage for the Pan-African orogenic cycle. The two limits of this time range correspond to the approximate time of initiation of rifting (1200 Ma) of the Pan-African arc-basins of the Arabian shield (Stoeser and Camp, 1985) and also that of the Dahomey-Pharusian belts (Cabey et al. 1981, Black et al., 1979, Black, 1984) and the final cratonization (500 Ma).

Globally, the older age limit is believed to be the time of initial fragmentation of a

Proterozoic supercontinent (Sawkins, 1976; Windley, 1977, Kroner, 1979), although there are counter arguments that maintain that this fragmentation did not take place until after 570 Ma on the basis of palaeomagnetic data (e.g. Piper, 1982). The later age coincides with the peak of basement rejuvenation ages in older orogenic belts, i.e. the tectonothermal event of Kennedy (1964), and signifies the approximate age of cratonization of the Gondwana supercontinent at its final stage of aggregation.

Thus, in its geographic context, the Pan-African is used to refer to, not only orogenic belts in Africa but also genetically related Late-Proterozoic belts in the rest of the Gondwana continents (Mc Williams, 1981; Porada, 1979, 1989; Black, 1984; Bernasconi, 1983, 1987). Tectonically, the term also applies not only to newly accreted belts, like the Red Sea fold belt (Kazmin, 1971), discussed above, but also to older polycyclic mobile belts, in which Late-Proterozoic wide scale isotopic resetting (Cahen et al., 1984) has taken place. The Mozambique belt, the Zambezi belt and the exteriors of the Dahomey - Pharusian belt (Caby et al., 1981; Black et al., 1979; Black, 1984) of Africa and the Montiqueira belt (Bernasconi, 1987) of NE south America are important examples of this second category.

In this thesis the usage of the terms Mozambique belt, Red Sea fold belt and the Pan-African is, unless other wise stated, as described in the above review. The use of the Pan-African orogeny as is suggested (Jackson and Ramsay, 1980) to denote events at around 500 Ma is avoided in this work also. The other term "Mozambiquian orogeny" is also not used because it is even more controversial and is quoted arbitrarily and locally (see Muhongo et al. 1987 and the references there in, also Hepworth, 1979).

CHAPTER THREE

ROCK UNITS

Introduction

Precambrian rocks outcropping over a large part of the Sagan-Afelata area are generally polydeformed and metamorphosed at medium to high grades. Quartzofeldspathic rocks, which are derived from both sedimentary and igneous rocks and foliated granitoids are the predominant rock types. Next in abundance is a semi-pelitic and pelitic migmatitic biotite gneiss, with intercalations of subordinate rock types, that include thin units of amphibolites, and quartzofeldspathic rocks with variable amounts of hornblende and biotite. Independent units of amphibolite and mafic granulite also form mappable units. Ultramafic schist, calcsilicate rocks, quartzite, garnet - plagioclase schist and sillimanite - muscovite schist occur as volumetrically insignificant parts of larger units in the eastern part of the area.

These metamorphic rocks are unconformably overlain by Tertiary and more recent volcanic rocks. The volcanic rocks are most extensive in the western part of the area, where they floor the Sagan half-graben, which is at the southern termination of "The Main Ethiopian Rift" (Mohr, 1967). Volcanic rocks also cover the escarpments and highlands to the west, east and south of this half graben. In contrast, in the central and eastern part of the area, outcrops of volcanic rocks are limited to a few basalt flows, which are generally thin and occur in small isolated outcrop areas. However, in these parts of the

area lateritic soil is common, and at places grades into regoliths containing small outcrops of weathered basalt. This gradation and the confinement of the thickest outcrops of the volcanic rocks to valleys suggest that most of the present land surface in the central and eastern part of this project area is a close approximate to the unconformity between the Tertiary volcanic rocks and the Precambrian basement (Gichile et al.1986).

This chapter describes lithologic and petrographic characteristics of the major Precambrian - Paleozoic metamorphic and plutonic rock units and outlines their distribution and contact relationships. Informal "lithostratigraphic" names assigned to major rock groups formerly considered as stratigraphic units (Kazmin, 1973; Kazmin et al. 1978; Warden, 1976 and Warden and Horkel, 1984) are referred to, in order to relate the present study to previous work on the geology of the Ethiopian Precambrian. Table 3.1 shows the names of the main "stratigraphic" units (more correctly tectono-metamorphic units) shown on the geological map of Ethiopia (Kazmin, 1973) and their relationship to rock units recognized in this work.

The order in which rock units are described is not necessarily stratigraphic, but wherever a time relation could be inferred the relationship is pointed out in the descriptions of the relevant rock units.

The description is aided by subdivision of the area into three domains (Fig. 1) which are from west to east the Sagan, Fincha and Afelata domains. These are distinguished by combined differences in lithological assemblages, structural style, and to a lesser extent metamorphic grade. The boundary between the eastern Afelata domain and the central Fincha domain is a major scale tectonic boundary, the Kolle-Altuntu lineament of Gichile

Table 3.1 Tectonometamorphic units to which main rock units within the Sagan - Afelata area belong, and locality based names used in this work.

Map unit designation in this work (Fig. 1)	Tectonometamorphic unit to which the unit belonged on the geological map of Ethiopia (Kazmin, 1973).	Position in the three complex classification of the Ethiopian Precambrian (Kazmin, 1973).	Locality based names used in this work.
AD 3	unrecognized	Upper complex	Korolle pyroxenite
AD 2	Adola group	Upper Complex	Hiddi Asasu amphibolite
AD 1	Alghe gneiss	Lower Complex	Sebbeto tonalite
FD 8	post - tectonic granite	.....	Bergudda complex
FD 7	Yabello gneiss	Lower complex	Kinsho granite
FD 6	syntectonic granites ?	.....	small foliated granitoids
FD 5	Awata gneiss	Lower complex	Altuntu granite
FD 4	Yabello gneiss	Lower complex	Fincha gneiss
FD 3	Awata gneiss	Lower complex	Melu gneiss
FD 2	Burji gneiss	Lower complex	Burji gneiss
FD 1	Awata gneiss	Lower complex	Bokossa granite gneiss
SD 1	Konso gneiss	Lower complex	Sagan granulites

et al., 1986, marked by a large (tens of kms long in southern Ethiopia) lineament which has been photogeologically traced over hundreds of kms farther to the north and south (Vail, 1983, see also lineaments in Chapter 4). The boundary between the Fincha domain and the Sagan domain to the west may also be tectonic. However, the nature of this boundary cannot be ascertained because it is obscured by extensive Tertiary - Quaternary volcanism and faulting related to the development of the East African rift system.

3.1. The Sagan domain (SD)

The Sagan domain, in the westernmost part of the project area underlies the Sagan half-graben. Only two small isolated not more than 3 km x 5 km wide outcrops of Precambrian rocks are known in this domain. The predominant rock type in both outcrop areas is mafic granulite with subordinate quartzofeldspathic rocks, also of probable granulite grade (map unit SD 1). Unique to the northern outcrop is an E - W strike of the foliation, transverse to the N - S trend, that is predominant in the other domains and also within the Mozambique belt in general (Kazmin, 1972, Getahun and Alula, 1987).

3:1:1 Mafic granulites (SD 1)

SD 1 mafic granulites are part of the "Konso Gneiss" of Kazmin (1973). Banded to massive mafic granulites predominate over minor intercalations of quartzofeldspathic and quartzitic rocks. The mafic granulites, are characteristically light to dark grey. Felsic components (feldspar and quartz) are darker than in lower grade equivalents, plagioclase is light greyish and oppalecent while quartz is commonly bluish grey.

In the southern outcrop area, banded mafic granulite predominates over massive types. Dark, pyroxene - rich, layers with or without garnet porphyroblasts, alternate with thicker and lighter plagioclase rich layers (Plate 3.1). Individual layers vary, in thickness, from thin (thin section scale, Plate 3.2) to up to 3 cm. Banded mafic granulites along the southern bank of the Sagan river, are also cross - cut by quartz - plagioclase veins (Plate 3.3). Some of these veins are less continuous as the rocks grade to more massive, less veined, pyroxene rich types with relatively minor amounts of plagioclase and quartz. Granulites in the northern outcrop area are, as described by Getahun and Alula (1987), commonly greenish black, medium grained, weakly foliated to massive rocks, that are dark grey on weathered surfaces.

In both outcrop areas, plagioclase, quartz, pyroxene (both calcium pyroxenes and orthopyroxene), hornblende, less commonly garnet, K feldspar and opaque minerals are the major component minerals of the SD 1 mafic granulite. In outcrops along the northern bank of the Sagan river garnet porphyroblasts are unusually coarse and are rimmed with plagioclase grains. Approximate mineral proportions of representative specimen from these rocks are given in Table 3.2 (Appendix I).

The Sagan granulite are generally fine grained. Relatively coarser grains of quartz, are often lenticular and elongated in the direction of the foliation giving the rock a strong planar fabric (Plate 3.4). Plagioclase (An = 42%), occurs in polysynthetically twinned, commonly anhedral, grains. Orthopyroxene (pale green to pink pleochroic hypersthene) is fine grained and invariably anhedral. The typical calcium pyroxene is pale green, faintly pleochroic diopside, and occurs as fine anhedral grains. Pyroxene grains occur in

clusters (Plate 3.2), in some specimens. Hornblende, pleochroic in shades of green, replaces both pyroxenes along cleavage planes or more commonly forms rims. Rims assume the form of clusters of barely identifiable very fine (crystallites) grains (Plate 3.5) or an optically continuous shell of a single large grain wholly or partly enclosing pyroxene grains (Plate 3.6).

Trace amounts of acicular sillimanite and minor muscovite are present in a specimen of Garnet granulite from the southern outcrop. Other minor constituents include opaque minerals, which commonly occur where hornblende replaces pyroxenes, trace amounts of apatite, titanite and zircon. Biotite is present in trace amounts in few specimens. Subordinate rocks within unit SD 1 include generally quartzitic or quartzofeldspathic rocks, which appear to be more common in the northern outcrop area (Getahun and Alula, 1987).

Equivalent mafic granulites in the Konso region, from where the name Konso gneiss (Kazmin, 1973) is derived, are thought to have been derived from interlayered mafic to intermediate volcanic, possibly pyroclastic and associated mafic hypabbysal rocks (Davidson, 1983). From compositional primary layering seen in outcrops of mafic granulite (Plates 3. 1 and 3.2) of the southern outcrop area, and the general mineralogical composition of these rocks it may be said that similar mafic to intermediate volcanic rocks may have been the protolith for these rocks also.

3:2 The Fincha domain (FD)

This domain underlies the central and largest part of the project area. The rocks

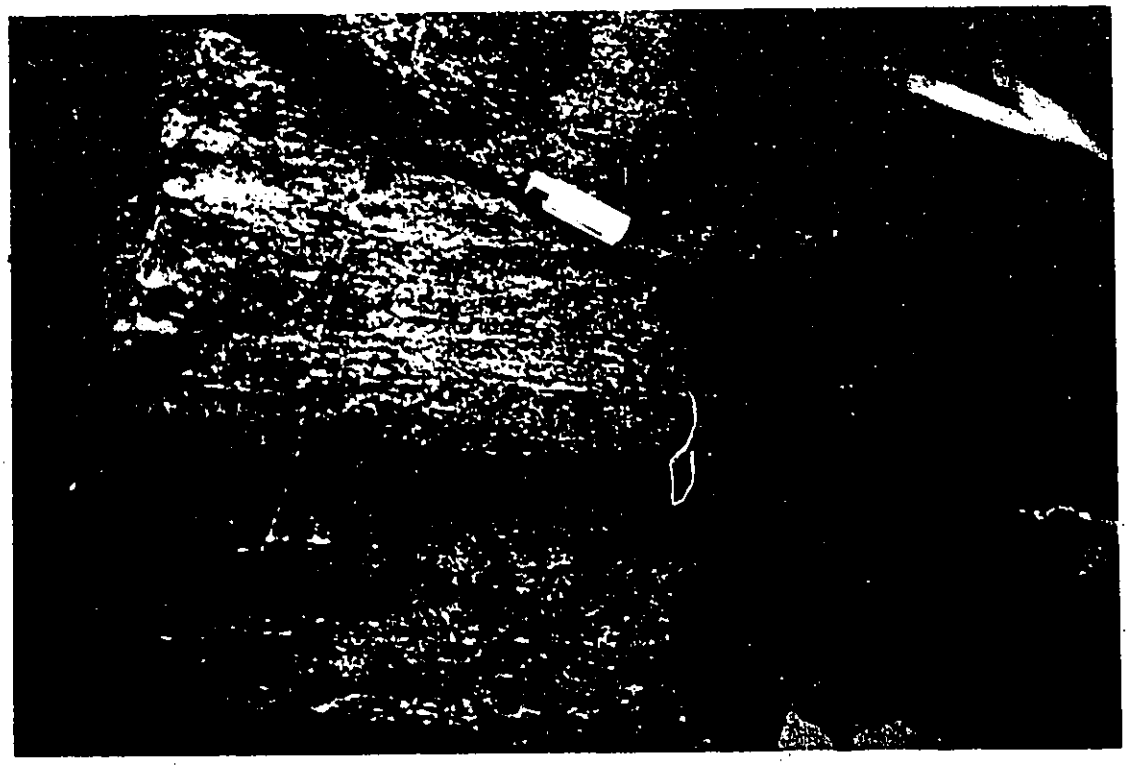

Plate 3.1 Compositional layering in an outcrop of SD 1 mafic granulite. Darker layers are richer in pyroxenes and hornblende and the lighter in quartz and plagioclase. Sagan river valley, north of the Yabello-Konso bridge.

Plate 3.2 Thin section scale layering in mafic granulite (SD 1). Greenish (Cpx and Hbl), pinkish (Opx) and light (Qtz and Pl). Plane polarized light, field of view 9 mm.

Plate 3.3 Quartz-plagioclase veining in SD 1 mafic granulite. Note some are related to late fractures (see displacements in the lower right half). Sagan valley, southern bank, south of the Yabello-Konso bridge.

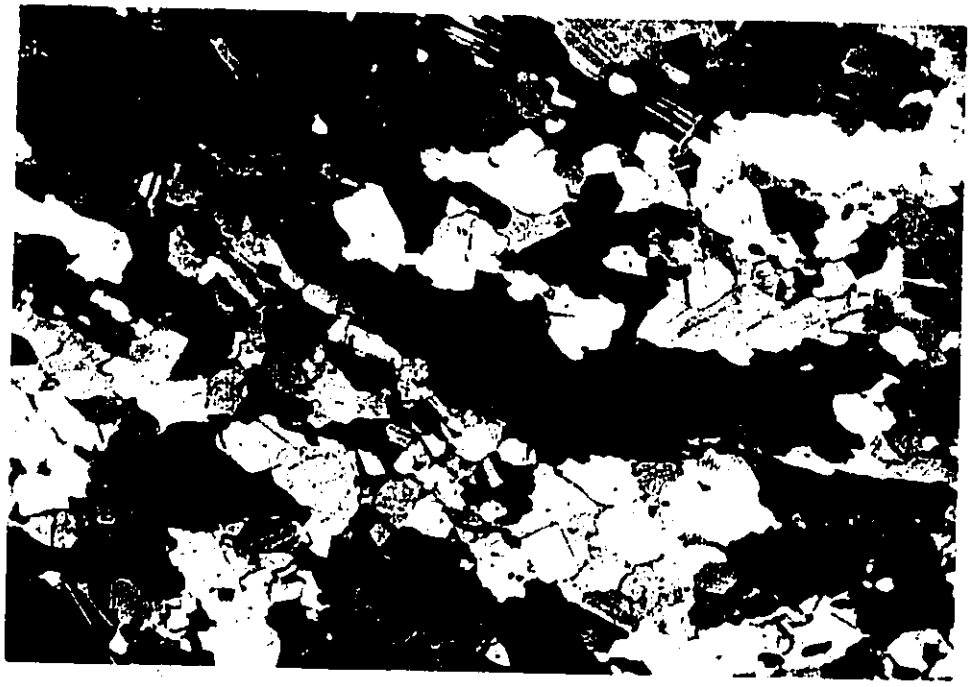

Plate 3.4 Relatively coarser lenticular quartz (dark), in a dark fine grained granoblastic groundmass. Lower left (dark) opaque mineral rim around orthopyroxene grain (lighter). Crossed Nicols, field of view 4.5 mm.

included in this domain are the "Yabello", "Burji", and "Awata" gneiss of Kazmin (1973). Except for the Burji gneiss (FD 2), which is dominated by layered biotite gneiss, the domain is predominantly underlain by quartzofeldspathic gneiss and granites with minor mafic components. Metamorphic grade varies from amphibolite facies in the eastern and central part of the domain to granulite facies in the west central where there are patches of charnockitic rocks (see Fig. 5.1).

3:2:1 Granitic gneiss (FD 1)

This unit is best exposed along the escarpment bounding the Wolena-Bokossa ridge on the west from which the local name "Bokossa gneiss" is given to these rocks. Along this escarpment the rock occurs in large outcrops with apparent coarse (outcrop scale) "layering" which is accentuated by jointing parallel to foliation (Plate 3.7). Layering is also seen at smaller scales (cm scale), as alternate mafic and felsic discontinuous bands (Plate 3.8). Biotite and pyroxene (both calcium pyroxenes and orthopyroxenes) with minor opaque grains are important constituents of the mafic bands, while the lighter coloured bands contain some biotite and magnetite but are rich in pink perthitic feldspars and quartz. Elsewhere, to the east and south, the unit does not show the small scale compositional layering. The main mineral foliation (S_1) is generally defined by the preferred alignment of fine grains of reddish biotite. In mafic bands the main mafic silicate minerals (ortho- and calcium pyroxenes) also show a weak preferred alignment (Plate 3.9). Quartz shows pronounced elongation parallel to the biotite foliation.

Biotite is pleochroic from red to pale reddish - yellow. Plagioclase is twinned and the

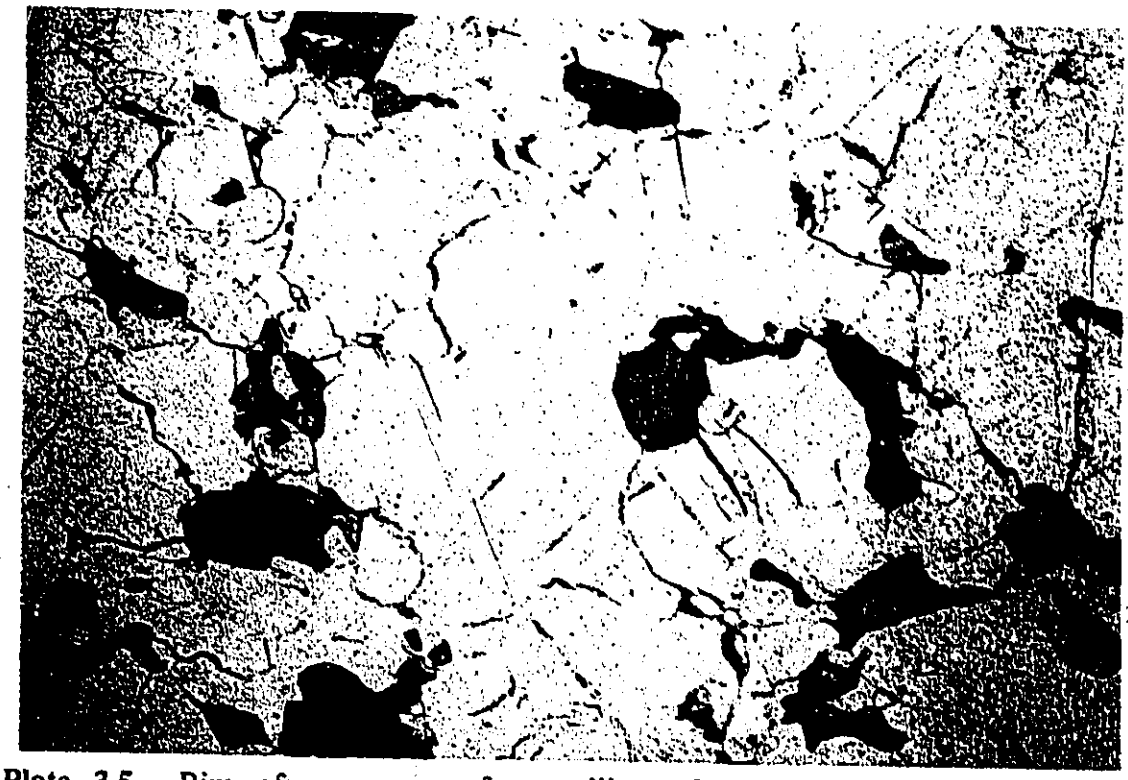

Plate 3.5 Rim of aggregates of crystallites of hornblende (green) around an orthopyroxene grain (round, yellowish grain), SD 1 mafic granulite. Plane polarized light, field of view 2.3 mm.

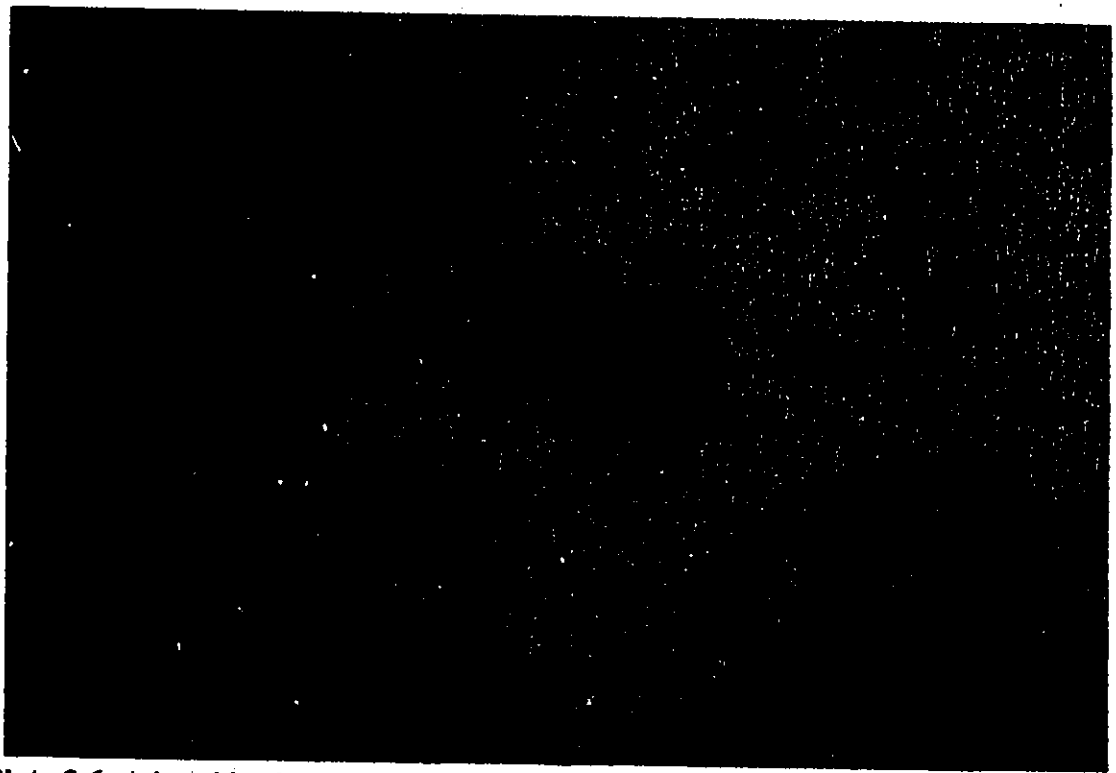

Plate 3.6 A hornblende crystal (centre dark green) enclosing a calcium pyroxene crystal (lighter green), in SD 1 mafic granulite. Note also crystallites around an orthopyroxene grain in continuity. Plane polarized light, field of view 2.3 mm.

twin lamellae are commonly bent. Both feldspars and quartz show undulose extinction. Polygonization of grains is also common in coarser grains of quartz and feldspar.

This charnockitic unit (FD 1) was formerly (Kazmin, 1973) regarded as a part of the Awata gneiss. However, from both its gross lithological features and its mineralogy and texture it appears to have a plutonic protolith and has no similarity with either the meta-sedimentary or meta-plutonic units constituting the Awata gneiss elsewhere. The rock is also metamorphosed at higher grades (probably granulite facies) than rock units in the Awata gneiss (see also Chapter 5). Getahun and Alula (1987) report inclusions of biotite gneiss (Burji gneiss, FD 2) in this rock. This has not been seen during this work. The unit is intruded by the steep sided Bergudda plutonic complex (FD 8) along its eastern margin.

3:2:2 Layered biotite gneiss (FD 2)

This unit outcrops in the western part of the Fincha domain, along the slopes and on top of the southern part of the Amaro horst and in the low lands north of the Sagan valley, west and south - south west of the Wolena-Bokosa ridge (Fig. 1). The unit is distinguished from the adjacent granitic gneiss (map unit FD 1) by the predominance of layered biotite gneiss which is distinctly of sedimentary origin and the wide variety of lithologic units associated with the latter.

According to Kazmin (1973) this unit which, is referred to as "The Burji Gneiss" is characteristically composed of uniform schist and gneiss derived from semi-argillaceous fine grained sediments. Consequently, in regional syntheses (e.g. Warden 1976, Warden and Horkel, 1984.) the unit is considered as a more homogeneous unit than warranted

Plate 3.7 Layered outcrop of FD 1 granite gneiss, layering dips east (right side of picture). Western escarpment of Wolena Bokossa ridge.

Plate 3.8 Small scale layering in FD 1 granite gneiss. Darker bands are rich in pyroxenes biotite and opaque mineral grains, lighter layers are quartzofeldspathic. Wolena Bokossa area, south of the Soyema - Yabello road.

from the variety of rock types it encompasses.

The Burji gneiss, as recently described (Getahun and Alula, 1987), is composed of various proportions of biotite gneiss, biotite - hornblende gneiss, hornblende - biotite gneiss, and quartzofeldspathic gneiss. Rare layers of diopside bearing gneiss, often of 5 - 10 cm scale thickness are at places interlayered with hornblende gneiss and hornblende - biotite gneiss. Thin units of amphibolite, often boudinaged, are abundant. Gneissic granite and pegmatite veins up to 5 m thick are also abundant.

Biotite gneiss, the dominant rock type, is commonly fine to medium grained (1 - 4 mm), melanocratic and well layered (Plate 3.10). The layering varies from mm to tens of cm in thickness and is commonly defined by alternating biotite and/or hornblende rich mafic layers and felsic layers that are mainly granitic to pegmatitic leucosomes and veinlets. Such layering is interpreted to be of metamorphic origin. In some cases layering defined by contrasting proportions of biotite, or of biotite and hornblende is preserved within the mafic bands. This latter layering is compositional, and apparent in a few specimens down to thin section scale; it is often accompanied by variations in grain size between alternate layers. In such cases, layers with coarse grains of biotite are poor in or do not contain hornblende. This perhaps primary layering is also parallel to the coarser migmatitic layering defined by granitic leucosomes and the accompanying mineral foliation. A strong alignment of hornblende prisms and biotite flakes and flattened quartz grains defines the mineral foliation.

The migmatitic layering and mineral foliation appear to have been preceded by a yet earlier set of migmatitic or gneissic layering (S_1', chapter 4) which is folded and

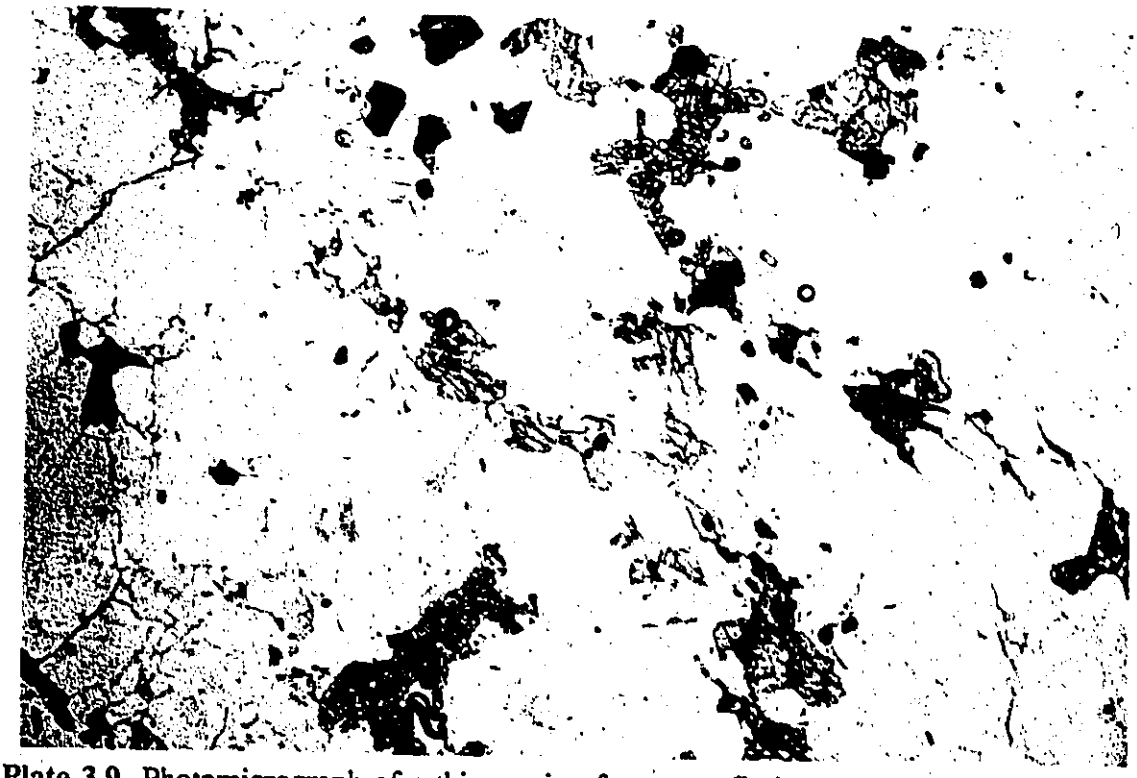

Plate 3.9 Photomicrograph of a thin section from a mafic layer of FD 1 granite gneiss in the Bokossa area. Pyroxenes (Opx and Cpx, grey, with cleavage), biotite (brownish), the dark grains are opaque minerals. Note weak alignment and also perthitic feldspar (left centre). The light mineral grains are of feldspar and quartz. Plane polarized light, field of view 2.3 mm.

Plate 3.10 Metamorphic layering in an outcrop of FD 2 layered biotite gneiss (Burji gneiss). Hammer-head points north. Koromo area, west of Soyema village.

transposed and is only preserved in rootless intrafolial F_1 folds.

The major minerals constituting the biotite gneiss are brown biotite, plagioclase, and quartz with subordinate and less commonly present hornblende and garnet. Hornblende is dark green (Z), and is inclusion free or with minor inclusions of fine quartz. Biotite is deep brown and free of inclusions. Grains of both K feldspars and plagioclase are anhedral, free of inclusions and often not twinned. Most grains of quartz are also inclusion free. Accessory minerals include opaque minerals, zircon, apatite and titanite.

Other than the major unit i.e. biotite gneiss, which is distinctly of sedimentary origin, the subordinate units within the Burji gneiss appear to be largely of magmatic origin. These include mafic units with hornblende as an essential mineral and some of the quartzofeldspathic units. The hornblende - biotite rocks are fine to medium grained, and may have been derived from intermediate hypabbysal intrusives as suggested by their intact magmatic textures. The biotite - hornblende rocks are finer grained and have undergone more pronounced metamorphic recrystallization and were perhaps of volcanic origin. Some of the felsic fine grained units have blastoporphyritic textures (Plate 3.11) and appear to be derivatives of feldspar porphyritic volcanic rocks or perhaps porphyry dykes, emplaced at shallow levels. The abundance of hornblende and biotite in the fine grained matrix of these rocks suggests that they may be of intermediate compositions. More over they appear not to have undergone the higher grade metamorphism that the layered biotite gneiss has been subjected to. It is possible that some of these units were emplaced as subvolcanic intrusives at a later date than the early migmatization (S_1').

Biotite rich gneiss are often more weathered and friable. Thus, the estimates of mineral

proportions shown in Table 3.3 (Appendix I), is of the more resistant, but volumetrically subordinate, lithologies with hornblende as an important constituent.

3:2:3 Paragneisses (FD 3)

This name is used to refer to several rock types (collectively), which could not be mapped out distinctly because of their limited outcrops and the scale of this work. This group of rocks, the "Melu gneiss" (Gichile et al., 1986) were thought to constitute the western apparently "non - granitic" part of the "Arero Gneiss" (Kazmin, 1970). In later works and on the geological map of Ethiopia (Kazmin, 1973) the unit is regarded as a part of the Awata gneiss.

The predominant rock type in this group of "gneissic" units, is shown as FD 3a on the geological map (Fig. 1). It lies east of the main highway between quartzofeldspathic gneiss (FD 4a) and augen granite (FD 5) building the Melu ridge from which the name "Melu gneiss" was given (Gichile et al., 1986) to map unit FD 3a. FD 3a is typically medium grained biotite bearing to rich, quartz - feldspar rock (commonly about 1mm size grains) that weathers to light grey or yellowish. It possesses a mineral foliation defined by the alignment of grains of biotite and subordinate and sporadically occurring muscovite. Although, quartz streakings are apparent, in handspecimen, the rock has no distinct gneissic layering and in thin sections the foliation in the rock is rarely apparent. It also doesn't have sufficient amounts of micaceous minerals to be called a schist. It is a strongly foliated granite looking rock similar to those that elsewhere have been referred to as foliate (Ashton and Leclair, 1990).

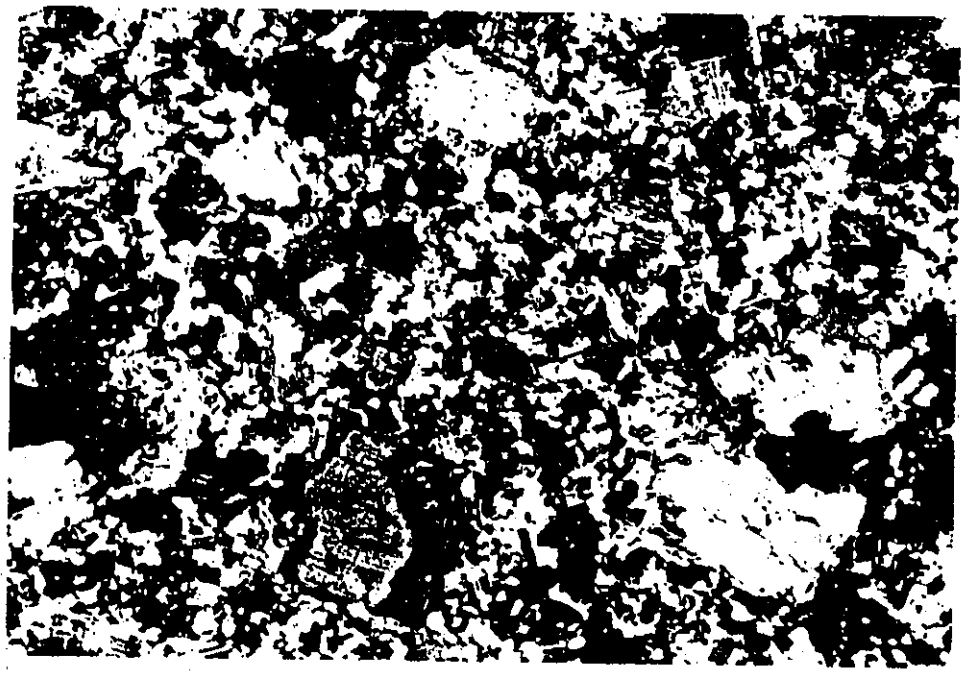

Plate 3.11 A flelsic blastoporphyritic (K feldspar phenocrysts) fine-grained (dyke ?) rock in unit FD 2 (Burji gneiss). Recrystallization is limited to the matrix; dark grains in the groundmass are of hornblende, biotite and opaque minerals. Crossed Nicols, field of view 4.5 mm.

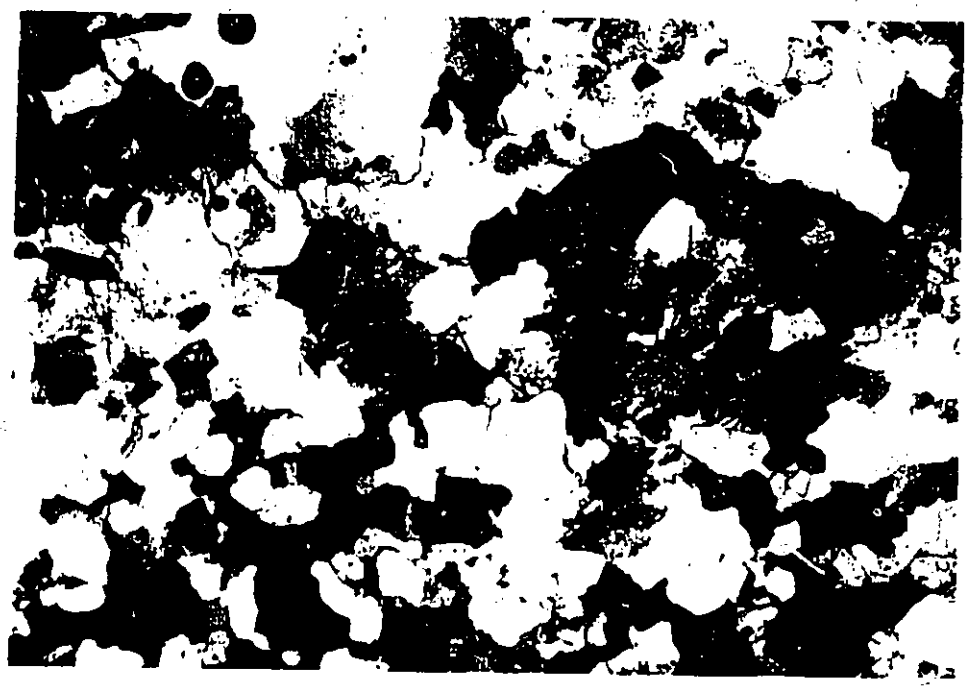

Plate 3.12 Photomicrograph of a specimen of FD 3b calc-silicate gneiss. Calcite (rhombic cleavage trace), biotite (dark), hornblende and diopside (lighter grey), quartz and feldspars (light). Note grain size layering (upper half coarser than lower half). Crossed Nicols, field of view 2.3 mm. Melu ridge.

In thin sections, both feldspar and quartz are xenoblastic. Quartz grains are some times drawn - out and define the mineral foliation, with fine grains of biotite, which are generally intergranular and only weakly aligned. Feldspar grains tend to be equant. Both biotite and often the intergrown muscovite grains have "dirty looks" due to fine opaque inclusions. Consequently biotite is pleochroic from light yellow to (almost black) dark brown. The rock is both texturally and to a lesser extent mineralogically homogenous, in all outcrops. Thus, one can not rule out the possibility of its being derived from a granitoid protolith.

However, map unit FD 3 is regarded as paragneissic, because of the presence of thin, but persistent, interlayers of metasedimentary rock units within FD 3a The more persistent of these sedimentary units, calcsilicate gneiss (FD 3b) and sillimanite - muscovite gneiss (FD 3c) are approximately shown on the geological map (Fig. 1). FD 3b is found in many places but by far the most persistent layer extends in the east central part of the map area whereas FD 3c is limited to a locality to the north.

FD 3b calcsilicate gneiss contains variable amounts of blue green hornblende, tremolite and/or diopside, epidote and up to 4% recrystallized carbonates (calcite) besides quartz and feldspar. Hornblende grains in this rock type are generally fine, xenoblastic, and contain inclusions of opaque minerals. Quartz and feldspar grains are also xenoblastic, and commonly polygonized. The thin layering in these rocks is sometimes seen in thin sections as alternate bands of contrasting grain sizes (Plate 3.12).

FD 3c sillimanite - muscovite gneiss essentially consists of the two feldspars and quartz besides sillimanite and muscovite. It occurs in very small and friable outcrops in the

locality shown (Fig. 1) and is often associated with muscovite bearing granitic gneiss.

An amphibolitic unit (FD 3d), with subordinate intercalations of biotite - rich schists lies near the southern extremity of the FD 3 unit. The amphibolites of FD 3d are fine grained finely layered (Plate 3.13) and at most places contain epidote. Fine porphyroblasts of garnet occur in some of the more leucocratic and schistose amphibolitic rocks. Some of the garnet porphyroblasts are poiklioblastic and contain inclusions of fine grains of quartz (Plate 3.13). The garnet bearing amphibole schists also contain actinolite grains in parallel growth with blue green hornblende (Plate 3.13). The coarser layers are generally poorer in mafic minerals and contain elongated xenoblastic grains of quartz and feldspar defining a strong fabric. The fabric is also defined by well aligned grains of the two amphiboles which give a general schistose texture to these rocks. Table 3.4 in Appendix I lists estimates of the approximate mineral proportions in thin sections of selected samples from different lithologies in map unit FD 3.

Map unit FD 3 is bound to the east by a large unit of foliated megacrystic granite (FD 5), along a poorly defined boundary. The nature of this boundary is unknown due to lack of exposures, but was thought to be gradational (Kazmin, 1970, Gichile et al., 1986). An interpretation that followed from this relation was that the granitic unit (FD 5) was derived from the rocks of unit FD 3 by anatexis. However, this relation can not be demonstrated in the field because of Cenozoic volcanic and alluvial cover. Furthermore, geochemical data from the granite (Chapter 6) do not support this relation.

3:2:4 Quartzofeldspathic gneiss (FD 4)

This unit is mainly a layered, leucocratic, fine grained gneiss (FD 4a), and outcrops in the central part of the eastern half of the project area. The predominant lithology (FD 4a) was initially distinguished as "Fincha gneiss" named after the Fincha village, which is situated in the east-central part of the Sagan-Afelata area, by Gichile et al. (1986) from the rest of the "Yabello gneiss" of Kazmin (1973). The latter (Yabello gneiss) includes map units FD 4 and FD 7 of this work (Table 3.1).

The Fincha gneiss (FD 4a) is a fine grained gneiss essentially composed of microcline, quartz, and significant amounts of opaque minerals and is characterized by thin layering (Plate 3.14). Layers are commonly defined by magnetite - rich laminae accompanied by a weak mineral foliation, which is also on a fine scale (Plate 3.15). This layering is best seen in road cuts near the Surruppa village south of this thesis area. Layering is also defined by variations in grain size in relatively magnetite poor parts of this rock. In such rocks aggregates of quartz and feldspar grains of contrasting size define the foliation, which sometimes shows in thin sections (Plate 3.16). Mineral foliation is better developed where the rock contains appreciable amounts of biotite. In such cases, the alignment of fine grains of biotite defines a relatively stronger mineral foliation.

Mineralogically the unit is homogeneous, and is mainly composed of abundant microcline, up to 25% quartz, significant amounts of opaque minerals and trace amounts of biotite (Table 3.5) and alanite. Microcline is anhedral, polysynthetically twinned, and commonly contains fine grained characteristically subrounded inclusions of quartz (Plate 3.17). Quartz grains are generally anhedral, finer grained than the associated feldspar

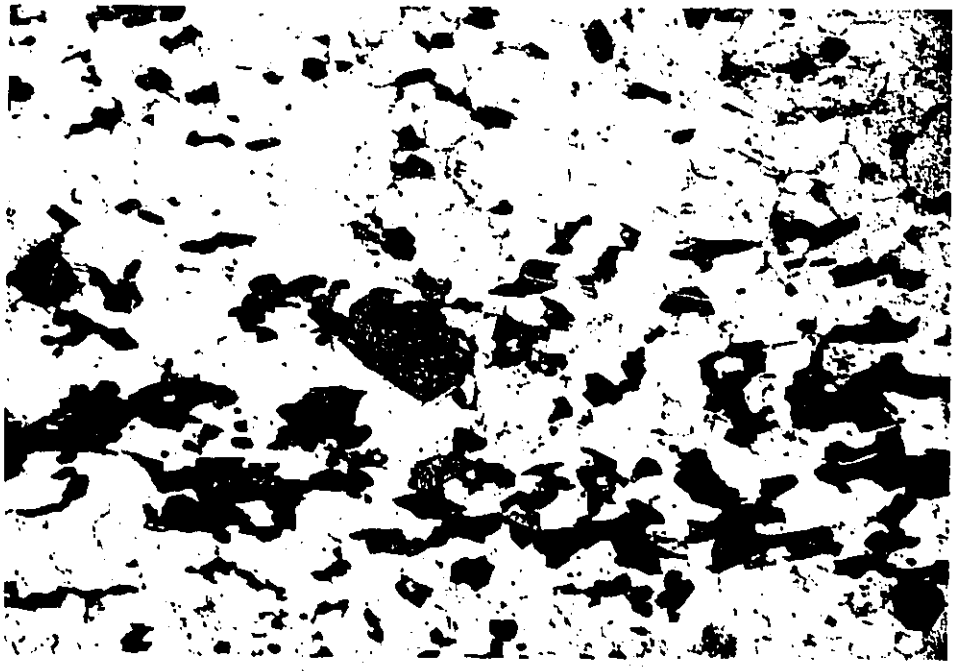

Plate 3.13 Fine layering in a garnet bearing amphibole schist of unit FD 3d. Garnet porphyroblast (centre) with inclusions of fine grained quartz. Hornblende (dark) replacing actinolite (lighter in a relatively large amphibole grain (above and to the right of garnet porphyroblast) and also in others. Plane polarized light, field of view 4.5 mm. Kilkille area.

Plate 3.14 Fine layering in an outcrop of the Fincha gneiss (FD 4a). Dark relatively eroded layers are more pelitic and uncommon in the unit. Layering dips west, see below for a close up. Road cut near Surruppa village (15 km south of the thesis area).

grains, typically subrounded (Plate 3.17) and do not show significant grain elongation. Sillimanite and muscovite bearing more leucocratic gneiss typically in small patchy intercalations occurs in the Doga hill and at the southeastern foot of the Surruppitti hill. The rock is more schistose than the typical Fincha gneiss (FD 4a) and may perhaps represent more aluminous pockets within the predominant quartzofeldspathic unit (FD 4a).

Unit FD 4b, a quartz rich rock with lenses of tremolite - plagioclase schist outcrops in a NW trending narrow zone along the western boundary of FD 4a with FD 7, and extends to the north out of this area. Apart from the lenses of ultramafic schist the rock is almost mono - mineralic, with quartz as the only mineral. Similar quartz rich rock in perhaps the same zone mapped to the south (Kiros and Kinetibeb, 1987) is known to be manganiferous (Kazmin, 1970). Quartz grains in this rock are anhedral, coarse and do not show strong recrystallization features. However, the preferred alignment of these strongly flattened grains defines a foliation. In outcrop the foliation appears to be accompanied by a parallel textural (grain size) layering, which gives the rock a layered appearance. Tremolite grains in dark tremolite - plagioclase schist, lenses within unit FD 4b are skeletal and generally coarser than coexisting plagioclase grains. Both plagioclase and tremolite grains show a preferred orientation defining a mineral foliation. The equivalents of this schist, in an extension of the same zone, 15 km north of the map area and west of the Agere Mariam village are known to contain serpentine (Hundie Beyene, personal communication, 1986). This association tremolite - serpentine - plagioclase and the lack of quartz (within the schist) suggests an ultramafic to mafic igneous protolith, rather than a sediment for the schistose lenses in FD 4a. The zone in which these rocks (dykes ?)

Plate 3.15 Closer view of layering (Plate 14 above) in the Fincha gneiss (FD 4a); dark layers are magnetite rich. Pencil points north.

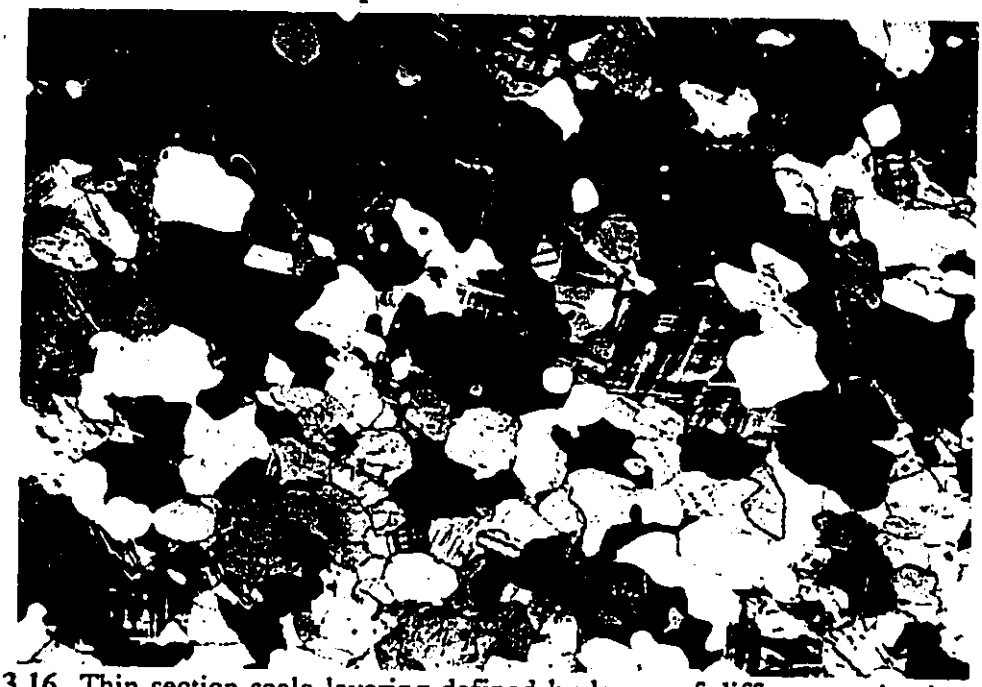

Plate 3.16 Thin-section scale layering defined by layers of different grain sizes, upper right coarser than lower left, in Fincha gneiss (FD 4a). Note also the rounded grains of quartz that are characteristic of this unit. Crossed Nicols, field of view 4.5 mm. Didiga area.

occur extends for over 35 kms N - S and may mark a significant discontinuity [see section on Precambrian lineaments in Chapter 4].

3:2:5 Meta - megacrystic granite (FD 5)

Granite (unit FD 5) outcrops as a large N - S elongated body along the eastern margin of the Fincha domain. The major outcrops form a topographic high trending approximately N - S, with prominent peaks which are from south to north, Hilintisa, Tula Boko, Altuntu and Finikotu. The local name "Altuntu granite" is given to this unit from the central peak (Altuntu) in this ridge (chain of peaks). The eastern slopes of this ridge form a major topographic break between the eastern lowlands and the higher land to the west. This boundary is a major structural boundary between the contrasting eastern Afelata domain and the central Fincha domain.

The FD 5 Altuntu granite is medium grained, commonly with megacrysts of microcline and pinkish in colour. The granite is slightly heterogenous, partly marked by changes in relative proportions between phenocryst-phase and the groundmass and also intensity of deformation (compare Plates 3.18 and 3.19). This textural difference is some times apparent in a single outcrop (Plate 3.20) and could be related to both strain and chemical gradients. In general, a mineral foliation is defined by strongly aligned biotite and to a lesser extent hornblende grains and elongate quartz -feldspar aggregates. Mineralogical heterogeneity is manifested mainly in the relative proportion of biotite and hornblende. In extreme cases hornblende, is absent in some parts of the granite. The granite is commonly crossed by micro - granitic and pegmatitic dikes and veins of cm to metre

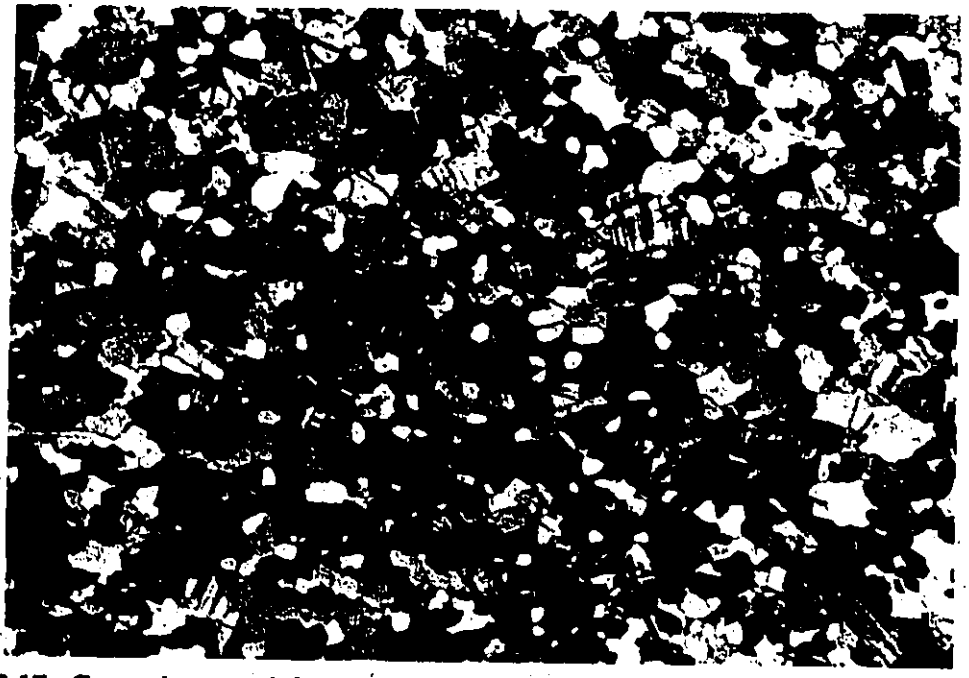

Plate 3.17 General textural features of the Fincha gneiss (FD 4a) in thin section. Note subrounded anhedral grains of quartz both in the groundmass and also as inclusions in feldspar grains. Crossed Nicols, field of view 2.3 mm. Burkitu Megadda area.

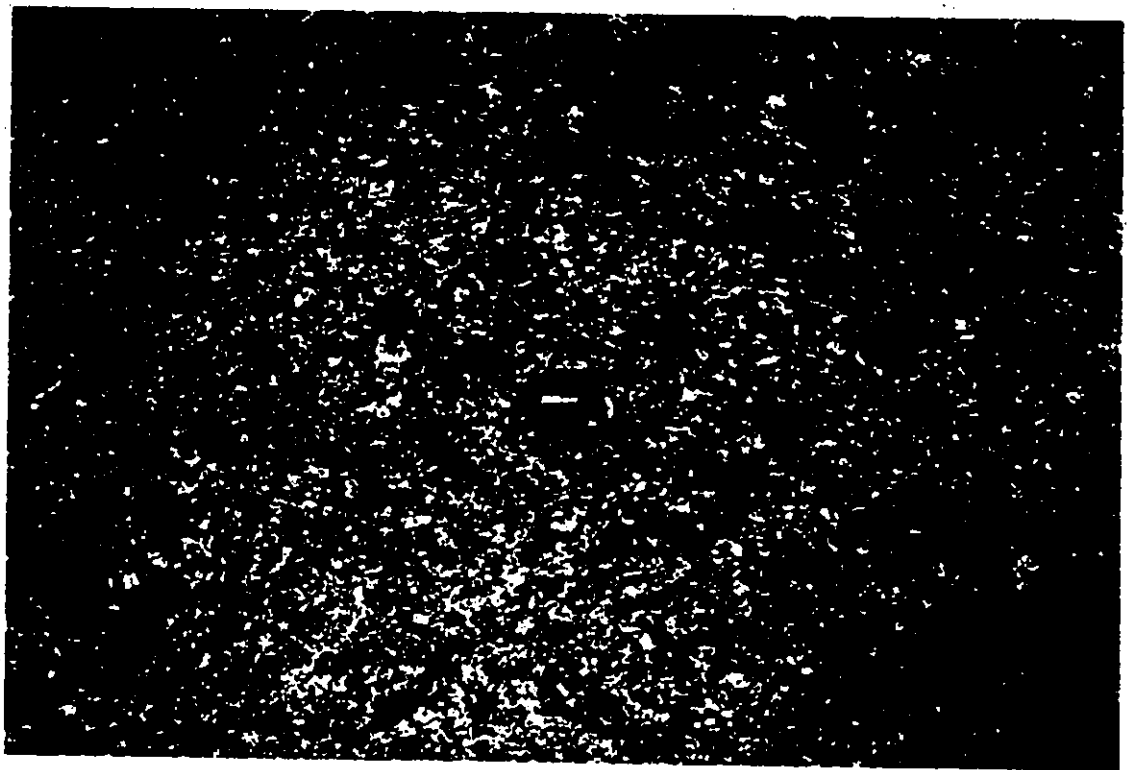

Plate 3.18 The Altuntu megacrystic granite (FD 5). Megacrysts are dominantly of microcline. In this outcrop the rock is relatively poor in megacrysts, richer in biotite than average and weakly deformed. Altuntu peak.

scale thicknesses.

The granite also contains fine grained mafic inclusions that are rich in biotite (Plate 3.20); these commonly occur in northern exposures. The inclusions are tens of centimetres long and are commonly a few centimetres thick. They share the same fabric with the enclosing granite and shown no indication of a pre -intrusion fabric (see also Chapter 4).

Megacrysts in the Altuntu granite are commonly polysynthetically twined grains of pink microcline (Plate 3.21) and reach up to 1 cm across. Plagioclase grains, also form phenocryst phases, but are more common in the groundmass. The phenocrysts are subhedral, but the fine to medium grained grains in the groundmass are anhedral, and show solid state recrystallization features such as straight boundaries and triple junctions (Plate 3.21). Intergrowths of plagioclase and K feldspars are rare and limited to the occurrence of a few fine patches of K feldspar in some plagioclase grains.

Mafic silicate minerals within the FD 5 granite are biotite and hornblende. At most places biotite is predominant over hornblende, but at a few places like in the Tula Boko ridge and in the Bonkokiti area hornblende predominates over biotite. In the Tula - Boko ridge the rock is unusually finer grained, free of phenocryst phases and is relatively weakly deformed. Biotite grains are generally medium grained, pleochroic from dark brown to faintly greenish yellow, and euhedral. They are generally free of inclusions, but sometimes contain fine grains of titanite, opaque minerals and apatite. Hornblende is pleochroic from bright deep green (Z) to olive green (Y) to yellow green (X). Grains are medium in size, xenoblastic, and commonly poikilioblastic. They contain inclusions of quartz, titanite, feldspar, biotite, apatite and zircon. The FD 5 granite has characteristically

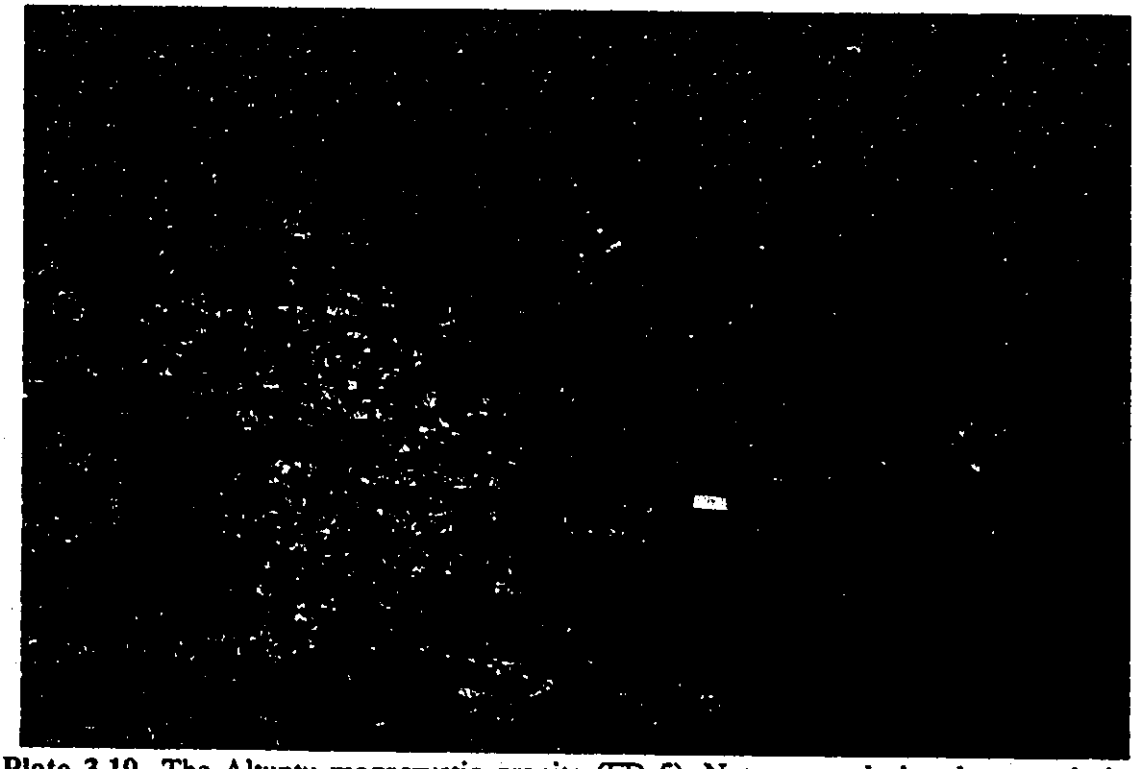

Plate 3.19 The Altuntu megacrystic granite (FD 5). Note general abundance and also orientation of feldspar megacrysts. Here rock is moderately deformed (compare with plate 3.19 above). Altuntu peak.

Plate 3.20 Textural variation in a single outcrop of the Altuntu granite (FD 5). This variations appear to be related to a gradient in magnitude of strain across the fabric. Chemie area, north of the Baya Gundi - Agere mariam road. Pencil points north.

high contents of titanite (approximately up to 4%) in some specimens. Titanite grains are in some cases euhedral but they may occur as massive grains clustered into polygranular aggregates of up to 3 mm across. Individual grains may reach up to 1 mm; they are commonly associated with biotite. Approximate proportions of minerals in representative thin sections studied from unit FD 5 are shown in Table 3.6 (Appendix I).

Both the eastern and the western boundaries of the granite are covered by soil and patches of volcanic rocks. The eastern boundary is relatively sharp (a few tens of metres wide) in the south; where it bounds unit AD 2 of the Afelata domain. However, a direct contact of these two units is not observable. In the north, the granite is bound by the meta - tonalitic unit (AD 1) of the Afelata domain. In this northern area the contact is characterized by a zone of pegmetites, and mafic dykes. At some places mafic dykes are accompanied by abundant quartz veins related to numerous minor dextral shear zones. Angular blocks of gneissose tonalite (unit AD 1) are also present in the mega-crystic granite of this area suggesting the tonalite was engulfed by the granite. The elongate (sheety) shape of the FD 5 granite pluton suggests that it was emplaced along a structural discontinuity (see also Chapters 4 and 7).

3:2:6 Small foliated granitoid bodies (FD 6)

FD 6 includes several plutonic bodies of generally small size that are intrusive into gneissic units within the Fincha domain. The first group of these bodies (FD 6a) are granite plutons which are sheet like and concordant to the regional foliation and the second (FD 6b) are qurtzdioritic bodies with oval or pear shaped map outlines (Fig. 1).

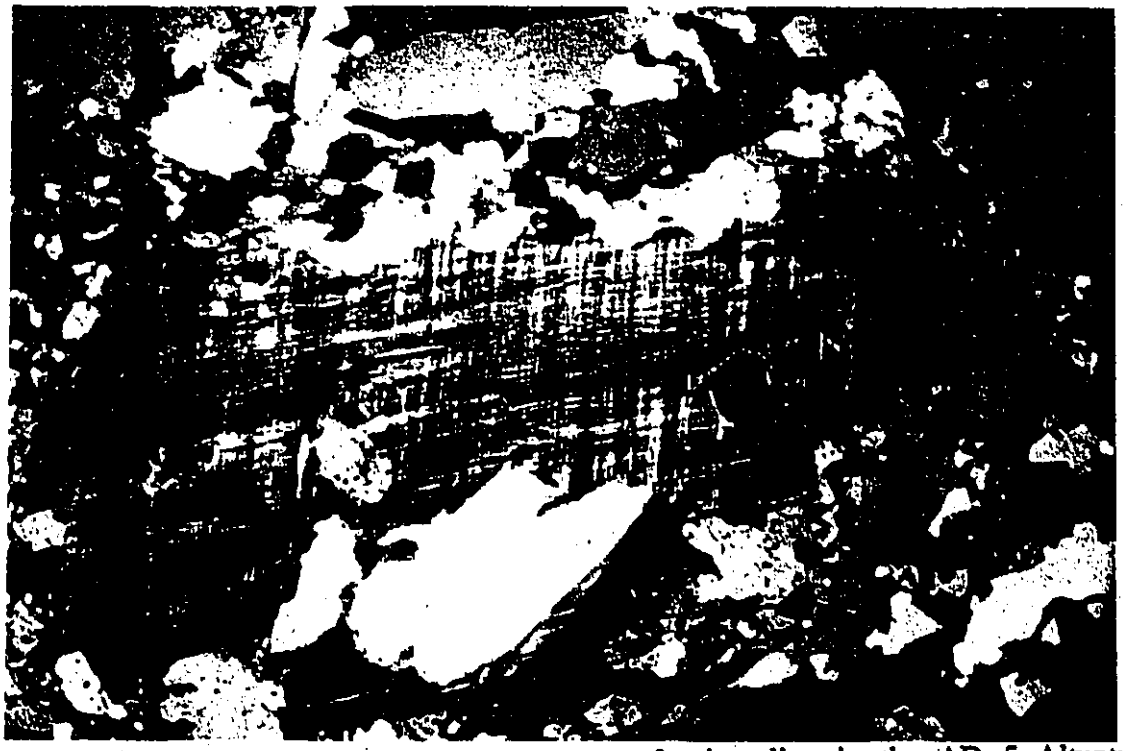

Plate 3.21 Photomicrograph of a megacryst of microcline in the AD 5 Altuntu megacrystic granite. Margins of the megacryst are marked by recrystallized finer grains of microcline. Crossed Nicols, field of view 9 mm.

Plate 3.22 Photomicrograph of a thin section of a specimen from the Kinsho granite (FD 7). Note unfoliated granitic texture, interstitial quartz (white), subhedral cross section of aegirine (centre) and anhedral interstitial (longitudinal sections) to the left and also lower centre. Crossed Nicols, field of view 4.5 mm.

They are all foliated and the foliation in the host rock follows their margins (Fig. 4.1).

In general FD 6a granites are composed of K - feldspar (microcline), plagioclase (oligoclase), biotite, quartz and minor opaque mineral grains and accessory minerals like zircon and apatite. They are commonly fine to medium grained and non porphyritic. An exception to this is, one of the FD 6a granitic bodies, outcropping in small outcrops in the Jigessa area which is relatively coarser grained and also porphyritic. This body also contains, unlike the other granites, significant amounts of hornblende besides biotite.

Although only its northern end outcrops in this area, one of the bigger of the FD 6a granitic intrusives, is the Dek-Bor granite, at the south central margin of the map area. This body trends N - S and was probably emplaced as a sheet concordant to the regional foliation and lithologic boundary perhaps during the later stages of the D_1 deformation (chapter 4). The granite is pink, medium grained, equigranular, foliated and at places lineated.

The FD 6b quartzdioritic bodies are similar in lithologic characteristics. They are predominantly made of grey weathering, mesocratic, fine to medium grained quartz diorites. The bodies are in some cases cross-cut by more leucocratic dykes, perhaps later phases of the same intrusions and contain fine grained hornblende rich inclusions. Apart from the weak alignment of biotite grains, recrystallization features are limited to the fine grained matrix, and the bulk of these rocks have retained their plutonic textures.

3:2:7 Foliated aegirine - bearing leucogranite (FD 7)

FD 7 is a light coloured fine to medium grained granite, with weak foliation that forms

N - S trending ridges (Kinsho and Welmel) in the east central part of the Sagan - Afelata area (Fig 1). The granite chain continues to the south and includes the Daddim ridge, about 10 km south of this area (Kiros and Kinetibeb, 1987) which appears to have the same petrochemical (peralkaline) characteristics (Chapter 6). The chain continues farther southeast of the Yabello village a village 70 km south of this area and from which the name Yabello granite (Kazmin, 1970, 1973) was given to this rock unit.

Outcrop is generally scarce and exposures of this peralkaline granite are limited to the ridges mentioned above. The granite contains uniformly high proportions of alkali feldspar (up to 75%), some plagioclase (maximum 15%), quartz and up to 15% of the alkali pyroxene aegirine. Opaque minerals form up to 5% and biotite is a very minor component or absent. Estimates of the approximate mineral proportions in thin sections of representative specimens from this unit are given in Table 3.7 (Appendix I).

The alkali feldspar is microcline and occurs commonly as anhedral to subhedral grains that contain rounded inclusions of fine grains of quartz. Plagioclase grains are finer and commonly inclusion free, but occur as inclusions in bigger grains of alkali feldspar. Perthitic intergrowths are absent unlike some comparable peralkaline granites in the Pan African of northeast Africa (e.g. Abdel-Rahman, 1986). Quartz is generally an interstitial mineral in this rock. It contains inclusions of both aegirine and alkali feldspar grains. The aegirine of this granite is pleochroic from bright green (X) to yellow green (Z). The grains are generally fine and subhedral. However, elongate anhedral grains interstitial between quartz and feldspar grains are also common (Plate 3.22). Aegirine grains are generally free of inclusions but in rare cases they contain inclusions of quartz, suggesting

that the pyroxene did not necessarily form early in the crystallization sequence. Trace amounts of titanite are present in some specimen. It commonly forms massive aggregates rimming opaque mineral grains. A weak foliation is observable in outcrops of this rock, but in thin sections it is rarely apparent (Plate 3.22). However, a general alignment of aegirine and elongate quartz and feldspar grains can be seen in some specimens. Metamorphic recrystallization is not evident and the rock has a well preserved granitic (plutonic) texture marked by interlocking grains (Plate 3.22). It is on the basis of these textural features i.e weak or no metamorphic textures, and the late stage of peralkaline magmatism in the tectono - magmatic evolution of similar Pan African terranes, e.g. northeast Egypt (Abdel Rahman and Martin, 1990) and the Arabian shield (Jackson, 1986) that this body is considered as younger than the calc-alkaline intrusives (AD 1 and FD 5) in this area (see also Chapters 6 and 7).

3:2:8 Meta - pyroxene - hornblende plutonic complex (FD 8).

The term complex is applied to this large body of a pyroxene - bearing hornblende rich in the central part of the Sagan - Afelata area, because it appears to consist of compositionally different (see Chapter 6 for a discussion of the geochemistry) and texturally varied but spatially and to a lesser extent temporally associated and perhaps genetically related rock types. The outer rim of this complex (building most of the Bergudda ridge from which the name Bergudda complex is given to this body except, the Cheleleka hill, the Meti Gola ridge and a small knob in the Hida Korma area) is a pink, pyroxene - bearing hornblende granite. In contrast, the dark greenish inner core, which

mainly forms the Bergudda Cheleleka hill and a knob to the north contains hornblende, orthopyroxene, calcium pyroxene, plagioclase, K feldspar and quartz. The core rock, has greasy dark-green appearance and looks massive in handspecimen and foliation is only faintly observable in some outcrops. However, in thin section the rock shows strong recrystallization features like triple junctions (Plate 3.23) and also weak preferred mineral grain alignment (Plate 3.24).

The alkali feldspar in the core rock is perthitic, intergrowths containing about equal amounts of both plagioclase and K feldspar and varying in morphologic types; string perthites being the predominant (Plate 3.25). Plagioclase also occurs in subhedral polysynthetically twinned crystals. Both feldspars may contain fine inclusions of pyroxenes. Orthopyroxene which is rare is yellowish (Plate 3.26) and faintly pleochroic. Calcium pyroxene is faintly pleochroic, pale green diopside. Hornblende is the major mafic constituent of this rock; it forms coarse crystals and also replacement rims around pyroxene grains (Plate 3.27). Biotite is a sporadic minor component; it typically occurs in sheaves, forming aggregates of radiating fine grained crystals but also as needles (Plate 3.26).

Mineralogically, the core rock can be classified as a hypersthene quartzmonzonite of the IUGS classification (Streckeisen, 1976) or mangerite (Park, 1989) of the charnockite suite. This classification is also supported by its general dark greasy appearance, perthitic texture of the K feldspar, hornblende coronas around orthopyroxene and sagentic exsolution (?) texture of biotite, which is thought to indicate high titanium contents; all of which are features considered as diagnostic of the rocks of the charnockite suite (Park,

1989).

The pink pyroxene - bearing hornblende granite outer rim, is composed of hornblende, biotite, perthitic K feldspar, plagioclase and quartz. It also displays a variety of perthitic intergrowth of feldspars. The planar fabric (foliation), in this outer rim, is fairly strong and penetrative at outcrop (Plate 3.27) and handspecimen scales, in the outer parts of this rim of the complex; whereas foliation is only weakly developed in the inner regions (Plates 3.28). In thin sections, even with in the strongly deformed pink outer rim both grain alignment and strong recrystallization features are limited to the matrix (Plates 3.29).

The approximate mineral proportions of selected specimen from the FD 8 plutonic complex are given in Table 3.8. Veins from the pink granite forming the outer rim of the Bergudda complex are intrusive to the granitic gneiss (FD 1) and cut across the gneissosity in this latter unit (Plate 3.30). The origin and tectonic significance of this rock is considered in Chapter 6, where its petrochemistry and probable tectonic setting are discussed.

3:2:9 Massive granite (FD 9)

A small body of apparently undeformed granite intrudes the nose of a south plunging (F_2) antiform (Fig. 4.1) close to Fincha village, in the central part of the area. From air photo interpretations it appears to be slightly elliptical in plan and the long axis is oriented N - S parallel to the regional structural grain in the country rock.

The granite is biotite - bearing, fine grained, massive and pinkish grey. The K feldspar

Plate 3.23 Solid state growth texture in the matrix of a specimen from the dark core of the Bergudda complex (FD 8). Plane polarized light, field of view 2.3 mm. Bergudda Cheleleka hill.

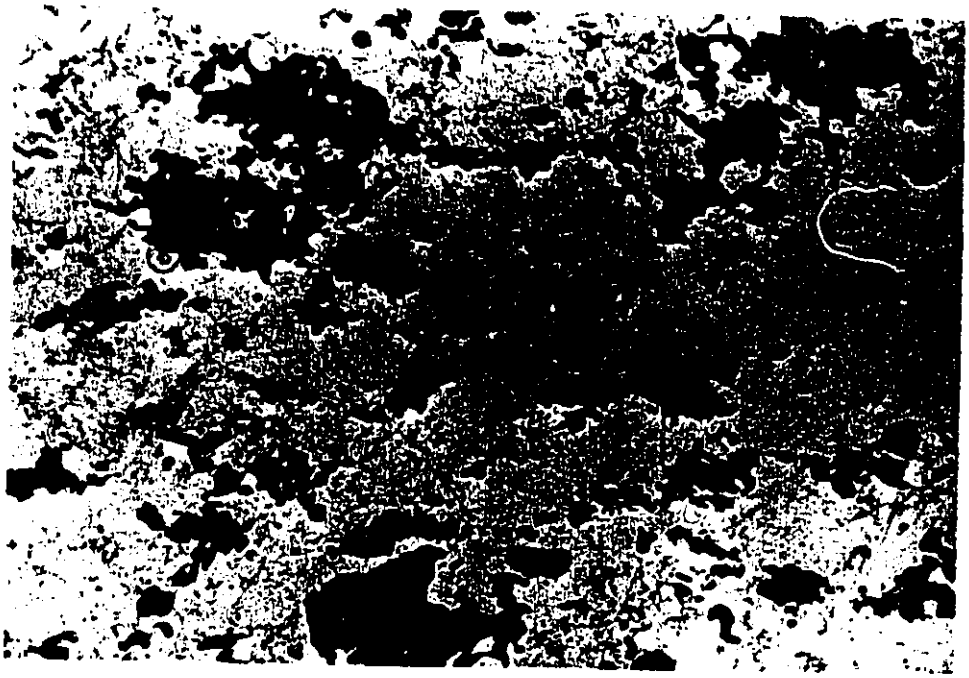

Plate 3.24 Preferred alignment of mineral grains, in a thin section of a specimen of the dark core of the Bergudda complex (FD 8). Pyroxenes stubby, high relief; hornblende coarser skeletal anhedral grains. Alignment is roughly parallel to length of photo. Plane polarized light, field of view 4.5 mm.

Plate 3.25 Example of perthitic intergrowth of feldspars in the dark core of the Bergudda complex (FD 8): combined strings and blebs of albite (white) in K feldspar (dark). Note also sheave texture of biotite characteristic of the rocks of this complex. Crossed polars, field of view 2.3 mm.

Plate 3.26 An orthopyroxene grain (centre) in a thin section of a specimen of the dark core of the Bergudda complex (FD 8). Dark grains are of opaque minerals and large greenish grains are of hornblende, and needles are of biotite (also characteristic of the biotite of this complex). Plane polarized light, field of view 2.3 mm.

is polysynthetically twinned microcline. Its grains are anhedral and in rare cases contain inclusions of fine grains of quartz and plagioclase. Plagioclase grains are fine, subhedral, polysynthetically twinned, and mostly sericetized. Biotite grains are fine and have partly been replaced by green chlorite. Quartz occurs as both fine and medium grained anhedral grains. The fine grains are subrounded, inclusion free and are the most common constituents of the interstices. Some of these show signs of re-equilibration, straight edges and triple junctions.

Although no mineral foliation is apparent, the recrystallization of fine quartz grains, partial chloritization of biotite and sericitization point out, that this small body may be late metamorphic.

3:3 Afelata Domain (AD)

Only three map units are distinguished in this domain. All the three units are magmatic. However, the domain also contains several thin intercalations of metasedimentary units (within map unit AD 2) which are treated below only briefly. The megacrystic granite (FD 5) of the Fincha domain is as shown in Chapter 6, genetically related to the magmatic units of the Afelata domain from which it is separated by a structural discordance.

3:3:1 Meta - tonalite (AD 1)

A gneissose tonalite (AD 1) is exposed in the northeastern corner of the Sagan - Afelata area. The unit is a relatively small part (about 65 km^2) of a body in a front of other

Plate 3.27 Strongly developed foliation in the pink granite forming the outer rim of the Bergudda complex. Hida Korma area, northern Bergudda.

Plate 3.28 Weakly foliated outcrop of the pink pyroxene-hornblende granite, in the inner regions of the pink granite of the Bergudda complex (FD 8). Xenolith is of FD 1 granite gneiss. Hammer head points N, Wodedera area, Soyema - Yabello road.

similar bodies underlying the area stretching N - S along the western margin of the Megaddo region [Chater, 1971, see also the geologic map by Kozyrev et al. (1985) and chapter 4]. In the Sagan-Afelata area the unit is best exposed along the Sebbeto valley from which the name Sebbeto tonalite is given to it.

The rock is a fairly homogeneous, dark greyish, medium grained, commonly gneissose hornblende bearing biotite tonalite. Minor inhomogeneities that are seen in this body are mostly textural, like the intensity of development of foliation. However, there is also a slight variation in the ratio of hornblende to biotite from place to place, and also in the relative abundance of quartz. Plagioclase, quartz, biotite, hornblende and titanite are the important constituents of this rock. K feldspar and in some cases epidote are present but always in minor quantities. Table 3.9 in Appendix I gives the approximate proportions of minerals from representative samples of this rock. Plagioclase in the oligoclase range is the predominant mineral (up to 70% by volume). The grains are generally anhedral, fine to medium in size, and commonly inclusion free. In some specimens some of the relatively larger grains of plagioclase are porphyrocrysts (Plate 3.31). These appear to be grains preserved as relict from an original igneous mineralogy, surviving gneissification and complete recrystallization. Finer grains of plagioclase form the recrystallized matrix (Plate 3.31) with equally fine quartz grains. Quartz grains are generally anhedral, mostly equant but some are elongated and show coarse polygonization. Quartz is generally free of major mineral inclusions. Biotite is the most important mafic mineral. It occurs in well formed laths that define the strong mineral foliation (Plates 3.31). Hornblende is pleochroic from bright green (Z) to olive green (Y) to yellow green (X). The grains are

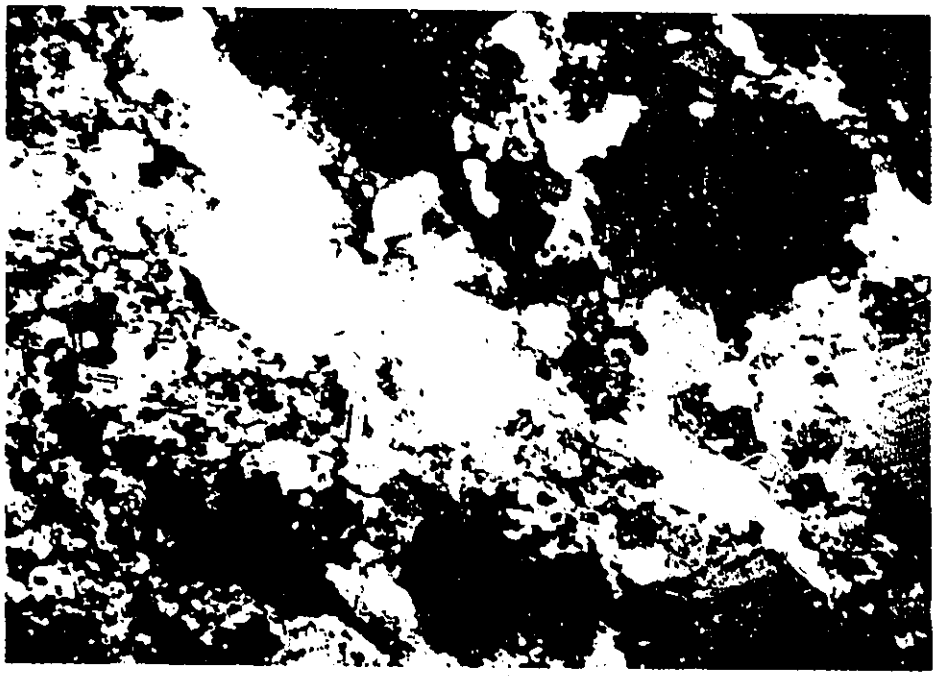

Plate 3.29 General texture of strongly deformed pink rim of the Bergudda complex. Note large grains of feldspars (dark) are relatively intact. Quartz has recrystallized into strings and the matrix is thoroughly comminuted and recrystallized into fine grains of quartz and feldspar. Crossed polars, field of view 9 mm. Hida Korma area, northern Bergudda.

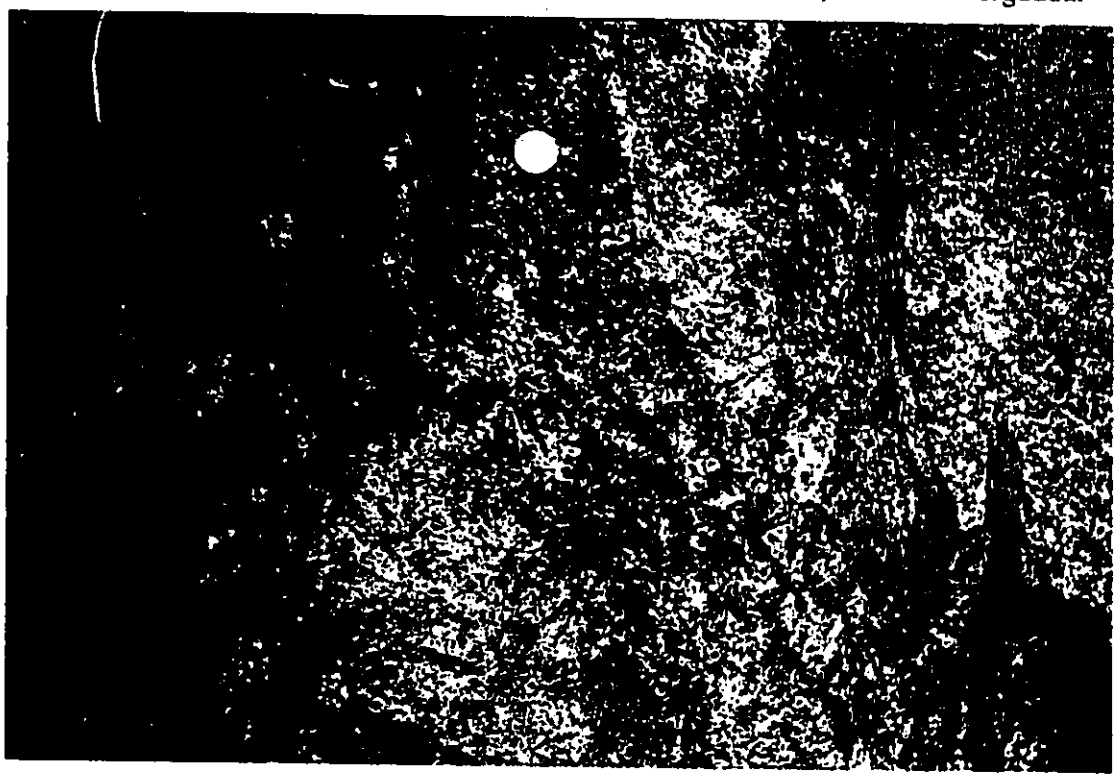

Plate 3.30 A vein of the pink pyroxene - hornblende granite rim of the FD 8 Bergudda complex (dark and coarse) intruding an outcrop of the FD 1 granite gneiss. Earlier fabric (S_1) in FD 1 (not clear in picture) is parallel to the crosscut vein (lighter and inclined) and has been crosscut by the vein and a later fabric that developed parallel to the crosscutting vein (vertical). Biyo area about 3 km south of the Biyo river.

commonly anhedral and relatively coarser grains form clots mostly with biotite. At places such clots form knots along the mineral foliation and intensify the planar fabric in outcrops. In some specimens both biotite and hornblende have skeletal grains. In such specimen the coarser grained quartz and feldspar grains are lacking; instead the rock is fine grained with thoroughly recrystallized mozaics of quartz and feldspar grains. In outcrop these appear more gneissose; they lack relicts of the original plutonic texture and mineralogy.

Titanite is minor but a characteristic mineral in this rock as in the megacrystic granite (FD 5) to the west. Fine massive (anhedral) grains, are common; more rarely the grains are medium sized and subhedral or euhedral. Occasionally, titanite grains form large clusters (up to 2.5 mm across) with subordinate finer grains of apatite. Subhedral epidote is occasionally a minor component.

The metatonalite is strongly deformed and in most outcrops gneissose. Veins of leucotonalitic compositions and of quartz are generally abundant and parallel the foliation in this rock (Plate 3.32) at most places. At some places earlier sets of discordant veins are also present. The meta-tonalite is also cross-cut by relatively late finer grained, leucocratic, tonalitic dykes. Due to the strong gneissosity and this veining, which at places resembles migmatitic layering (Plate 3.32) the meta-tonalite was considered, as a part of a high grade biotite gneiss in the "lower group" (Chater, 1971) of the Precambrian of Southern Ethiopia (Chater and Gilboy, 1968). This gneissic appearance and the domal structure in the region in which the tonalite outcrops (Chapter 4) led earlier workers to consider the unit as basement (presumed Archean), to the more heterogenous clastic units

constituting the "middle complex" of the Ethiopian Precambrian (Kazmin, 1970, 1973; Kazmin, et al. 1978; Warden and Horkel, 1984; Gichile et al., 1986).

However, as pointed out previously (Gichile, 1990a, 1990b, 1991b), the gneissose tonalite is an Upper Proterozoic calc-alkaline intrusive. Its genesis and that of similar rocks belonging to the same chain, is shown in Chapters 4, 6 and 7, to be related to that of the low-grade metavolcanic - metasedimentary rocks of the Adola arc.

3:3:2 Amphibolite (AD 2)

Amphibolites and associated rocks (AD 2) outcrop in the southeastern corner of the Sagan - Afelata area. Most rocks in this map unit have clear magmatic precursors, including schists derived from ultramafic rocks (AD 2b) and amphibolites (AD 2a) derived from basic volcanic rocks and subvolcanic intrusives. Although amphibolites are predominant (approx. > 95%), the unit also contains various metasedimentary (pelitic, semipelitic, and calcsilicate) rocks.

Fine - grained well - foliated amphibolite (Plate 3.33) and medium - grained more massive types (Plate 3.34) have similar metamorphic mineralogy. Hornblende and plagioclase make the bulk of these rocks. Epidote is more common in the medium grained than in the fine grained; in which plagioclase, titanite and quartz are relatively more important. Hornblende grains are generally subhedral in both (Plates 3.33 to 3.34) but tend towards euhedralism in the coarser massive amphibolite (Plate 3.34). Some porphyroblastic hornblende grains which are coarser than the average tend to grow across the mineral foliation in the fine amphibolites. These appear to be late-kinematic with

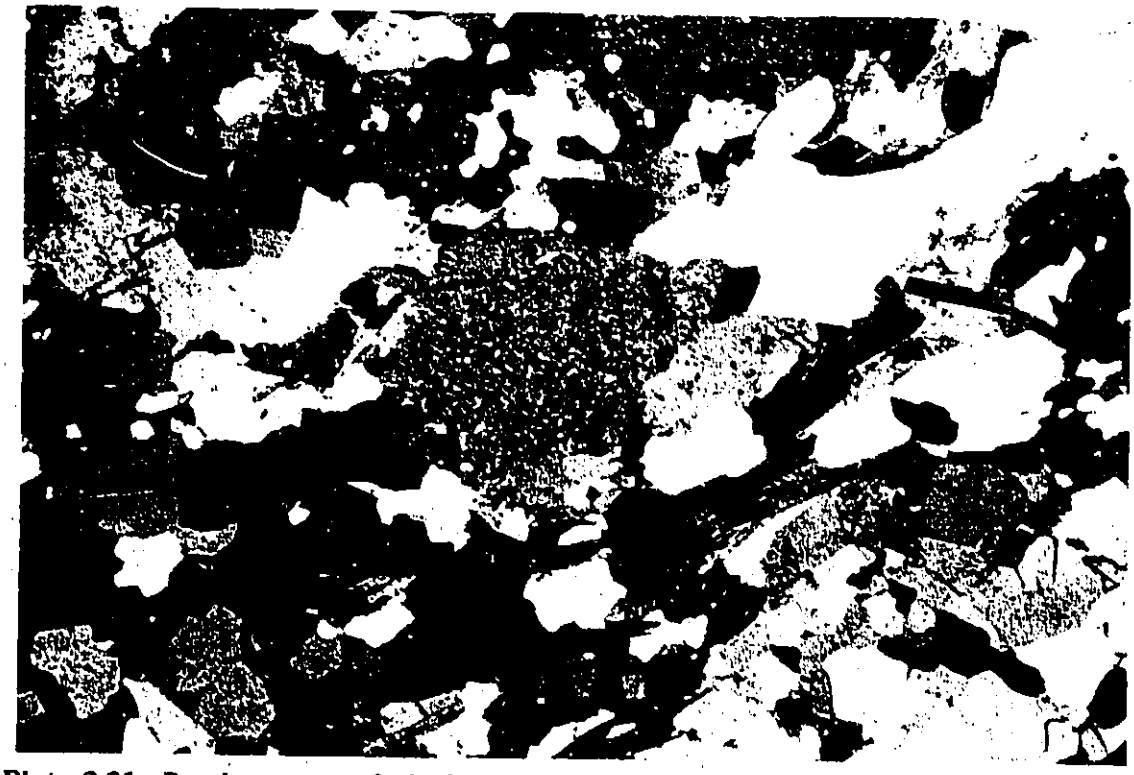

Plate 3.31 Porphyrocryst of plagioclase in a thin section of a sample of the Sebbeto meta-tonalite (AD 1). This and similar grains are relicts from igneous mineralogy. Note also strong alignment of biotite and elongated grains of quartz and feldspar. Crossed Nikols, field of view 4.5 mm.

Plate 3.32 Quartzofeldspathic veins parallel to foliation/gneissosity in the Sebbeto meta-tonalite (AD 1). Sebbeto valley east of the Fincha - Baya road.

respect to the strong foliation defined by the finer hornblende grains in this rock.

In the fine grained amphibolites plagioclase (approx. An = 36%) grains are fine anhedral and interstitial. However, these grains bound each other along straight, metamorphic, grain boundaries. Plagioclase grains are sometimes sericetized and also contain inclusions of fine hornblende and quartz grains.

In contrast, in some of the relatively massive medium grained amphibolites plagioclase grains are coarser and appear to be predominantly igneous. In some of these rarely present metamorphic grain boundaries appear to be at the initial stages of development, as they show features transitional between igneous (plutonic) and metamorphic textures. In these types recrystallization of plagioclase grains is seen accompanied by simultaneous crystallization of epidote released from the more calcic plagioclase.

Calcium - pyroxene, generally minor or absent in the fine grained amphibolites, is diopsidic in both the fine and medium grained amphibolites. Calcium - pyroxene grains in the medium grained amphibolites are very faintly pleochroic or do not show pleochroism. The grains are anhedral, and at different stages of replacement by hornblende grains. The clinopyroxene is thus igneous as is most of the plagioclase. In some cases pyroxene grains probably had an ophitic texture.

Injection type (lit par lit) migmatitic veining in AD 2a amphibolites is particularly strongly developed in the Reko valley (Fig. 1) in the south eastern margin of the unit (Plate 3.35). The migmatites are in the fine grained rather than in the massive medium grained amphibolites. This observation and the metamorphic mineral assemblage and textures described above for the massive amphibolite, appear to indicate lower

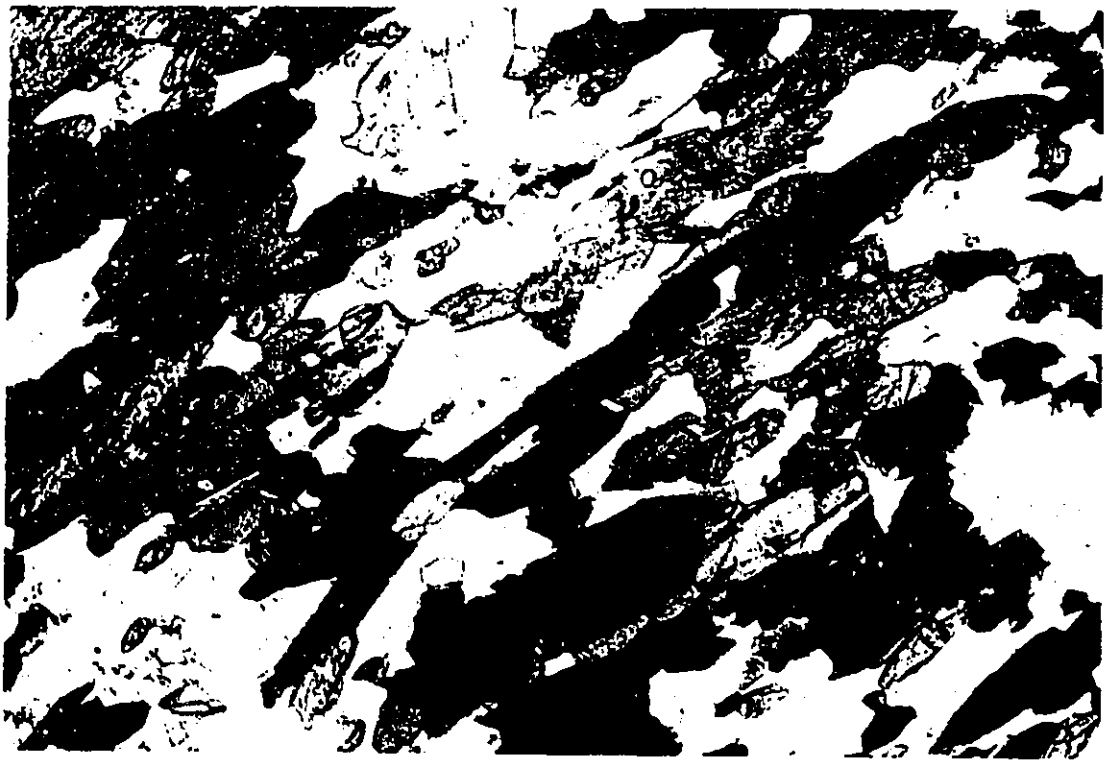

Plate 3.33 General texture of the fine-grained amphibolite of AD 2 at the scale of a thin section. Hornblende (dark, prismatic grains), Plagioclase and quartz (light), titanite (fine, massive, high relief). Plane polarized light, field of view 2.3 mm.

Plate 3.34 General texture of the medium-grained amphibolite of AD 2 at the scale of a thin section. Hornblende (grey grains with cleavage), plagioclase and quartz (light), titanite (fine, massive, high relief). Section normal to a mineral lineation defined by hornblende grains, plane polarized light, field of view 2.3 mm.

temperature conditions than implied by Chater (1971), for similar migmatitic amphibolites in the adjacent Megaddo region to the east.

Calc-silicate rocks (AD 2d), and semipelitic gneiss (AD 2e) are minor components of map unit AD 2. The calc-silicate rock is commonly well layered and locally contains abundant (up to 12%) apatite (Plate 3.36) and an unusually high proportion of epidote (approx. 25%). Elsewhere, diopside is the predominant calc-silicate mineral and quartz is present.

Minor thin units of muscovite - quartz schist are present within the AD 2 amphibolites. Well formed muscovite grains and elongate recrystallized grains of quartz are the main components of this rock but at one locality the rock contains kyanite and sillimanite (Plate 3.37). Table 3.10 in Appendix I is an estimate of the relative mineral proportions in the different rock types, in the Hiddi Asasu amphibolite (unit AD 2).

The AD 2 amphibolites appear to be intruded by the AD 1 tonalite to the northeast however this relation is not clear. Unit AD 2 appears to be in tectonic contact with the Altuntu granite (FD 5) to the west, along a regionally significant structural discontinuity (see chapters 4, 6, and 7).

3:3:3 Meta - pyroxenite (AD 3)

Meta-pyroxenite, associated with minor metagabroic rocks, forms three small hills near the contact of the AD 1 tonalite with the AD 2 amphibolites. The map outline of the body (Fig. 1) is delineated from air photos and the hills form smaller areas than shown.

The meta-pyroxenite is dark green and mainly composed of lustrous, coarse, stubby

prismatic decussate crystals of tremolite (approx. 65%), with talc (approx. 15%); chlorite, opaque minerals and serpentine are subordinate. The coarse tremolite crystals appear to be pseudomorphed mosaics of clino-pyroxene crystals that formerly made up the bulk of the rock. Aggregates of talc and serpentine grains evidently pseudomorph olivine crystals originally enclosed by the coarse clinopyroxene grains. Fine opaque mineral grains are abundant along the cleavage planes of tremolite grains (Plate 3.38). The composition of the opaque mineral(s) has not been determined. Pyrite or pyrothite are not visible in handspecimen, and the opaque grains are likely magnetite segregations, released as a product of the serpentinization of olivine (Moody, 1976). These grains are lacking or minor along the rims of replaced olivine grains (Plate 3.38).

The meta-pyroxenite appears to have had originally a cumulate igneous texture (Wager et al., 1960; Irvine, 1982) in which olivine was the cumulate and clinopyroxene the intercumulate phase.

The relationship between the meta-pyroxenite and the tonalitic unit AD 1, is not observable because of intervening thick lateritic soil. The virtually intact plutonic texture and the low grade, apparently static thermal metamorphism suggested by the pseudomorphs, could indicate that the pyroxenite was emplaced at the waning stages of metamorphism and deformation as suggested earlier (Gichile et al., 1986). However, it is also possible that the meta-pyroxenite represents a cumulate ultramafic phase in the sub-arc magma chamber, that was transported upwards by the tonalitic pluton during its emplacement.

Plate 3.35 Migmatitic veining in an outcrop of AD 2a amphibolite. Reko valley; fold is an F_2 minor fold.

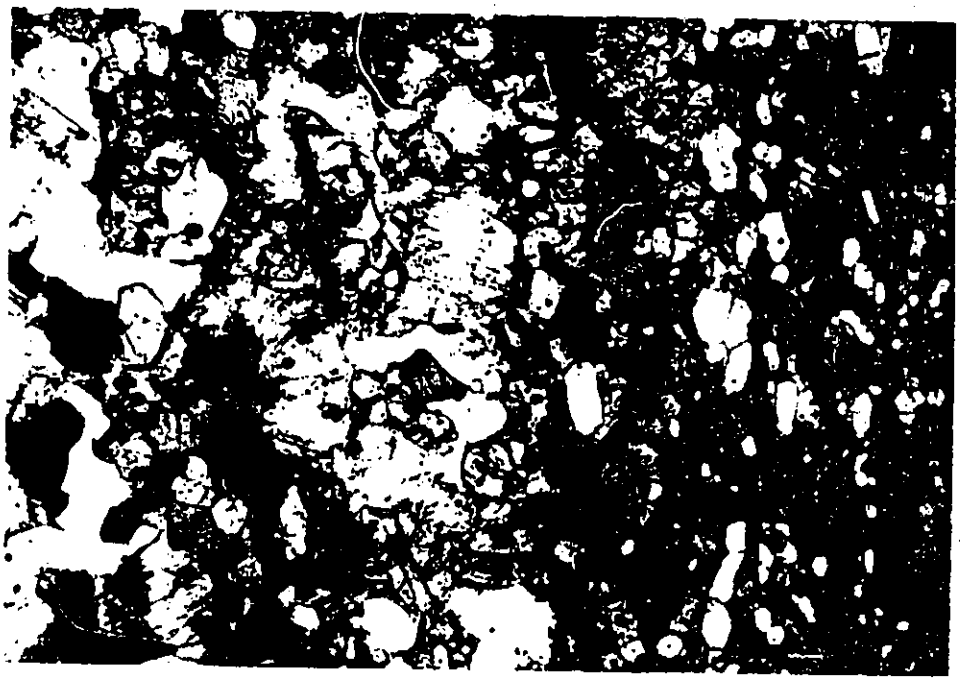

Plate 3.36 Layering in calc-silicate gneiss (AD 2d) of unit AD 2. This sample has unusually high contents of apatite (fine, subhedral, hexagonal, white grains in the darker band). Grey grains are of epidote, minor diopside and hornblende. Light large grains are of plagioclase and quartz. Plane polarized light, field of view 4.5 mm.

CHAPTER FOUR

STRUCTURES

Introduction

This chapter describes structures and fabrics developed during ductile deformation of the metamorphic rocks in the Sagan - Afelata area. Large brittle fractures and faults that form prominent photolineaments, most of which are related to the development of the East African rift system (Tertiary and younger), are not included in the descriptions. The chapter describes structures and fabrics of three generations (4:1), analyzes orientation data for structural domains and subdomains (4:2), summarizes the structural data (4:3) correlates the structural development in the Sagan-Afelata area to that of neighbouring regions (4:4) and considers Precambrian lineaments (4.5).

Sparsity of outcrops and the reconnaissance nature of the work do not allow a detailed structural analysis. However, in several places, a foliation (S_1) and at places, a parallel primary layering (S_o), are affected by two generations of later structures, thus indicating three phases of deformation designated D_1, D_2, and D_3. The structural elements developed during each of these phases are referred to as (S) planar fabric, (L) linear fabric and (F) fold, with the corresponding suffixes S_1, L_1, and F_1 for D_1 structural elements etc. A fourth phase (D_1') preceeding all other phases including D_1, is inferred from observations in one locality and is discussed only briefly. Its significance is however considered in

Plate 3.37 Photomicrograph of a sillimanite - kyanite - quartz schist of unit AD 2. Kyanite (large prisms), sillimanite (fibrous), quartz, feldspar and muscovite. Plane polarized light, field of view 4.6 mm.

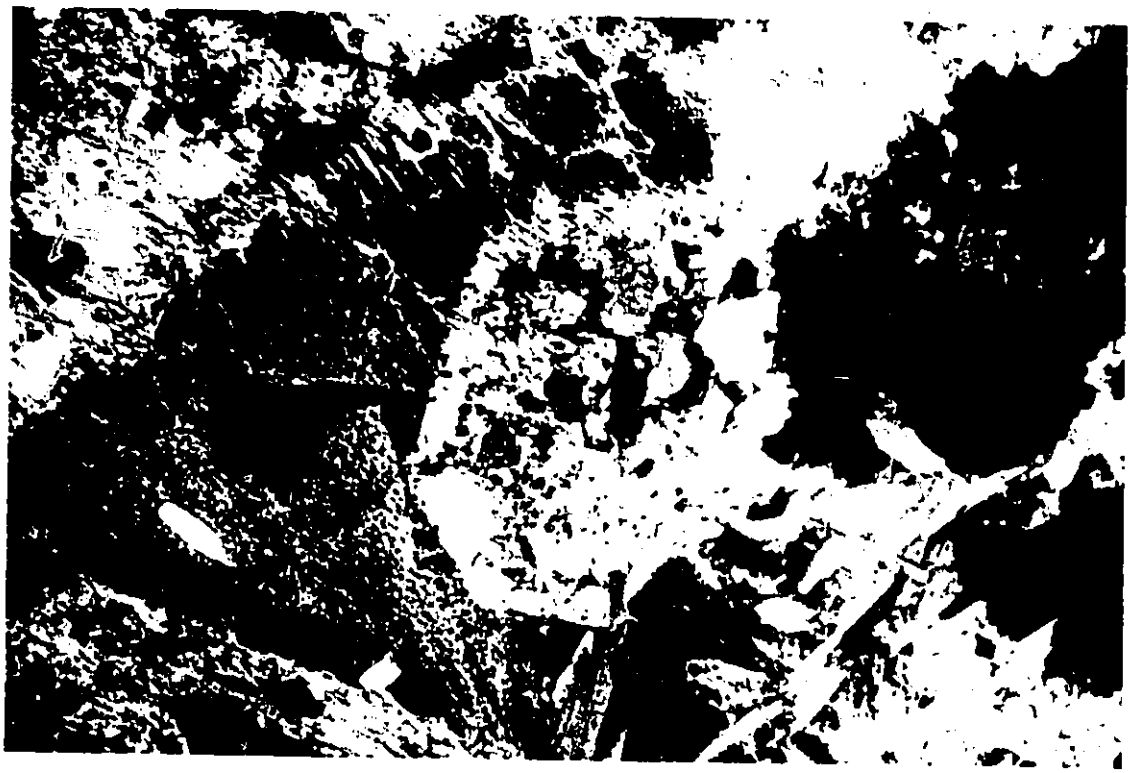

Plate 3.38 Cumulate texture of the Korolle pyroxenite (unit AD 3). Serpentine (dark grey), talc (pink and green), chlorite (light grey, platy), tremolite (dark). Black spots are of opaque minerals. Note that tremolite is free of opaque mineral grains adjacent to the olivine grain. Crossed Nicols, field of view 2.3 mm. Kuppi Korolle.

regional correlations (4:4).

4:1 Structural generations

4:1:1 D_1' structures

The D_1' deformation is an event that is inferrable in a few gneissic units from the tectonic/metamorphic nature of a planar surface S_1' that has been affected by F_1 folding.

S_1' in FD 2 layered biotite gneiss is defined by migmatitic layers parallel to compositional layering (S_o), that have completely been transposed parallel to S_1 foliation during the F_1 folding. This layering S_1' is a very distinct tectonic surface that is folded by F_1 rootless intrafolial folds in FD 2 (Plate 4.1 to 4.4). It is, however, not clear if the parallelism of S_1' to the compositional layers S_o is due to pre F_1 isoclinal folding F_1' that is related to a different period of deformation.

Similarly in FD 4a quartzofeldspathic gneiss, in the Burkitu Megadda area, pegmatitic veins parallel to a compositional layering S_o have been isoclinally folded by F_1 mesoscopic folds (Fig. 1). It is inferred that these veins were related to pre F_1 migmatization/deformation, although there could have been progressive deformation with veining at an early stage of the D_1 event.

4:1:2 D_1 structures

The D_1 deformation imparted a penetrative foliation (S_1) to most of the metamorphic rocks in the Sagan-Afelata area. Major D_1 structures, if present, were not seen.

Plate 4.1 Rootless F_1 intrafolial fold in an earlier migmatitic layering (S_1'). Note that the present gneissic layering (S_1) is axial planar to the fold. Pen points north. Layered biotite gneiss (FD 2), Siego area.

Plate 4.2 Preserved hinge zones of F_1 minor folds in the layered biotite gneiss of unit FD 2. Foliation and layering S_1 is axial planar to these folds. Koromo area, Pen points north.

4:1:2:1 S_1 foliation

The main structural element developed during the D_1 deformation is, foliation S_1, inferred to be originally subhorizontal which is folded by later structures and varies in orientation from subhorizontal to subvertical. S_1 differs in mode and intensity of development from domain to domain and in different rock units within a single domain. In mafic granulites (SD 1) of the Sagan domain, S_1 is defined by the preferred orientation of pyroxene and hornblende crystals and highly elongate lenticular quartz grains (Plate 3.5). This mineral foliation is accompanied by a distinct parallel compositional layering, S_o, of probable primary origin (Plates 3.1 and 3.2) and in some cases quartz-plagioclase veining (Plate 3.3) which gives it a migmatitic appearance. Similar compositional layering (S_o) in mafic granulites 10 to 15 km farther west is ascribed to possible pyroclastic layering (Davidson, 1983).

In the central Fincha domain, S_1 is highly variable in both intensity and physical character. In semipelitic and pelitic gneisses (FD 2), S_1 is defined by the preferred orientation of biotite and less commonly hornblende grains. In most places a strong gneissic layering parallels the mineral foliation (Plate 3.11) often with parallel quartzofeldspathic leucosomes. In contrast, in quartzofeldspathic gneiss (FD 4a), S_1 is defined by persistent magnetite rich and magnetite poor layers (Plate 3.15), and/or layers of different grain size (Plate 3.16), most of which may be transposed sedimentary layering. Locally, in the Megadda area, chlorite in parallel growth with biotite crystals define the foliation (S_1) in an atypical variety of the FD 4a gneiss.

In amphibolites (AD-2) of the eastern Afelata domain, S_1 is defined by the preferred

Plate 4.3 F_1 asymetric Z folds in pre-S_1 leucosome within layered biotite gneiss of FD 2. Burji gneiss, E of Siego village. Pen points N.

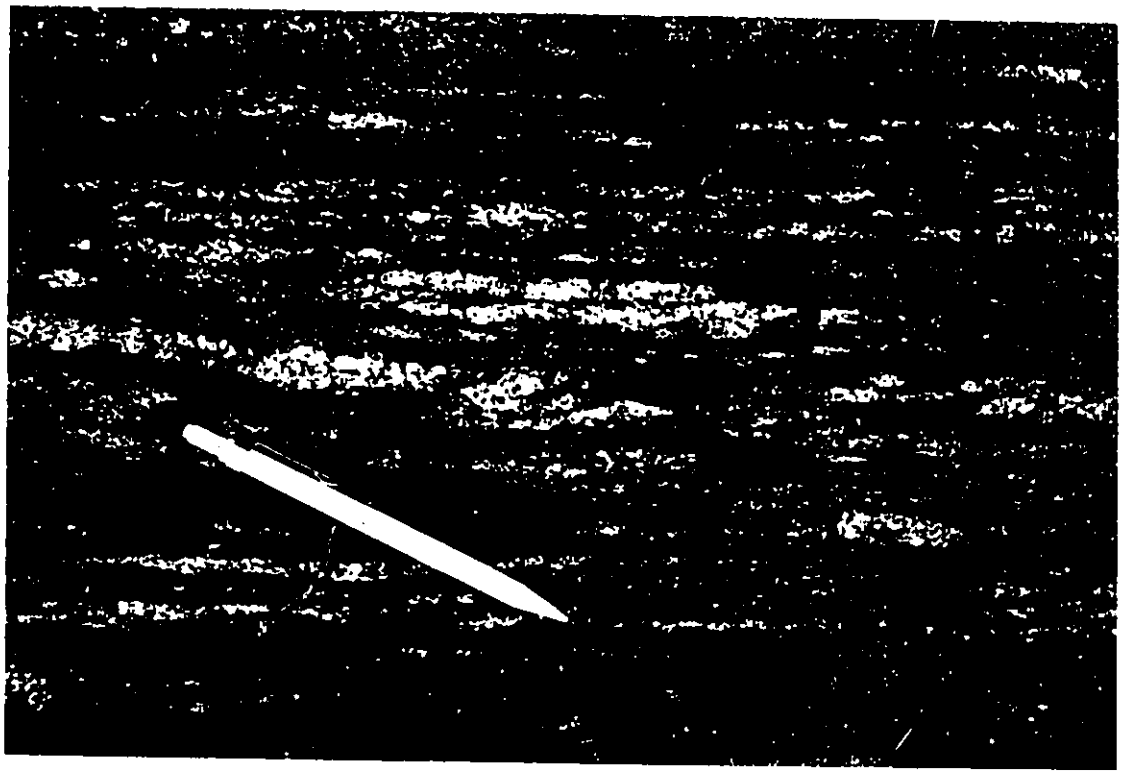

Plate 4.4 A pre-S_1 leucosome (thick) forming the limb of an F_1 minor fold, at an oblique angle to S_1 foliation (parallel to long side of picture). Leucosome is folded. Burji gneiss (FD 2), E of Siego village. Pen points N.

alignment of hornblende grains and at a few places, it is accompanied by injection type lit-par lit (Meinhert, 1968) migmatitic veins (Plate 3.35). These veins are common, particularly in the southern and eastern extremities of the unit (AD 2).

S_1 also varies considerably in expression in the granitoid rocks. Generally, in early to synkinematic granitoids, FD 5 megacrystic granite, FD 6 granite and quartzdiorite, AD-1 gneissose tonalite and possibly FD 1 granitic gneiss, S1 is defined by aligned biotite and occasionally biotite and hornblende grains, and is often accompanied by a gneissic layering. In AD 1 tonalite this foliation is in most places accompanied by persistent gneissic layering, granitic leucosomes and veining (Plate 3.32).

In contrast, foliation is weakly developed or totally lacking in the late - kinematic FD 7 leucogranite and the inner charnokitic core of the FD 8 pyroxene - hornblende plutonic complex. Foliation is barely observable in this complex, in outcrops of the inner part (Plate 3.28) and also in some areas in the exterior regions of the pink outer rim. In contrast, at some places the exterior regions are strongly deformed and show a strongly developed foliation (Plate 3.27). However, anisotropy due to elongation of quartz crystals and a weak preferred alignment of pyroxene, hornblende, and feldspar grains is observable in thin sections of both the dark core (Plate 3.23 and 3.24) and the pink outer rim (Plate 3.29).

The variations in the development of foliation in the other plutonic units appears to be due to the differences in time of pluton emplacement relative to deformation. However, it can also be due to contrasts in mineralogy, essentially the abundance of "ductile minerals" such as quartz and micas compared to "non ductile minerals" essentially

feldspars (Vernon and Flood, 1988).

Microcline megacrysts are common in FD 5, (Plates 3.18 to 3.21). Hetrogenous non - coaxial deformation is indicated in a few cases by the oblique orientation of the larger axes of some of these augened megacrysts to foliation S_1. However, among the few oriented specimen studied none contains reliable kinematic indicators (Simpson and Schmid 1983; Passchier and Simpson, 1986).

4:1:2:2 L_1 lineations

L_1 lineations are few and restricted to localities displaying F_1 minor folds for example in the eastern half of the map area in the Burkitu-Megadda area in unit FD 4a, and also unit SD 1 (Fig. 1). L_1 is subhorizontal and is defined by hinge zones of the folds and associated local mineral lineations.

4:1:2:3 F_1 folds

No major F_1 folds are recognized. F_1 minor folds are present in the Burikitu Megadda area (Fig. 1) of the Fincha domain, localized in the hinge zone of a major F_2 antiform folding FD 4a quartzofeldspathic gneiss and also at several places in the layered biotite gneiss (FD 2). The outlines of F_1 minor folds in FD 4a, are defined by a fine layering produced by alternating quartz - feldspar layers rich and poor in magnetite with or without biotite. Most of the minor folds, are typically small, with wavelengths of <20 cm and amplitudes of <15 cm, and are tight, recumbent intrafolial folds (Plate 4.5). The hinge lines of F_1 minor folds are not fully exposed anywhere, but the appearance of the profiles

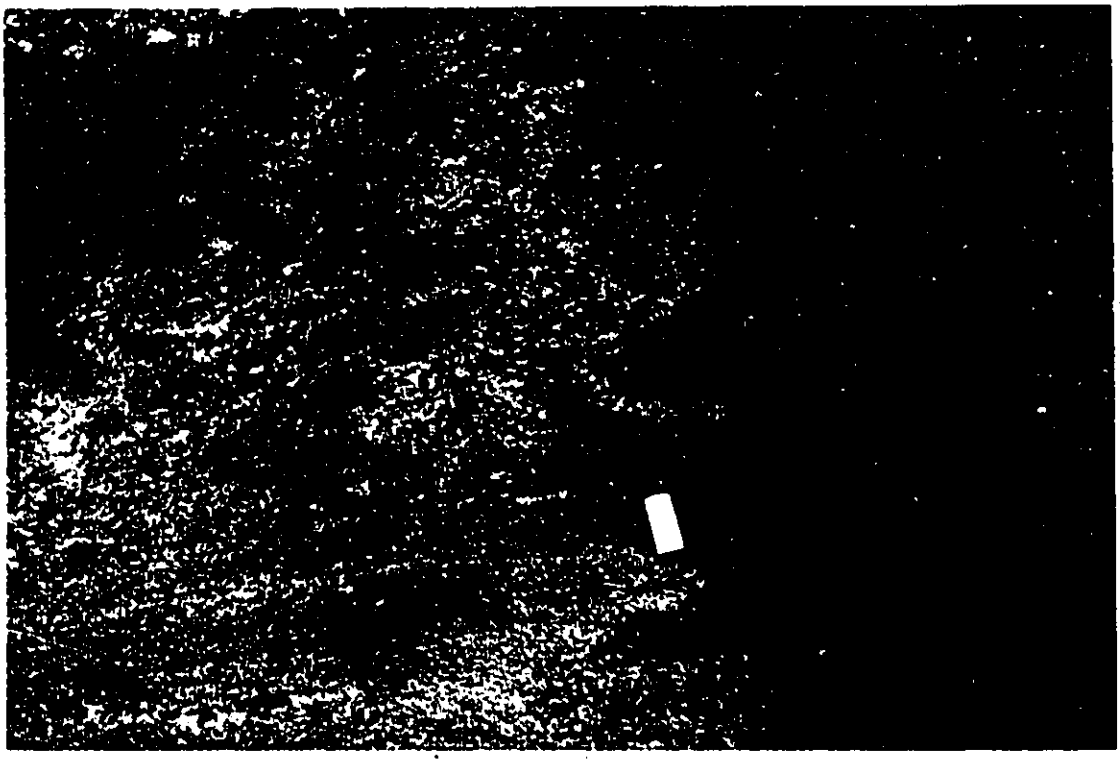

Plate 4.5 F_1 minor fold in quartzofeldspathic gneiss (FD 4a). Dark layer is richer in magnetite. Scale 1.5 cm.

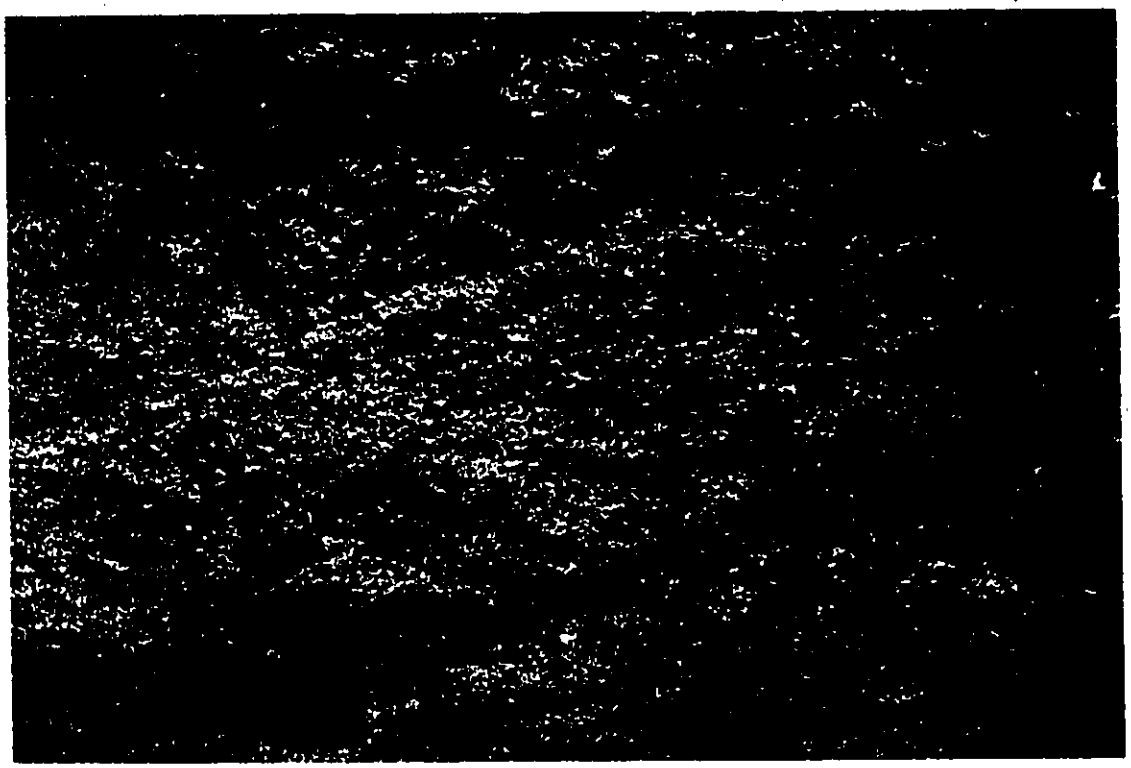

Plate 4.6 A weak second foliation defined by opaque mineral and biotite grains (dark) cross-cutting an earlier layering/gneissosity (S_1) which is approximately parallel to the longer side of picture. Leucocratic layer of FD 1 granite gneiss, Bokossa area.

of these folds on N - S trending subvertical outcrop faces and the attitudes of associated L_1 lineations suggests that hinges are subhorizontal and trend about E - W. The hinge zones are commonly angular and sometimes show thickening (Plate 4.5).

An axial planar fabric is weakly developed and mostly not evident in the hinge zones of the F_1 minor folds in the Fincha gneiss (FD 4a), but appears to be parallel to the S_1 foliation which envelops the folds. However, in the FD 2 layered biotite gneiss minor F_1 folds have a strong axial planar fabric which at most places is defined by a strong schistosity S_1 and an accompanying migmatitic layering and/or veining.

Some pegmatite and quartz veins near F_1 minor folds in FD 4a gniess are also folded isoclinally with S_1 as the axial planar fabric. This suggests a pre-S_1 (S_1') or an early S_1 event of pegmatization so that more than one generation of folds may be grouped as F_1. The evidence is more substantial in the FD 2 layered biotite gneiss where F_1 minor folds fold an earlier migmatitic layering S_1' (see section 4:1:1). Minor F_1 intrafolial folds in FD 2 layered biotite gneiss are typically isoclinal (Plate 4.1), and fold early (pre S_1) migmatitic layering S_1', which itself is parallel to compositional layering S_o. In most outcrops the limbs of these minor folds have been detached by boudinaging and only relatively thickened hinge zones of the folds are preserved (Plate 4.2). Asymmetric folds in the early migmatitic leucosomes (S_1') are also preserved as relicts in many outcrops (Plates 4.3 and 4.4).

4:1:3 D_2 structures

F_2 major folds and possibly associated faults control the mapped disposition of rock

units, and most geomorphologic features of the area, except in the Sagan domain where limited outcrops of Precambrian rocks make this control not obvious.

4:1:3:1 S_2 foliation

S_2 foliation is generally poorly developed and is restricted to the hinge zones of F_2 minor folds. Thus in paragneissic units in FD 3 and FD 4 of the Fincha domain S_2 usually occurs in the hinge zones of F_2 minor folds as parallel and up to 1 cm apart subvertical planes. Close examination reveals an alignment of biotite grains.

In FD 1 granite gneiss in the Welena Bokossa area, a weak secondary foliation (Plate 4.6) cuts across the main S_1 gneissic layering (Plate 3.8). This fabric is defined by the alignment of opaque mineral grains and minor biotite flakes and does not contain minerals of the high grade assemblage (orthopyroxene and calcium pyroxene) which are in the assemblage defining the earlier (S_1) foliation and gneissic layering (Plate 3.8). This later fabric may locally be an S_2 foliation, but minor folds to which it can be related are not apparent.

4:1:3:2 L_2 lineations

Lineations (L_2) are important D_2 minor structures (Fig. 1). They are present in all deformed rock units except in the Sagan domain (SD 1) mafic granulites and some late intrusive units like the FD 8 plutonic complex. L_2 consists of mineral lineations defined by hornblende grains in ampibolites (FD 3d, AD 2a) and biotite hornblende gneisses in

FD 2, biotite in most biotite-bearing or biotite-rich gneisses (units FD 2, FD 3, FD 4), and granitoids (FD 6) and (AD 1) and mineral aggregate lineations defined mostly by quartz and feldspar grains but also less commonly by biotite clots of a few mm diameter.

A very localized linear feature distinct from the above and defined by quartz blades (Plate 4.7) but most commonly ridges (Plate 4.8) is present in quartzofeldspathic gneiss unit FD 4a, in the Megadda area only. Accompanying F_2 minor folds have not been observed in the locality. It is considered as L_2 because it is similar in orientation to L_2 lineations elsewhere in the Fincha domain. This lineation is in its nature and perhaps origin unlike the L_2 lineations. L_2 intersection lineations (S_1/S_2 ?) may be inferred in the FD 1 granite gneiss from the attitudes of S_1 and the superimposed weaker planar fabric (S_2 ?) but this has not been observed in the field.

L_2 lineations are most developed in the Fincha structural domain (see section 4.2) in which most plunge at variable angles between NNW and NNE, and fewer plunge southward (Fig. 4.9). This spread (variation) in plunge may locally be ascribed to among other things the superimposition of later F_3 upright folds in this domain (Fig. 4.1) on initially subhorizontal L_2 lineation.

4:1:3:3 F_2 minor folds

F_2 minor folds are common in most metamorphic rocks in the area except, as for L_2, in the Sagan domain mafic granulites (SD 1). F_2 minor folds are generally tight, upright folds with rounded to angular hinge zones; they affect S_1 and parallel layering (Plate 4.9). Amplitudes and wavelengths of F_2 minor folds vary, but are commonly in the range of

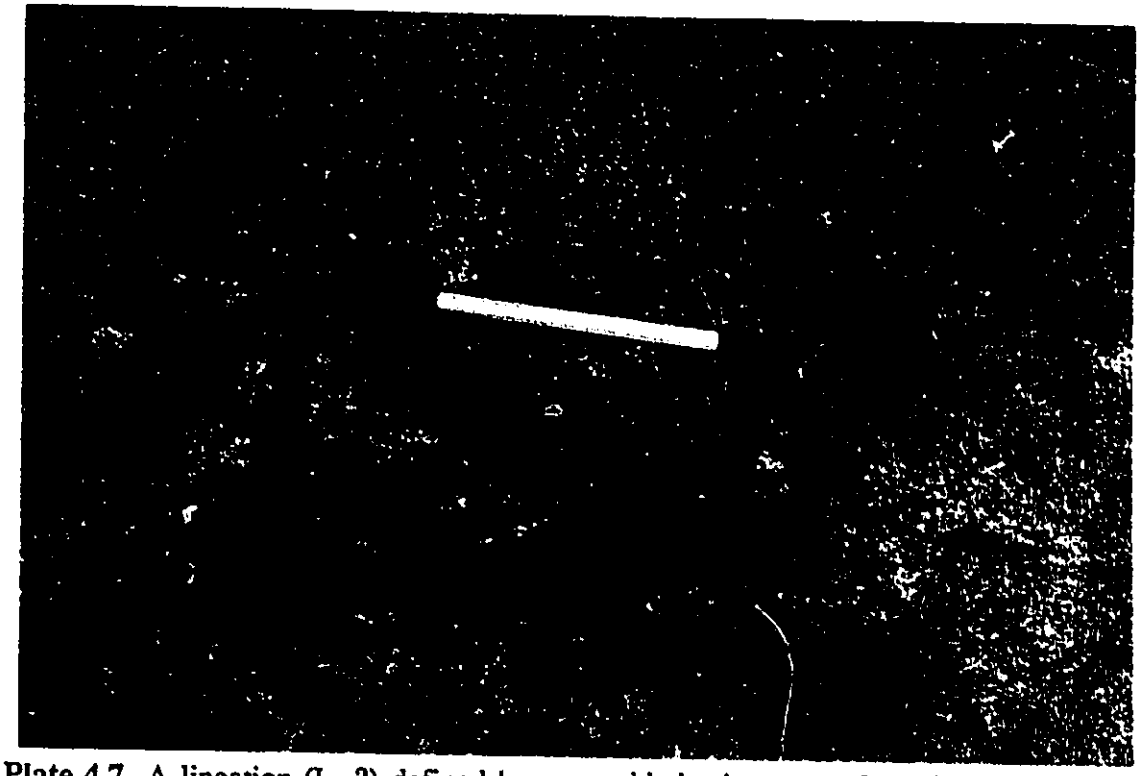

Plate 4.7 A lineation (L_2 ?) defined by quartz blades in quartzofeldspathic gneiss (FD 4a). Megadda area, Teppa valley. Pen points north.

Plate 4.8 A lineation (L_2 ?) defined by ridges in FD 4a quartzofeldspathic gneiss. Megadda area, Teppa valley. Pen points north.

10 to 20 cm. In a few cases, limbs reach upto 2 m in length, for example in the Afelata domain in migmatitic AD 2 amphibolites (Plate 3.35), in the north central parts of the Fincha domain in FD 4a and FD 3 (Plate 4.9) and also FD 2 layered biotite gneiss (Plates 4.10). Similarly the interlimb angles vary from unit to unit, perhaps depending on relative competency. The interlimb angles are generally lowest in schistose units where the folds are almost isoclinal (Plates 4.9 and 4.10).

Most F_2 minor folds plunge at shallow angles (<=10°) north or south parallel to L_2 lineations. However, a few exceptions include steeply north plunging folds affecting relatively more competent granitic units that are often associated with zones of intense pegmatization within FD 4a quartzofeldspathic gneiss. Such folds are very localized and the steep plunges appear to have no regional significance.

A few tight folds affect the gneissic tonalite (AD 1) of the Afelata domain. The folds are best seen in the Sakie Gundi valley (Fig. 2). These folds are mostly folds in S_1 foliation, and thus are F_2 or later structures. The folds are typically intrafolial, and have high amplitude to wavelength ratios and angular hinges (Plates 4.11 and 4.12). A few fold quartz veins emplaced parallel to foliation (S_1), and have smaller amplitude to wave length ratios.

4:1:3:4 F_2 major folds

Major D_2 structures are mainly shallow plunging N - S trending folds with subvertical or steeply inclined axial surfaces. Few F_2 major folds are precisely delineated (Fig. 4.1) in the Fincha domain. Generally the closures of antiforms are broader and axial traces are

Plate 4.9 F_2 minor upright antiform (up is to left of photo) in layers of biotite schist (dark) and calc-silicate (above hammer) and the parallel foliation (S_1) in the Melu gneiss (FD 3). Road cut, 3 km southeast of Fincha village.

Plate 4.10 East verging F_2 minor synform in S_1 foliation and parallel layering S_o, FD 2 layered biotite gneiss. Burji gneiss, Shershero valley. East is to right hand side of photo.

located with more certainty than those of synforms, that appear to be tight with obscure hinge zones (Figs. 1 and 4.1).

The axial surface traces of adjacent F_2 major antiforms are 2 to 12 km apart and can be traced confidently only over a few kms, except for one antiform in FD 5 granite in the northeastern corner of the Fincha domain (Fig. 4.1) which could be traced for over 15 km N - S. In the Fincha structural domain some F_2 major antiforms are doubly plunging, in a few cases perhaps as a result of the superimposition of later E - W system of F_3 folds. F_2 folds generally die out along their axial surfaces over a short distance.

A synclinorium mapped south and east of the study area by Chater (1971) may extend into the AD 2 amphibolitic unit in the southern part of the Afelata domain. However, this has not been demonstrated at the scale of the present work and consequently is not shown on the geological maps (Figs. 1 and 4.1).

4:1:4 D_3 structures

D_3 structures are of relatively local importance, restricted to the eastern part of the Fincha domain (FD) and the Afelata domain (AD). They are also present in adjacent areas to the south (Kiros and Kinetibeb, 1987). F_3 minor folds described in FD 2 layered biotite gneiss in the western extremity of the Fincha domain by Getahun and Alula (1987) have not been observed.

D_3 structures comprise minor and possibly major folds (F_3) and axes of crenulations and are designated as (L_3). S_3 foliations are unknown, however late crenulation cleavages defined by chlorite growth in some ultramafic schists (AD 2b) in the Afelata domain and

Plate 4.11 Intrafolial folds (F_2 ?) in Sebbeto tonalite (AD 1). Sakie Gundi valley, 5 km east of Kuppi Korolle. Hammer head points N.

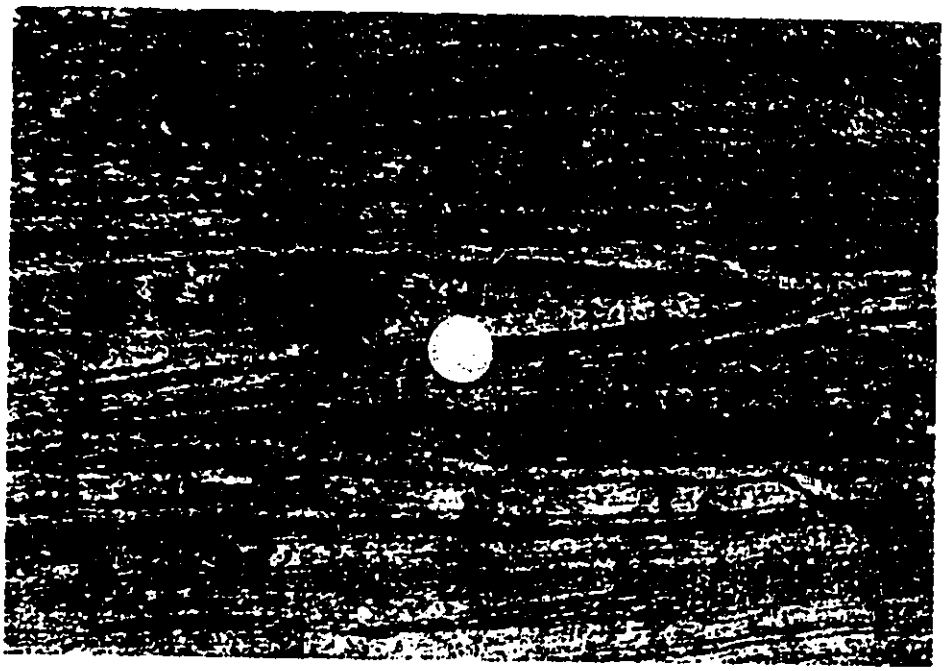

Plate 4.12 A close view of one of the intrafolial (F_2 ?) folds in Plate 4.11. Folds have typically angular hinges and affect S_1 gneissic layering.

steep E-W trending foliations in epidotized amphibolite horizons in unit FD 3 in the Kilkille area (Fig. 1) may be related to the axial surfaces of these folds.

4:1:4:1 L_3 lineations

L_3 lineations are of two types, hinge lines of F_3 minor folds and axes of crenulations related to D_3 deformation. The first are few and observed in the Afelata domain in the AD 2 amphibolite unit and trend E-W (Figs. 1 and 4.1). The second are best developed in quartzofeldspathic gneiss (FD 4) in the Surruppa area (Kiros and Kinetibeb, 1987), 15 km south of this thesis area.

4:1:4:2 F_3 minor folds

Minor folds of D_3 generation are closed to open folds, with broad and round hinge zones. They are generally short limbed and thus have high wavelength to amplitude ratios. Their axial surfaces are subvertical commonly with no associated mineral foliation and generally trend E - W. These folds could only be observed in the extreme east of the Sagan-Afelata area in FD 2 amphibolites (Fig. 1).

4:1:4:3 F_3 major folds

F_3 major folds are not distinctly mappable. These folds are inferred as superimposed on F_2 major folds (Fig. 4.1) to create doubly plunging, elongate outcrop patterns in the east of the Fincha domain and also in the Gariboro region to the east (Gilboy, 1970). To

the south of the thesis area, F_3 major folds are expressed as systematic array of deflections (open curves) in lithologic boundaries and structural (S_1) trend lines (Kiros and Kinetibeb, 1987). The deflections in lithologic boundaries and the S_1 foliation are concave to east or west and the bisectors of these curves trend about E - W, and are considered as axial surface traces of F_3 folds. Some of the latter type of folds have been shown on Fig. 4.1 in the eastern half of the Fincha structural domain.

4:2 Orientation data

As elsewhere in the Mozambique belt the predominant trend of the foliation (S_1/S_2) and major structures (D_2) is approximately N - S or NNE - SSW with minor deviations to the east and west. An exception is the approximate E - W strike of foliation in the western granulites of the Sagan domain. Other deviations are near F_2 fold closures, synkinematic to late-kinematic intrusions or in minor shear zones (Figs. 1 and 4.1). For the purpose of presenting the orientation data the area is subdivided in to structural domains (sD) that are distinct from the more general geological domains (D).

4:2:1 Structural domains (sD)

In contrast to the three more broad geologic domains (D), the area can be subdivided into five structural domains (sD) that are fairly distinct, based on orientations of S_1 foliation and parallel layering. However, none of these five domains can be considered as structurally homogeneous (Turner and Weiss, 1963) and domain boundaries are arbitrarly chosen to follow lineaments or faults. From west to east, these are (Fig. 4.1),

the Sagan structural domain (SsD), where granulites are characterized by about E - W striking foliation (particularly in the northern outcrop area) and moderate dips, the Burji structural domain (BsD), with N to NNE striking foliation that dominantly dips steeply WNW (Fig. 4.2), the Bokossa structural domain (BksD), characterized in the granitic gneiss (FD 1) by moderately easterly dipping foliation (Fig. 4.3), the Fincha structural domain (FsD), in which foliation dips vary from horizontal to steep, and strikes are mainly NNW to NNE (Fig. 4.4), and the Afelata structural domain (AsD), with moderate to steep foliation striking variably NNW (Fig. 4.5).

4:2:1:1 The Sagan structural domain (SsD)

The granulites in the northern outcrop of this structural domain strike uniformly east - west and in the southern outcrop WNW - ESE. In both areas dips are moderate and consistently to the south (Figs. 1 and 4.1).

4:2:1:2 The Burji structural domain (BsD)

FD 2 layered biotite gneiss of this structural domain is characterized by a penetrative S_1 mineral foliation accompanied by a strong gneissic layering and not uncommonly by a compositional layering (S_o) which at most places is paralleled by the pre S_1 S_1' migmatitic layering. S_1 consistently strikes N to NNE (Figs. 4.1 and 4.2 see also Fig. 1) and dips steeply most commonly westward but locally eastward.

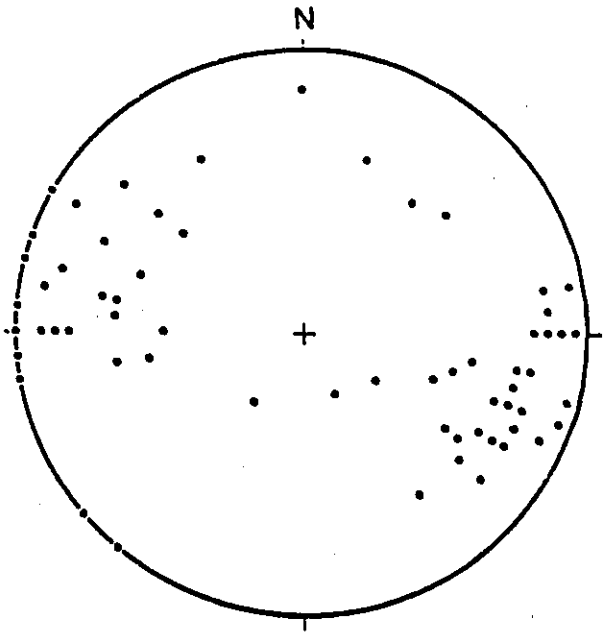

Fig.4.2 Lower hemisphere equal area projection of poles to S_1 foliation in the Burji structural domain (BsD).

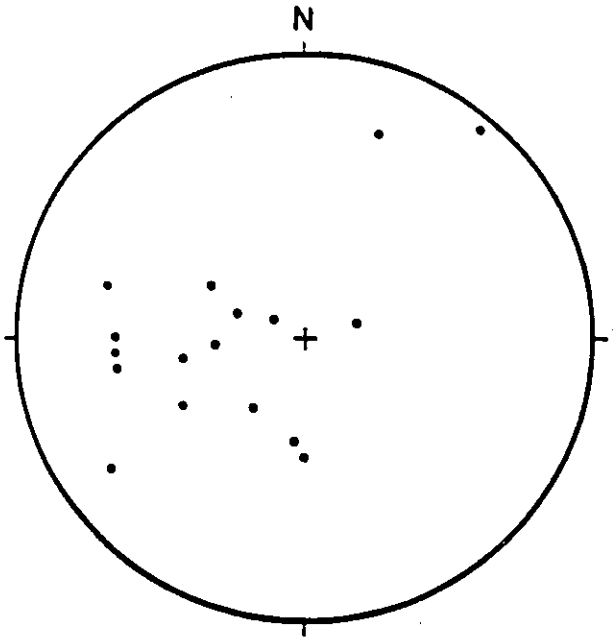

Fig.4.3 Lower hemisphere equal area projection of poles to S_1 foliation in the Bokossa structural domain (BksD). The foliation in FD 8 plutonic complex is not included.

4:2:1:3 The Bokossa structural domain (BksD)

As in BsD, in the Bokossa area (Fig. 4.3) S_1 layering and foliation dominantly strike northward but dips vary from shallow to moderate angles to the east in the FD 1 granite gneiss. Unique to this unit is the development of a second planar fabric (S_2 ?) in the FD 1 gneissose granite (Plate 4.6).

A steep fabric is developed in the FD 8 Bergudda plutonic complex (not included in Fig. 4.3) that appears different in orientation from the shallow dipping foliation accompanied by gneissic layering (S_1) in adjacent outcrops of FD 1 granitic gneiss hosting this pluton.

4:2:1:4 The Fincha structural domain (FsD)

The western part of this structural domain is the poorest in outcrop. However, the fold pattern seen in Fig. 4.1, is outlined from the structural measurements obtained with addition of air photo interpretations. S_1 foliation and the accompanying gneissic layering or primary layering (S_o) in this domain have variable strikes (Fig. 4.4). Where dips are relatively steep, S_1 generally strikes NNE - SSW or NNW - SSE, delineating the boundaries of the adjacent plunging folds. The few approximately E - W strikes in S_1 (Fig. 4.4) are from noses of plunging folds, the boundaries of intrusives and minor E - W striking shear zones (Fig. 1).

A weakly developed second foliation, is best seen in this domain than elsewhere. This foliation (S_2), is localized in the hinge zones of F_2 minor folds. It generally trends between NNE - SSW and NNW - SSE (i.e. parallel to the axial planes of F_2 major folds)

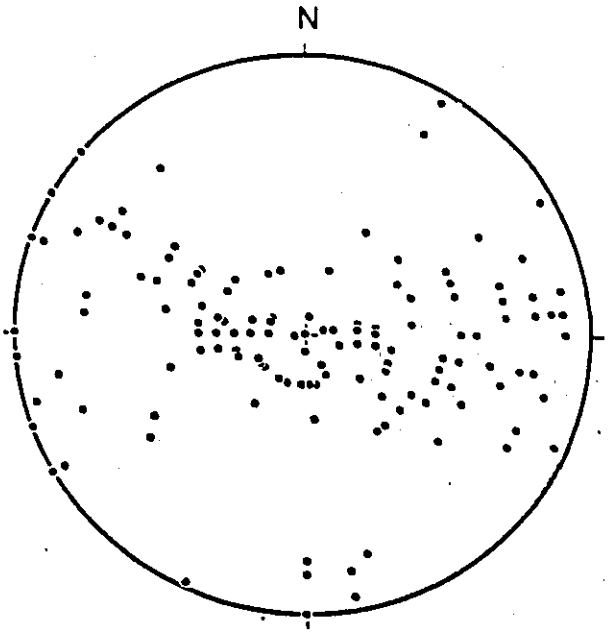

Fig.4.4 Lower hemisphere equal area projection of poles to S_1 foliation in the Fincha structural domain (FsD).

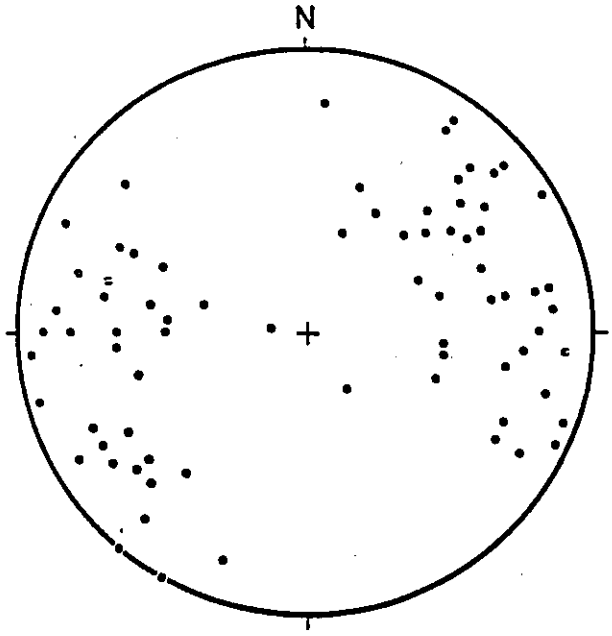

Fig.4.5 Lower hemisphere equal area projection of poles to S_1 foliation in the Afelata structural domain (AsD).

but its occurrences is sparse compared to that of S_1. Similarly the foliation observed in late-kinematic plutons like the FD 7 of this domain may in part be an early S_2 foliation or a ghost structure retained from gneissic rocks that host the plutons.

4:2:1:5 The Afelata structural domain (AsD).

The strike of S_1 foliation in the Afelata structural domain is variably NNW - SSE (Fig. 4.5). Dips mainly vary from moderate to steep, both east and westward. The few examples of shallow dips are from the northern AD 1 tonalitic unit (Fig. 4.6), in which foliation is often accompanied by gneissic layering and the relatively steeper dips (Fig. 4.7) are from the amphibolitic unit (AD 2) to the south. A general curve convex to the west and southwest (Fig. 4.1) distinguishes this domain from the domains to the west.

This curvature is on a regional scale, part of a general trend observed in the western part of the Megaddo region [see also maps in Chater, (1971), Warden and Horkel, (1984) and Kozyrev, (1985)]. The curvature may be related to movement between the Afelata and Fincha domain crustal blocks along the Kolle-Altuntu lineament (see section 4.5).

4:3 Summary and discussion

The regional foliation, the most important metamorphic fabric, is termed S_1 in all domains. However, one can not demonstrate if the same foliation continues throughout. For example S_1 foliation in mafic granulites SD 1 of the Sagan domain strikes E - W, whereas in the adjacent biotite gneiss (unit FD 2) of the Fincha domain, S_1 strikes N-S Fig. 4.1. No continuity can be established between the two domains because of the

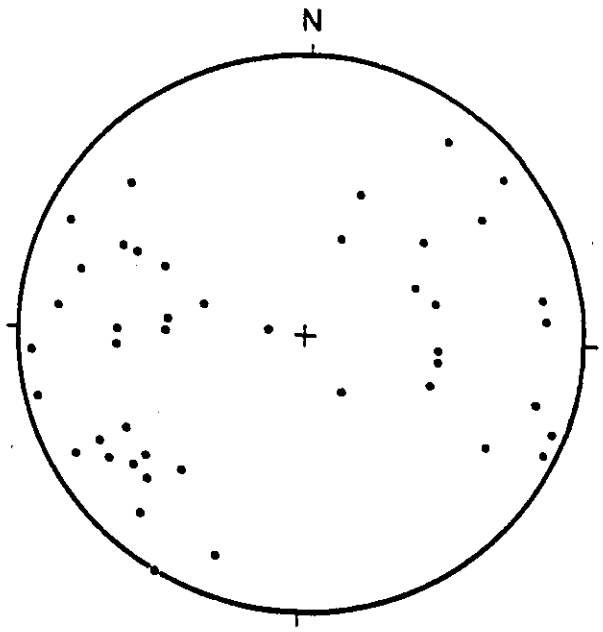

Fig. 4.6 Lower hemisphere equal area projection of poles to S_1 foliation in the northern half of the Afelata structural domain (AsD).

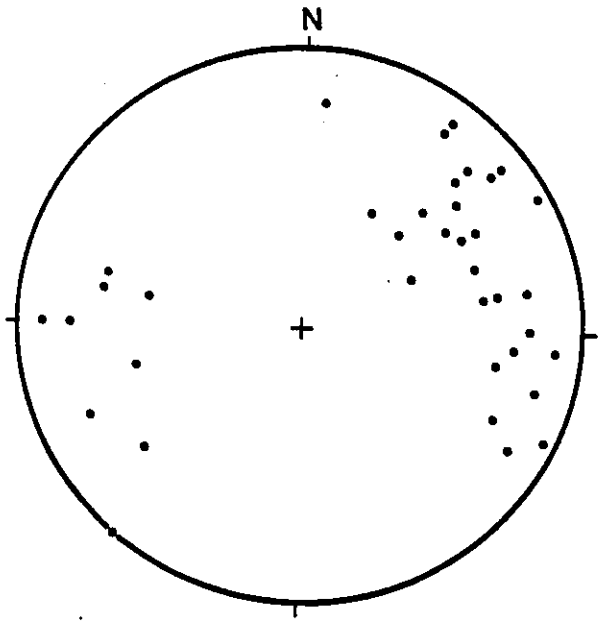

Fig. 4.7 Lower hemisphere equal area projection of poles to S_1 foliation in the southern half of the Afelata domain (AsD).

isolation of the two small outcrops of mafic granulite (Fig. 1). Thus, it is not clear if the N-S striking foliation in the Fincha domain was formed through the transposition of the E - W foliation in the Sagan structural domain, the development of a younger fabric or indicates the juxtaposition of domains of different structural history.

Similarly although a crosscutting relationship between the foliations in the Fincha and Afelata domains can not be established in this area, it is clear from larger maps that also cover the area to the south and east (Chater, 1971, Kazmin, 1973 and Kozyrev et al., 1985), that there exists a major discontinuity between the two domains (Fig. 4.8 and see also section 4.5).

Three phases of deformation (D_1 to D_3) can readily be recognized in the Sagan-Afelata area. The significance of an earlier event D_1' is not clear because the associated structure S_1' appears to have been preserved only in the Burji structural domain and one locality (Burkitu-Megadda area, Fig. 1) in the Fincha structural domain. In the latter area it can not be demonstrated if the S_o compositional layer-parallel pegmatitic veining is a D_1' structure or is a product of an early D_1 pegmatization. In this domain the D_1 phase of deformation is regarded (for simplicity) as possibly including more than one generation of structures. In general the D_1'-D_1 phase(s) of deformation or D_1 appears to have resulted in flat-lying foliation S_1 as inferred from the shallow plunges of F_2 major folds. In the Sagan domain, however, F_2 folds are not recorded (Fig. 4.1). From a correlation of this phase(s) of folding to similar early event(s) in the adjacent portions of the Mozambique belt (see section 4.4) and the widely accepted tectonic models for the evolution of the belt (Shackleton, 1977, 1979; Key et al., 1989) it can be said that this flat-lying early foliation

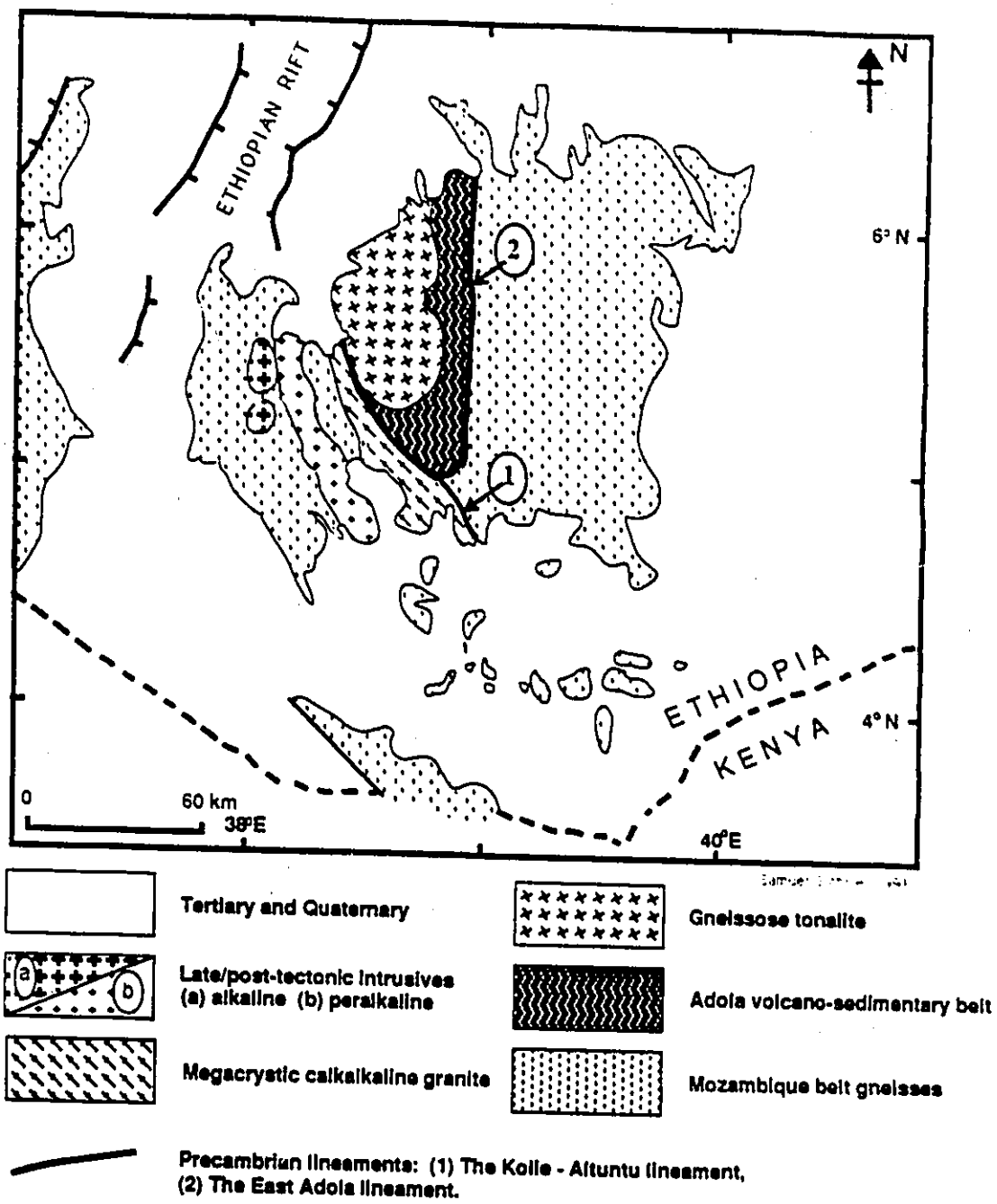

Fig. 4.8 Simplified geological map of southern Ethiopia (modified from Kazmin, 1973; Chater, 1971 and Kozyrev, 1985).

was due to subhorizontal transport that was mainly directed E-W. As will be shown in chapter 5, from the association with high pressure metamorphism major scale thrusting may have been involved, such as that related to Himalayan type of continental collison (Newton and Perkins, 1982).

D_2 produced major folds (F_2) with NNW to NNE trending axes and also a fairly penetrative L_2 lineation best seen in the Fincha structural domain (Fig. 4.9) roughly parallel to the axes of these folds and the axis of the orogen (Mozambique belt). This important phase of deformation is interpreted as due to an oblique compression (transpression), and must have resulted in significant ductile continental shortening across (E-W) the orogenic belt.

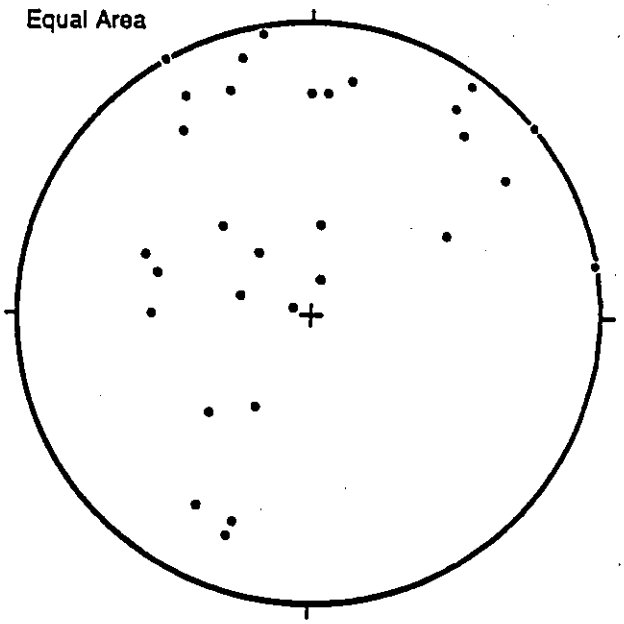

Fig. 4.9 Lower hemisphere equal area projection of L_2 lineations in the Fincha structural domain (FsD).

The only large structures related to the D_3 deformation are a few possible F_3 E-W folds localized in the east of the area. These folds, which are locally important in adjacent parts of the Mozambique belt of Kenya (Key et al., 1989) and southern Ethiopia (Gilboy, 1970, Chater, 1971, Kiros and Kinetibeb, 1987), may be related to compressions longitudinal (N-S) to the orogenic belt which could be the result of later collisional events in the N.

4:4 Correlation with other areas

A correlation of the structural elements developed during the various events recognized in this work, to similar structures recognized by other independent works in the immediately adjacent regions is presented in Table 4.1. As seen in this table, the general sequence of structural development and the structural elements in the adjacent gneissic terrains is similar. This similarity is particularly striking in the case of the Hamar domain of the Konso region 15 km to the west (Davidson, 1983, Davidson et al., 1973 and 1976) and the Gariboro region 60 km to the east (Gilboy, 1970).

However, a slightly different sequence is apparent in the Megaddo region (Chater, 1971) which bounds the Sagan-Afelata area on the east, although there is a definite physical continuity in both rock units and structures between this region and the adjacent Afelata domain. The important difference is that Chater's F_3 folds are developed only locally, in a narrow zone of greenschist facies metamorphism and major discontinuities in his upper group rocks. This zone appears to be unique and seems to have no equivalents in both the gneissic rocks to the east (Gilboy, 1970) and this area. Another

Table 4.1 Correlation of structural elements in the Sagan-Afelata area to that of neighbouring regions.

	Konso area	Gariboro region	Megaddo region
This work	Hamar Domain (Davidson et al. 1973, 1976, Davidson, 1983).	(Gilboy, 1970)	(Chater, 1971)
S_1	gneissosity/foliation	S_1 schistosity & foliation in Middle & Lower group gneisses and early gneissose granites, and locally in actinolite - chlorite schists	planar fabric S_1 in gneissose rocks defined by micas, parallel to but distinguished from S_2 only in the hinge zones of F_2 minor folds. Also parallel to migmatitic layers in ampibolites and S_0 in layered rocks. Not developed in "Upper Group" rocks.
L_1	probably the NW & W plunging local lineations in E of area	not recognized	not known
F_1	meso-rootless intrafolial folds with AXP foliation thought to fold an early gneissosity	not recognized; but inferred F_1 isoclinal recumbent folds to which S_1 is an axial plane fabric	F_1 rare, very small, always isoclinal folds of variable styles with rounded or angular hinge zones.
S_2	weak axial plane foliation steeper than the gneissosity folded by meso-folds	mica schistosity, S_1, axial planar to F_2 meso-folds & F_2 crenulation cleavage	S_2 more developed in the hinge zones of F_2 minor folds in micaceous rocks, also parallel to the folded S_1; not present or accentuated by new mineral growth in mica-free rocks.
L_2	strong NW, N also oppositely plunging lineation, related to F_2 folds, v. important	N & NNW plunging L_2, various types of lineations related to F_2 folds, v. important	L_2 most abundant, in varied forms including S_1/S_0 intersections, continuous between folded and unfolded rocks, very important.

Table 4.1 cont'd.

F_2	NW, N also oppositely plunging major and minor folds locally folding F_1 minor folds; most important phase of folding.	N to NNW plunging F_2, close to tight folds with subvertical axial surfaces, some refolding coaxially late in the same event. Most important phase of folding. Not seen in conglomerates of the Upper Group.	F_2 tight to isoclinal, may be close folds, with rounded to angular hinge zones; close to similar folds in shape; coaxially refolded locally during same event.
S_3	unknown	E-W trending crenulation cleavage S_3, paralleled by biotite growth, in the hinge zone of an F_3 antiform.	S_3 no mineral growth, parallel to axial surfaces of F_4* folds.
L_3	unknown	L_3 gently to moderately NW- to NNW-plunging hornblende and mica mineral lineations	L_3 axes of F_4 folds only
F_3	unknown	F_3, steeply inclined or upright open folds with wavelengths of 15-20 km, E-W axial traces & subhorizontal axes.	F_3 minor F_4 folds are tight and limited to the west, parallel (style), with rounded hinge zones, not seen folding earlier structures.

* Note that Chater's F_3 folds are limited to the east of the Megaddo region, where the "Upper Group" rocks outcrop, but his F_4 folds are equivalent to F_3 folds of both this and the Gariboro region to the east [see text for discussion].

important difference is coaxial refolding of early F_2 folds by later folds also considered to be F_2, a relation not observed in both the Gariboro region (Gilboy, 1970) and this area. The late E-W folds (F_3) are however recognized both in the Gariboro area and in gneisses underlying the western part of the Megaddo area. These folds are referred to as F_4 folds by Chater (1971).

Thus, apparently there is a general structural continuity in the high-grade gneissic rocks of southern Ethiopia. This sequence is also similar to that in high-grade gneisses of western Ethiopia (Ayalew and Moore, 1990; Mengesha and Berhe, 1987; Kazmin et al, 1978; de Wit, 1977) except for the absence of equivalents of F_3 folds and the non recognition of a pre S_1 fabric equivalent to the S_1' of this work. However, the structural similarity does not imply that the various structural elements developed in these areas are definitely contemporaneous.

Boglioti (1989) considers that all rock units within the Adola area, which includes the Megado and Gariboro regions of Chater (1971) and Gilboy (1970) respectively, had the same structural history and interference patterns. The sequence of folding proposed can not be used for correlation purposes, mainly because the geographic distribution of the structural data is unknown, and interpretations were made on the basis of few stereographic projections of a few sets of data.

Regional work due south of the thesis area in the northernmost high grade basement of Kenya (Key et al., 1989) has distinguished several major thermo-tectonic episodes of post Kibaran age (1200 Ma). Three to four of the more regional events may tentatively be correlated with the deformation in the structural sequence described here on the basis

of regional significance, relative ages, sequence and style of deformation.

The two oldest events, the Samburuan and the Sabachian took place under high grade metamorphic conditions (amphibolite to granulite facies). The events are very close in age and are interpreted to be responsible for the formation of a subhorizontal gneissosity at about 830 Ma (Samburuan) and subsequent recumbent folding and low angle thrusting directed transverse to the present N-S trend of the Mozambique belt at about 826 Ma (Sabachian). Equivalent events and corresponding structures have not been identified unequivocally in the Sagan - Afelata or in adjacent areas. However, these two events, which can be regarded as essentially indistinguishable in time, may be correlative with D_1'/D_1.

The age of the possibly separate D_1' event is unknown, but the age of D_1 can be approximated at 700 - 750 Ma at least in the Afelata domain from the age of the pre D_1 Sebbeto tonalite (765 Ma U-Pb) which pocesses an S_1 fabric, and the late syn-kinematic FD 6 Dek Bor granite (710 Ma U-Pb) in the Fincha domain.

NNW - SSE / NW - SE folds important in controlling the physiographic features in the north Kenyan basement were produced by the Baragoian event (Key et al., 1989), dated at 620 Ma (Rb-Sr). This event is correlated with D_2 which produced similarly oriented and equally important major folds, the F_2 folds of this area, which are equivalent to similar major folds mapped throughout the basement of southern Ethiopia (Davidson, 1983; Gilboy, 1970; Chater, 1971).

The D_3 structures which are E-W F_3 folds localized in the eastern half of the thesis area and farther east (Chater, 1971, Gilboy, 1970), may be correlatable to the Kipsingian E -

W asymmetric warps dated at 530 Ma (Rb-Sr) in the south of the region mapped by Key et al. (1989). These relatively late structures are also known to be structures produced at relatively high structural levels and as for F_3 are associated with localized low grade metamorphism.

This correlation implies that the northern part of the Mozambique belt evolved coherently and that the different phases of deformation were controlled by the same sequence of tectonic events and perhaps mechanisms that operated at the same stages but at different times in different segments of the orogenic belt. The discrepancy in the chronology is apparent at least for the earliest event(s), assuming that the D_1 event or D_1'-D_1 event(s) of this area (dated at 710-760 Ma) and the corresponding events in Kenya (dated at 826-830 Ma). This diachroneity may be a necessary result of the obliqueness of the continental collision responsible for the development of this belt (de Wit and Chewaka, 1981). Such a diachroneity in structural development due to oblique collision can be exemplified by the on going collision between the Luzon arc and Taiwan (Suppe, 1983, 1987).

4:5 Precambrian Lineaments

Most lineaments are not discussed because a large number may perhaps be the result of Tertiary rift tectonics. However, the following appear to be important.

4:5:1 The Kolle - Altuntu lineament

The Kolle-Altuntu lineament (Fig. 4.10) is a N-S structural break between the Fincha

and Afelata domains. The Altuntu megacrystic granite (FD 5), which is elongated along the lineament, may have been intruded along it as a sheet. Most lineations within the granite, which has a deformational augen texture, plunge to the north at shallow angles. The granite is weakly sheared along discreet zones, which may in part be post intrusion. The few oriented specimen studied from this area show no kinematic indicators. However, in a wider zone to the north the rock displays stronger shear fabrics (Getahun Seyid, pers. comm.). The granite may have facilitated the movement along this lineament, at least partially at the early stages of development of the fault zone. Lubrication by syndeformation granites has been suggested for large shear zones, for example the Proterozoic Great Slave Lake shear zone (Hanmer and Connely, 1986), and also for shear zones in the Variscan of western Europe (Strong and Hanmer, 1981) and the Pan-African of the Nubian shield (Almond et al., 1989). The subhorizontal N-S trending lineations in the granite, although indistinguishable from possible L_2 stretch lineations, suggest that movement along this lineament had a transcurrent (N-S) component.

To the south and east (Kazmin, 1973; Kozyrev et al., 1985; Chater, 1971), the lineament abruptly terminates (Fig 4.8) the Adola belt (Kozyrev et al., 1985; Kazmin, 1973; Kazmin et al., 1978). Thus, it juxtaposes an island arc and oceanic terrane (Afelata domain and Adola ophiolitic terrane (Kazmin, 1976) with a terrane of more continental characteristics (Chapters 3, 6 and 7). On continental scales the lineament has been traced to the Didessa river lineament in western Ethiopia and beyond, to the Ingesana hills of the Sudan (Vail, 1983) over a distance of about 1,600 km, and to the southeast to the Mutito fault zone of Kenya. If this extrapolation is correct, the fault can be compared in

its length and strike (although its segment in the Sagan-Afelata area is more northerly than north westerly) with the major north westerly late Pan-African fault and shear zones as the Najid fault system of the Arabian shield (Brown and Jackson, 1960, Brown, 1972, Stern, 1985, Stoeser and Camp, 1985). It may also be compared with other East African Late Precambrian fault zones such as the Surma mylonitic domain of south western Ethiopia (Davidson, 1983), and the Aswa fault zone to the south. However, unlike in these other fault zones, distinctly mylonitic faults are lacking and the zone itself is much narrower, at least in the Sagan-Afelata area.

Some of the movement along the Kolle-Altuntu lineament is perhaps penecontemporaneous with and/or younger than the Altuntu granite (FD 5) which engulfs the Sebbeto tonalite (AD 1), and the latter is dated at about (765 Ma). This implies that the lineament is younger than 760 Ma. It is perhaps much younger and may be within the age range of similar late Pan-African faults such as the Najid fault zone which is dated at about 630 - 550 Ma (Stoeser and Camp, 1985).

4.5.2 The Doga - Didiga lineament

The Doga - Didiga lineament unlike the Kolle - Altuntu lineament is defined by a line of ultramafic rocks, with subordinate quartzitic and epidote rich perhaps calcsilicate rocks which may include the N-S line of ultramafic hills noted by Kazmin (1970) in the Surruppa area to the south (see also Kiros and Kinetibeb, 1987).

In the Sagan - Afelata area the zone is defined by a north-northwesterly line of outcrops of low grade (tremolite rich) schists associated with quartzitic rocks (unit FD 4b,

Fig. 1). Further north the zone has been traced to a zone of serpentine bearing rocks (Hundie Beyene, pers. comn., 1985). Thus the lineament, which extends for over 70 km NNW - SSE, has apparently been accompanied by dyke injection and later green schist facies metamorphism, perhaps related to movements along the zone. To the south of the Sagan-Afelata area the line of ultramafic rocks in the Surruppa area occur in short en echelon segments which together are disposed (en echelonly) to the east of the segment in this study area. Thus the zone may be comparable with the en echelon array of major N - S trending shear or straightening zones in the Mozambique belt to the south (Hepworth, 1967). These zones are however much wider and are also associated with folding and shearing. In northern and central Kenya two major shearing and folding events related to such zones have been dated at about 580 - 570 Ma (Key et al., 1989). The older (580 Ma) of these is associated to dextral ductile shearing (Barsaloian) and the later (Loldaikan) to brittle sinistral shearing.

The Doga-Didiga lineament is sub-parallel to and bounds on the east the "geochemically anorogenic"Kinsho granite (unit FD 7). This granite forms a chain which continues southeast of Yabello village, 70 km south of this area. It is interpreted (chapters 6 and 7) to be emplaced during the later stages of the tectonic evolution of the Sagan-Afelata area i.e. during post -tectonic rifting of the newly thickened crust underlying the area in Late Proterozoic times. It is thus possible that the lineament is a remnant of a deep fault zone that may have controlled the emplacement of the granite and ultramafic rocks along the zone. The fault zone could have been wider before obliteration by emplacement of the anorogenic granite (FD 7), in accord with the wider zone of

ultramafic intrusions in the Surruppa area to the south (Kiros and Kinetibeb, 1987).

Similar N - S trending late shear zones in the Pan African of the Sudan are also known to be sites of anorogenic magmatism. As discussed above, the late N-S faults assumed to be marked by the lineaments, although younger than 660 Ma (Almond et al., 1989), appear to be older than those in the Mozambique belt of Kenya.

CHAPTER FIVE

METAMORPHISM

Introduction

The first section of this chapter (5:1) outlines relevant mineral assemblages of representative rock types from the Sagan, Fincha and Afelata domains and determines the P-T conditions during metamorphism from the stability of the assemblages . Mineral assemblages from mafic, ultramafic, calc-silicate and pelitic rocks are considered because they can be used in combination or individually to infer ranges of temperature and/or pressure conditions. This approach is sufficient to make overall estimates of metamorphic conditions because one or more than one of the four rock types are present in each domain, although in different proportions. The assumption made is that metamorphic quenching has taken place at approxmately the same time in an area for which a set of metamorphic reactions are considered; areas are generally no larger than "a quadrangle" (i.e. 60 km^2) as used by Carmichael (1978). It is also assumed that a field outlined from the P - T conditions for some reactions in a few adjacent quadrangles can indicate the approximate overall conditions of regional metamorphism for the corresponding domain. In the second section (5:2) this petrographic approach is further strengthened by P-T estimates from the mineral chemistry of three units.

In the final section (5:3) the data are integrated, and the overall variation in metamorphic conditions across the area at the present erosional levels is reviewed. The

conditions of metamorphism are also compared to those in adjacent areas.

The relevant mineral assemblages and estimates of P-T conditions are summarized in Table 5.7 and on a simplified metamorphic map of the area (Fig.5.1).

5:1 Metamorphic mineral assemblages

5:1:1 Sagan domain (SD)

This most westerly domain (Fig. 1) is dominated by mafic granulites associated with subordinate rock types (see also 3:2). The mafic rocks are suitable for general estimates of pressure and temperature conditions of metamorphism.

Table 3.2 lists the mineral assemblages and proportions of selected specimens of the mafic granulites from the Sagan domain. The important paragenetic assemblages in these associations can be represented by the following:

Plagioclase - Ca pyroxene - Orthopyroxene - Hornblende - Quartz

Orthopyroxene - Ca pyroxene - Hornblende - Plagioclase - Biotite - Quartz

Plagioclase - Orthopyroxene -Ca pyroxene -Biotite -Garnet - Hornblende - Quartz - Sillimanite

Orthopyroxene indicates metamorphic temperatures corresonding to regional granulite facies conditions (Winkler, 1974, Turner, 1981). Additionally, the following reactions suitable for placing limits on pressure can be suggested for the mafic granulites with garnet - plagioclase and quartz (above).

Plagioclase + Orthopyroxene = Garnet + Quartz (1)

more specifically

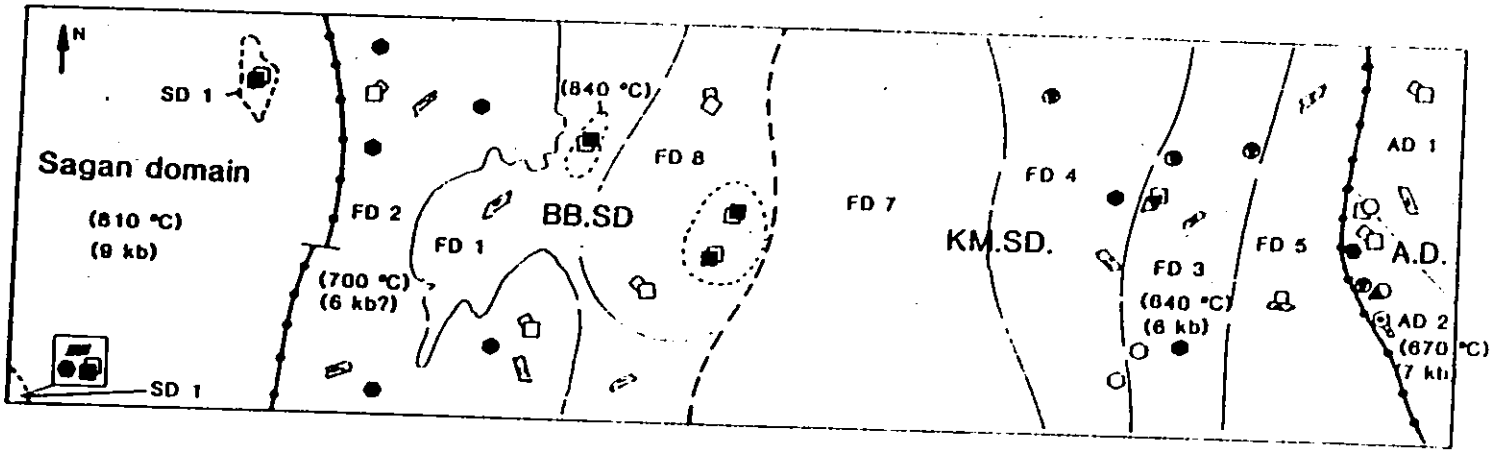

Fig. 5.1 Simplified metamorphic map

- Grt
- Opx-Cpx
- Hbl-Di
- Bt
- Ms-Kfs-Sil
- Di-Cal-Tr-Qtz
- Ep
- Hbl-bt
- Di-Ep
- Ky-Sil
- Ath-Tlc
- Granulite facies (approx. outcrop)
- Lithologic boundary (major & approx.)
- Domain boundary
- Subdomain boundary

KM.SD. Kinsho-Melu subdomain
BB.SD. Burji-Bokossa " } Fincha domain
A.D. Afelata domain

SD 1 etc Lithologic symbols as in text

$(Anorthite)^{Pl}$ + $(Enstatite)^{Opx}$ = $(Grossular + Pyrope)^{Grt}$ + Quartz

and

Plagioclase + Calcium pyroxene = Garnet + Quartz (2)

more correctly

$(Anorthite)^{Pl}$ + $(Diopside)^{Cpx}$ = $(Grossular + Pyrope)^{Grt}$ + Quartz

Note: $(Anorthite)^{Pl}$ means Anorthite component in Plagioclase, same for other components.

The univariant curves for these two reactions are shown as curves (1) and (2) in Fig. 5.2. As shown in this figure these two reactions indicate metamorphic pressures of about 12 kbars at temperatures between 600 and 900 °C (Newton and Perkins, 1982). These values are however the upper limits of pressure as the reaction curves were determined for the pure end member compositions ie. 100% enstatite and 100% anorthite. A realistic estimate for the Sagan garnet granulites is shown in Fig 5.2 see section 5.2 for a more specific P-T estimates for these rocks.

Hornblende in mafic granulites of the Sagan domain is a replacement of both calcium rich clinopyroxene and calcium - poor orthorpyroxene (see 3.2.1. and Plates 3.5 and 3.6). The same textural relation has been reported from the Konso granulites west of this area where the association is interpreted as retrogressive (Davidson, 1983).

Biotite is a minor constituent of these granulites and occurs in only a few specimens. However, it appears not to be retrogressive as estimates of metamorphic temperatures using the garnet - biotite geothermometry, according to Kretz's calibration (1990) is well within the range of temperatures of granulite facies metamorphism. Furthermore, the

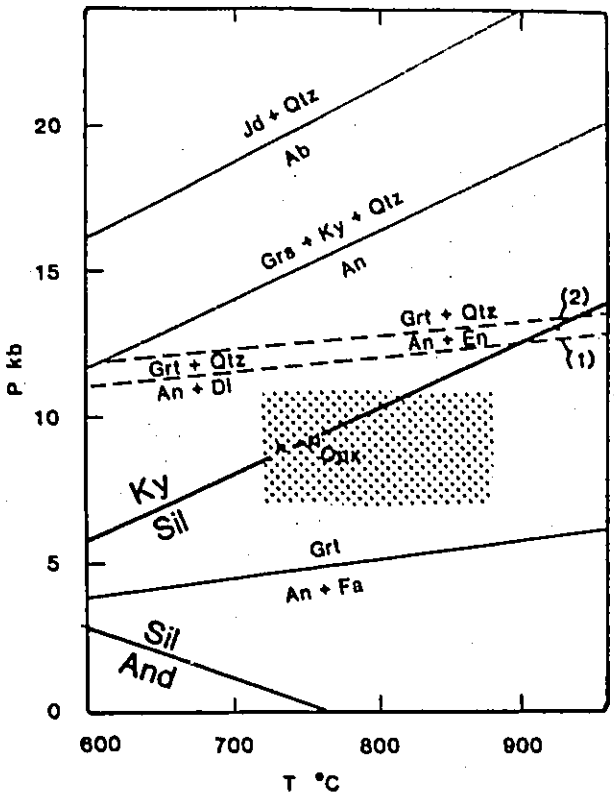

Fig. 5.2 Equilibrium curves for metastable (dashed lines), and stable (solid lines) mineral reactions used in geobarometry in the temperature range 600 °C to 950 °C (from Newton, 1983). Kyanite-Sillimanite-Andalusite stability fields are after (Holdaway, 1971). Numbers in brackets refer to equations in text. Dotted area is the approximate stability field for the Sagan granulites based on the pressure value obtained from sample NG 77a (point X in dotted area) using one of the geobarometric relations of Newton and Perkins, (1982) [equation (c) in section 5:2:3 of this chapter].

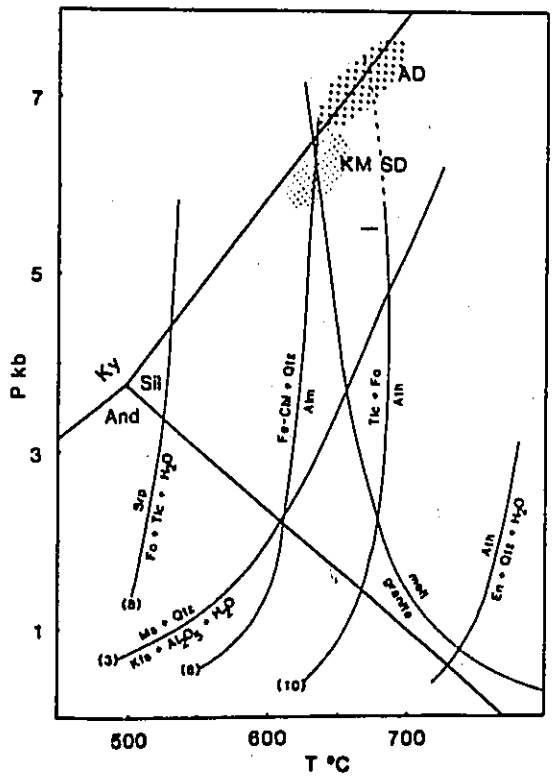

Fig. 5.3 Univariant curves for some reactions in pelitic, mafic and ultramafic rocks in the temperature range 500 - 800 °C. Sources for stability relations are in text; see also Greenwood (1976). Stability fields of the Al_2SiO_5 polymorphs are after Holdaway (1971). Numbers in brackets refer to numbers of corresponding equations in text. Marked regions show the approximate T-P fields of the dominant metamorphic event in the Afelata domain (AD) crosses, and the Kinsho - Melu subdomain (KM SD) dotted.

estimate is close to that obtained from the two pyroxene thermometry and the clinopyroxene solvus thermometry (Kretz, 1981) indicating biotite crystallized at approximately the same temperature as the coexisting pyroxenes (see 5.3.1.1).

5:1:2 Fincha domain (FD)

Most of the rock uits in this domain are quartzofeldspathic gneisses, except in the western extremity, where biotite gneiss, biotite hornblende gneiss, and amphibolites are predominant.

The Fincha domain is subdivided into a western (Burji - Bokossa) and an eastern (Kinsho - Melu) subdomains. The Burji - Bokossa subdomain consists of layered biotite gneiss (unit FD 2) and granite gneiss (FD 1) and the Kinsho - Melu subdomain essentially consists of quartzofeldspathic gneiss (FD 4) and a heterogenous paragneissic unit (FD 3) comprizing semipelites, pelites, calc-silicate rocks and amphibolites. Discussion of metamorphic conditions in the Fincha domain is therfore made for the two subdomains separately.

5:1:2:1 Burji - Bokossa subdomain

Two lithologies are dominant in map unit FD 2 underlying the western half of this subdomain, layered biotite and biotite -hornblende gneiss with subordinate amphibolites.

Mineral assemblages from these rock units and the subordinate lithologies are given in Table 3.3. The assemblages partly diagnostic of metamorphic conditions are:

Plagioclase - Hornblende - Biotite - K feldspar - Quartz

Biotite - K feldspar - Plagioclase - Garnet - Hornblende - Quartz

The map unit, (FD 2), does not contain any pelitic units with assemblages consisting of any of the aluminosilicate minerals (kyanite, sillimanite or andalusite) or corderite, staurolite or orthopyroxene making estimates of precise P - T conditions from mineral assemblages difficult. However, layered gneiss in map unit FD 2 is also commonly migmatitic (Plates 3.10 and 4.1 to 4.4).

Furthermore, mineral assemblages in associated mafic rocks (amphibolites and hornblende gneiss) contain hornblende without actinolite, and plagioclases (anorthite > 20%) and no epidote indicating temperatures are in the range of at least amphibolite facies metamorphism (Winkler, 1979, Turner, 1981). [see 5.3.2.2 for the geothermometric estimates based on coexisting garnet and biotite]. Although orthopyroxene is not seen as a stable phase, the estimate suggests that metamorphic conditions may have been transitional to lower granulite facies conditions. The absence of orthopyroxene may be due to non parallelism of isograds to local isotherms as seen in some metamorphic terrains (e.g. the Adrionacks, Valley et al., 1990).

Pressure estimates are difficult to make in this unit because no mineral paragenessis describable by reactions with suitably low P/T gradients can be proposed. However, cordierite is virtually absent and garnet is common in biotite gneisses, suggesting that methamorphic pressure is is not particularly low in this unit.

Granitic gneiss, Unit FD 1, where well-exposed, along an escarpment close to the contact with unit FD 2, forms coarse mafic and felsic layers up to 10 cm thick (Plate 3.10). The mafic layers suitable for inferring the conditions of metamorphism have the

assemblage:

Orthopyroxene - Clinopyroxene - Plagioclase - K feldspar - Biotite - Quartz - Opaque minerals

Both pyroxenes are anhedral and show weak preferred grain alignment that can be ascribed to metamorphic recrystallization (Plate 3.9). At many places within this unit, magnetite and biotite grains defining a second planar fabric indicate the growth of secondary metamorphic minerals (Plate 4.6) cutting across the gneissic layering.

Close to its margin map unit FD 1 is intruded by the granitoid plutonic complex of unit FD 8 (see chapter 6 for a complete discussion of the geochemistry and compositional zoning within the complex, and Chapter 3 for a detailed petrographic description).

Two other interesting assemblages in this subdomain occur in this metamorphosed plutonic complex. These are:

Hornblende - Biotite - Perthitic K feldspar - Plagioclase - Quartz

Hornblende - Biotite - Perthitic K feldspar - Plagioclase - Quartz - Calcium pyroxene

Hornblende - Orthopyroxene - Calcium pyroxene - Plagioclase - Perthitic K feldspar - Quartz

The first two of these assemblages are from the rim and the last one is from the core of the pluton. Table 3.8 lists the approximate mineral proportions for this pluton.

These assemblages and the texture of at least the core of this pluton indicate it has recrystallized under temperature conditions of granulite facies metamorpism. However, no specific reaction assemblages that can give an approximate estimate of the pressure conditions during metamorphism could be suggested.

In summary rock units in the Burji - Bokossa subdomain appear to be at least partly metamorphosed to granulite facies but were perhaps overprinted by amphibolite facies metamorphism at a later date. Temperatures of metamorphism, in the subdomain may not have fallen below 700 °C and pressures probably no lower than 6 kb.

5:1:2:2 Kinsho - Melu subdomain

The western map unit in this sub domain, unit FD 4, has no mineral assemblages that are characteristic of certain P-T ranges of metamorphism. However, small pelitic intercalations in the Doga hill and around the Surruppitti hill (Fig. 1) have the important paragenetic assemblage:

Plagioclase - K feldspar - Muscovite - Sillimanite - Quartz.

A thin section from a small outcrop of layered quartzofeldspathic gneiss west of Fincha village (Fig. 1) contains crystals of an isotropic yellowish mineral which upon probe analysis proved to be garnet.

Quartzofeldspathic rocks in the Megadda area contain fine euhedral crystals of biotite in parallel growth with green chlorite.

The mineral assemblages for the various lithologic units in map unit FD 3 (Melu paragneiss) in the eastern part of the Fincha domain are shown in Table 3.4. The important paragenetic associations in the different lithologies can be represented by the following:

In calc-silicate rocks, unit FD 3b:

Diopside - Epidote - Quartz

Diopside - Calcite - Tremolite - Quartz

In pelitic gneisses, unit FD 3c:

Muscovite - K feldspar - Sillimanite - Quartz - Plagioclase

In amphibolite intercalations unit FD 3d in the Kilkille area:

Hornblende - Plagioclase - Epidote - Quartz

Hornblende - Plagioclase - Epidote - Quartz - Biotite

Hornblende - Plagioclase - Epidote - Quartz - Actinolite

In garnet bearing quartz - plagioclase schists associated with amphibolites unit FD 3d:

Garnet - Plagioclase - Hornblende - Actinolite - Quartz

The following reactions based on some of the above assemblages can be used to approximate the pressure and temperature conditions of metamorphism.

$$\text{Muscovite} + \text{Quartz} = \text{K feldspar} + \text{Sillimanite} + H_2O \quad (3)$$

$$\text{Dolomite} + \text{Quartz} = \text{Diopside} + 2\ CO_2 \quad (4)$$

$$\text{Tremolite} + 3\ \text{Calcite} + 2\ \text{Quartz} = 5\ \text{Diopside} + 3\ CO_2 + H_2O \quad (5)$$

Reaction (3) with equilibrium curve (3) shown in Fig. 5.3 is commonly taken as defining the lower boundary of upper amphibolite facies metamorphism at relatively low (< 4 Kbar and $P_{H2O} = P_f$) pressures.

Diopside in calc-silicate rocks may have formed by either of reactions (4) or (5). However, from the paragenetic assemblage

Diopside - Tremolite - Calcite - Quartz

in these rocks, reaction (5) appears to be more probable, but the pressure - temperature conditions for this reaction depend on the prevailing P_{CO_2} values and the minimum temperature of metamorphism is generally higher than 600 °C for $X_{CO_2} > 0.2$ at an experimental total fluid pressure of 6.00 Kbar (Fig. 5.4, curve 5).

The assemblage in a garnet bearing quartz - feldspar schist with in unit FD 3d, suggests the reaction

Fe chlorite + Quartz = Almandine garnet (6)

The equilibrium curve (6) for this reaction (Hsu, 1968) shown in Fig. 5.3 suggests temperatures greater than 600 °C at pressures greater than or equal to 2 kbar.

Judging from the pressure values (about 6.5 kbar) at the intersection of curve (6) with the Kyanite - Sillimanite boundary of Holdaway (1971), Fig. 5.3, and the stability of sillimanite rather than kyanite it may be assumed that the metamorphic pressure at a temperature of about 600 to 650 °C did not exceeded about 6.5 kbar.

Thus, we may tentatively conclude that conditions at the peak of the dominant metamorphic event, in the Kinsho - Melu subdomain were approxmately (620 - 670 °C) at pressures of about 6 kbar (5.8-6.5 kbar).

5:1:3 The Afelata domain

The Afelata domain consists of two major units, a synkinematic gneissose tonalite (AD 1), in the easternmost corner of the project area and a dominantly amphibolitic unit, the Hiddi Asasu amphibolite (AD 2) to the south. The later unit consists of minor intercalations of pelites, semipelites and calc-silicate rocks which help in inferring

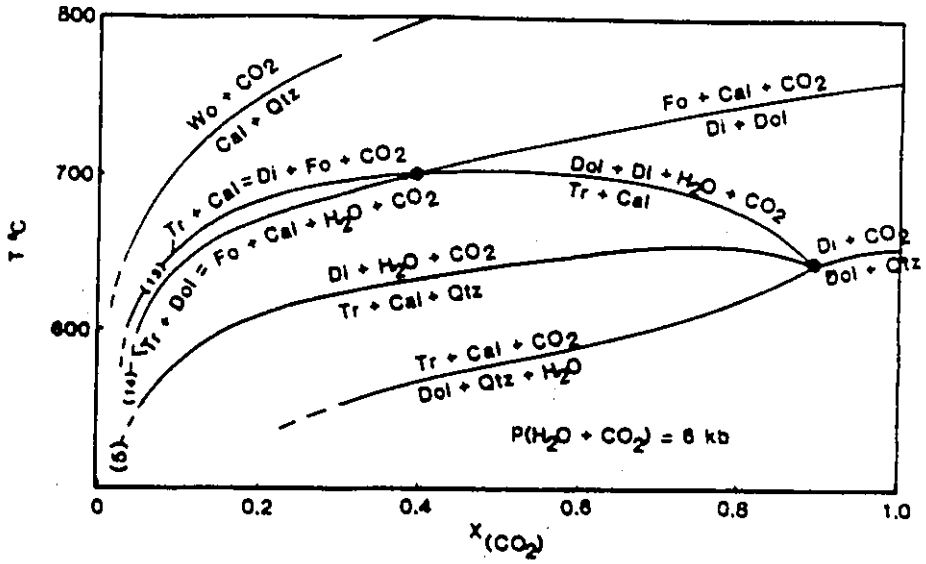

Fig. 5.4 Equilibrium curves in the T - X_{co2} field at 6 kb for reactions in fluid-saturated marbles and calc-silicate rocks (after Valley, et al, 1990). Numbers in brackets refer to numbered reactions in text.

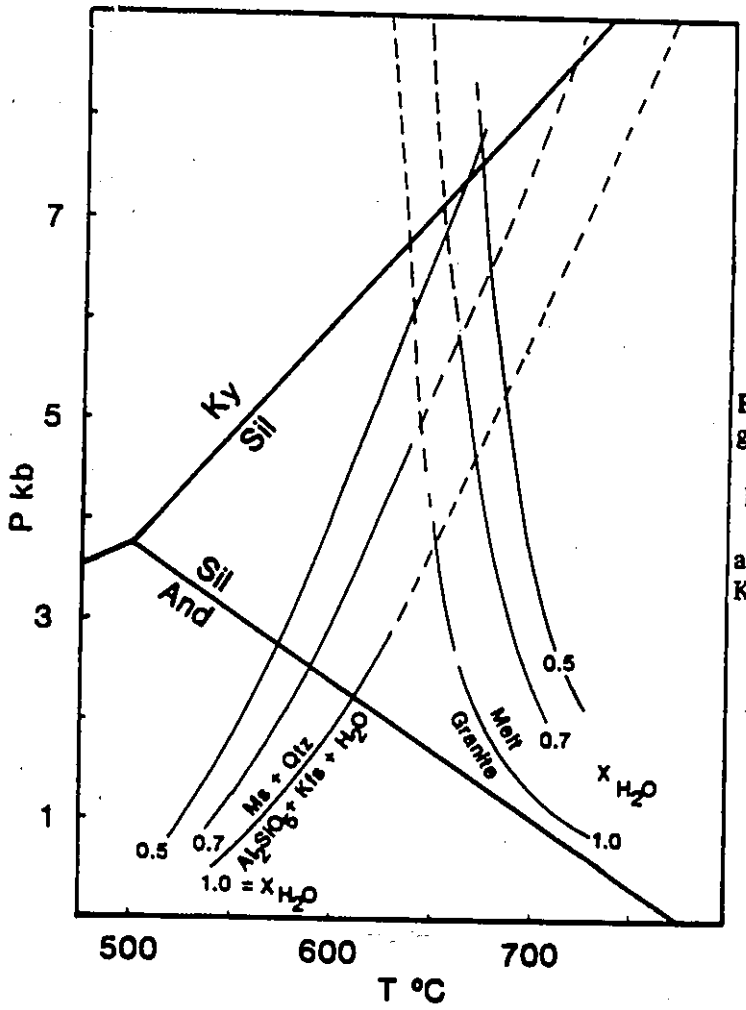

Fig. 5.5 P-T curves for granite/melt and the reaction

$Ms + Qtz = Al_2SiO_5 + Kfs + H_2O$

at different X_{H2O} values (after Kerrick, 1972).

conditions at the peak of metamorphism.

Approximate estimate of mineral proportions in the gneissose tonalite (AD 1) and the amphibolitic unit (AD 2) and the minor intercalations in the later are given in Appendix I Tables 3.9 and 3.10 respectively. Important paragenetic assemblages are:

Biotite - Hornblende - Plagioclase - Quartz

Biotite - Diopside - Hornblende - Plagioclase - Quartz

in AD 1 tonalite

Plagioclase - Hornblende - K feldspar (?) - Quartz

Diopside - Hornblende - Plagioclase - Quartz

Garnet - Hornblende - Plagioclase - Quartz

in AD 2 amphibolites

Kyanite - Sillimanite - Plagioclase - K feldspar - Quartz

in a pelitic gneiss intercalated within AD 2 amphibolite

Textural relations (Plate 3.37) suggest sillimanite replaces kyanite in the last assemblage.

Talc - Tremolite - Antigorite

Talc - Tremolite - Cummingtonite - Actinolite

in ultramafic schists in AD 2 amphibolites

Diopside - Epidote - Plagioclase - Kfeldspar - Quartz

in calcsilicate rocks in AD 2

The main foliation in the cummingtonite-bearing rock is crenulated and secondary chlorite grows along the axial planes of these crenulations. This later mineral growth is perhaps related to the late F_3 folds (Chapter 4) which are observable at mesoscopic scales

in this area. The common assemblages in the Afelata domain in general are suggestive of medium grades of metamorphism (Winkler, 1979). This fact is also apparent from field observations, like the presence of migmatitic phases in both the AD 2 amphibolites (Plate 3.35) and the AD 1 gneissose tonalite (Plate 3.32).

To constrain the pressure and temperature of metamorphism in the Afelata domain more closely, the univariant curves of a few mineral reactions are considered below.

The amphibolite unit AD 2 consists of metamorphosed pelitic, calc-silicate, and ultramafic rocks within a bulk of amphibolites.

A possible reaction in a pelitic unit with coexisting sillimanite and kyanite (in which the former appears to replace the later) is the reaction

Kyanite = Sillimanite (7)

with an equilibrium represented by the univariant curve after Holdaway (1971), in Fig. 5.3. Garnet appears in associated amphibolites suggesting many possible garnet generating reactions, of which the following appears as the most probable for such a mafic amphibolite.

Fe-chlorite + Quartz = Almandine (6)

Thus, reactions (6) and (7) combined constrain the lower limits of P and T at about 6.5 Kbar and 640 °C.

A metamorphosed ultramafic rock in this unit contains tremolite, cummingtonite and talc in an equlibrium relationship. Talc may have formed by a lower temperature dehydration reaction, probably the reaction:

5 Serpentine = 6 Forsterite + Talc + $9H_2O$ (8)

and tremolite at a slightly lower temperature by the reaction:

5 Serpentine + 2 Diopside = Tremolite + 6 Forsterite + $9H_2O$ (9)

(Evans and Tromsdorff, 1970)

The equilibrium curve for the first of these, reactions (8), is shown as curve (8) in Fig. 5.3 after (Bowen and Tuttle, 1949).

Kyanite bearing schists associated with garnetiferous amphibolites in continuity with this amphibolitic unit are ubiquitous in the Megadda area (Chater, 1971., Kozyrev et al.,1985). Thus, it may well be that the pressure of regional metamorphism in the Afelata domain may have at least reached as high as 6.5 kbar (curve 6 Fig. 5.3).

Two possible reactions that may have generated diopside in calc-silicate rocks are:

Dolomite + Quartz = Diopside + CO_2 (4)

and/or

Tremolite + Calcite + Quartz = Diopside + CO_2 + H_2O (5)

As shown in Fig. 5.3 curves 4 and 5 at experimental pressures ($PH_2O + P_{CO_2}$) of 6 kbar and $X_{CO_2} > 0.2$ equilibrium temperatures in the range of 600 - 630 °C are predicted by these reactions.

The pelitic unit in this domain with the assemblage

Sillimanite - Kyanite - Muscovite - Quartz - K feldspar - Plagioclase

suggests the relation:

Muscovite + Quartz = K feldspar + Sillimanite (3)

in addition to reaction 7 (above).

Reaction (3) takes place at a higher temperature of metamorphism than most of the

previous reactions for $P_{H2O} = P_f$. However, as can be seen from Fig. 5.5 it may require relatiely lower temperature for $P_{H2O} < P_f$ values (Kerrik, 1972). The lowest pressure estimate that can be made with certainty from the reaction curve in Fig. 5.5 for an assemblage with coexisting kyanite and sillimanite can be as high as about 7.2 kb at X_{H2O} values of about 0.5. The corresponding temperature estimate is about 670 °C and is about the same as the estimate based on relation (10) above and the Kyanite - Sillimanite boundary. Assuming P_{H2O} values (> 0.50) the P-T ranges of metamorphism within this domain can approximately be represented by the region shown in Fig. 5.3.

5:2 Geothermometry and geobarometry

Introduction

To supplement data on pressure and temperature of metamorphism inferred from the mineral assemblages (5:2), the P-T conditions were determined from mineral chemistry for three samples of mafic granulites (SD 1) from the Sagan domain (SD), two from the northern and one from the southern outcrop, and three samples within the Burji - Bokossa subdomain, two from garnet-biotite gneiss in layered biotite gneiss (FD 2) and one from the mafic layer of the granitic gneiss (FD 1).

Minerals analyzed: Analyses were done on pyroxenes, calcium pyroxene and calcium poor orthopyroxene, garnet, biotite and plagioclase from mafic granulites (SDI) and a mafic layer from the granitic gneiss (FD 1), and garnet and biotite from layered garnet-biotite gneiss (FD 2). Analyses of garnet and biotite grains were also obtained for a

sample of mafic granulite (SD 1) from the southern outcrop area. Table 5.1 lists the samples analyzed from each unit and the major minerals constituting each of these samples.

Both calcium-poor orthopyroxene (Opx) and the calcium clinopyroxene (Cpx) grains from the mafic granulites (SD 1) are anhedral, well recrystallized fine to medium sized, and show no signs of zoning. A few of the crystals are rimmed by hornblende but such crystals were excluded from analysis to avoid lower pressure and temperature estimates corresponding to later retrogression and/or uplift (Newton and Perkins, 1982., St-Onge, 1985).

All biotite crystals analyzed from a mafic granulite sample (NG 77a) were petrographically selected primary (non retrogressive) biotites. This is confirmed from the temperature estimates obtained from the garnet-biotite thermomery based on reactions involving biotite which are close to those obtained independently from the two pyroxene thermometry. Biotite grains analyzed are generally fine grained and commonly euhedral to subhedral.

Garnet crystals analyzed from the layered biotite gneiss (FD 2) are medium to fine-grained but generally coarser than those in specimens from the mafic granulite (SD 1). In specimens from both units, garnet commonly contains quartz inclusions.

In analyzing the coarser grained garnets, two to five points were probed along a traverse across the grain, to detect compositional zoning (Tracy, 1982) which could reflect conditions of metamorphism post-dating the peak of the granulite facies metamorphism. However, zoning, though present in few grains, was insignificant. Averaged mineral

Table 5.1 Mineralogy of specimen studied for Geothermometry and Geobarometry.

Unit (SD 1) mafic granulite

sample No.	Qtz	Pl	Kfs	Opx	Cpx	Grt	Hbl	Bt	Mag	Ilm	Sil
NG 77a	+	p	+	p	p	p	+	p	+	+	tr
GS 537	+	p	+	p	p	-	+	p	+	+	-
GS 539	+	p	+	p	p	-	+	p	+	+	-

Unit (FD 2) Layered biotite gneiss

sample No.	Qtz	Pl	Kfs	Bt	Hbl	Grt	Mag	Ilm
GS 449	+	+	+	p	+	p	+	+
GS 486a	+	+	+	p	+	p	+	+

Unit (FD 1) Granitic gneiss (Charnockite)

sample No.	Qtz	Pl	Kfs	Opx	Cpx	Grt	Hbl	Bt	Mag	Ilm
OG 90b	+	+	+	p	p	-	-	+	+	+

\+ present
\- not present
p analyzed by microprobe

analyses are shown in Tables 5:2 to 5:6.

Instrument and analytical techniques: Polished sections were prepared from specimens selected for their relative freshness and suitability due to mineralogic compositions. The polished sections, after appropriate marking of the minerals to be analyzed, were carbon coated and analyzed by microprobe. Microprobe analyses were obtained with a CAMECA CAMEBAX instrument at McGill University, Montreal. The instrument operated at an accelerating voltage of 15.0 kV and a beam width of 5 um. Natural minerals were used as standards.

5:2:1 Two pyroxene geothermometry

Temperature estimates were obtained using equations based on the calcium-rich pyroxene (Cpx) slope of the solvus surface, i.e. the calcium content of Cpx, and also the Mg - Fe^{2+} distribution coefficient, which is determined by the temperature dependent exchange reaction.

$$\underset{\text{(in Opx)}}{MgSiO_3} + \underset{\text{(in Cpx)}}{CaFeSi_2O_6} = \underset{\text{(in Opx)}}{FeSiO_3} + \underset{\text{(in Cpx)}}{CaMgSi_2O_6}$$

The equations used for both methods (below) are those of Kretz (1981) and accordingly for the Cpx slope of the solvus surface:

$$T = 1000 / (0.054 + (0.608 \times X_{CPX}) - 0.304 \ln (1\text{-}2\ [Ca])) \quad \text{(for } T < 1080\ C) \qquad (a)$$

and for for the exchange reaction

$$T = 1130 / (\ln K_D + 0.505) \qquad (b)$$

where T is the absolute temperature (in K)

$X_{CPX} = Fe^{2+} / (Mg^{2+} + Fe^{2+})$ in Cpx

$[Ca] = Ca / (Ca + Mg + Fe^{2+})$ in Cpx

$K_D = [X_{OPX}/(1\text{-}X_{OPX})] / [X_{CPX} / (1\text{-}X_{CPX})]$

$X_{OPX} = Fe^{2+} / (Mg + Fe^{2+})$ in Opx

$X_{CPX} = Fe^{2+} / (Mg + Fe^{2+})$ in Cpx

$(Fe^{2+} / (Fe_2^{+} + Fe^{3+}) = 0.89$ was assumed for all calcium pyroxenes analyzed because the ratio $Fe^{2+} : Fe^{3+}$ was not determined analytically.

5:2:1:1 Sagan domain (SD)

Analyses of the pyroxenes from the three granulite samples are shown in Tables 5.2 and 5.3. Substituting calculated values of X_{CPX} and [Ca] in equation (a) above yields temperatures of about 720 °C for the sample from the southern granulite area (NG-77a) and temperatures of about 840 °C and 720 °C for the two samples (GS-537 and GS-539 respectively) from the northern granulite outcrop. Estimates based on equation (b) for the three samples are in contrast 840 °C for sample NG-77a, and about 940 °C and 880 °C

Table 5.2 Analyses[1] and formulae[2] of orthopyroxenes (Opx)

	SAMPLE No.			
wt%	GS 539[3]	NG 77a[4]	GS 537[5]	OG 90b[6]
SiO_2	50.62	50.40	50.45	52.51
Al_2O_3	2.66	2.62	2.90	3.52
Fe_2O_3	0.00	0.00	0.00	0.00
FeO	25.73	26.51	26.77	22.11
MgO	19.96	18.81	19.57	22.22
MnO	1.00	1.51	1.31	1.53
CaO	0.61	0.60	0.67	0.96
Na_2O	0.00	0.03	0.02	0.03
K_2O	0.02	0.01	0.01	0.01
TiO_2	0.07	0.07	0.06	0.10
Total	100.67	100.56	101.58	99.99
Formulae				
Si	1.91	1.92	1.90	1.97
Al (iv)	0.09	0.08	0.10	0.02
sum	2.00	2.00	2.00	1.99
Al (vi)	0.03	0.03	0.03	-
Ti	0.00	0.00	0.00	0.00
Fe^{+3}	0.00	0.00	0.00	0.00
Fe^{+2}	0.81	0.84	0.84	0.69
Mn	0.03	0.05	0.04	0.05
Mg	1.12	1.07	1.10	1.24
Ca	0.02	0.02	0.03	0.04
Na	0.00	0.00	0.00	0.00
K	0.00	0.00	0.00	0.00
sum	1.98	2.01	2.04	2.02

1 Analyses by microprobe; total Fe expressed as FeO
2 Formulae based on 6 Oxygen atoms
3 mean of 2 analyses, unit (SD 1)
4 " 6 " , " (SD 1)
5 " 4 " , " (SD 1)
6 " 7 " , " (FD 1)

Table 5.3 Analyses[1] and Formulae[2] of calcium pyroxenes (Cpx).

	SAMPLE No.			
wt%	GS 539[3]	NG 77a[4]	GS 537[5]	OG 90b[6]
SiO_2	50.57	50.04	49.77	52.10
Al_2O_3	3.99	4.22	4.55	1.30
Fe_2O_3	1.22	1.23	1.39	1.36
FeO	9.83	9.92	11.21	11.03
MgO	11.89	11.88	11.86	13.92
MnO	0.46	0.03	0.55	0.68
CaO	20.48	20.40	20.05	20.34
Na_2O	0.84	0.78	0.72	0.78
K_2O	0.01	-	-	-
TiO_2	0.30	0.30	0.33	0.16
Total	99.09	98.80	100.43	101.67
Formulae				
Si	1.90	1.90	1.87	1.94
Al(iv)	0.10	0.10	0.13	0.06
sum	2.00	2.00	2.00	2.00
Al(vi)	0.08	0.09	0.08	-
Ti	0.01	0.01	0.01	0.00
Fe^{+3}	0.03	0.04	0.04	0.04
Fe^{+2}	0.31	0.31	0.35	0.34
Mn	0.01	0.00	0.02	0.02
Mg	0.67	0.67	0.67	0.77
Ca	0.83	0.83	0.81	0.81
Na	0.06	0.06	0.05	0.06
K	0.00	-	-	-
sum	2.00	2.01	2.03	2.04

1 Analyses by microprobe; Fe_2O_3 estimated by assuming FeO/FeO(T) = 0.89
2 Formulae based on 6 Oxygen atoms
3 mean of 4 analyses, unit (SD 1)
4 " 6 " , " (SD 1)
5 " 5 " , " (SD 1)
6 " 5 " , " (FD 1)

for samples GS-537 and GS-539 respectively.

5:2:1:2 Fincha domain (FD)

The same method was also used to estimate the temperature of metamorphism (charnockitization) in the granitic gneiss of map unit FD 1. Pyroxene analyses from sample OG 90b of this unit are shown in Tables 5:2 and 5.3.

For this sample, unlike the samples from the mafic granulite, estimates based on both equations (a) and (b) (above) were identical, and are about 900 °C.

Figure 5.6 shows the compositions of analyzed pyroxenes in the Ca, Mg, Fe^{2+} space. As seen in this figure both calcium-rich pyroxenes and calcium-poor orthopyroxenes from the charnockitic gneiss are more magnesian than those from the mafic granulites. Calcium - rich pyroxenes from the mafic granulite unit show a large spread in values of their calcium contents and thus show a larger range of solvus temperatures from about 700 °C to about 1000 °C with most grains clustering in the lower half of this temperature range. Calcium-rich pyroxenes from the charnockitic unit, in contrast, cluster at about 900 to 1000 °C. Fig. 5.6 also shows a comparison of the mean compositions of pyroxenes analyzed from each sample with that of pyroxenes from those of the Skaergaard intrusion (Sk) and granulite facies metamorphic rocks of Quairading (Q). As seen in this comparison pyroxenes analyzed from both the mafic granulite (unit SD 1) and the felsic charnockitic gneiss (FD 1) have compositional means close to that of the Quairading granulite suite than to those of the Skaeregaard intrusion except for a single grain of pyroxene from the mafic granulite (Fig. 5.6). The comparison suggests that all the

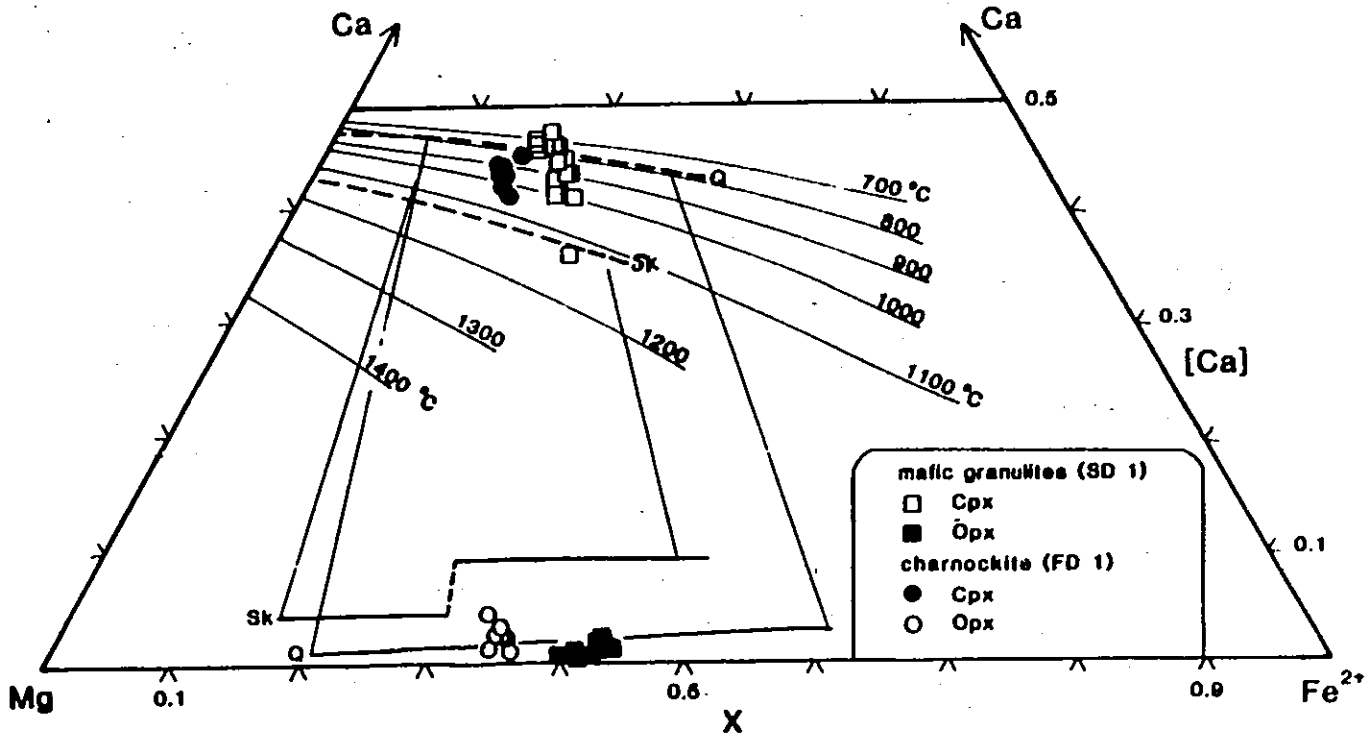

Fig. 5.6 Plots of pyroxenes analyzed from the mafic granulites (SD 1) and the charnockitic granite gneiss (FD 1) in the pyroxene quadrilateral. Isotherms (full lines) are from Kretz (1981). Thicker lines are lines through plots of calcium-pyroxenes (dashed) and orthopyroxenes (solid) from the Qairadig metamorphic terrane (Q) and the Skaergard intrusion (Sk). Note that most pyroxenes analyzed from both granulites of the Sagan-Afelata area are compositionally closer to the metamorphic pyroxenes.

pyroxene grains analyzed are of metamorphic orign than of igneous origin.

5:2:2 Garnet - biotite geothermometry

Introduction

The garnet - biotite geothermometer has been calibrated by a number of workers, including Thompson (1976) and Goldman and Albee (1977). The calibrations by Ferry and Spear (1978) and Perchuk and Lavrent'eva (1983) are experimental, and appear to be in common use for estimating temperatures of metamorphism.

In this work estimates were made by using an equation, (equation (c) below), proposed by Kretz (1990) based on a re-evalution of the Ferry and Spear (1978) and Perchunk and Lavrent'eva (1983) data and experimental procedures. The equation gives estimates that compromise between those obtained by the Ferry and Spear (1978) and Perchunk and Lavrent'eva (1983) relations.

The equation is

$$\ln K_D = 2780 / T_{(K)} - 1.51 \qquad (c)$$

Where K_D is the distribution coefficient (as defined above) after correction for the calcium content in the garnet.

T is the absolute temperature of metamorphism in K.

Correction, for the effect of the calcium content in garnet on the value of the distribution coefficent (K_D), was made using the equation

$$\ln K_D = \ln K'_D - 2.5 \times 10^{-2} [Ca] \qquad (d)$$

for $0 < [Ca] < 25$, (Kretz, 1990)

and Where K'_D is the distribution coefficient for Fe^{2+} and Mg in coexisting garnet and biotite.

and

K_D is the distribution coefficient after correction for the Ca content of garnet.

This geothermometer was used principally to estimate the temperature at the peak of metamorphism in the layered biotite gneiss of unit FD 9 with greater precision than is possible from petrography alone. This was felt necessary because this unit is bound on either side by granulite facies rocks, while it appears to be in the amphibolite facies.

The method was also applied to mafic granulites in which garnet and biotite coexist to get an independent estimate besides that from the two - pyroxene geothermometry.

5:2:2:1 Sagan domain (SD)

From this domain only a sample of mafic garnet and biotite- bearing granulite (NG 77a) from the southern outcrop area of unit SD 1 was used to estimate temperature by this method according to equation (c).

Seven garnet and three biotite crystals from a polished section of this sample were analyzed, the mean of the analyses are shown in Tables 5.4 and 5.5. In the following calculations, the means of values from several spot analyses of each garnet grain were averaged out and the average values for each grain were then averaged to obtain a mean for several grains in a thin section (see footnotes, Tables 5.4 and 5.5). Estimates of temperatures obtained from this sample (NG 77a) using the above equation (c) is about 740 °C.

5:2:2:2 Fincha domain (FD)

Garnet and biotite grains from two samples (GS 449 and GS 486a) were analyzed from the layered biotite gneiss (FD 2) in this domain (Table 5.4). The temperature estimates from the two samples, using equation (c) above, are about 770 °C and 670 °C for samples GS 449 and 486a respectively.

Table 6.7 lists the estimates of metamorphic temperatures for all samples considered above.

5:2:3 Geobarometry

Introduction

In this work, estimates of the pressure of metamorphism were obtained using one of the two geobarometric expressions (equations (e) and (f) below) of Newton and Perkins (1982). These equations are derived from the following equilibrium relations in garnet - bearing granulites.

Table 5.4 Garnet analyses[1] and formulae[2]

	SAMPLE No.		
	NG 77a[3]	GS 486a[4]	GS 449[5]
SiO_2 (wt%)	38.80	37.72	37.96
Al_2O_3	21.22	20.71	21.02
Fe_2O_3	0.99	1.01	0.68
FeO	23.97	23.93	27.70
MgO	6.63	3.66	3.89
MnO	1.09	5.32	3.72
CaO	7.27	7.44	5.45
TiO_2	0.06	0.05	0.26
Total	100.02	99.84	100.68
Formulas			
Si	6.01	5.99	5.99
Al	3.87	3.87	3.90
Fe^{+3}	0.11	0.12	0.08
sum	3.98	3.99	3.98
Fe^{+2}	3.10	3.18	3.65
Mn^{+2}	0.14	0.72	0.50
Mg	1.53	0.87	0.91
Ca	1.21	1.27	0.92
sum	5.99	6.02	5.99

[1] Microprobe analyses results
[2] Formulae based on 24 Oxygen atoms
[3] Mean of 13 analyses on 7 grains, unit (SD 1)
[4] " 5 " 2 " , " (FD 2)
[5] " 21 " 9 " , " (FD 2)

Table 5.5 Biotite analyses[1] and Formulae[2]

	SAMPLE No		
	NG 77a[3]	GS 486a[4]	GS 449[5]
SiO_2(wt%)	36.49	35.90	35.56
Al_2O_3	14.96	15.15	17.05
Fe_2O_3	2.24	2.78	2.74
FeO	13.75	17.08	16.81
MgO	14.23	10.94	10.82
MnO	0.03	0.29	0.10
CaO	0.07	0.04	0.03
Na_2O	0.05	0.07	0.16
K_2O	9.47	9.72	9.85
TiO_2	3.42	4.22	3.48
Cr_2O_3	0.01	0.01	0.04
H_2O	4.03	3.95	3.97
Total	98.74	100.14	100.57
Formulae			
Si	5.50	5.44	5.35
Al (iv)	2.50	2.56	2.65
sum	8.00	8.00	8.00
Al (vi)	0.16	0.14	0.37
Ti	0.39	0.48	0.39
Fe^{+3}	0.25	0.32	0.31
Fe^{+2}	1.73	2.16	2.11
Mg	3.20	2.47	2.43
Mn	0.00	0.04	0.01
sum	5.73	5.61	5.62
K	1.82	1.88	1.89
Na	0.01	0.02	0.05
Ca	0.01	0.01	0.00
sum	1.85	1.91	1.94
OH	4.00	4.00	4.00

1 Cations by microprobe, H_2O by calculation
2 FeO by assuming FeO = 0.86 x FeO(T)
3 Formulae based on 22 Oxygen atoms
4 mean of 3 analyses, unit (SD 1)
5 " 5 " , " (FD 2)
" 8 " , " (FD 2)

Plagioclase + Orthopyroxene = Garnet + Quartz

$(An)^{Pl} + (Fs)^{Opx} = 1/3\ (Gr)^{Grt} + SiO_2$

P_{OPX} (bars) = 3944 + 13.07 T (K) + 3.5038 T ln K_A (e)

and

Plagioclase + Clinopyroxene = Garnet + Quartz

$(An)^{Pl} + (Hd)^{Cpx} = 2/3(Gr)^{Grt} + 1/3\ (Py)^{Grt} + SiO_2$ for which

P_{CPX} (bars) = 675 + 17.179 T + 3.5962 ln K_B (f)

Where

$K_A = (a_{Ca} \times a_2M_g)^{GT} / (a_{Ca})^{Pl} \times (a_{Mg2+})^{OPX}$

$K_B = (a^2_{Ca} \times a_{Mg})^{GT} / (a_{Ca})^{Pl} \times (a_{Ca.Mg})^{CPX}$

T = metamorphic temperature in K

$(a_m)^n$ is the activity of component m in mineral n

P_{OPX} and P_{CPX} are the pressure estimates according to equations (e) and (f) respectively.

The uncertainities in pressure estimates according to equations (e) and (f) are +/- 1500 bars and +/- 1600 bars respectively (Newton and Perkins, 1982).

5:2:3:1 Sagan domain (SD)

Pressure estimates based on geothermometric calibrations using mineral chemistry was only done for the mafic granulites (SD 1) of the Sagan domain.

The sample used (NG 77a from the southern outcrop area) was chosen for containing the equilibrium assemblage garnet - pyroxene (orthopyroxene and calcium-rich clinopyroxene) - plagioclase and quartz (Table 5.1). The compositions of the plagioclase grains (shown in Table 5.6) were also determined by microprobe analyses.

The pressure estimate obtained from sample NG 77a on the basis of the first expression (equation c) at an approximate temperature of 1000 K, (close to the temperature estimate for this sample by the Garnet - Biotite thermometry according to the Kretz (1990) equation is 8.9 +/- 1.5 kbar.

This estimate is the same as the average of pressure values obtained from twelve typical Precambrian granulite massifs (Newton and Perkins, 1982).

Estimates have not been made based on the clinopyroxene composition equation (f) because such estimates are known to be generally lower than estimates by both the first equation (e) and other known geobarometric methods and also have higher uncertainities (Newton and Perkins, 1982).

5:3 Summary and discussions

5:3:1 Metamorphic P-T conditions

The temperature of metamorphism varies from about 600 °C to 940 °C with the highest values atained in the west within granulites (SD 1 and FD 1). Pressure estimates are less constrained. An abrupt change of pressure from about 6 kbar in layered biotite gneiss in

Table 5.6 Analyses[1] of Plagioclase in sample NG 77a, unit (SD 1)

wt%	mean[2]
SiO_2	56.75
Al_2O_3	26.76
Fe_2O_3	-
FeO	0.08
MgO	0.00
MnO	-
CaO	8.56
Na_2O	6.36
K_2O	0.22
Total	98.73

Composition in terms of end members

	Ab	Or	An
	56.60%	1.30%	42.20%
atomic	Ca = 0.4162		Na = 0.5659

[1] analyses by microprobe
[2] mean of analyses of 8 plagioclase grains

unit FD 2 to about 9 Kbar in the Sagan granulites SD 1 over a distance of no more than a few kms (Fig 5.1) is significant, but the estimates of pressure in unit FD 2 are not well defined particularly on the higher side of pressure. Table 5.8 and Fig. 5.1 summarize the generalized pressure-temperature data from the project area.

5:3:2 Metamorphic gradients

Temperature gradients calculated from the generalized average temperature and pressure values in each domain are shown in Table 5.8. The highest estimate (38 °C/km) is recorded in the eastern part of the Burji Bokossa subdomain in the charnokitic granite gneiss (FD 1) intruded by the plutonic complex (FD 8), itself recording granulite facies metamorphic imprints. The lowest gradients are in the Sagan domain (SD 1 mafic granulites 25 °C/km) and the eastern Afelata domain in (unit AD 2, 26 °C/km). In general the metamorphic conditions (i.e. T/P gradients) suggest a Barrovian metamorphism.

5:3:3 Structure and metamorphism

The purpose of this short section is to access qualitatively the relative change in regional thermal conditions with time, more correctly the change in thermal conditions with phases of deformation. The reference taken for this relative comparison is the P - T conditions at the peak of the predominant metamorphic event, which are discussed in Chapter 5.

Table 5.7 Summary of approximate metamorphic conditions and implications in the Sagan - Afelata area.

Domain	Sagan Domain	Burji - Bokossa (sub-domain)		K-Melu (sub-D).	Afelata (Domain)
Map unit	(SD 1)	(FD 2)	(FD 1)	(FD 3)	(AD 2)
approx. mean T[a](°C)	810	720	900	650	670
" P[b](kb)	9	6	6	6	7
ave. gradient (°C/km)	25	32	38	28	26
approx. depth (km)	33	22	22	22	26
crustal thickness (km)	58	47	47	47	51

Note: [a] Estimated temperature ranges (°C) are approximately (720 - 940) for (SD 1), (700 - 900?) for (FD 1), (670 - 770) for (FD 2), (620 - 670) for (FD 3), and (600 - 720) for (AD 2).

[b] Estimated pressure ranges are approximately (kb) (7.40 - 10.40?) for (SD 1), (5 -7?) for (FD 2), (5 - 7?) for (FD 1), (5.8 - 6.5?) for (FD 3) and (5.8 - 7.6?) for (AD 2).

assumptions

1. that pressure is isostatic
2. geobarometric and geothermometric data are correct for the Sagan domain and the Burji - Bokossa subdomain, despite the relatively few measurements.
3. that metamorphic quenching took place at the same time in all units of a quadrangle as used by (Carmichael, 1978) and thus assemblages in a (domain or subdomain) can be combined to estimate approx. P-T conditions for the corresponding domain/subdomain.
4. that the present crustal thickness under the area is approximately 25 kms.
5. 1 kb pressure = 3.67 km of crustal load.

However, it is necessary to point out the difficulties involved in such an attempt, i.e. the reconaissance nature of this work and the geology of the area. Most metamorphic rocks in the project area possess a gneissic layering, which appears to have formed early in their metamorphic history or are deformed granitic rocks. The later do not give much information on changes in conditions of metamorphism and in the former any metamorphic signature that may have preceded the gneissic layering is likely obliterated. Similarly, metamorphic fabrics that postdate this layering are generally not as strongly developed as such a layering and the associated foliation on which they are superposed.

The predominant metamorphic event is structurally related to the first phase of deformation (D_1), that produced the S_1 foliation and the accomapanying gneissic layering in gneissose rocks. Any metamorphic fabric preceeding this strongly developed fabric (like the relict layering and/or foliation and pegamatite veins probably related to the event) folded by F_1 minor folds, in unit FD 4a, may have been obliterated during probable transposition, as the rootless intrafolial nature of these folds suggests (de Sitter, 1964). [see also section 4:1:1:1 above]

During the D_2 event a planar fabric was only weakly developed, but both this fabric (S_2) and the strongly developed linear fabric (L_2) are defined by the same minerals (Table 4.1) that define the preceeding S_1 foliation; essentially hornblende in amphibolites, quartz and feldspar aggregates (streaks on S_1) in quartzofeldspathic gneisses and granitoids, and biotite in semipelitic and pelitic gneisses except in the mafic granulites of the Sagan domain (SD). In the later, (SD), mafic minerals of the granulite facies assemblage (two pyroxenes) are rimmed by secondary hornblende suggesting a later amphibolite facies

event.

The recrystallization of the same S_1 forming minerals to form S_2 and L_2 in all other domains, qualitatively indicates that at least the same or overlaping ranges of temperature conditions prevailed during both the D_1 and the D_2 events. The observed strong development of L_2 in contrast to S_2 during D_2 contrary to the strong development of S_1 compared to L_1 appears to reflect the contrast in strain pattern. D_1 appears to have resulted in dominantly S tectonites, and D_2 superposed a strong L fabric on theses structurally anisotropic rocks (S tectonites of D_1).

The third deformational event, however, is both of local importance, being restricted to the eastern half of the area, and also did not effect any observable mineral growth. In the Surruppa area (Kiros and Kinetibeb, 1987), south of this thesis area, crenulations of this generation are observed. However, no petrographic studies were made, on oriented specimen, to detect any mineral growth along the axes of these crenulations. The openness and near concentricity of F_3 minor folds points out that the rocks had lower ductility during the D_3 deformation, which is likely to be due to the prevalence of lower temperature and/or short lived thermal event. This also seems to agree well with the absence of a clear D_3 planar fabric.

Indications of an earlier, pre D_1, phase of deformation (D_1') in this area, other than those seen in FD 2 layered biotite gneiss and FD 4a quartzofeldspathic gneiss, is unknown. Regarding the metmorphic conditions during a probably early deformational event D_1' which may have preceeded D_1, we can only speculate. Judging from the lowest estimates of temperature at which low temperature migmatization related to regional

metamorphism may begin (Kerrick, 1972), in a metamorphic terrain with predominantly quartzofeldspathic rocks. Thus a lower estimate on metamorphic temperature during D_1' may approxmately be at the greenschist - amphibolite facies transition. The relative importance of this event and the time gap between it and the following D_1 event are however unknown.

In summary, although an event D_1' preceeding D_1 may have been important in some of the gneissic rocks, the reliable and widely developed records in metamorphic rocks of this area indicate that the peak metamorphic temperatures were reached during or shortly after D_1 and probably the same or slightly lower thermal conditions were maintained through out D_2. An exception to this is in mafic granulies SD 1, and possibly the adjacent high grade rocks FD 1 and FD 2. In the later two D_1 metamorphism was probably in the granulite facies and the following D_2 metamorphism was in the amphibolite facies. This condition had, however, declined considerably during the D_3 event. Table 5.7 gives a qualitative summary of metamorphic conditions during the D_1 event.

5:3:4 Crustal thickness and metamorphism

Metamorphic pressures inferred from mineral assemblages or reactions are often considered as reflecting paleodepths during metamorphic quenching (Thompson and Norton, 1968, Carmichael, 1974, 1978). Estimates of denudation, related to uplift, shown in Table 5:7, were made for a crust of average density (2.7 gm/cm^3) assuming that tectonic and fluid pressure are negligble, and all pressure is lithostatic (e.g. Carmichael, 1974, 1978). Thus, according to this estimate, about 20 km thick of Precambrian crust has

been denuded over most of the area except in the Sagan graben where this value abruptly rises to 33 km. This implies that the Precambrian crustal thickness over most of the area must have been about 45 km. This value increases westward to nearly 60 km in the Sagan domain. as the geobarometric data although inconclusive because of the small number of analyses, indicate that the Sagan - ganulite (SD 1) formed under metamorphic pressures of about 9 kbar. This pressure falls in the range of (actually the mean) pressures obtained from some twelve Precambrian massifs, compiled by Newton and Perkins (1982).

Examples of such massifs, in the Precambrian basement of East Africa are found in the Labwor hills of Uganda (Nixon et al., 1973) and in the central granulite complex (Hepworth, 1972) of Tanzania. In the later, the Furua complex is kyanite bearing and on the high pressure side (9.3 -11.1 K bar at 800 °C) of this mean (Coolen et al., 1982). The ages of metamorphism in these areas are Archean, in the Labwar hills of Uganda and Proterozoic i.e 700 - 900 Ma in Tanzania (Spooner et al., 1970; Bell and Dodson, 1981; Muhongo, 1987; Malisa and Muhongo, 1990). The later age range (700-900 Ma) also includes the age of granulite facies metamorphism (charnockitization) in the Precambrian basement of Kenya (Key et al., 1989).

The Ugandan granulites are a continuation of the Tanzanian shield (Bell and Dodson, 1981) while the Tanzanian granulites are Mozambiquian, both in metamorphic age and perhaps in the emplacment age of the precursors (Malisa and Muhongo, 1990) and in their tectonic positions (Hepworth, 1972). The chronologic placment of the Sagan granulites of this area and the adjacent Konso granulites (i.e. the Konso gneiss collectively), in the "Stratigraphy" of the basement of Ethiopia (Kazmin, 1973, Kazmin et al., 1978) appears

to be based on the analogy of the "Watian" (granulite group) of the Ugandan basement (Hepworth and MacDonald, 1966). However, the continuation of the Watian basement of Uganda into southern Ethiopia has not been demonstrated by earlier work (Davidson, 1983) or this work. On the contrary Key et al., (1989) point out that the Hamar domain (the high grade domain, including Konso granulites) of the Omo project area (Davidson, 1983) continues in to northern Kenya (into the northern most of their map area). Furthermore as demonstrated in Chapter 4 of this work this later area in the Kenyan basement has a structural continuity with the Sagan - Afelata area. There also appears to be a similarity in both lithologic association and in tectonic setting between the Konso granulites of southern Ethiopia (as described by de Wit and Chewaka, 1981) and the central and eastern granulite complexes (Hepworth, 1972) of Tanzania. Thus, most probably the layered granulites of southern Ethiopia, including SD 1 of this area, are correlatable to the Mozambiquan (central and eastern Tanzanian and Kenyan) than to the Archean (Ugandan) granulites.

The attainment of such high pressures, in both the Archean and Proterozoic granulite massifs, are in general ascribed to regional thermal perturbations due to "instantaneous" overloading of a continental margin by another continental margin (Newton and Perkins, 1982). Such a phenomenon is expected to happen during, a Himalayan type, continental collision and consequent crustal doubling (e.g. Powell and Conaghan, 1975; Richardson and England, 1979). Thus, very likely, the layered granulites of southern Ethiopia including the Sagan granulites (SD 1) of this area, are also Proterozoic granulites that formed perhaps by such a continental collison event. This event may be one of the events

in the evolution of the the Mozambique belt which is being shown to be a Proterozoic collisional belt in regions south of Ethiopia (Muhongo, 1987, 1988, 1989; Shackleton, 1977, 1979; Key et al., 1989; Berhe, 1989). This logical deduction argues against the previous belief that the southern Ethiopian granulites are of Archean age (e.g. Kazmin, 1973, 1975, 1976; Kazmin et al., 1978).

5:3:5 Metamorphic conditions in adjacent areas

The Precambrian rocks underlying the Konso highlands (15 km) to the west, the Hamar domain of the Omo project area (Davidson, 1983, Davidson et al. 1973, 1976) have undergone regional metamorphism of upper amphibolite to granulite facies conditions. The Sagan granulites (SD 1) of this area are in isolated outcrops. However, amphibolite facies metamorphic rocks appear between these granulites and those of the Konso area. Thus, in both terranes it appears that granulites have a patchy distribution.

A N-S trending narrow belt of volcanic and sedimentary rocks subjected to greenschist facies metamorphism lies east of the study area. This belt is separated from the eastern Afelata domain by a wide (about 15 km) zone of sediments and mafic volcanic rocks subjected to amphibolite facies metamorphism (Chater, 1971; Kozyrev et al., 1985). The later zone is continuous with the amphibolitic unit (AD 2) in the Afelata domain.

CHAPTER SIX

PETROCHEMISTRY AND TECTONIC SETTING OF SELECTED IGNEOUS ROCKS

Introduction

This chapter complements the structural and metamorphic data by infering the tectonic setting, of four selected plutonic units and one volcanic unit from the Sagan-Afelata area on the basis of their bulk chemistry. Thus, the objective of the chapter is not to discuss the petrogenessis of the units but to infer the probable tectonic settings of emplacement and where possible the probable source materials for the corresponding magmas. The approach adopted is largely empirical and is based on the comparison of both major element and trace element abundances of the studied units to those of similar rocks from well known tectonic settings. In the case of the plutonic units and to a lesser extent the volcanic unit, the general lithologic characteristics, field relations and associations are also taken into consideration.

The chapter is subdivided into five major parts. In the first part (6:1), the regional geologic setting, outcrop features, the relationship to adjacent rock units, and the lithologic and general geochemical characteristics (including the degree of metamorphic alteration), of each of the magmatic units is briefly reviewed. The outcrop, and petrographic descriptions of each of the five units, Sebbeto tonalite (AD 1), Hiddi Asasu amphibolite (AD 2), Altuntu granite (AD 5), Kinsho granite (FD 7) and the Bergudda

plutonic complex (FD 8) are discussed in more detail in Chapter 3. The second part (6:2) deals with comparative descriptions of the geochemical characteristics and classification of the four granitoid units. In the third part (6:3), tectonic discriminant diagrams based on relative abundances of both major oxide and trace elements are used to suggest the probable tectonic settings of the granitoid units. This section also correlates the magmatic rocks of the Sagan - Afelata area with analogous Phanerozoic and Pan-African granitoids. The fourth part (6:4), deals with the description, geochemical classification and determination of the tectonic setting of the meta-volcanic unit. The final part (6:5) is devoted to summarizing the conclusions reached from this chapter and to discussing the implications in terms of establishing the tectonic settings of the Precambrian rocks of the Sagan-Afelata area in general. The tectonic implications of the results discussed in 6:5 are viewed in a more regional context in Chapter 7.

Sampling and analytical techniques

Samples collected for geochemical analyses each comprised about 700 g of chips, recovered from larger fragments by removal of all the weathered and veined portions.

Analyses were performed with a Phillips PW 1410/20 AHP x-ray fluorescence unit in the geochemistry laboratory of the University of Ottawa. Results were compared with the following Canadian natural rock standards commonly used by the laboratory: MRG-1 and SY-1 (Canadian Certified Reference Materials Project, Abbey, 1983), DR-N (Association Nationale de la Recherche Technique, Gordinardju, 1982) and GA (Centre de Recherches Petrographiques et Geochimiques, Govinadarju and de la Roche, 1977). Ferrous iron was

determined by wet chemical methods. REE analysis was done by neutron activation techniques at the laboratory of Ecole Polytechnique, Montreal. All analyses are presented in Appendix II.

6:1 Geologic setting, lithologic and geochemical characteristics

The general regional geologic setting of the Sagan - Afelata area is discussed in Chapters 1 and 2. The general distribution and map outline of the studied magmatic rocks within the Sagan - Afelata area are shown in Fig. 1 and in a simplified map (Fig. 6.1), and the main geochemical and lithological characteristics and the broad classifications of the granitoid units are presented in Table 6.1.

6:1:1 The Sebbeto tonalite (AD 1).

The Sebbeto tonalite is a unit of commonly gneissose, medium - grained, mesocratic, hornblende-biotite tonalite. It underlies the northeastern corner of the project area and more than half of the Afelata domain. Its relationship to the Hiddi-Asasu amphibolite to the south is not certain, but it appears to be intruded by the Altuntu granite along its western margin.

The tonalite occupies a N-S trending zone west of a mafic to ultramafic volcano-plutonic and lower grade metasedimentary belt (the Megaddo graben syncline of Kozyrev et al. 1985). The zone of intrusion is segmented into ellipsoidal portions in map view. Individual segments appear well in regional maps (Kozyrev, 1985, see also Chater, 1971) and may, as in the northern Afelata domain, be cored by gneissose plutonic bodies of

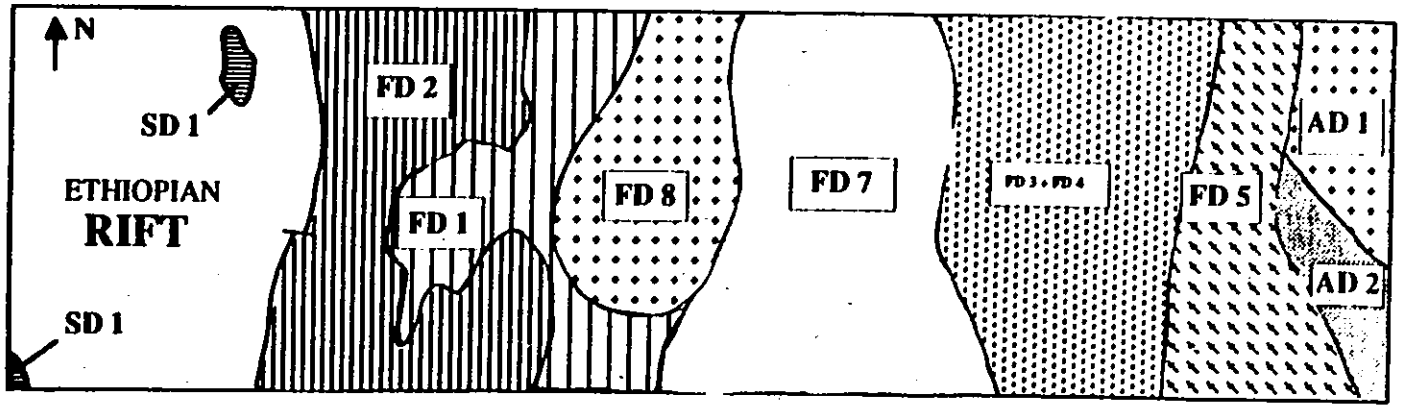

Fig. 6.1 Location map of granitoids studied from the Sagan-Afelata area. Unit designations are as in Fig. 1 and the text.

Table 6.1 Summary of the main characteristics and broad classification of the four granitoids studied from the Sagan Afelata area.

	Sebbeto tonalite (AD 1)	Altuntu granite (FD 5)	Kinsho granite (FD 7)	Bergudda complex (FD 8)
Lithology	med.gr. meso-tonalite	megacrystic meso-granite	fine-leuco-granite	dark-pink quartzmonzonite granite
Ferromagnesian minerals	Hbl, Bt	Hbl, Bt	Aegirine	Opx, Cpx Hbl, Bt
SiO_2 range (wt%)	61-69	67-76	73-76	58-71
Al_2O_3 range (wt%)	16-19	12-15	8-12	13-17
Total alkali ($K_2O + Na_2O$) wt%	3.07-6.18 $K_2O < Na_2O$	7.92-8.89 $K_2O > Na_2O$	7.03-8.80 $K_2O=Na_2O$	7.70-10.45 $K_2O=Na_2O$
Al/(Na+K+CA/2) (Pitcher, 1983)	1.28	1.40	0.14	0.83
Normative minerals	c,hy,di	c,hy,di	ac,hy,wo, hm,il	ol,ne,hy
$K_2)/SiO_2$ trend	0.7-1.72	3.54-5.23	3.27-4.78	3.45-5.26
$K_2O/(K_2O+Na_2O)$ wt%	0.13-0.31	0.45-0.59	0.42-0.62	0.45-0.55
A/CNK	1.22-1.35 (peraluminous)	1.07-1.13 (peraluminous)	0.81-1.06 (peralkaline-metaluminous)	metaluminous
AFM trend	calc-alkaline	Calk-alkaline	tholeiitic	tholeiitic
Rb/Sr range (wt%)	0.01-0.09	0.09-0.99	0.09-13.88	0.07-0.79
normative classification (Barker, 1979)	tonalite	granite	granite	granite
enclave type	Hbl rich (mafic)	Bt rich (mafic)	Bt rich (rare)	Hbl bearing (small,rare)
White & Chappel's (1983) classification	I type	I type	I type	I type
Pitcher's (1983) classification (wt %)	M type (island arc)	I type (cordilleran)	A type (post-orogenic)	A type (post-orogenic)

similar composition. To the southeast of, near the village of Gelebba, a pluton of similar composition but with lower grade metamorphic imprint and much smaller size has been mapped as quartz diorite (Chater, 1971).

In regional synthesis, the dome looking map configurations outlined by this pluton and other similar plutons to the north, were interpreted as being produced by superposed supposedly Archean E - W and Proterozoic N - S folding, of a high-grade gneiss (Warden and Horkel, 1984). In the geological map of Ethiopia (Kazmin, 1973) this unit and its probable equivalents to the north, were shown as a part of "the Alghie gneiss", one of the lower units in "the Arero Group" (Kazmin, 1973). The Arero Group was thought to encompass high-grade gneissic units dominated by biotite gneiss. It was believed to constitute the oldest (Archean) gneiss group that formed a basement to all the other "overlying" Proterozoic gneissic units.

However, contrary to these interpretations the Afelata domain (AD) of this work differs from the domains to the west in having predominantly intermediate to mafic magmatic rocks. Both the regional metamorphic foliation and lithologic layering in rocks of this domain appear to be discordant, to those in the adjacent Fincha domain (FD) to the west. The structural continuity and lithologic affinity of the rocks of the Afelata domain with those of the Megaddo region (Chater, 1971) suggest that the AD is related to the Proterozoic Adola belt to the east as pointed out earlier (Gichile, 1990a). A U/Pb (zircon) date of 765 +/- 2.5 Ma (EIGS, unpublished data), from the Sebbeto tonalite indicates that this relation is geochronologically sound. The Adola belt consists of mainly mafic volcanic rocks that partly include submarine flows (Chater, 1971), which are closely

associated with deep sea sediments and some ultramafic rocks (Kozyrev et al., 1985). This association within this narrow linear belt is regarded as ophiolitic (Kazmin, 1975; Shackleton, 1977; Berhe, 1989). The results of this thesis suggest that the association very likely represents the supracrustal sequences of an arc complex (see Chapter 7) of which the Sebbeto tonalite and other granitoid bodies in its chain form the plutonic root.

Analyses from the Sebbeto tonalite are shown in Table 6.2 (Appendix II). The rock has a wide range of silica content (61 - 69 wt%) and high alumina values (16 - 19 wt% Al_2O_3). It has low total alkali contents (3.07 - 6.18 wt%) with relatively low abundance of K_2O compared to Na_2O (K_2O = 13 - 31 wt% of total alkali) and has a low Rb/Sr ratio (0.01 - 0.09). Its high alumina content shows in its peraluminosity (A/CNK = 1.22 - 1.35) and the appearance of corundum in the norm (Table 6.2). However, it contains neither of the alumino-silicate polymorphs (kyanite, sillimanite or andalusite) nor muscovite in the mode.

6:1:2 The Altuntu granite (FD 5)

This pluton outcrops along the eastern margin of the central Fincha domain (FD). It appears to have been emplaced as a N - S elongated sheet. It has a minimum of about 5 km thickness in this area and extends for over 90 km N - S [see also Chapter 3]. It may be in fault contact with the Hiddi Asasu amphibolite (unit AD 2) of the Afelata domain to the east. To the north along its contact with the Sebbeto tonalite (in the Tatessa and Burka Daga areas) metre-scale angular blocks of tonalite embedded in the granite suggest it engulfed the tonalite. Its western contact with gneissic units in the Fincha domain to

the west is obscured by overburden [see also Chapters 3, 4, and 7]. The granite appears to be concordant to the regional structural grain and lithologic boundaries in the gneissic rocks to the west, but appears to be discordant to the foliation and lithologic layering in unit AD 2 to the east.

The pluton forms the core of a major F_2 antiform in foliation in the eastern part of the Fincha domain (FD). It has been mapped both to the north (Getahun Seyid, pers. comm., 1987) and to the south (Kiros and Kinetibeb, 1987). No geochronological data are available, however, its genetic relation (6.3) to the Proterozoic units (AD 1 and AD 2) and the block of AD 1 tonalite in it strongly suggest that it is younger than AD 1 (Sebbeto tonalite) and thus AD 2 (Hiddi Asasu amphibolite).

Table 6.3 in Appendix II, presents the analyses of this hornblende-bearing megacrystic biotite monzogranite. The granite has high silica content (67 - 76 wt%) and also high total alkali values ($K_2O + Na_2O$ = 7.92 - 8.89 wt%) with K_2O predominating over Na_2O (up to 59% by wt.). Alumina contents vary from 12 to 15% by weight, and the rock is peraluminous (A/CNK = 1.07 - 1.13). The Rb/Sr ratio is low (0.09 - 0.99).

6:1:3 The Kinsho granite (FD 7)

This aegerine-bearing leucogranite also outcrops in the Fincha domain (FD). It constitutes a part of the Yabello granites (Kazmin, 1970, 1973; Warden, 1976; Kazmin et al. 1978). This granite and all the other granites in the same chain were regarded as anatectic products of the Yabello gneiss of Kazmin (1970, 1973; Kazmin et al. 1978). What was known as the Yabello gneiss coresponds lithologically to unit FD 4a (the

Fincha gneiss) of this work. However, on the geological map of Ethiopia (Kazmin, 1973), the Yabello gneiss is shown as constituting units FD 4 and FD 7 of this work (Table 3.1).

There are no geochronological data for this unit, but as pointed out in Chapter 3 its age may be close to that of the Bergudda complex (unit FD 8) on the basis of the temporal position of similar granites in the tectonic evolution of Pan-African terranes of northeast Africa (e.g. Abdel-Rahman, 1986), and Arabia (e.g. Jackson, 1986, Ramsay et al., 1986, Stoeser, 1986), [see also discussion and summary and chapter 7].

Analyses from this leuco granite are shown in Tables 6.4 (Appendix II). The granite has very high silica values with a narrow range of 73 to 76 wt%. It also has high total alkali values (7.03 - 8.80 wt%) with K_2O about equal to Na_2O in wt%. In contrast, it is characteristically deficient in CaO (0.2 - 1.0 wt%) reflecting its high content of K-feldspar and the near absence of modal plagioclase. It also has both low absolute abundance of MgO (0.02 - 0.36 wt%) and a relative deficiency of Mg compared to Ca, shown by the appearance of wollastonite in the norm of most of the samples. The Kinsho granite is characterized by a high content of opaque minerals in the modal mineralogy, this shows in the norm as both hematite and ilmenite in all analyzed samples. The granite is peralkaline to metaluminous (A/CNK = 0.81 - 1.06) and has both a high range and high values of Rb/Sr ratios (0.81 to 13.88, with an average of 4.2).

6:1:4 The Bergudda plutonic complex (FD 8)

This plutonic complex was considered as a post-tectonic granite supposedly emplaced long after the Precambrian tectonism had ceased (Kazmin, 1970, 1973). Later, Gichile et

al. (1986), recognized granulite facies metamorphic imprint in the core rock and intense deformation along its eastern margin [see also Chapter 3] and suggested that it was perhaps a tectonically uplifted block.

The core of this plutonic complex is made of a weakly foliated to massive, dark greenish medium grained rock with granulite facies metamorphic mineral assemblages and texture. This core is rimmed by a pinkish pyroxene bearing hornblende granite which is much more deformed (see Chapter 3 for detailed petrography of the different parts of this pluton).

This plutonic complex outcrops in the Burji-Bokossa sub-domain of the Fincha domain and is intrusive into the Bokossa gneiss (FD 1). Xenoliths of the gneiss vary from small (centimetre-scale) polygonal blocks (Plate 3.28) to map - scale outcrops of leucocratic gneiss forming roof pendants in the southwestern part of this body (Fig. 1). Furthermore, marginal veins of this pluton (FD 8) intrude and cut across the gneissosity in the FD 1 granite gneiss (Plate 3.30).

Two U/Pb (zircon) ages obtained from this pluton (EIGS unpublished data) one from the granulitic core and the other from the intermediate zone, are 538 +/- 2.8 Ma and 528 +/- 8.4 Ma respectively.

Analyses from the Bergudda plutonic complex (FD 8) are presented in three sets in Appendix II (Tables 6.5a to 6.5c). These are from the dark core, the pink outer rim and an intermediate zone respectively. The complex has a wide range of silica values (58 - 71 wt%) with a general increase from core to rim. An extreme manifestation of the relative silica undersaturation of the more mafic inner core is seen as the appearance of

normative nepheline in a few, and normative olivine in one of the samples (SG 5572). The complex has high alkali values (7.70 -10.45 wt%) with about equal (wt%) values of K_2O and Na_2O, that increase towards the core. This increase in alkalis towards a silica poor core and the negative correlation between K_2O and Rb are known to be primary characteristics of A type alkaline ring complexes (Rogers and Greenberg, 1990, see also classification below).

However, in some plutonic units subjected to granulite facies metamorphism elemental distribution is known to be related to metamorphic processes rather than being primary (Tarney and Windley, 1977; Rollinson and Windley, 1980; Allen et al., 1985; Rameshwar Rao and Narayana, 1989). In this pluton although some differences in elemental abundance are related to the apparent primary compositional zoning some distributions may be secondary i.e. metamorphic.

6:1:5 The Hiddi - Asasu amphibolite (AD 2)

This map unit (AD 2) encompasses a variety of lithologies but amphibolites are predominant. The Hiddi Asasu amphibolites are, as discussed in Chapter 3, of basically two textural varieties: a fine - grained perhaps metavolcanic variety and a coarser - grained relatively massive metaplutonic variety. However, the analyses used in the following interpretations were obtained from the fine grained presumably metavolcanic variety only. The unit is perhaps intruded by the Sebbeto tonalite (AD 1) to the north (Chapter 3), but this relationship is not very clear.

Analyses were performed on six fresh samples (Table 6.6 in Appendix II) of non-

porphyritic, epidote and carbonate - free, fine - grained amphibolite. Analytical procedures and equipment are as for the granitic rocks. CIPW norms shown in Table 6.6 were calculated without adjustment for oxidation (i.e. Fe_2O_3/FeO ratio) and also conversion of normative nepheline to normative albite (Irvine and Baragar, 1971). No analyses were also done for volatiles (CO_2 and H_2O) and the LOI values have not been determied. Thus, the normative albite and nepheline values shown in Table 6.6 may not correspond to that of the fresh (unmetamorphosed) volcanic rock (e.g. Condie et al., 1977, Condie and Shadel, 1983).

These corrections were not done because in the following discussions and interpretations the norms of any of the analyzed samples is not used. Much emphasis is made of the contents of trace elements, which are regarded as relatively immobile (e.g. Winchester and Floyd, 1977, Pearce and Norry, 1979) to characterize this metavolcanic unit and make an inference about its tectonic setting.

6:2 Alteration and metamorphism

All granitoid units and the metavolcanic unit have been subjected to metamorphism, but to different degrees. Of the five rock units, the green rock forming the core of the Bergudda plutonic complex (FD 8) is the one metamorphosed under the highest temperature conditions. Metamorphic mineral assemblages and textures indicate that this rock has been subjected to granulite facies metamorphism. The two units in the Afelata Domain, the AD 1 tonalite and the AD 2 amphibolite have been subjected to at least mid-amphibolite facies metamorphism. Metamorphic conditions for the peralkaline granitic

unit (FD 7) are uncertain. The rock has a weakly developed foliation but a well-preserved granitic texture and the characteristic mafic mineral, aegirine, appears to be magmatic rather than metamorphic (Chapter 3). The rock is concordant to the planar fabric within the FD 4 quartzofeldspathic gneiss which has been metamorphosed under conditions transitional to upper amphibolite facies of regional metamorphism. However, the gneiss (FD 4a) and the FD 7 granite both show relatively weakly developed metamorphic grain orientation (Chapter 3). In the case of the pluton, the weak fabric may be ascribed to the lack of micaceous minerals (Vernon and Flood, 1988) also perhaps to late-kinematic emplacement.

6:3 Comparative geochemistry of the granitoid units

One of the most distinct compositional variations displayed by the four granitoid suites is the abundance of SiO_2 which is fairly high (> 73 wt%) in the Kinsho granite and in most of the analyses from the Altuntu granite. In contrast to the slightly wider range and lesser values of silica (approximately 60 - 69 wt%) in the Sebbeto tonalite and the Bergudda complex. This distribution of silica values is contrasted with that of alumina values which is relatively lower in the high SiO_2 Kinsho granite (8 - 12 wt%) and to a lesser extent in the Altuntu granite (12 - 15 %), in comparison to the less silicious Sebbeto tonalite and the Bergudda complex in which alumina values are higher (13 - 19 %).

The Bergudda complex has the highest values of total alkalis (7.70 - 10.45 %, Na_2O + K_2O). This high proportion of total alkalis and the slight under-saturation with respect

to silica is expressed in the CIPW norm (Table 6.5a) by the appearance of olivine in one of the analyses and the low value of normative quartz in the core of this pluton.

As is expected from the near absence of K-feldspar and the predominance of more calcic plagioclase (Chapter 3) alkali values expressed as the sum of K_2O and Na_2O are lowest (3.07 - 6.18 wt%) in the Sebbeto tonalite (Table 6.2). Intermediate values between 7.03 and 8.89 (wt%) are shown by the two other granitic units (Tables 6.3 and 6.4). The Kinsho granite is also unique in having very low contents of CaO (<0.5 wt% in 63% of the samples analyzed) and MgO (<0.25wt% in all but one sample).

The trace element compositions of the four granitoid units are shown in Tables 6.6 to 6.9. Among the LIL elements analyses for Ba, Rb and Sr, Sr has the highest abundance in the silica poor Sebbeto tonalite (Table 6.2). In contrast Rb is relatively more abundant in the megacrystic Altuntu granite (Table 6.3) and the peralkaline Kinsho granite (Table 6.4). The highest barium values are shown by the charnockitic core of the Bergudda granitoid complex (Table 6.5a). However, the LIL element distribution within this complex may also be influenced by the granulite facies metamorphism and subsequent retrogression as discussed above.

For the other three granitoid units, the elemental ratios Rb/Sr and Ba/Sr are relatively lower in the tonalite, in which Ba/Rb values are significantly higher (Table 6.2). These ratios imply that this body is the least - contaminated and most juvenile of all the four plutonic units considered in this chapter.

The large - ion high - field - strength elements Nb, Y and Zr are generally of lower absolute abundance in all the four granitoid units. Nb values are significant (> 10 ppm)

only in analyses from the Kinsho granite and the Bergudda complex and two of the analyses from the Altuntu granite. This distribution may in part be due to the low detection limit of the element but also, as will be shown later, due to the different tectonic settings i.e. magma source and degree of contamination of the two granitoid groups (Pearce and Gale, 1977, Pearce et al. 1984).

Y and Zr show more or less similar distribution patterns to that of Nb except for slightly higher values, than that of Nb, (up to > 20 ppm) in the calc-alkaline Sebbeto tonalite. These two elements are also detectable (> 10 ppm) in all analyses from the Altuntu granite. Relatively higher values of Y are, as that of Nb, from the more peralkaline Kinsho granite and the Bergudda complex.

6:4 Classification of the granitoid units

As shown in Table 6.2 in Appendix II, all samples from AD 1 tonalite are hypersthene normative except for two samples (SG 4932 and SG 4971) which are corundum normative. Samples from FD 5 granite have both hypersthene and corundum as normative minerals except for one sample (SG TA1) which has higher values of normative hypersthene than the rest (Table 6.3). The Kinsho granite (FD 7) is different from all the other three plutons in its peralkalinity (Fig. 6.4). This shows in the presence of aegirine as a normative mineral in 50 % of the analyses. All samples from this pluton also have hematite and ilmenite in their norms and most (63%) of the samples are wollastonite normative. On the basis of the proportions of normative, orthoclase, albite and anorthite (Oconner, 1964; Barker, 1979), analyses of the Sebbeto tonalite (AD 1) fall within the

tonalite field where as those from the other three plutons plot within the granite field (Fig. 6.2). However, this classification cannot distinguish the relatively silica-poor, dark core of the Bergudda complex, which as discussed in Chapter 3 may be classified as a hypersthene-bearing quartz monzonite on the basis of its mineralogy (Streckeisen, 1976).

All the four granitoids studied from the Sagan - Afelata area are sub -alkaline. On an AFM plot (Fig. 6.3) the two easterly granitoids, the Sebbeto tonalite and the Altuntu granite show calc-alkaline trends of differentiation, while the remaining two granites show mainly tholeiitic character.

The A/CNK [A = Al_2O_3, C = CaO, N = Na_2O, K = K_2O (molar)] values are relatively high (> 1) for the calc-alkaline granitoids in comparison to the lower values for the Kinsho and Bergudda granites (approx. <= 1). The A/CNK vs A/NK plot (Fig. 6.4) shows that the calc-alkaline granitoids are peraluminous. This is also seen in the appearance of corundum in the norms of some of these granitoids (Tables 6. 2 and 6.3). The other two granitic units are peralkaline to metaluminous. The peralkalinity of one of these, the Kinsho granite, is as shown above expressed by the appearance of the alkali pyroxene aegirine in the modal and normative (Morimoto, 1989) mineralogy in half of the analyses (Table 6.4).

As is seen in the Na_2O versus K_2O plot of the four granitoid units (Fig. 6.5) all can be categorized as I-type granites of White and Chappell (1983). Some samples from the megacrystic (Altuntu) granite (FD 5) fall within the A-type granitic field, however their field of distribution overlaps the field of I-type granites. As will be shown below this granite is an I - type cordilleran calc-alkaline granite.

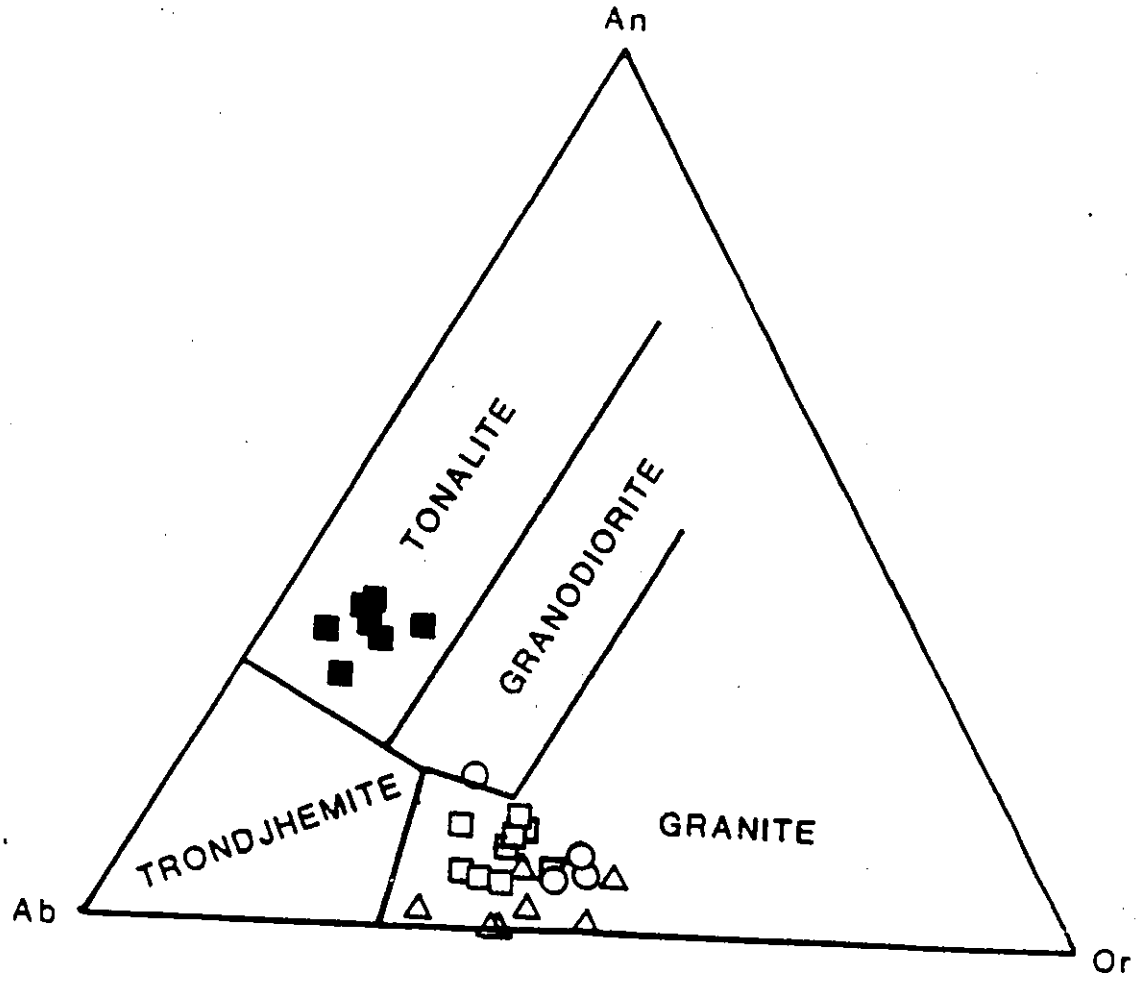

Fig. 6.2 Normative classification (Oconner, 1964, Barker, 1979) of the four granitoids studied from the Sagan-Afelata area.

Symbols: filled squares Sebbeto tonalite (AD 1),
open squares Bergudda complex (FD 8),
open triangles Kinsho granite (FD 7)
open circles Altuntu granite (FD 5).

Note these symbols are used in all diagrams in this Chapter.

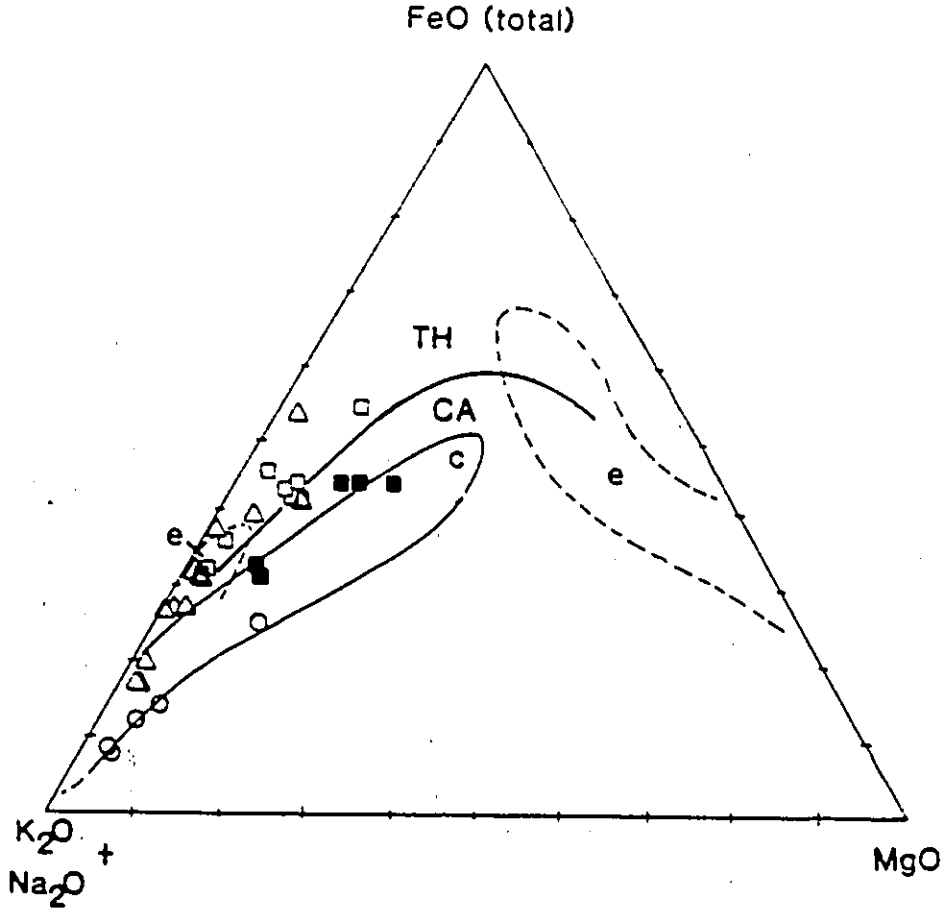

Fig. 6.3 AFM diagram of the four granitoids of the Sagan - Afelata area. Tectonic fields (c compressional i.e. subduction related, e extensional, are from Petro et al., 1979). Symbols as in Fig. 6.2.

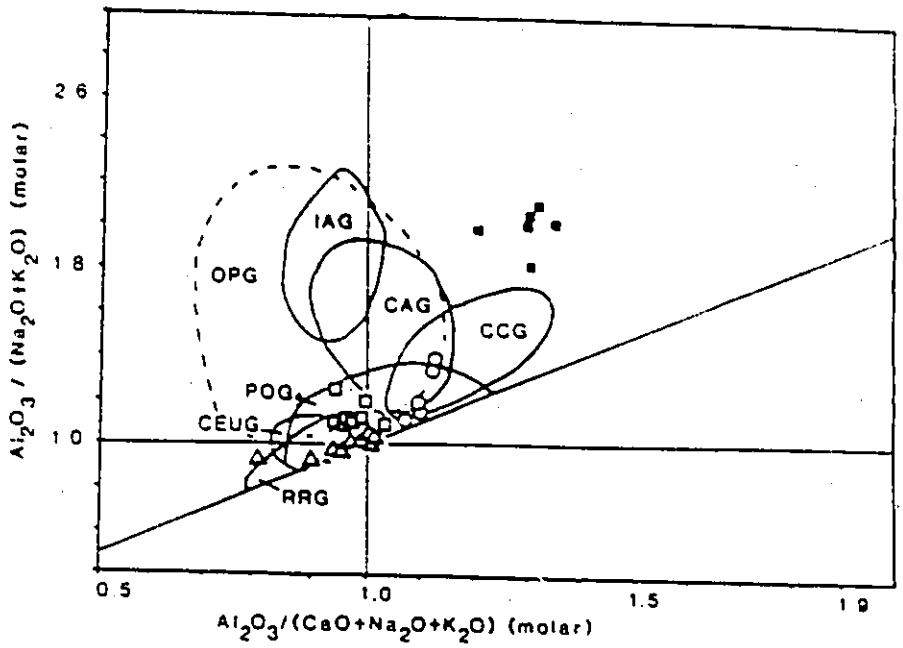

Fig. 6.4. A/NK vs A/CNK plot for the studied granitoids. Tectonic fields (IAG island arc granitoid, OPG oceanic plagiogranites, CAG continental arc granitoids, CCG continental collision granitoids, POG post orogenic granitoids, CEUG continental epirogenic uplift granitoids, and RRG rift related granitoids; are after Maniar and Picolli, 1989). Symbols as in Fig. 6.2.

Most analyses from the Sebbeto tonalite (AD 1) and the Bergudda complex (FD 8) plot outside of all the fields shown in this diagram. In the first case (AD 1) the Na_2O/K_2O ratio is high, which may be explained by the high proportion of sodic plagioclase (oligoclase) and a very low content of K feldspar. The samples from the Bergudda complex (FD 8) with high Na_2O values have on the contrary an approximate Na_2O/K_2O ratio of unity. This ratio may reflect the composition of the high temperature soda - rich K feldspar now seen as perthitic intergrowth of about equal amounts of sodic plagioclase and K feldspar (Chapter 3).

As seen in a brief summary of the main characteristics of these granitoids (Table 6.10) the Kinsho granite and the Bergudda complex with their largely perthitic K feldspar content, alkaline nature and possibly late-tectonic emplacement history can be classified as the A - type (anorogenic or post orogenic) granites (Collins et al. 1982, Whallen et al 1987, Rogers and Greenberg, 1990). This is particularly true of the peralkaline Kinsho granite which has the characteristics of the late - to post - orogenic granites of the Pan-African of west Africa (Boullier et al., 1986, Liegeois and Black, 1987), Egypt (Abdel-Rahman and Martin, 1990) and the Arabian shield (Harris and Marriner, 1980, Jackson 1986).

6:5 Tectonic setting of the granitoid units

The four granitoids of the Sagan - Afelata area can broadly be classified into two broad tectonic groups based on the relative contents of the trace elements Rb, Y and Nb (Fig. 6.6, Pearce et al. 1984). The two easterly suites (the Sebbeto tonalite and the Altuntu

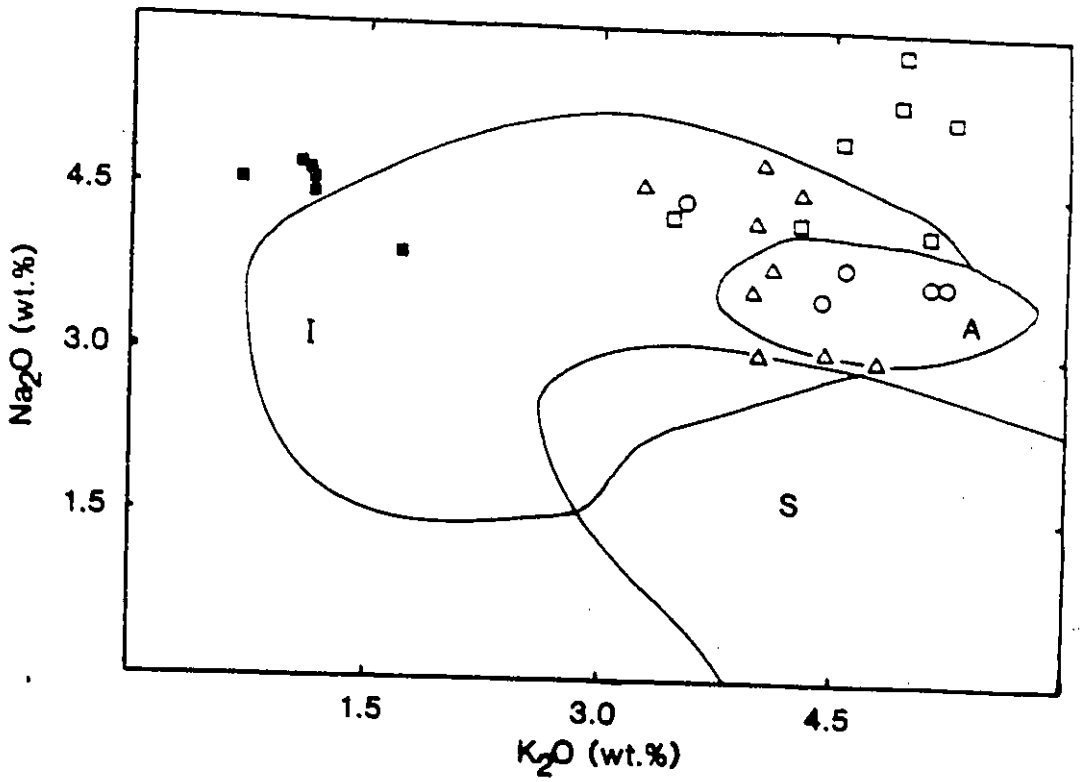

Fig. 6.5. Classification of granitoids of the Sagan-Afelata area on the basis of the Na_2O vs Ka_2O plot. fields after White and Chapell, 1983). (I) I-type, (A) A-type, (S) S type granitoid. Symbols as in Fig. 6.2.

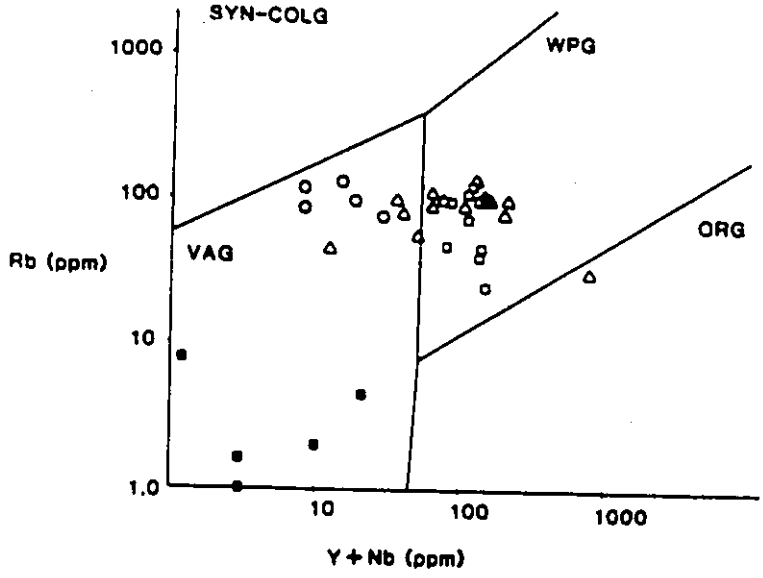

Fig. 6.6 Tectonic settings of the granitoids of the Sagan-Afelata area on the basis of Rb vs (Nb + Y) discriminant diagram of Pearce et al., (1984). Abbreviations: (syn-colg.) syn-collisional granitoids, (WPG) within-plate granitoids, (ORG) oceanic ridge granitoids, (VAG) volcanic arc granitoids. Symbols as in Fig. 6.2.

granite) have geochemical characteristics of volcanic arc granites and the remaining two granites those of within - plate (intracontinental or intraoceanic) granites.

Maniar and Piccoli (1989) proposed a discrimination scheme that classifies granitoids into seven tectonic groups (corresponding to seven tectonic settings) based on the major element chemistry only. Although the method is purely empirical and based on data acquired from Phanerozoic granitoids, it has been applied by the authors to Proterozoic granitoids with apparent success.

In this work, the boundaries between the fields of granitoids of different tectonic setting were approximately delineated (by the present author) from the original plots of the data compiled by Maniar and Piccoli (1989). Following the scheme, the K_2O vs SiO_2 plot (Fig. 6.7a) shows that none of the granitoids from the Sagan - Afelata area are oceanic plagiogranites. By combined use of the Al_2O_3 vs SiO_2 (Fig. 6.7b), [FeO (T)/FeO (T) + MgO] vs SiO_2 (Fig. 6.7c) and two other plots based on recalculated values from the traditional AFM and ACF (Figs. 6.7d and 6.7e respectively), the four granitoids of this area can be divided into two broad groups. The first group consists of the Sebbeto tonalite and Altuntu granite which are related to a continental arc or island arc setting or a continental collision environment. The other two granites constitute the second major group related to a continental extensional environment, i.e. related to epirogenic uplift (CEUG) or continental rifting (RRE). These two major tectonic groups are also distinct both from the trace element (Fig. 6.6) and the AFM-based discriminant plot (Fig. 6.3), although analyses from the Kinsho granite show some dispersed distribution.

The Bergudda and Kinsho granite (the second group) are, according to their TiO_2 vs

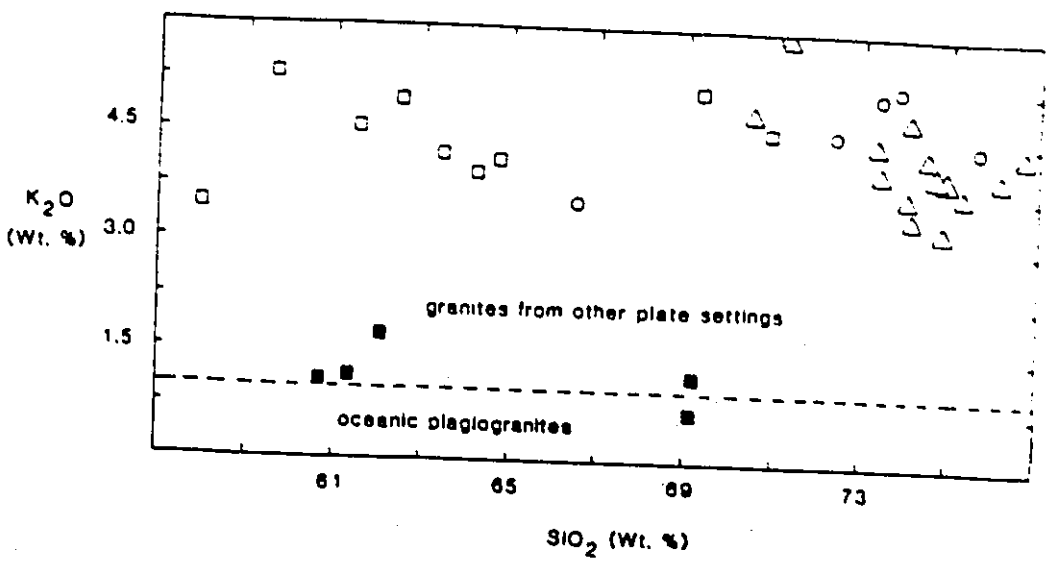

Fig. 6.7a Tectonic setting discrimination plot of the granitoids of the Sagan-Afelata area on the basis of the K_2O and Na_2O contents. Fields after Maniar and Picolli. (1989). Symbols as in Fig. 6.2.

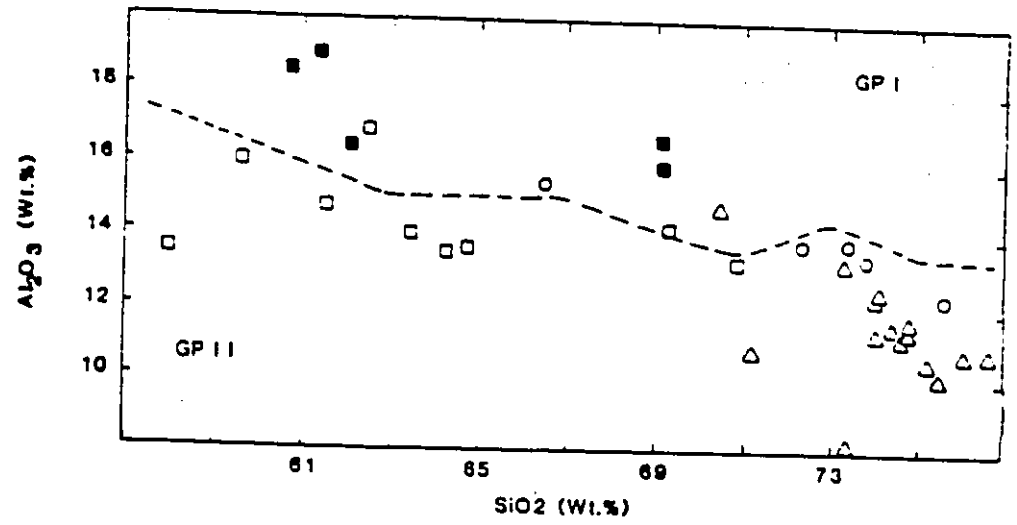

Fig. 6.7b Discrimination of the granitoids of the Sagan Afelata area into GP I (orogenic granitoids i.e. *IAG*, CCG and POG) and GP II (anorogenic granitoids i.e. RRG, CEUG and OP (oceanic plagiogranites) on the basis of the of Al_2O_3 Vs SiO_2 plot. see Fig. 6.4 above for the other abcreviations. Fields approxmately delineated from plots by Maniar and *Picolli* (1989). symbols as in Fig. 6.2.

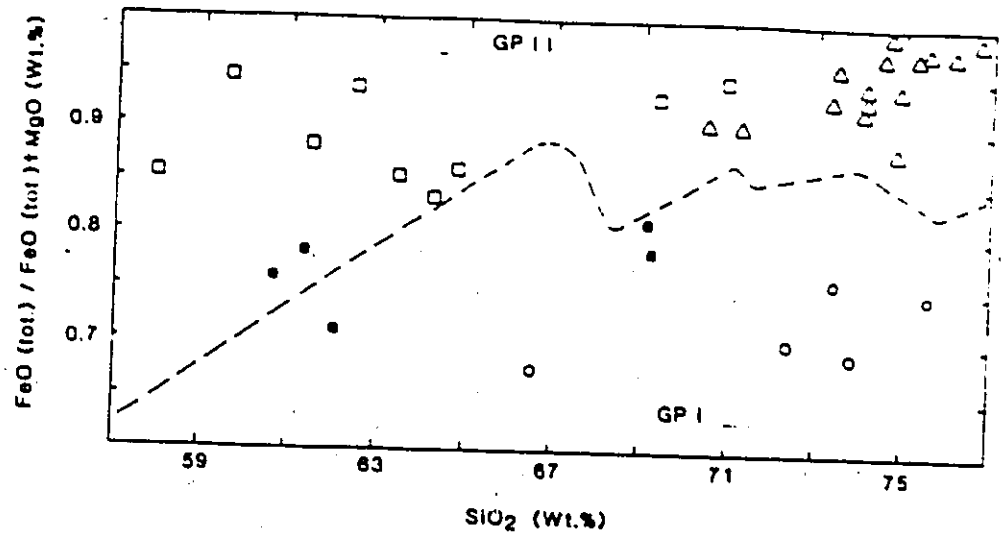

Fig. 6.7c Discrimination of the granitoids of the Sagan Afelata area into GP I (orogenic) and GP II (anorogenic) granitoids on the basis of FeO (total), MgO and SiO_2 values. see Fig. 6.4 above for the abbreviations. Fields approxmately delineated from plots by Maniar and Picolli (1989). symbols as in Fig. 6.2.

From AFM

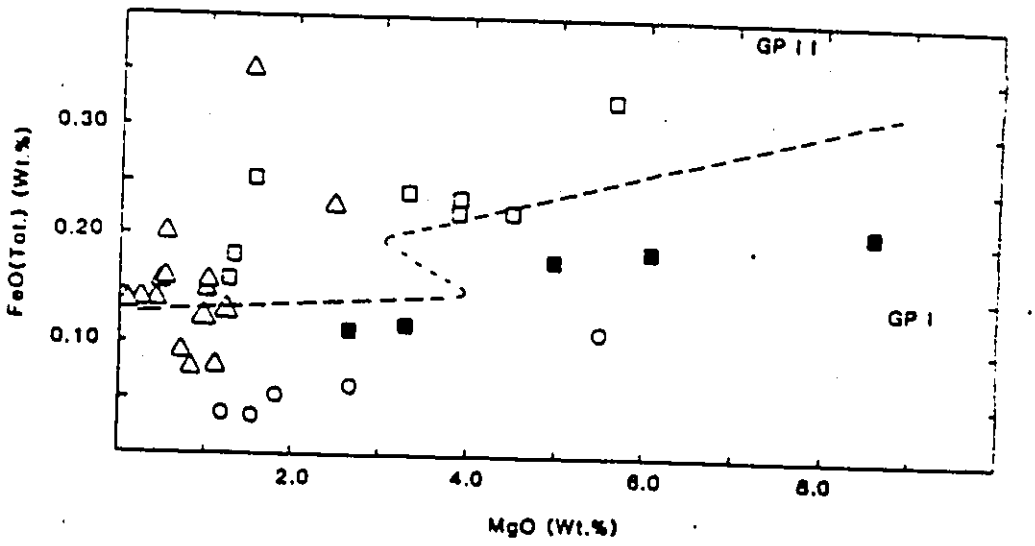

Fig. 6.7d Discrimination of the granitoids of the Sagan Afelata area into GP I (orogenic) and GP II (anorogenic) granitoids on the basis of FeO (total) Vs MgO, values recalculated from the AFM. Fields approxmately delineated from plots by Maniar and Picolli (1989). abbreviations as in Fig. 6.4 above. symbols as in Fig. 6.2.

SiO_2 (Fig. 6.7f) and also molar A/NK vs A/CNK based plot (Fig. 6.4), are intrusives related to continental rifting rather than to epirogenic uplift.

As shown above (Fig. 6.4), the analyses from the calc - alkaline arc - related granitoids (Sebbeto and Altuntu) plot on the A/NK vs A/CNK plot in the peraluminous field. In terms of the fields of tetonic settings, the analyses from the Altuntu granite plot in the region of overlap between continental collision and continental arc related granitoids $1.05 < A/NK < 1.15$; Maniar and Piccolli, 1989). The sheeted nature of emplacement along a tectonic boundary (for over 90 km) between two distinct domains (AD and FD), and the K feldspar megacrystic texture (Pitcher, 1983) and the high SiO_2 content of the Altuntu granite are in favour of a collisional origin for this granite.

However, the major and trace element geochemistry of this granite is not similar to that of collisional granites from the Himalayas (Vidal et al. 1982, Dietrich and Gansser, 1981) or the Hercynian of south western Europe (Harris et al. 1984). Compared to these collisional ganites, the Altuntu granite is slightly poorer in Al_2O_3 and K_2O and richer in Fe_2O_3 (T), MgO, CaO, TiO_2 but has approximately comparable values of Na_2O, and MnO. The Altuntu granite is also relatively enriched in Ba, Sr, and Zr but much poorer in Rb. Consequently it has lower Rb/Sr, K/Rb and Rb/Zr ratios.

Furthermore, on the basis of the relative proportions of the trace elements, Rb, Y and Nb (Pearce et al. 1984, Fig. 6.6) discriminant diagram and a Rb/Zr vs SiO_2 plot (Fig. 6.8, after Harris, 1984) used to distinguish Himalayan type syn - collisional leucogranites from volcanic arc granites, the analyses from the Altuntu granite plot in the field of volcanic arc - related granites. The monzogranitic mineralogy, the type of enclaves (Table 6.1) and

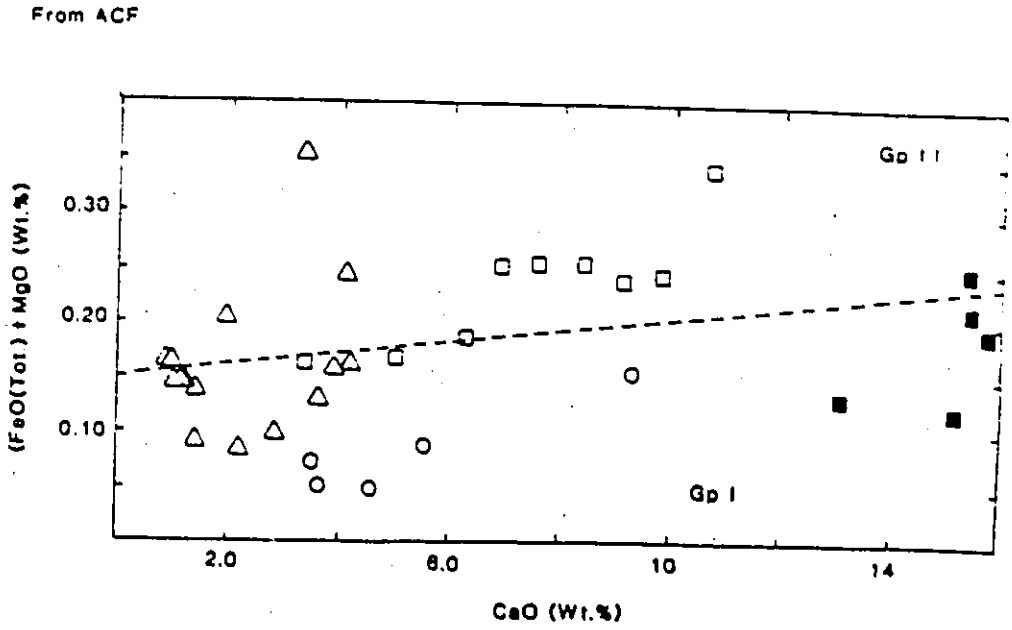

Fig. 6.7e Discrimination of the granitoids of the Sagan Afelata area into GP I (orogenic) and GP II (anorogenic) granitoids on the basis of FeO (total) and MgO vs CaO values recalculated from the AFM. Fields approxmately delineated from plots by Maniar and Picolli (1989). abbreviations as in Fig. 6.4. symbols as in Fig. 6.2.

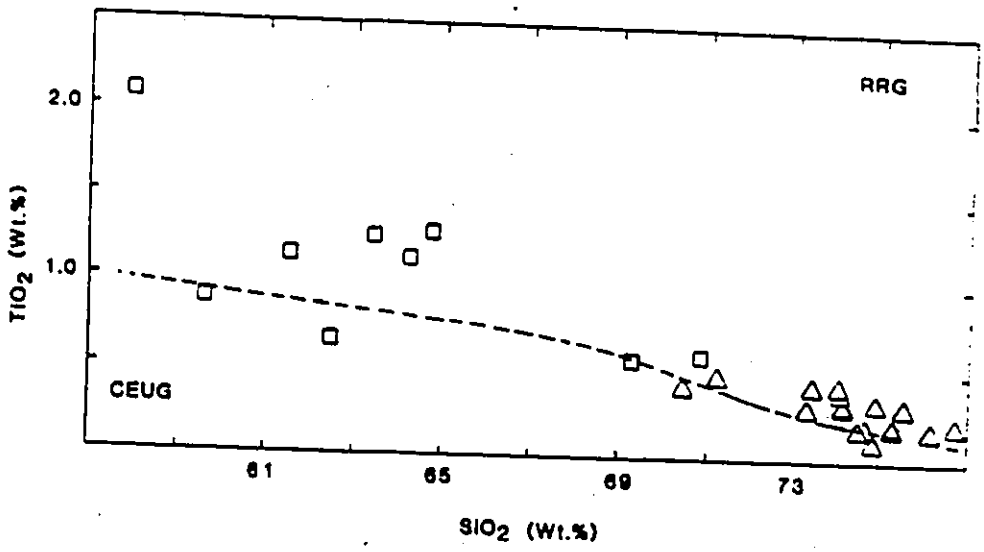

Fig. 6.7f Specific tectonic settings of the anorogenic granitoids (GP II) of the Sagan-Afelata area into RRG (rift relatd) and CEUG (continental epirogenic granitoids). Fields approxmately delineated from plots by Maniar and Picolli (1989). symbols as in Fig. 6.2.

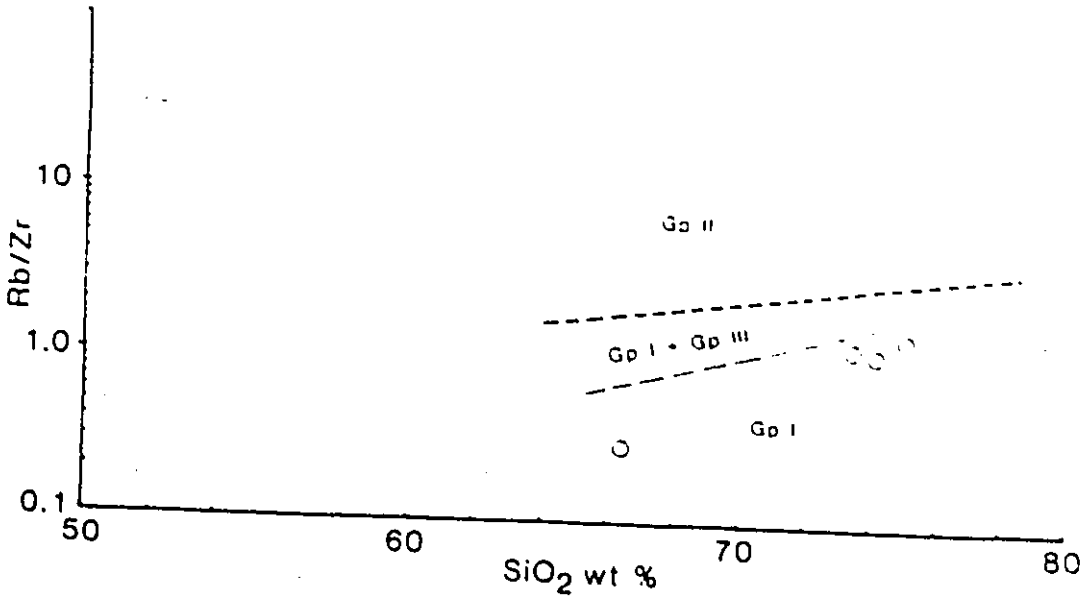

Fig. 6.8 Discrimination diagram used to distinguish the Altuntu granite from collisional granites (GP II) (GP I, precollison calc-alkaline) and (GP III, post collision calc-alkaline) granites. fields from Harris (1984) fine broken line added to original to differentiate GP I from the region of overlap with GP III granites.

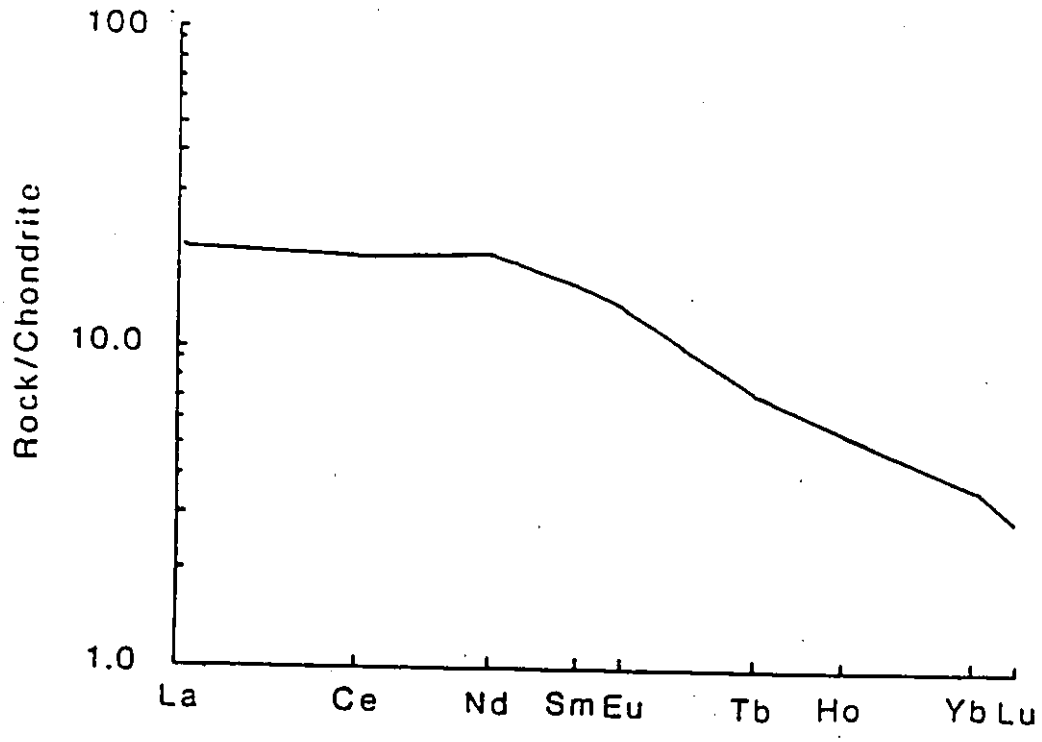

Fig. 6.9 Chondrite normalized REE pattern for a sample of the Sobbeto tonalite. Note the flat pattern and the general low absolute abundance of REE.

the field it plots in on the A/CNK vs A/NK plot (Fig. 6.4), further suggest that this granite is a continental arc granite rather than a collisional or an oceanic island arc granite.

Analyses from the Sebbeto tonalite plot in Fig. 6.4 outside all of the delineated fields. According to Maniar and Piccolli (1989) this rock may be considered as a continental collision granite because of its high A/CNK (> 1.15) values. However, this tonalite also has no lithologic, petrographic or geochemical similarity with known continental collision granites. As discussed above it has low K and Rb contents more typical of granitoids of non-crustal protoliths and relatively high Ba values suggestive of a mantle derived volatile component (e.g. Witt and Swager, 1989). This is also consistent with the relatively low Rb/Zr, Rb/Sr ratios and total REE contents (< 20 times that of chondrite values for the LREE) and relatively flat REE patterns (see also Fig 6.9) which suggest that it is juvenile i.e. derived from a more primitive mantle melt rather than an anatectic product of a recycled crustal material. The observed high peraluminosity of this rock is however not understood.

Table 6.7 is a preliminary list of the probable tectonic settings and the temporal relations of the four granitoid units to the dominant tectonothermal (collisional) event (chapter 7) in the Sagan - Afelata area, on the basis of the geochemical data.

6:6 Classification of the volcanic unit

The fine grained varieties of the Hiddi Asasu amphibolite appear from both the low SiO_2 values (Table 6.6 in Appendix II) and the alkali - silica based classification (Fig.

Table 6.7 Probable tectonic settings of the four granitoids studied from the Sagan-Afelata area.

	Sebbeto tonalite (AD 1)	Altuntu granite (FD 5)	Kinsho granite (FD 7)	Bergudda complex (FD 8)
Temporal relation to main deformation (Harris et al., 1986)	Group I (pre-collision)	Group I (pre-collision)	Group IV ? (post-collision)	Group IV ? (post-collision)
tectonic setting based on trace elements (Pearce et al., 1984 etc.)	VAG	VAG	WPG	WPG
tectonic setting based on major elements (Maniar & Piccolli, 1989)	CCG	CAG	RRG	RRG
based on combined criteria	IAG	CAG	post-collisional rifting ?	post-collisional rifting ?

Abreviations

VAG volcanic arc granitoid
WPG within plate granitoid
CCG continental collision granitoid
CAG continetal arc granitoid
RRG rift related granitoid
IAG island arc granitoid

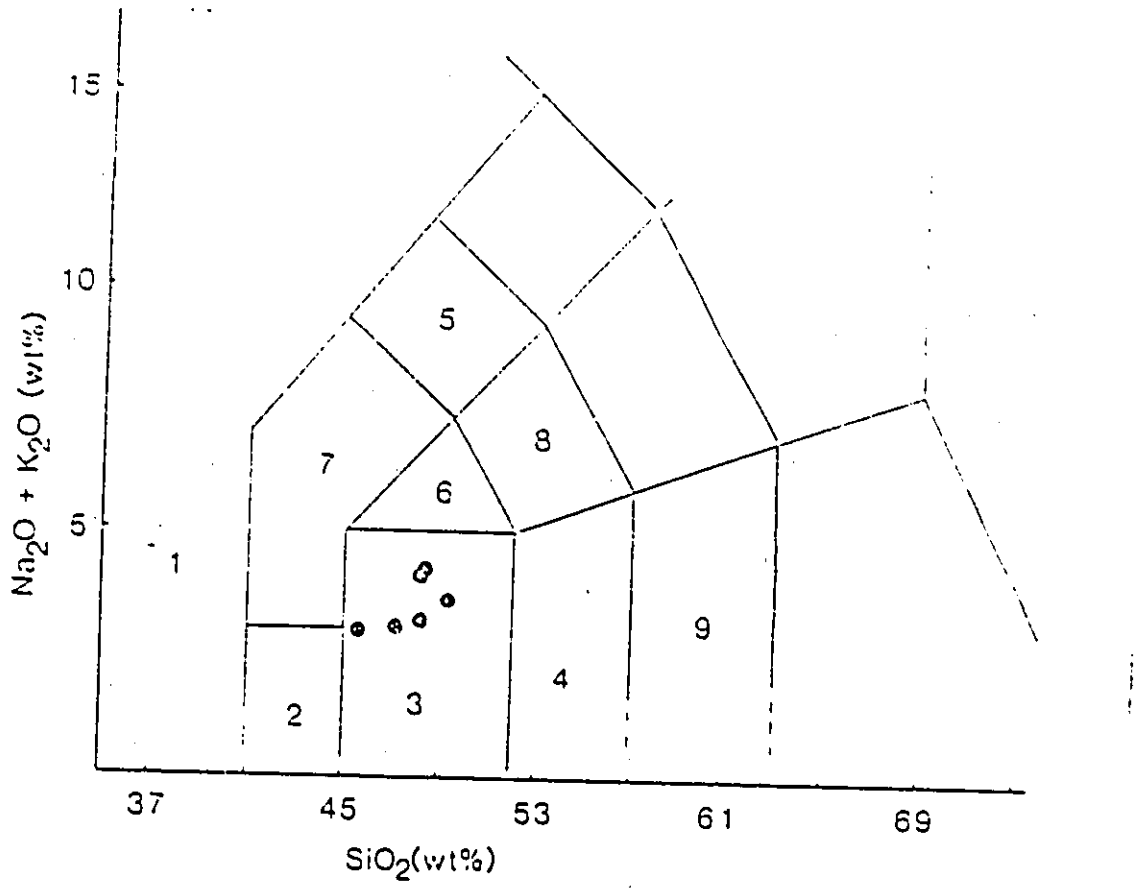

Fig. 6.10 Classification of the Hiddi Asasu amphibolite on the basis of the total alkali and silica values (after Le Bas et al., 1986). fields (2) picro-basalt, (3) basalt, (4) basaltic andesite, (6) trachy basalt etc.

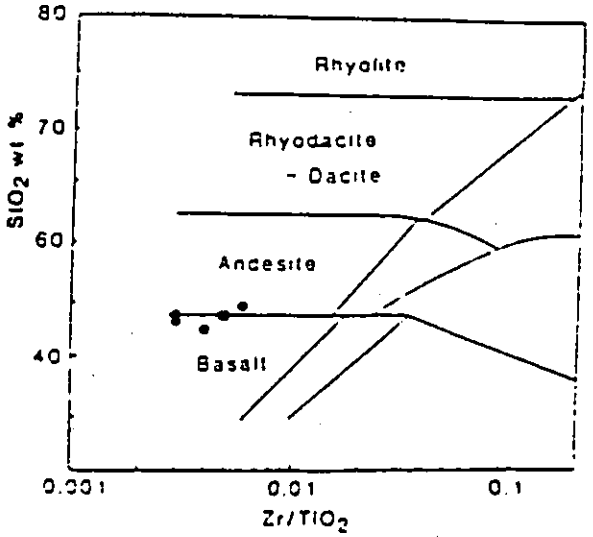

Fig. 6.11 Classification of the Hiddi Asasu amphibolite on the basis of Zr/TiO_2 Vs SiO_2 binary diagram. (after Winchester and Floyd, 1977).

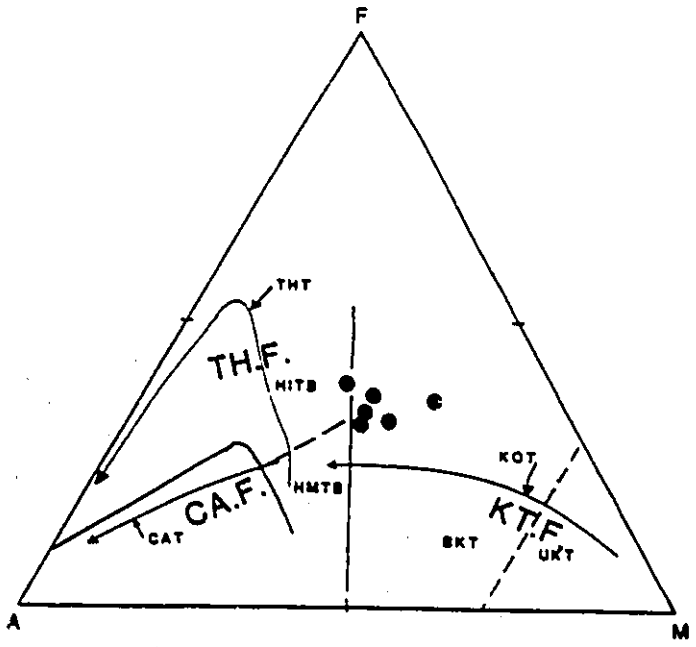

Fig. 6.12 Jensen (1976) plot for the Hiddi Asasu amphibolites. fields (F): KT.F. komatiitic, TH.F. tholeiitic, CA.F. calc-alkaline, UKT ultramafic komatiite, BKT basaltic komatiite, HMTB high magnesium tholeiitic basalt and HITB high iron tholeiitic basalt. Arrows show differentiation trends i.e. KOT komatiitic, THT tholeiitic and CAT calc-alkaline. A = Al_2O_3, F = FeO(T) - TiO_2 and M = MgO (in molar proportions).

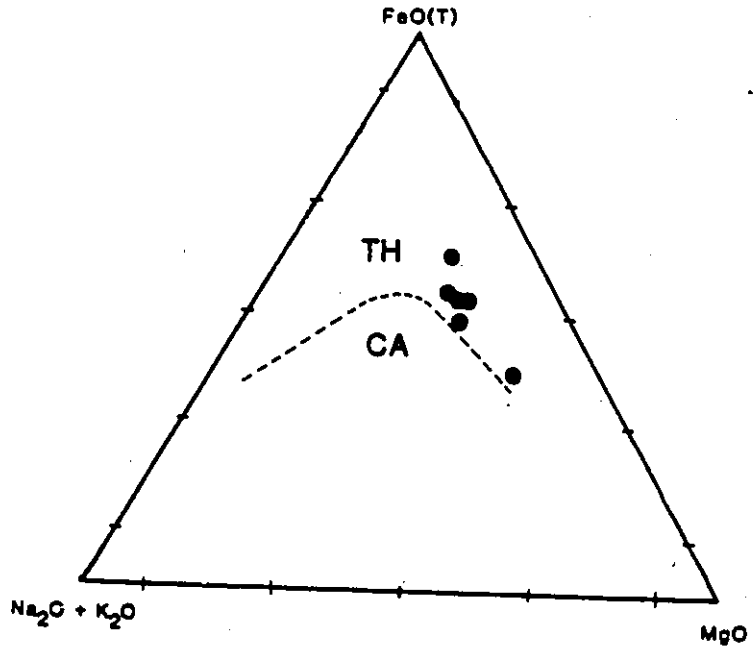

Fig. 6.13 AFM diagram for the Hiddi Asasu amphibolites. TH tholeiitic, CA calc-alkaline field. boundary curve from Irvine and Baragar (1971).

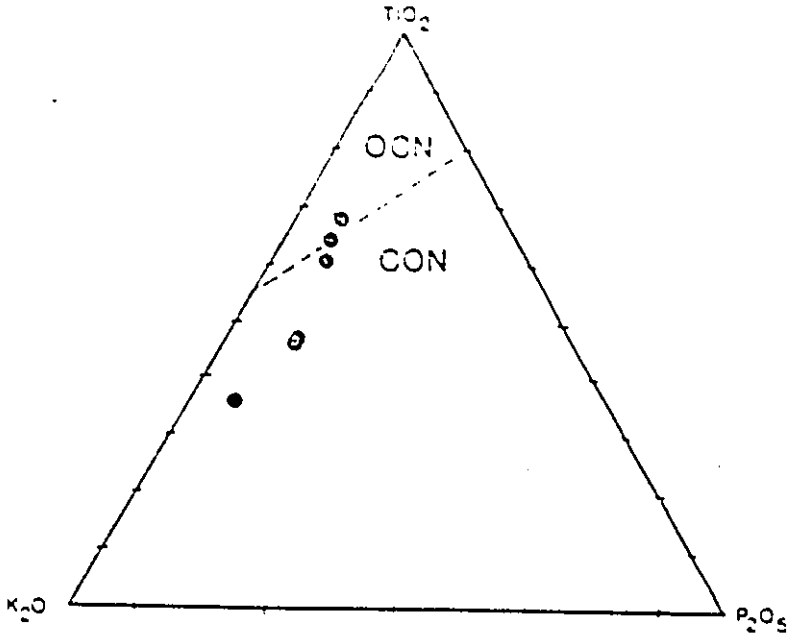

Fig. 6.14 K_2O-TiO_2-P_2O_5 ternary plot for analyses from the Hiddi-Asasu amphibolite. Fields OCN oceanic and CON conunental basalts, from Pearce et al. 1975. Note the plotting of most of the analyses within the CON field is due may be due to secondary enrichment in K than primary (see text for discussion).

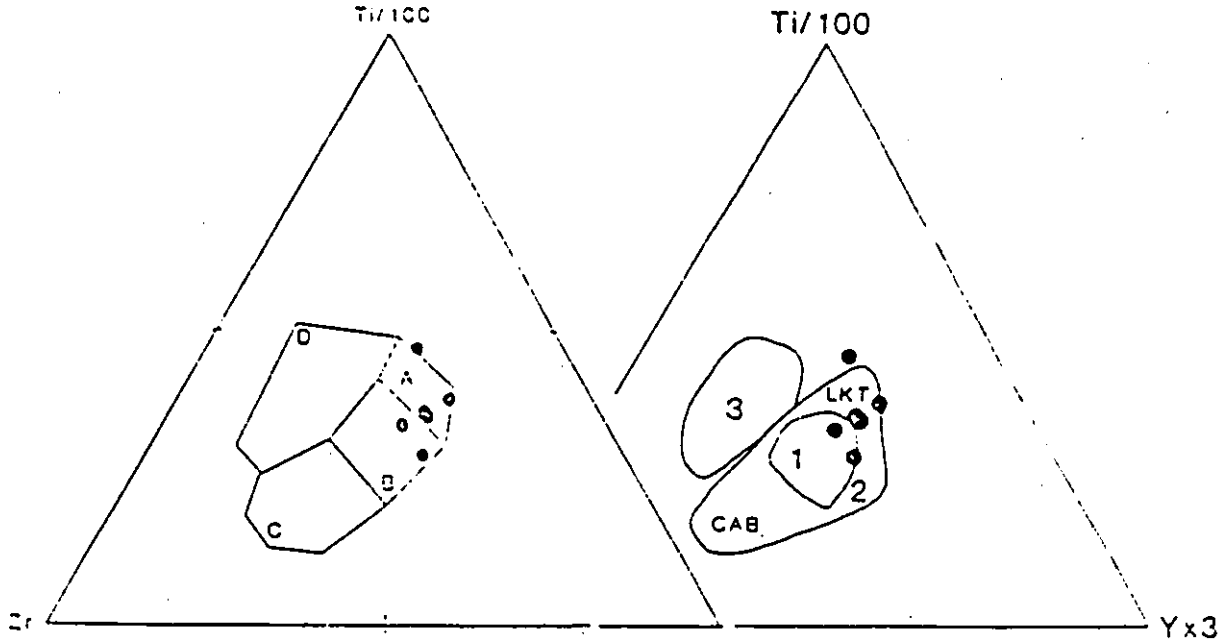

Fig. 6.15 Tectonic setting of the Hiddi Asasu amphibolite on the basis of (a) the Ti-Zr-Y ternary diagram of Pearce and Cann (1973) and (b) a modification of the same (Hull, 1987). fields: (A) low-K tholeiite, (B ocean floor basalt (C) calc-alkali basalt, and (D) within plate basalts. (1) ocean floor basalts, (2) island arc basalts (3) within plate basalts, CAB continental arc basalt, LKT low potash tholeiite.

6.10) of Le Bas et al., (1986), to have been derived from basaltic lava. This is also confirmed by the (Zr/TiO_2) - SiO_2 classification of volcanic rocks (Fig. 6.11) proposed by Winchester and Floyd (1977). Except for one of the analyses, that plots in the high-iron tholeiitic basalt (HITB) field, all of the analyses plot in the field of komatitic basalt on the Jensen (1976) plot (Fig. 6.12). However, these basalts show an iron (Fe) enrichment trend of differentiation shown by tholeiitic basalts on the AFM plot (Fig. 6.13).

6:7 Tectonic setting of the volcanic unit

On the K_2O - TiO_2 - P_2O_5 ternary diagram of Pearce et al. (1975), which is used to discriminate between oceanic and continental basalts (Fig. 6.14), four of the six analyses plot as continental basalts. However, on the basis of both the Ti - Zr - Y discriminant diagram (Pearce and Cann, 1973) and a modified version of the same diagram (Hull, 1987) , Figs. 6.15 and 6.15b respectively, four of the analyses plot as low K tholeiites. The remaining two analyses plot in the field of ocean floor basalts, but none of the analyses plot as within plate basalts (i.e. continental and ocean island basalts). This apparent contradiction between the tectonic setting indicated by the Ti - Zr - Y and K_2O - TiO_2 - P_2O_5 ternary diagrams, can be explained by a relative enrichment in K during metamorphism and also a slight loss of Ti to sea water. These processes are expected to result in the displacement of the plots of analyses of oceanic basalts into the field of continental basalts on this diagram (Pearce et al. 1975).

Two more diagrams used to discriminate between oceanic basalts of different tectonic

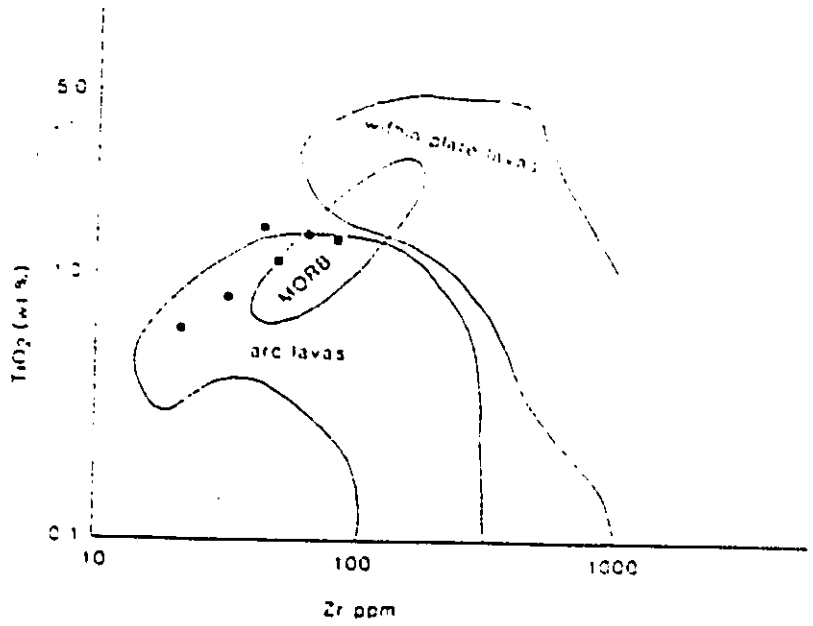

Fig. 6.16 Tectonic setting of the Hidh Asasu amphibolite on the basis of TiO_2 vs Zr plot. Field after [illegible] (1982). MORB mid oceanic basalt.

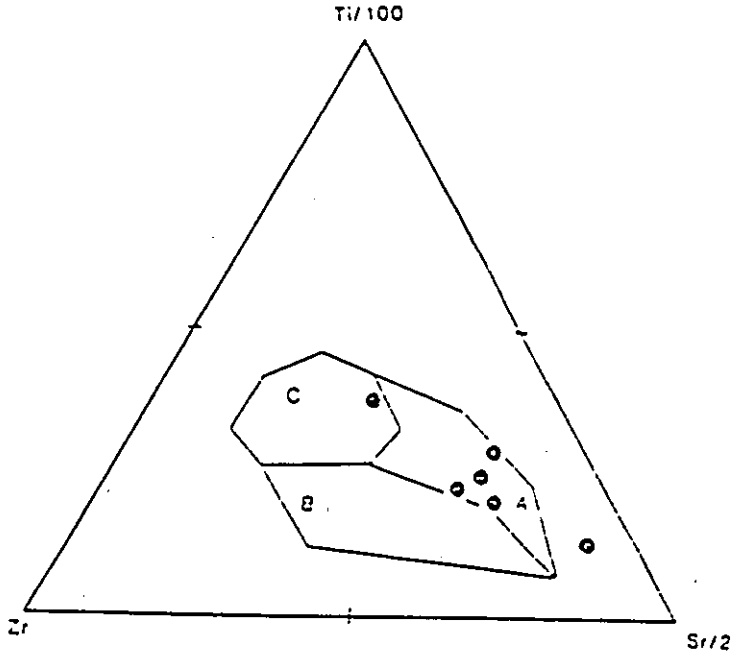

Fig. 6.17 Tectonic setting of the Hidh Asasu amphibolite on the basis of the Sr-Zr-Ti terna[illegible] diagram fields A low K tholeiites, B calc-alkali basalts, C ocean floor basalts, fields after Pearce and Cann (1973)

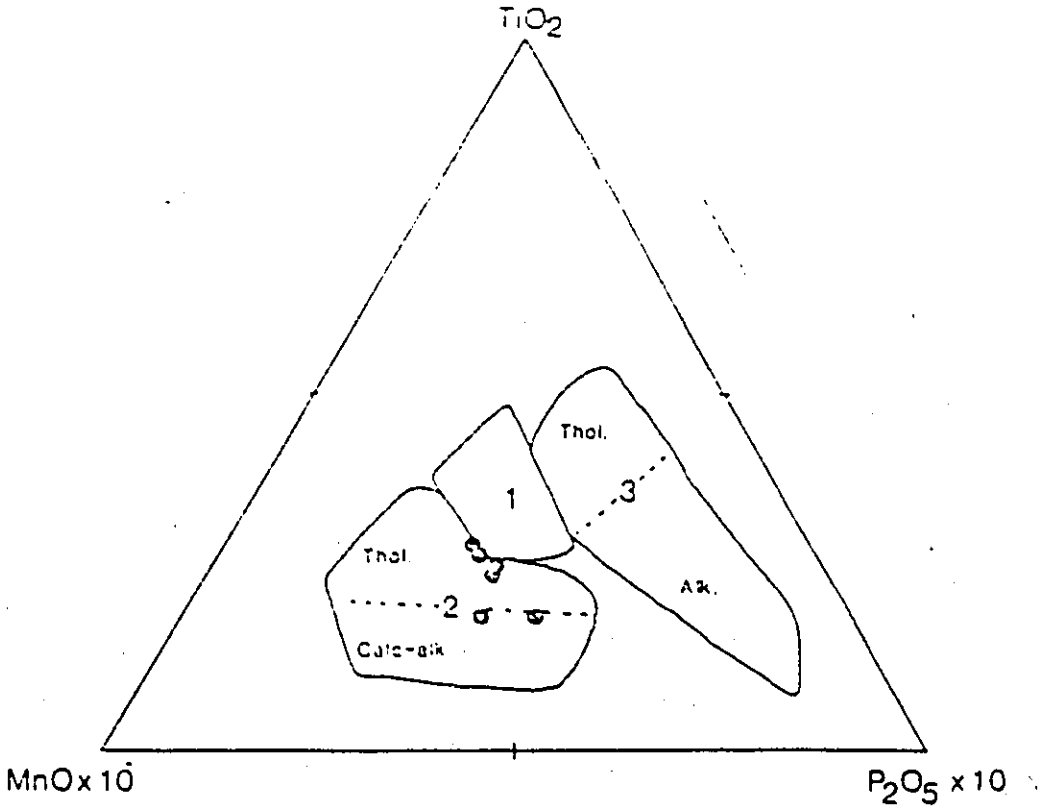

Fig. 6.18 Tectonic setting of the Hidi Asasu amphibolite on the basis of the K_2O-MnO-P_2O_5 ternary diagram, fields 1, ocean ridge basalt, 2, volcanic arc basalt, 3, oceanic island basalt, after Mullen, 1983., Thol. tholeiitic, Calc-alk Calc-alkaline, Alk. alkaline.

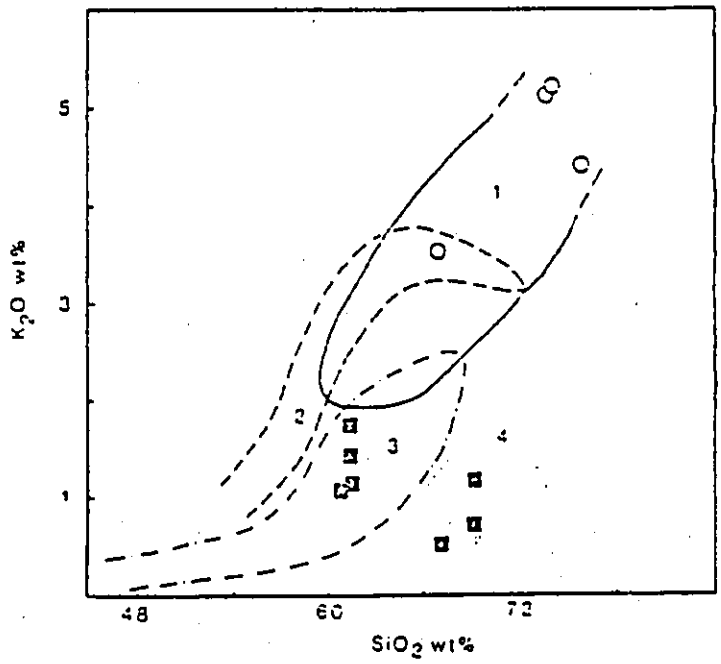

Fig. 6.19 A comparison of the K_2O-SiO_2 fields defined by the analyses from the Altuntu granite (circles) and the Sebbeto tonalite (filled squares) with that of Phanerozoic arc-related granitoids: (1) the Sierra Nevada batholith (Bateman and Doge, 1970), (2). granitoids of the Peruvian Andes (Atherton et al., 1979), (3). plutons of Solomon and New Britain island arcs (Chivas, 1978, Hine and Mason, 1978) and (4). granitoids from the Fiji arc (Gill and Stock, 1979).

settings, the TiO_2 - Zr (Fig. 6.16) and the Ti - Zr - Sr diagrams (Fig. 6.17) suggest that at least 4 or 5 of the six samples from the Hiddi Asasu amphibolite are from oceanic (island arc) settings. Furthermore, on the basis of a plot based on relative proportions of the oxides TiO_2, MnO and P_2O_5 (Fig. 6.18) used to distinguish the specific tectonic settings of basaltic and andesitic lavas of oceanic regions (Mullen, 1983), all the six analyses plot in the volcanic arc field. Thus, a combination of the classification and discrimination schemes considered above suggest that the protolith to the Hiddi Asasu amphibolite are low K tholeiitic basalts that were extruded in an island arc setting. It is also known that low K tholeiitic magmatism is characteristic of immature island arcs e.g. in the Aleutians, (Kay et al., 1982). Similar rocks are also known from the lower Pan - African of the Arabian shield (Roobol et al., 1983) and the Arabo - Nubian shield in general (Gass, 1981).

These results are in agreement with inferred tectonic setting of the adjacent plutonic rock, the Sebbeto tonalite (AD 1). This interpretation is also also supplemented by the subaqueous (marine) environment of extrusion indicated by the existence of pillowed volcanic rocks associated with deep marine sediments in amphibolites in continuity with the Hiddi - Asasu amphibolite in the Megaddo area to the immediate east (Chater, 1971, Kozyrev et al., 1985).

6:8 Discussion and conclusions

The geochemistry of both the Sebbeto tonalite and the Hiddi Asasu amphibolite of the Afelata domain indicate that the magmatism within this domain took place in an oceanic

island arc setting. This inference is also supported by the virtual absence of both lavas and plutonic rocks of more felsic compositions which are predominant in continental arc settings, both in this area and the neighbouring Adola area (Chater, 1971, Gilboy, 1970, Kozyrev et al. 1985, Kazmin, 1973). This Proterozoic island arc is in here referred to as the Adola arc, and the name Adola arc-basin is used to refer to the proto-arc (Adola) basin.

The Altuntu granite (FD 5) appears to have been emplaced as a sheet along a large scale discontinuity between the Afelata and the Fincha domains. The presence of blocks of Sebbeto tonalite within this granite in the Tatessa and Burka Daga areas in the northern outcrops suggest that this granite had engulfed the Sebbeto tonalite during its emplacement along this major structural break.

The Altuntu granite has higher $K_2O/(Na_2O + K_2O)$ and Rb/Sr ratios and higher but narrower ranges of SiO_2 values than the Sebbeto tonalite. It also has more biotite-rich enclaves that appear to be of sedimentary origin and is in general more evolved. It appears that it is at least partly derived from or contaminated by crustal rocks than the adjacent Sebbeto tonalite. Such crustal rocks could however include calc-alkaline rocks emplaced during the early accretionary stage of plate margin magmatism along the western edge of the Adola arc-basin as in some late Precambrian Pan-African terranes of the Nubian shield, e.g. Abdel-Rahman (1986).

A comparison of the K_2O - SiO_2 fields of both the Altuntu granite and the Sebbeto tonalite with some Phanerozoic arc-related plutonic rocks (Fig. 6.19) shows that the Altuntu granite has an analogue in the cordilleran Sierra Nevada batholith (Bateman and

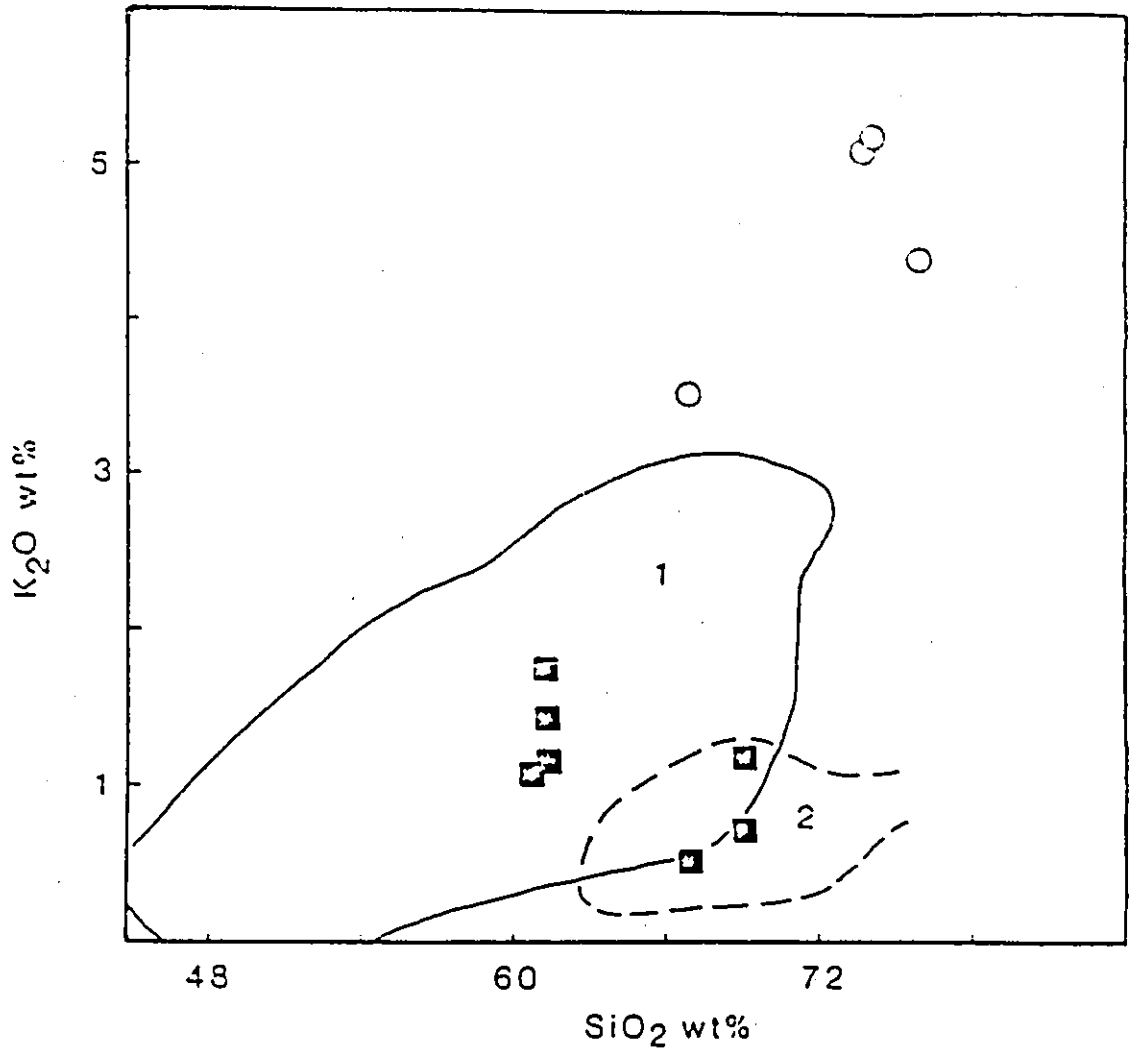

Fig. 6.20 A comparison of the K_2O-SiO_2 fields of the calc-alkaline plutonic rocks of the Sagan-Afelata area with that of similar granitoids of the Asir supersuite (Jackson, 19[illegible] in the Pan African of the western Arabian shield. fields (1) granodiorite and tonalite associations, (2) trondjehemite associations.

Dodge, 1970) and in the high K and high SiO_2 end member granitoids of the Peruvian Andes (Atherton et al., 1979). These data strengthen the above hypotheses and point out that perhaps the Altuntu granite was emplaced at a continental plate margin that may have in part been thickened by magmatic underplating. This implies that it may have atleast partially been derived from the partial melting of older magmatic rocks that underplated the continental margin during the early stages of the subduction process.

In contrast, the Sebbeto tonalite is similar in this aspect i.e. in terms of the K_2O-SiO_2 field, to the low-K island arc plutonic rocks of Solomon islands and New Britain (Chivas, 1978, Hine and Mason, 1978). The relatively more siliceous (> 65 wt% SiO_2), perhaps trondhjemitic members analyzed from the Sebbeto tonalite plot in the field of the island arc plutonic suites of Fiji (Gill and Stork, 1979).

As mentioned in the introduction (Chapter 1) and also in the general geology chapter (Chapter 2) the rocks constituting the Adola belt have much in common and are genetically related to similar rocks in the Arabo - Nubian shield. Fig. 6.20 compares the K_2O - SiO_2 fields of both the Altuntu granite and the Sebbeto tonalite with the accretion stage plutonic rocks of the "Assir super suite" of the western Arabian shield (Jackson, 1986, see also Ramsey et al., 1986 and Jackson et al. 1984). It is clear from this figure that the analyses from the Altuntu granite have higher SiO_2 values, are more potassic and fall outside the fields of the Asir super suite accretionary stage plutonic rocks of the western Arabian shield. However, most of the analyses from the Sebbeto tonalite fall within the field of "the granodiorite and tonalite associations" (Ramsey et al., 1986, Jackson, 1986) of the Asir supersuite. The high silica relatively more leucocratic varieties

are comparable with the "trondjhemite association" of the supersuite.

Both plutonic and volcanic rocks of the Assir supersuite are known to be products of predominantly oceanic island arc magmatism (see also Chapter 2) between 600 and 900 Ma (Stoeser and Camp, 1985, Jackson, 1986, Ramsay et al. 1986, Stoeser, 1986, Roobol et al., 1983). From the above and the late Precambrian age of the Sebbeto tonalite, it appears that both the Sebbeto tonalite and the Hiddi Asasu amphibolite of the Afelata domain developed in similar (oceanic island arc) tectonic settings within the same time range as the comparative juvenile Late Precambrian rocks of the Arabian shield. However, the above discussions and the above comparison (Fig. 6.19) suggest that the Altuntu granite is a more evolved and very likely more contaminated (Cordilleran) calc-alkaline pluton emplaced in a continental arc setting.

As discussed above, the other two plutonic units, the peralkaline Kinsho granite (FD 7) and the Bergudda complex (FD 8) have geochemical characteristics of within - plate granites. This is particularly true for the peralkaline Kinsho granite which has the characteristics of the late - to post - orogenic granites of the Pan-African of west Africa (Boullier et al. 1986, Liegeois and Black, 1987), Egypt (Abdel-Rahman, 1986, Abdel-Rahman and Martin, 1990, and the Arabian shield (e.g. Harris and Marriner, 1980, Jackson, 1986). The late-tectonic age assumed for this granite is based on its weak foliation and similarity to those Pan-African granites which were essentially intruded at a late stage in the Pan-African of the Arabo-Nubian shield (Stoeser, 1986, Jackson, 1986).

The Bergudda complex has a negative K_2O - SiO_2 correlation, different from the rest of the plutonic units. This aspect of its chemistry is similar to that of the

anorthosite/rapakivi anorogenic granite or the ring complex anorogenic granite classes of Rogers and Greenberg (1990). [see also discussion above on elemental distribution within this complex]. The apparent absence of anorthositic rocks in association with this pluton (at present erosional level) and lack of rapakivi textures further makes it similar to alkaline ring complexes of this scheme of classification.

The Bergudda complex is also similar to ring complex anorogenic granites of Rogers and Greenberg (1990) in having a negative relationship between Rb and K_2O. Furthermore, U/Pb ages obtained from the intermediate and inner core of the complex have an age difference of 10 Ma which suggests that the different parts of the complex were intruded as different pulses.

A direct comparison with rocks of the Pan-African basement of the Arabo-Nubian shield, in temporal, geochemical and lithological properties is deferred for the Bergudda complex until the above is resolved by further work. Some ring complexes show some similarities but most of these complexes have a reverse order zoning than seen in this complex.

CHAPTER SEVEN

SUMMARY AND CONCLUSIONS

Introduction

The first section of this chapter (7.1) summarizes the most important conclusions reached from the previous chapters and discusses the possible tectonic implications of the data. The second section (7.2) makes some constraints on any possible tectonic models that may be proposed to explain the evolution of the Sagan-Afelata area. This last part of the chapter also presents a simple tectonic model for late Proterozoic (Pan African) crustal accretion to the Precambrian crust of southern Ethiopia and suggests further work towards a complete tectonic model.

7:1 Summary and discussion

7:1:1 Lithology and stratigraphy

The rocks of the Sagan - Afelata area were previously (Kazmin, 1973) classified into the "lower complex" presumed to be Archean basement and the "upper complex" Late Proterozoic Red Sea fold belt related rocks (see Chapter 3, Table 3.1).

The data of this thesis show that the granitoid rocks Sebbeto tonalite (AD 1), Altuntu granite (FD 5), Kinsho granite (FD 7) and the Bergudda complex (FD 8) and the metavolcanic unit, Hiddi Asasu amphibolite (AD 2), are products of Late Proterozoic Pan-

African plate margin magmatism and subsequent late to post - collisional intracontinental plutonism. The granitic units which were previously (Kazmin, 1973) regarded as a part of the hypothetical "Archean basement" must be considered as time correlatives to units in the "upper complex" of Ethiopia, which is presumed to be of Late-Proterozoic age. Similarly all late-tectonic granites within the Sagan - Afelata area may also be regarded as related to this latest orogenic cycle (see 7.1.3 and 7.2 below) in the evolution of the Precambrian basement of southern Ethiopia.

It is also suggested although on the basis of the lithologic characteristics of paragneissic units, particularly the abundance of K_2O rich sediments (Chapter 3) and structural continuity with better studied areas in the Mozambique belt (Chapter 4), that all layered gneissic units within the Sagan - Afelata area are derived from Proterozoic clastic sediments, rather than reworked Archean basement as thought earlier (Kazmin, 1973, Kazmin et al., 1978).

7.1.2 Structure and metamorphism

In general this work shows that the structural and metamorphic grade of the rocks in the western half of the Sagan - Afelata area is similar to that of the rocks in the Hamar domain of the Omo project area (Davidson, 1983) while those of the eastern half of the Sagan - Afelata area resembles that of the Megaddo and Gariboro regions (Chater, 1971, Gilboy, 1970). Similarly there is a structural and metamorphic continuity between the Sagan-Afelata area and the Mozambique belt of northern Kenya (Key et al., 1989).

At least three phases of deformation (D_1'-D_1) to (D_3) have been distinguished in the

Sagan - Afelata area. The first (D_1'-D_1) is associated with early high grade regional metamorphism. Although limited in quantity, geobarometric data for the Sagan - granulite (SD 1) indicate mean metamorphic pressure of about 9 kbar has been reached. Although various hypotheses have been advanced for the origin of granulite facies terranes (see reviews by Newton, 1987), this suggests that the metamorphism was related to crustal doubling (Chapter 5). Such crustal doubling is commonly believed to be due to overthrusting of a continental margin by another continental margin during a Himalayan type continental collision (Newton and Perkins, 1982).

The high pressure metamorphism in the Sagan granulites (SD 1) is regarded as correlative with similar high grade event(s) related to collision and thrusting thought to be responsible for the evolution of the Mozambique belt to the south (Schackleton, 1977, Key et al., 1989, Muhongo, 1987). This suggestion is also in contrast to an earlier view (Kazmin, 1972) that the Sagan granulites (and generally "Konso gneiss", Kazmin, 1973) are relicts of an Archean basement within the Mozambique belt comparable to the "Watian" of the Ugandan basement (Hepworth and Macdonald, 1966). The extension of the Ugandan basement which is the northerly extension of the Archean Tanzanian craton (Bell and Dodson, 1981) is not apparent from both this work and an earlier work in the adjacent Omo project area (Davidson, 1983), whereas structural continuity between the Proterozoic basement of northern Kenya and that of southern Ethiopia has been demonstrated in chapter 4.

Amphibolite facies metamorphism and a nearly pervasive (except in the Sagan domain) dominantly N-S trending lineation (L_2) was overprinted on all rocks of the Sagan

- Afelata area, during the following D_2 major N-S folding, regardless of their tectonic positions. (D_2) is interpreted as signifying eastwesterly transpression and ductile crustal shortening across the Mozambique orogenic belt subsequent to the collision.

The third phase of deformation (D_3) is a weak, perhaps upper crustal warping about E-W axes and did not affect rocks in the Burji-Bokossa subdomain and the Sagan domain in the western half of the Sagan-Afelata area where retrograde granulite rocks outcrop. Structures of this phase are also unknown in areas farther west (Davidson, 1983), but are present in regions to the east (Chater, 1971, Gilboy, 1970). These E-W folds are spatially associated with the Adola belt and regions bounding it to the east (Gilboy, 1970) and the west (Gichile et al., 1986, Kiros and Kinetibeb, 1987). D_3 folds, as suggested in Chapter 4, may be related to longitudinal compressions of the orogenic belt due to late-collisional sublongitudinal crustal movements that may have taken place to the north.

7:1:3 Magmatism

As shown from the petrochemistry (chapter 6) the magmatic rocks studied are products of magmatism at island arc setting [the low K Sebbeto tonalite (unit AD 1) and the Hiddi-Asasu basalts (unit AD 2)] and of an intracontinental setting [(the Kinsho granite (unit FD 7) and the Bergudda complex (unit FD 8)].

The island-arc rocks represent a late Proterozoic (Pan African), subduction-related juvenile accretion to the Precambrian crust of southern Ethiopia at about 750 Ma. The intracontinental plutonic rocks, originated from later (post-accretion) partial melting of tectonically thickened crust (at about 530 Ma). The cordilleran type Altuntu granite (FD

5) represents plate-margin magmatism at a later stage of the accretionary process than the island-arc magmatism represented by the Sebbeto tonalite (unit AD 1) and the Hiddi Asasu amphibolite (unit AD 2). The Altuntu granite (unit FD 5) may, as pointed out in chapter 6, have been produced by partial melting of the magmatic underplate of the newly thickened, late Proterozoic crust of southern Ethiopia. This interpretation and the petrochemical and geochronological data show that early views (Kazmin, 1973, 1975; Kazmin et al., 1978 and Warden and Horkel, 1984) that regard these rocks as products of Archean granitization (units FD 5 and FD 7) and Archean orthogneissic (grey-gneiss) basement (unit AD 1) are erroneous.

7.2 A Model for late Proterozoic crustal accretion

In the following **conjectural** section a **largely speculative model** is presented to explain the sequence of events involved during late Proterozoic continental accretion to this portion of the basement of southern Ethiopia. The model is largely based on the general lithological characteristics, bulk chemistry (chapters 3 and 6), geochronology and spatial distribution and geological relations between magmatic units studied from within the Sagan-Afelata area. However, early studies particularly on the adjacent Adola belt (Gilboy, 1970; Chater, 1971; Kazmin, 1976; Kozyrev, 1985; Baraki et al., 1989) and also general models for the tectonic evolution of the Ethiopian basement (de Wit and Chewaka, 1981; Kazmin, et al., 1978) have been relied upon to some extent.

7.2.1 The model

The main assumption in the model is that subduction is to the west (Fig. 7.1) based on the disposition of the high-K Altuntu granite to the west of the low-K Sebbeto tonalite, both of which are calc-alkaline plutonic rocks considered to be generated above the same subduction zone. Similarly the Adola belt is regarded as an ophiolitic belt as previously propsed (Kazmin, 1976), but is interpreted as consisting of largely volcanic and deep marine sedimentary rocks of an arc complex, rather than a complete section of an oceanic floor as are many Phanerozoic ophiolites (Hamilton, 1988). According to the hypothetical model proposed, the sequence of tectonic events in the Sagan - Afelata area was perhaps as follows:

1. Basin opening (Fig. 7.1a): A basin in the northeastern segment of the Mozambique belt developed into a narrow oceanic basin (the Adola basin). The width of this basin may not have exceeded a few 100 to 1000 km because of constraints imposed by Proterozoic palaeomagnetic data (Piper, 1982; Kazmin, 1976) as well as the small volume of plutonic rocks emplaced during subduction, which indicates a relatively short lived period of underplating. The time at which this basin opened may not be older than 1070 Ma (the Rb-Sr whole rock date obtained from metasedimentary rocks in the eastern part of the Adola area by Chater (1971)). This age (1070 Ma) may record a metamorphic event prior to late Proterozoic plate-margin magmatism in southern Ethiopia.

2. Subduction (Fig. 7.1b) A west dipping subduction zone developed in the ocean and

underplated the Sagan - Afelata area from the east. Basic volcanic rocks, including the Hiddi Asasu amphibolite (unit AD 2) of this area (Fig. 1) and other similar rocks known in the Megaddo area of the Adola belt to the east (Chater, 1971, Kozyrev et al., 1987) were extruded and calc-alkaline plutons (Sebbeto tonalite, unit AD 1 and others in its chain, Chater, 1971 and chapter 3) were intruded at about 765 Ma in to the newly formed island arc crust above the subduction zone.

3. Collision (Fig. 7.1c and d) The collision that followed the closure of the Adola basin, was accommodated by easterly tectonic transport of the upper plate consisting of the supracrustal arc sequence and perhaps an oceanic crust at the leading edge of the arc complex. This took place on east verging (west dipping) thrusts in the Adola area such as deduced by Kazmin (1976) and described by Beraki et al., (1989). The closure and subsequent collision is envisaged as a two stage process:

(a) collision of the eastern continent with the Adola arc by the closure of the oceanic basin in front of the arc (Fig. 7.1c).

(b) subsequent impingement of the western continent by the newly accreted arc-continent complex (Figs. 7.1d and 7.1e) and subsequent continent-continent collision.

The later stage (b) may have involved the uplift of the remanent basin behind the arc on west verging thrusts contemporaneous with continued westerly subduction (Fig. 7.1d). This is favoured, rather than reversal of subduction due to the preceding arc-continent collision, which is the common phenomena during arc-continent collisions (Hamilton,

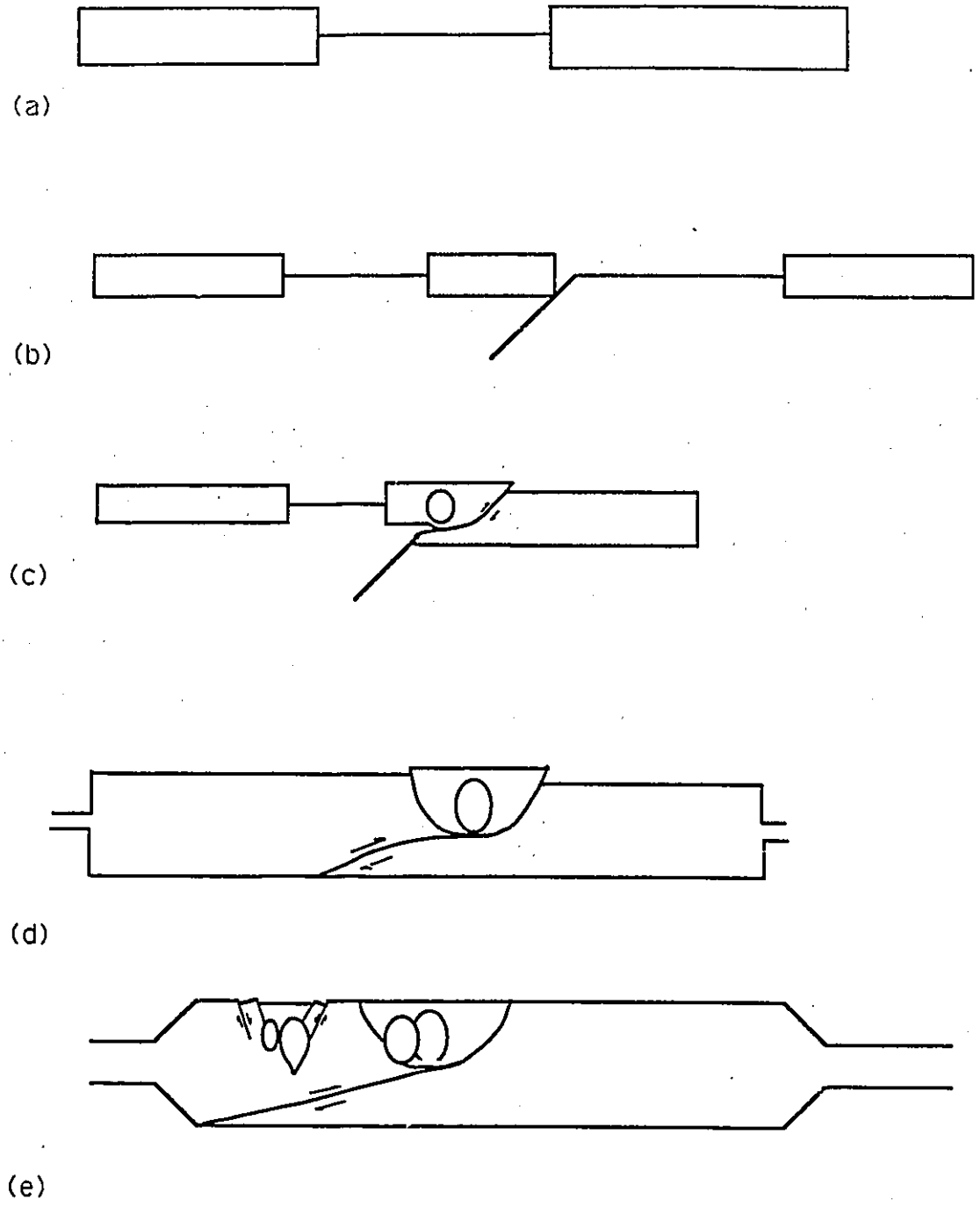

Fig. 7.1 Schematic diagram depicting the stages in the evolution of a part of the Precambrian basement of southern Ethiopia.

1988), because of its simplicity and also because it accounts for the disposal of the high K Altuntu granite (unit FD 5) to the west of the low K Sebbeto tonalite (unit AD 1) along the thickening margin of the western continent.

According to this model the chain of ultramafic rocks in the eastern part of the Adola area (Gilboy, 1970; Chater, 1971; Kazmin, 1976; Kozyrev et al., 1985) represents slices of the oceanic crust at the leading edge of the volcanic island arc complex. Similarly the extensive basic volcanic sequence and associated deep sea sediments in the Adola area (the Adola and Mormora groups of Kazmin, 1973) represent the supracrustal sequence of the Adola volcanic arc. This sequence which is at present disposed to the east of the plutonic root represented by the Sebbeto tonalite (unit AD 1) and granitoids in the chain, may have been detached from the latter (plutonic root) by eastward thrusting and consequent delamination.

Whatever the mechanisms, the later stages in this model very likely involved early transpression and late largely transcurrent motion along the Kolle-Altuntu lineament. The Altuntu granite, as discussed in Chapters 3 and 6, was emplaced as a sheet along this lineament. As discussed in chapter 4 the granite was affected by and may have facilitated a largely strike-slip movement along this zone at least in the early stages of movement along this lineament.

5. Late to post-collisional thickening, extension and magmatism (Fig. 7.1e) This stage is subsequent to final collision and suturing and follows limited continental overriding (D_1) and thickening (F_2 folding) of the continental lithosphere and regional

metamorphism. The stage may have involved cooling and fracturing of the thickened crust as suggested for comparable Pan-African terranes e.g. by Abdel-Rahman (1986) although comparable dyke injection is not observed.

The uplift might have culminated in incipient continental rifting at upper (brittle) crustal levels perhaps aided by gravitational instability (Dewey, 1988) of the thickened crust. This rifting is inferred from the bulk-chemistry (chapter 6) of the late to post-collisional alkaline to peralkaline plutonism (the Kinsho granite (unit FD 7) and the granitoids of the Bergudda complex (unit FD 8)).

The approximate age of this final cratonization stage can be taken at about 530 to 600 Ma based on the 538 and 528 Ma U-Pb (Zircon) dates obtained from two different phases of the Bergudda complex (unit FD 8) and the approximate period of widespread late-tectonic magmatism in the Precambrian basement of Ethiopia (Gilboy, 1970, Chater, 1971., Ayalew et al., 1989) which coincides with the late Precambrian tectonothermal event over most of Africa (Kennedy, 1964). The age is also within the age range of similar post-collisional magmatism in the Pan-African of northeast Africa and Arabia (e.g. Gass 1981; Stoeser and Camp, 1985; Jackson, 1986; Abdel-Rahman and Martin, 1987; Rogers and Greenberg, 1990; Stoeser, 1986).

7:2:3 Evaluation of the model and suggestions for furtner work.

The westerly directed subduction explains the increase to the west of the K-content of the calc-alkaline subduction-related plutonic rocks in the Sagan-Afelata area notably the disposition of the Altuntu granite (unit FD 5) to the west of the Sebbeto tonalite (unit AD

1). According to this model the peralkaline rocks represented by the Kinsho granite chain (unit FD 7) originated in the upper plate as for equivalent plutonic rocks in the Pan African of the Arabo-Nubian shield (e.g. Greenberg, 1981; Abdel-Rahman and Martin, 1990; Rogers and Greenberg, 1990). The model agrees well with the westerly subduction suggested for the Kenyan segment of the Adola-Moyale ophiolitic belt in the Moyale area to the south (Berhe, 1989). This model is also in agreement with an easterly direction of tectonic transport conjectured by de Wit and Chewaka (1981) and thrusting-over of the lower grade ophiolitic assemblage in the Adola area over the relatively high grade gneissic rocks suggested by Beraki et al., (1989), although no clear structural evidence for such thrusting has yet been established.

Despite the above positive sides to the model the time gap between the collisional event taken at approximately 710 Ma (the age of the syn-kinematic Dek Bor granite) and the stage of post collisional alkaline magmatism approximately 530 Ma (the age of the Bergudda complex) and of general post-tectonic magmatism in the basement of Ethiopia (about 500-600 Ma) is about 110 to 180 my. This gap is much greater than the maximum of the typical range of time-lag (25 to 75 My) between a collisional event and related post-tectonic magmatism for many collisional belts including the Pan African of the Afro-Arabian shield (Jackson, 1986, Pallister et al,, 1988, Sylvester, 1989). The discrepancy in time may possibly be explained by isotopic resetting in the Bergudda complex by Ordovician (granulite facies ?) metamorphism (chapter 5) which needs to be accounted for tectonically.

Although the task to explain the tectonic evolution of southern Ethiopia is beyond the

scope of this thesis, it is conjectured that the evolution involved diachronous processes that have been active over a time length of at least 110-180 my, of which the accretion of the Adola arc (this model) is only one (may be the last) In which case the evolution may have involved yet earlier event(s) of basin opening and closure such as suggested by Davidson (1983) to explain the origin of the protoliths of the mafic granulites in the Konso area to the west and magmatic accretion - collision events such as that proposed for the western branch of the Red Sea fold belt in western Ethiopia (Ayalew et al., 1990 and chapter 2).

A comprehensive model that can account for all these observations can only be proposed after more systematic regional work covers a large part of the basement of southern Ethiopia, including the Konso (Davidson, 1983) and Adola (Kozyrev et al., 1985) areas. It is suggested that such a work should emphasize the acquisition of detailed geochemical and geochronological data on volcanic and plutonic rocks including mafic granulites of this area (unit SD 1) and Konso area (Davidson, 1983). It should also include interpretation of the Adola basin sedimentary facies in a plate tectonic context (Mitchell and Reading, 1978, Ingersoll, 1988) and a compilation and interpretation of the E - W geological crossection across the Mozambique belt at the latitude of the Sagan - Afelata area.

REFERENCES

Abbey, S., 1977. Studies in standard samples for use in the general analysis of silicate rocks and minerals. Geological Survey of Canada Paper 77-34, 31p.

Abdel-Rahman and Martin (1990). The Mount Gharib A-type granite, Nubian Shield: petrogenesis and role of metasomatism at the source. Contrib. Mineral. Petrol., 104: 173-183.

Abdel-Rahman, A.M., and Martin, R.F. 1987. Late Pan-African magmatism and crustal development in northeastern Egypt. Geol. J. 22, 281-301.

Abdel-Rahman, A.M., 1986 Plutonism and tectonic evolution of the Ras-Gharib segment of the northern Nubian Shield, Egypt. Ph.D. Thesis, McGill Univ., Montreal, Canada.

Allen, P., Condie, K.C. and Narayana, B.L., 1985. The geochemistry of prograde and retrograde Charnockite-gneiss reactions in southern India. Geochimica et cosmochimica Acta, Vol. 43, pp. 323-336.

Almond, D.C., 1984. The concepts of "Pan-African Episode" and "Mozambique Belt"in relation to the geology of east and north-east Africa. In: Al Shanti, A. (ed.), Evolution and Mineralization of the Arabian-Nubian Shield. Institute of Applied Geology Bulletin, Jeddah. Pergamon Press, 6, pp. 71-87.

Almond, D., Darbyshire, D., and Ahmed, F., 1989. Age limits for major shearing episodes in the Nubian Shield of NE Sudan. J. Afr. Earth Sci., V. 9, no. 3/4, pp. 489-496.

Al Shanti, A.M.S., and Gass, I.G., 1983. The upper Proterozoic ophiolite melange zones of the easternmost Arabian Shield. Journal of the Geological Society of London, 140, pp. 867-876.

Al Shanti, A.M.S., and Mitchell, A.H.G. 1976. Late Precambrian subduction and collision in the Al Amar - Idsas region, Arabian Shield, Kingdom of Saudi Arabia. Tectonophysics, 30, pp. 41-47.

Andreoli, M.A.G., 1984. Petrochemistry tectonic evolution and metasomatic mineralisation of Mozambique granulites from S. Malawi and Tete (Mozambique). Precambrian Research, 25, 161-186.

Ashton, K.E. and Leclair, A.D. 1990. Foliate a useful term to complement the textural classification of foliated metamorphic rocks. Can. J. Earth Sci. 27, 1095-1097.

Atherton, M.P., McCourt, W.J., Sanderson, L.M., and Taylor, W.P., 1979. The geochemical character of the segmented Peruvian coastal batholith and associated volcanics. In: Atherton, M.P. and Tarney, J. (eds.), Origin of Granitic Batholiths-Geochemical Evidence. Shiva Publishing, UK., pp. 65-75.

Ayalew, T., 1989. Geology, Geochemistry, Age and Tectonic Setting of the Gore-Gambella Plutonic Rocks, Western Ethiopia. Unpublished Ph.D. thesis, Carleton University, Ottawa, 247p.

Ayalew, T.W., Bell, K., Moore, J. and Parrish, R., 1990. U-Pb and Rb-Sr geochronology of the western Ethiopian Shield. Geol. Soc. Am. Bull., V. 102, p. 1309-1316.

Ayalew, T.W. and Moore, J., (compilors) 1989. Final report of the Gore-Gambela geotraverse, western Ethiopia. IDRC. 153 p.

Bakor, A.R., Gass, I.G. and Neary, C.R. 1976. Jobal al Wask, northwest Saudi Arabia, an Eocambrian back-arc ophiolite. Earth and Planetary Science Letters, 30, 1-9.

Barker, F., 1979. Trondhjemite - definition, environment and hypothesis of origin. In: Barker, F. (ed.), Trondhjemites, Dacites, and Related Rocks. Elsevier, Amsterdam, pp. 2-5.

Bateman, P.C. and Dodge, F.C.W., 1970. Variations of major chemical constituents across the central Sierra Nevada batholith. Geological Society of America Bulletin, 81, pp. 409-420.

Bell, K., and Dodson, M.H., 1981. The geochronology of the Tanzanian Shield. Journal of Geology, 89, pp. 109-128.

Beraki, W.H., Bonavia, F.F., Getachew, T., Schmerold, R. and Tarekegn, T., 1989. The Adola fold and thrust belt, southern Ethiopia: a re-examination with implications for Pan-African evolution. Geol., Mag. 126(6), 647-57.

Berhe, S.M., 1989. Ophiolites in Northeast and East Africa: implications for Proterozoic crustal growth. J. Geol. Soc., London, Vol. 147, pp. 41-57.

Bernasconi, A., 1983. Geological comparison of Precambrian and early Paleozoic terrains between the southern west coast of Africa and the south-east of South America. Precambrian Res., 23: 9-31.

Bernasconi, A., 1987. The major Precambrian terranes of eastern South America: a study of their regional and chronological evolution. Precambrian Res., 37: 107-124.

Berthé, D. and Brun, J.P. 1980 Evolution of folds during progressive Shear in the south Armorican shear zone, France. J. of Structural Geology, V. 2, No. 1/2, pp. 127-133.

Berthé, D., Choukroune, P., and Jegouzo, P., 1979. Orthogneiss, mylonite and non-coaxial deformation of granites: The example of the South American Shear Zone: Journal of Structural Geology, V. 1., No. 1, pp. 31-42.

Beyth, M., 1971. Geology of Central and Western Tigre. Unpublished report, Ethiopian Institute of Geological Surveys.

Black, R., 1984. The Pan-African event in the geological framework of Africa. Pangea, 2, pp. 6-16.

Black, R., Caby, R., Moussine-Pouchkine, A., Bayer, R., Bertrand, J.M., Boullier, A.M., Fabre, J. and Lesquer, A. 1979. Evidence for late Precambrian plate tectonics in West Africa. Nature, V. 278. pp. 223-226.

Bogliotti, C., 1989. A reinterpretation of the large-scale structure of Precambrian rocks in the Adola gold field (Ethiopia) based on two generations of interference pattern. Precambrian Res., 44, 289-304.

Boullier, A.M., Liégeois, J.P., Black, R., Fabre, J., Sauvage, M. Bertrand, J.M., 1986. Late Pan-African tectonics marking the transition from subduction-related calc-alkaline magmatism to within-plate alkaline granitoids (Adrar des Iforas, Mali). Tectonophysics 132, 233-246.

Bowen, N.L. and Tuttle, O.F. 1949. The System Mgo-SiO_2-H_2O. Bull. geol. Soc. Am. 60, 430-60.

Brhun, R.L., Stern, C., and deWit, M.J., 1978. The bearing of new field and geochemical data on the origin and development of a Mesozoic volcano-tectonic rift zone and back-arc basin in southernmost South America. Earth Planet Sci. Lett., 41: 32-46.

Brown, G.F., 1972. Tectonic map of the Arabian Peninsula. Map AP-2, Dir. Gen. Min. Res., Jeddah.

Brown, G.F. and Jackson, R.D., 1960. The Arabian shield. Int. Geol. Congr. XIX 9, 69 - 77.

Burke, K. and Sengor, A.M.C., 1986. Tectonic escape in the evolution of the continental crust. Am. Geophys. Union, Geodynamics Ser., 14:41-53.

Caby, R., Bertrand, J.M.L. and Black, R. 1981. Pan-African ocean closure and continental collision in the Hogger-Iforas segment, Central Sahara. In: A. Kroner (ed.) Precambrian plate tectonics. Elsevier, Amsterdam. pp. 407-451.

Cahen, L., Snelling, N.J., Delhal, J., and Vail, J.R., 1984. The Geochronology and Evolution of Africa. Clarendon Press, Oxford, 512 p.

Carmichael, D.M., 1974. Metamorphic bathograds: A measure of the depth of post-metamorphic erosion on the regional scale: Geol. Soc. America. Abs. with programs, V. 6, p. 680-681.

Carmichael, D.M., 1978. Metamorphic bathozones and bathograds: a measure of the depth of post-metamorphic uplift and erosion on the regional scale. American Journal of Science, 278, pp. 769-797.

Chappell, B.W., and White, A.J.R., 1974. Two contrasting granite types. Pacific Geology, 8, pp. 173-174.

Chater, A.M., 1971. The Geology of the Megado area of Southern Ethiopia. Unpublished Ph.D. thesis, University of Leeds, Leeds, U.K.

Chater, A. and Gilboy, C., 1968. Preliminary report on the Geology of the Mozambique belt in Sidamo province, Southern Ethiopia. Report No. W, Research Institute of African Geology, University of Leeds. Leeds, U.K.

Church, W.R., 1982. The northern Appalachians and the Eastern desert of Egypt (abstract). Precambrian Res., 16, A13.

Clark, M.D., 1985. Late Proterozoic crustal evolution of the Midyan region, northwestern Saudi Arabia. Geology, V. 13, p. 611-615.

Clifford, T.N., 1970. The structural framework of Africa. In: Clifford, T.N. and Gass, IG. (eds.), African Magmatism and Tectonics. Edinburgh, Oliver and Boyd, pp. 1-26.

Cobbold, P.R. and Quinquis, H., 1980. Development of Sheath folds in shear regimes. J. of Structural Geology, V. 2, No. 1/2, pp. 119-126.

Collins, W.J., Beams, S.D. White, A.J.R., Chappell, B.W. 1982. Nature and origin of A-type granites with particular reference to southeastern Australia. Contrib. Mineral. Petrol. 80: 189-200.

Condie, K.C. and Allen, P., 1984. Origin of Archean Charnockites from southern India. In Archean Geochemistry A. Kroner, A.M. Goodwin and G.M. Hanson (eds), Springer-Verlag, Berlin.

Condie, K.C. and Shadel, C.A. 1984. An early Proterozoic volcanic arc succession in southeastern

Wyoming. Can. J. Earth Sci. 21, 415-427.
Condie, K.C., Viljoen, M.J., and Kable, E.J.D. 1977. Effects of alteration on element distributions in Archean tholeiites from the Barberton greenstone belt, South Africa. Cont. Min. Petrol., 64, pp. 75-89.
Coolen, J.J.M.M.M., Prien, H.N.A., Verdurmen, E.A.TH. and Verschure, 1982. Possible zircon U-Pb evidence for Pan-African granulite-facies metamorphism in the Mozambique belt of southern Tanzania Precamb. Res., 17, 3140.
Davidson, A. (Compiler), 1983. The Omo River Project: Reconnaissance Geology and Geochemistry of parts of Illubabor, Kefa, Gemu Gofa and Sidamo, Ethiopia. Ethiopian Institute of Geological Surveys Bulletin 2 and Canadian International Development Agency, 89 p.
Davidson, A., Moore, J.M., Davies, J.C., Gebre Leul, E., Shiferaw, A., Degeffu, A., Guyassa, A., Wolde Rufael, A., and Gelatta, M., 1973. Preliminary report on the geology and geochemistry of parts of Sidamo, Gemo Gofa and Kefa provinces, Ethiopia; Imperial Ethiopian Govt., Ministry of Mines, Omo River Project Rept., No. 1, 21 p.
Davidson, A., Moore, J.M., Davies, J.C., Shiferaw, A., Teferra, M., Degeffu, A., Wolde Rufael, A., Gelatta, M. and Hintsa, N., 1976. Preliminary report on the geology of geochemistry of parts of Gemo Gofa, Kefa and Ilubabor provinces, Ethiopia, Ethiopian Govt., Ministry of Mines and Power, Omo River Project Rept., NO. 2, 28 p.
Delfur, J., 1979. Upper Proterozoic volcanic activity in the northern Arabian Shield, Kingdom of Saudi Arabia. In: Evolution and Mineralization of the Arabian-Nubian Shield. In: A.M. Al Shanti (ed). Evolution and Mineralization of the Arabian-Nubian Shield. V. 2, pp. 59-75. Pergamon press, Oxford.
de Sitter, L.U., 1964. Structural Geology (2nd edition). McGraw Hill book company, New York, 551 p.
Dewey, J.F., 1988. Extensional collapse of orogens. Tectonics, Vol. 7, No. 6, pp. 1123 - 1139.
de Wit, M.J., 1977. Notes on the Geology of Part of Sheet NC-36-16 (Gore map sheet). Ethiopian Institute of Geological Surveys, Note 56.
de Wit, M.J., and Chewaka, S., 1981. Plate tectonic evolution of Ethiopia and the origin of its mineral deposits: An overview. In: Chewaka, S. and de Wit, M.J. (eds.), Plate Tectonics and Metallogenesis: Some Guidelines of Ethiopian Mineral Deposits. Ethiopian Institute of Geological Surveys, Bulletin 2, pp. 115-119.
Didier, J., 1973. Granites and their enclaves: the bearing of enclaves on the origin of granites. Elsevier, Amsterdam, 393 pp.
Dietrich, V. and Gansser, A. 1981. The leucogranites of the Bhutan Himalaya (crustal anatexis versus mantle melting). Bull. Suisse Mineral. Petrogr., 61, 177 - 202.
El Nadi, A.H., 1983. Geology of the late Precambrian Nafirdeib volcanics. Northeastern Sudan. Progress report. 12th Colloq. on Afrian Geology, Brussels, Abstracts, pp. 29.
El Nadi, A.H., 1990. Late Precambrian volcanism in northeastern Sudan and the evolution of the Nubian shield. J. of African Earth Sciences. V. 9., No 3/4, pp. 467 - 480.
Embleton, J.C.B., Hughes, D.J., Klemenic, P.M., Poole, S., and Vail, J.R., 1982. A new approach to the stratigraphy and tectonic evolution of the Red Sea Hills, Sudan [Abs:] Precamb. Res., V. 16, p. A19.
Engel, A.E.J., Dixon, T.H., and Stern, R.J., 1980. Late Precambrian evolution of Afro-Arabian crust from ocean arc to craton. Geological Society of American Bulletin, 91, pp. 699-706.
Evans, B.W. and Trommsdorff, V., 1970. Regional metqmorphism of Ultramafic rocks in the central Alps. Schewiz. Mineral. Petrog. Mitteil., 50, 481 - 492.
Ferry and Spear, 1978. Experimental caliberation of the partioning of Fe and Mg between biotite and garnet. Contributions to Mineralogy and Petrology. 66, 113 - 117.
Fitches, W.R., Graham, R.H., Hussein, I.M., Ries, A.C., Shackelton, R.M., and Price, R.C., 1983. The late Proterozoic ophiolite of Sol Hamed, N.E. Sudan. Precambrian Research, 19, pp. 385-411.
Fleck, R.J., Greenwood, W.R., Hadley, D.G., Anderson, R.E., and Schmidt, D.L., 1980. Age and evolution of the southern part of the Arabian Shield. In: Al Shanti, A. (ed.), Evolution and Mineralization of the Arabian-Nubian Shield, Institute of Applied Geology, Jeddah. Pergamon Press, Oxford, 4, pp. 1-17.
Gabriel, T., 1987. Preliminary report on the geology of Subsheets G and H of Map Sheet NB 37-10 (The Agere Mariam Sheet). Unpublished report, Ethiopian Institute of Geological Surveys. Addis Ababa, Ethiopia.

Garland, C.R., 1980. Geology of the Adigrat area. Memoir No. 1, Ethiopian Institute of Geological Surveys. 52 pp.

Garson, S. & Shalaby, I.M., 1976. Precambrian-lower Paleozoic plate tectonics and metallogenesis in Red Sea region. Geol. Ass. of Canada Special Paper, 14, 574-596.

Gass, I.G., 1977. The evolution of the Pan-African crystalline basement in NE Africa and Arabia. Journal of Geological Society of London, 134, pp. 129-38.

Gass, I.g., 1979. Evolutionary model for the Pan-African crystalline basement. In: Al Shanti, A. (ed), Evolution and Mineralization of the Arabian-Nubian Shield. Institute of Applied Geology Bulletin, Jeddah. Pergamon Press, 1, pp. 11-29.

Gass, I.G., 1981. Pan-African (Upper Proterozoic) plate tectonics of the Arabian-Nubian Shield. In: Kroner, A. (ed.), Precambrian Plate Tectonics, pp. 388-405.

Gass, I.G., 1982. Upper Proterozoic (Pan-African) calc-alkaline magmatism in northeastern Africa and Arabia. In: Thorpe, R.S. (ed.), Andesites, Orogenic Andesites and Related Rocks. Wiley, New York, pp. 591-609.

Geist, D., Baker, B. and McBirney, A. 1985. GPP: a program package for creating and using geochemical data files.

Getahun, S. and Alula, H.G. (1987). Preliminary report on the geology of Sub-Sheets N and O of NB-37-10 (The Agere Mariam Sheet), EIGS Unpublished report.

Gichile, S., 1987. Reconnaissance Geology of parts of the Agere Mariam Map Sheet (NB 37-10) and its implications on the Stratigraphy of the basement gneisses of Ethiopia. Congress on Ethiopian Geology, unpublished manuscript, Ethiopian Institute of Geological Surveys, Addis Ababa, Ethiopia. 9pp.

Gichile, S., 1990a. Petrochemistry and tectonic setting of granitoids, Mozambique belt, Southern Ethiopia, (East Africa). Abstract, Central Canada Geological Conference, Ottawa, p. 70.

Gichile, S., 1990b. Geologic implications of new U/Pb dates from the Precambrian basement of southern Ethiopia. Unpublished report. Regional mapping department, Ethiopian Institute of Geological Surveys. Addis Ababa, Ethiopia.

Gichile, S., Fyson, W.K. and Lalonde, A.E., 1991a. Pan-Afrian island arc accretion in the Mozambique belt of Southern Ethiopia. Geological Association of Canada - Mineralogical Association of Canada - Society of Economic Geologists. Annual meeting (1991). Toronto, Canada. Abstract with programms. V 16, p. A 44.

Gichile, S., Fyson, W.K. and Kretz, R., 1991b. Deformation and metamorphism of Precambrian rocks in the Sagan-Afelata area and the tectonic evolution of the Mozambique belt in southern Ethiopia. (Abstract) Central Canada Geological Conference (1991). Hamilton, Canada.

Gichile, S., Kiros, M., Solomon, B., and Taddese, A., 1986. Preliminary report on the Geology of Subsheets P and Q, Agere Mariam Sheet (NB 37-10). Ethiopian Institute of Geological Surveys. Addis Ababa, Ethiopia. 34 pp.

Gilboy, C., 1970. The Geology of the Cariboro Region of Southern Ethiopia. Unpublished Ph.D. thesis, University of Leeds, Leeds, U.K.

Gill, J.B., and Stork, A.L., 1979. Miocene low-K dacites and trondhjemites of Fiji. In: Barker, F. (ed.), Trondhjemites, Dacites and Related Rocks. Elsevier, Amsterdam, pp. 629-649.

Greenberg, J.K. 1981. Characteristics and Origin of Egyptian Younger granites: Summary. Geol. Soc. Am. Bull., Part I, V. 92, p. 224-232.

Greenwood, H.J., 1976. Metamorphism at moderate temperatures and pressures. In: Bailey, D.K. and Macdonald, R. (eds) The evolution of the crystalline rocks, Academic Press. N.Y., pp. 187-259.

Greenwood, W.R., Hadley, D.G., Anderson, R.E., Fleck, J.R., and Schmidt, D.L., 1976. Late Proterozoic cratonization in southwestern Saudi Arabia. Royal Society of London Philosophical Transactions, A 280, pp. 517 - 527.

Goldman, D.S and Albee, A.L., 1977. Correlation of Mg/Fe partioning between garnet and biotite with 180/160 partioning between quartz and magnetite. American Journal of Science, Vol. 277, pp. 750 - 767.

Hall, A., 1987. Igneous Petrology, Longman group, U.K. 573 pp.

Hanmer, S.K. and Connelly, J.N., 1986. Mechanical role of the syntectonic Laloche batholith in the Great

Slave Lake shear zone, district o Mackenzie, N.W.T. Paper Geological Survey of Canada. 86-1b. P. 811 - 826.

Harris, N.B.W., and Marriner, G.F., 1980. Geochemistry and petrogenesis of a peralkaline granite complex from the Midian mountains, Saudi-Arabia: Lithos, V. 13, p. 325-337.

Harris, N.B.W. 1983. Possible source regions for "within-plate" magmatism in northeast Africa and Saudi Arabia. Nature 289, 394-396.

Harris, N.B.W., Pearce, J.A , and Tindel, A.G., 1986. Geochemical characteristics of collision-zone magmatism. In: Coward, M.P., and Ries, A.C. (eds.), Collision Tectonics. Geological Society Special Publication. 19. Blackwell Scientific Publications, London, pp. 67-81.

Hepworth, J., 1967. The Photogeological recognition of ancient orogenic belts in Africa. Q. J. Geol. Soc. Lond. 123, 253 - 292.

Hepworth, J., 1972. Charnockitic granulites of some African cratons. Int. Geol. Congr. XXIV, Sec. 1, 126-134.

Hepworth, J.V., 1979. Does the Mozambique orogenic belt continue into Saudi Arabia? In: Evolution and Mineralization of the Arabian-Nubian Shield. Institute of Applied Geology, Jeddah, 3, pp. 39-51.

Hepworth, J. & MacDonald, R., 1966. Orogenic belts of the northern Ugandan basement. Nature 210, 726-727.

Hine, R. and Mason, D.R. 1978. Intrusive rocks associated with Porphyry Copper Mineralization, New Britain, Paupa, New Guinea. Economic Geology. Vol. 73, pp. 749-760.

Hoffman, P., 1988. United plates of America, the birth of a craton; Early Protenzoic assembly and growth of Laurentia: Ann Reviews of Earth and Planetary Sciences, V. 16, p. 543-603.

Hoffman, P., 1989. cambrian geology and tectonic history of North America. In: Bally, A.W. and Palmer, A.R. (ed he Geology of North America - An overview: Boulder, Colorado, Geol. Soc. Am., The Geology of a America, V.A., pp. 447-512.

Holdaway, M.J., tability of Andalusite and the aluminum silicate phase diagram. American Journal of Science, 27 131.

Holmes, A.B., he sequence of Precambrian orogenic belts in south and central Africa. 18th International al Congress, 14, pp. 254-269.

Hsu, L. C., 19 cted phase relationships in the system Al-Mn-Fe-Si-O-H. A model for garnet equilibria. J. 9, Part 1, 40 - 83.

Ingersoll, R.V., Tectonics of sedimentary basins. Geol. Soc. Am. Bull. V. 100, p. 1704 - 1719.

Irvine, T.N., 19 rminology for layered intrusions., J. Petrol. 23, 127-162.

Irvine, T.N. an gar, W.R.A., 1971. A guide to the chemical classification of the common volcanic rocks. Cana Journal of Earth Sciences, 8, pp. 523-528.

Jackson, N.J., 6. Petrogenesis and evolution of Arabian plutonic rocks. Journal of African Earth Sciences, 4, p. 47-59.

Jackson, N.J. and Ramsay, C.R., 1980. What is the "Pan-African"? A consensus is needed. Geology (Boulder), Vol. 8, No. 5, p. 210 - 211.

Jackson, N.J., Walsh, J.N. and Pegram, E., 1984. Geology, geochemistryand petrogenesis of Late Precambrian granitoids in the central Hijaz region of the Arabian Shield. J. Geol. Soc. Lond. 137, 617-628.

Jensen, L.S., 1976. A new cation plot for classification of common volcanic rocks. Ontario Division of Mines. Miscellaneous paper 66, 22 p.

Johnson, R.J., 1968. Structural history of the western front of the Mozambique belt in northeast southern Rhodesia. Kay, S.M., Kay, R.W., Brueckner, H.K. and Rubenstone, J.L. 1983. Tholeiitic Aleutian arc plutonism: The Finger Bay Pluton, Adak, Alaska. Contrib. Min. Petrol. 82: 99-116.

Kang, D.E , 1971. Origin and development of marginal basins in the western Pacific. J. Geophys. Res., 76:2542

Kay, S.M. Kay, R.W., and Citron, G.P. 1982. Tectonic controls on Aleutian Tholeiitic and calc-alkaline magma ism. J. Geophys. Res. 87: 4051-4072.

Kazmin, V., 1970. Geological map of the Yavello area; U.N. - Ethiopia Mineral Survey Report. Ethiopian Institute of Geological Surveys, Addis Ababa, Ethiopia.

Kazmin, V., 1971. Precambrian of Ethiopia. Nature, Physical Science, 230(16), pp. 176-177.
Kazmin, V., 1972. Granulites in Ethiopian basement. Nature, Physical Science, 240, 90-92.
Kazmin, V., 1972. Some aspects of Precambrian development in east Africa. Nature, 237, pp. 160.
Kazmin, V., 1973 (compiler). Geological map of Ethiopia. Lat. 4°00' to 18°00', Long. 34°00' to 48°00', Scale 1:2,000,000. Ethiopian Institute of Geological Surveys.
Kazmin, V., 1975a. Explanation of the geological map of Ethiopia. Ethiopian Institute of Geological Surveys, Bulletin 1.
Kazmin, V., 1975b. The Precambrian of Ethiopia and some aspects of the geology of the Mozambique Belt. Geophysical Observatory Bulletin. Addis Ababa, 15, pp. 27-43.
Kazmin, V., 1976. Ophiolites in the Ethiopian basement. Ethiopian Institute of Geological Surveys, Note 35, 16p.
Kazmin, V., 1978. Geology of the Ethiopian basement and possible relation between the Mozambique and the Red Sea belts. Egypt. J. Geol., 22, No. 1, 73-86.
Kazmin, V., 1979. Relationshiop between rifts and Precambrian basement in East Africa. Annals of Geological Survey of Egypt, 9, pp. 54-60.
Kazmin, V., Alemu Shiferaw, and Tilahun Balcha, 1978. The Ethiopian basement: stratigraphy and possible manner of evolution. Geologische Rundschau, 67(2), pp. 531-546.
Kazmin, V., Mengesha Tefera, Seife M. Berhe, and Senbeto Chewaka, 1979. Precambrian structure and metallogeny of western Ethiopia. Annals, Geological Survey of Egypt, 9, pp. 1-18.
Kennedy, W.Q., 1964. The structural differentiation of Africa in the Pan-African (+ 500 Ma) tectonic episode. Ann. Rep. Inst. Afr. Geol., Leeds University, 8.48.
Kerrick, D.M., 1972. Experimental determination of Muscovite + Quartz stability with $PH_2O < P_{total}$. Am. J. of Sci., V. 272, p. 946-958.
Key, R., Charsley, T., Hackman, B., Wilkinson, A. and Rundle, 1989. Superimposed Upper Proterozoic collison-controlled orogenies in the Mozambique Orogenic belt of Kenya. Precambrian Res., 44, 197-225.
Kiros, M. and Kinetibeb, Y., 1987. Preliminary report on the Geology of subsheets U and V os Map Sheet NB 37-10 (the Agere Mariam sheet). Unpublished report, Ethiopian Institute of Geological Surveys. Addis Ababa, Ethiopia.
Kozyrev, V., Girma, K., Safanov, Yu., Bekele, W.M., Gurbanovich, G., Tewolde Medhin, T., Kaitvkov, Arijapor, A., 1985. Regional geological and exploration work for gold and other minerals in the Adola goldfield, V. II, Regional geological mapping and prospecting. Report; Ethiopian Mineral Resources Development Corporation. Addis Ababa, Ethiopia.
Kretz, R. 1981., Site-occupancy interpretation of the distribution of Mg and Fe between Orthopyroxene and Clinopyroxene in metamorphic rocks. Canadian Mineralogist, 19(3), pp. 493-500.
Kretz, R., 1982. Transfer and exchange equilibria in a portion of the pyroxene quadrilateral as deduced from natural and experimental data. Geochemica et Cosmochimica Acta, Vol. 46, pp. 411-421.
Kretz, R., 1983. Symbols for rock-forming minerals. American mineralogist, V. 68, pp. 277-279.
Kretz, R., 1990. Biotite and garnet compositional variation and mineral equilibria in Grenville gneisses of the Otter Lake area, Quebec. J. Met. Geol., 8, 493-506.
Kroner, A., 1977. The Precambrian geotectonic evolution of Africa: Plate accretion versus plate destruction: Precambrian Res., V. 4, p. 163-203.
Kroner, A., 1977. Precambrian mobile belts of southern and eastern Africa - ancient sutures or sites of ensialic mobility? A case for crustal evolution towards plate tectonics. Tectonophysics, 40, pp. 101-135.
Kroner, A., 1979. Pan-African mobile belts as evidence for a transitional tectonic regime from intraplate orogeny to plate margin orogeny. In: Evolution and mineralization of the Arabian - Nubian shield. Institute of Applied Geology. King Abdulaziz University, Jeddah. Vol. 1, Pergamon, Oxford. pp. 21-37.
Kroner, A., 1985. Ophiolites and the evolution of tectonic boundaries in the late Proterozoic Arabian-Nubian Shield of North East Africa and Arabia. Pen. Res., 27:277-300.
Kroner, A., Greiling, R., Reischmann, T., Hussien, I. Stern, R., Dürr, S., Krüger, J., and Zimmer, M. 1987. Pan-African crustal evolution in the Nubian segment of northeast Africa. In: A. Kroner (ed). Proterozoic lithospheric evolution. Geodynamic series, V. 17, pp. 235-257.

Le Bas, M.J., Le Maitre, R.W., Streckeisen, A. and Zanettin, B., 1986. A Chemical classification of volcanic rocks based on the total Alkali-silica diagram. J. of Petrology, Vol. 27, Part 3, pp. 745-750.

Le Fort, P., 1981. The Mansalu leucogranite: a collision signature of the Himalaya, a model for its genesis and emplacement. J. of Geophys. Res., V. 86, No. B11, p. 10545-10568.

Leggo, P.J., 1971. Discordant Zircon U-Pb ages from Uganda basement. Nature 231, 81-86.

Levitte, D., Columbia, J., and Mohr, P.A. 1974. Reconeissance geology of the Amaro horst, Southern Ethiopia: Geol. Soc. Am. Bull., V. 85, p. 417-422.

Liégeois, J.P., and Black. R., 1987. Alkaline magmatism subsequent to collision in the Pan-African belt of the Adrar des Iforas (Mali). In: Fitton, J.G. and Upton, B.G.J. (eds). Alkaline igneous rocks. Geol. Soc. London Spec. Public. 30: 381-401.

Lister, G.S., and Snoke, A.W., 1984. S-C mylonites: Journal of Structural Geology. 6: pp. 283-298.

Loiselle, M.C., and Wones, D.R., 1979. Characteristics of anorogenic granites, Abstracts, Geological Society of America, Annual Meeting, 1979, p. 539.

Maboko, M.A.M., Bolerrijk, N.A.I.M., Priem, H.N.A., and Verdurmen, E.A.TH. 1985. Zircon U-Pb and biotite Rb-Sr dating of the Wami river granulites, eastern granulites, Tanzania: evidence for approximately 715 Ma old granulite-facies metamorphism and final Pan-African cooling approximately 475 Madago. Macfarlane, A., 1969. Preliminary report on the geology of the Central Serengeti, N.W. Tanzania. Ann. Rep Res. Inst. Afr. Geol., Univ. Leeds, 13: 14-16.

Maniar, P.D. and Piccoli, P.M., 1989. Tectonic discrimination of granitoids. Geol. Soc. Am. Bull., V. 101, p. 635-643.

Malisa, E. and Muhongo, S., 1990. Tectonic setting of gemstone mineralization in the Proterozoic metamorphic terrane of the Mozambique belt in Tanzania. Precambrian Res., 46 (1-2), pp. 167 - 176.

Martin, H. and Porada, H., 1977. The intracratonic branch of the Damaran orogen in South West Africa. I-Discussion of geodynamic models. II. Relationships with the Pan-African mobile belts system. Precambrian Res. 5, 311-338, 339-357.

McConnel, R.B., 1979. A Precambrian origin for the Proto-Rift dislocation zone of eastern Africa. In: Geodynamic Evolution of the Afro-Arabian Rift System. Academia Nazionale Dei Lincei, Roma. P. 35-44.

McWilliams, M.O., 1981. Paleomagnetism and Precambrian tectonic evolution of Gondwana. In: A. Kroner (Ed.), Precambrian plate tectonics. Elsevier, Amsterdam, pp. 649-687.

Mehnert, K.R., 1968. Migmatites and the origin of granitic rocks. Elsevier, Amsterdam.

Mengesha, T., 1987. The geology of the Kurmuk and Asosa map sheets (NC-36-7 and Nc 36-8)., report (in progress) Ethiopian Institute of geological surveys. Addis Ababa Ethiopia.

Mengesha, T. and Seife M. Berhe, 1987. Geology of sheet NC 36-16 (Gore sheet). Ethiopian Institute of Geological Surveys. (Unpublished manuscript).

Mengist, T., 1986. Petrology and Geochemistry of Supracrustal and Intrusive Rocks fromt he Birbir Domain of the Gore-Gambela Geotraverse. Unpublished M.Sc. thesis, Addis Abeba University, 102 p.

Mitchell, A.H.G., and Reading, H.G., 1978. Sedimentation and tectonics. In: Reading, H.G. (ed.), Sedimentation and Tectonics. Elsevier, pp. 439-476.

Mohr, P., 1967. The Ethiopian Rift System. Bull. Geophys. Obs., Addis Ababa, V. 11, p. 1-65.

Mohr, P., 1979. Lithology and structure of the Precambrian rocks of Eritrea. In: Al Shanti, A.M.S. (ed.). Evolution and mineralization of the Arabian-Nubian Shield, V. 2., pp. 7-16, Pergamon Press, Oxford.

Moore, J.M. Morgan, J., Mengesha Teferra, and Mengist Teklay, 1987. Geology of the Gore-Gambella geotraverse, western Ethiopia. In: Matheis, G. and Schandelmeier, H. (eds.), Current Research in African Earth Sciences, Balkema, Rotterdam/Boston. pp. 109-112.

Morton, W.H., 1981. Geology and mineralization of the Tsehafi Emba copper prospect, Western Tigre. In: Chewaka, S. and deWit, M. (ed.) Plate tectonics and metallogenesis. Bull. No. 2, Ethiopian Institute of Geological Surveys. Addis Ababa. Ethiopia, p. 75-82.

Muhongo, S. and Schandelmeir, H. and Kramers, J.D., 1987. Rb/Sr Whole rock dating of the granulite complex of the Ulguru mountains, Tanzania and some speculations on the age of the Mozambique orogeny. In: Current research in Africa earth Sciences. Matheis and Schandelmeier (eds)., Balkema, Rotterdam.

Mullen, E.D., 1983. $MnO-TiO_2-P_2O_5$: a minor element discriminant for basaltic rocks of oceanic environments and its implications for petrogenesis. Earth. Plan. Sci. Lett. 62, 53-62.

Newton, R.C., 1983. Geobarometry of high-grade metamorphic rocks: Am. Jour. Sci., V. 283-A, p. 1-28.

Newton, R.C. and Perkins, D., III, 1982. Thermodynamic calibrations of geobarometers for charnockites and basic granulites based on the assemblages garnet-plagioclose-orthopyroxene - (clinopyroxene) - quartz, with applications to high grade metamorphism. Am. Mineral. 67: 203-222.

Nixon, P.H., Reedman, A.J. and Burns, L.K., 1973. Sapphirine-bearing granulites from Labwor, Uganda. Mineralogical Magazine, 39, 420-428.

Pallister, J.S., Stacey, J.S., Fischer, L.B. and Premo, W.R., 1987. Arabian Shield ophiolites and Late Proterozoic microplate accretion: Geology, V. 15, p. 320-323.

Pallister, J.S., Stacey, J.S., Fischer, L.B., and Premo, W.R., 1988. Precambrian Ophiolites of Arabia: geologic settings, U-Pb geochronology, Pb isotope characteristics and implications for continental accretion: Precamb. Res., V. 38, p. 1-54.

Park, A., 1989. Charnockite suite. In: D.R. Bowes (ed.). The Encyclopedia of Igneous and Metamorphic petrology. Nostrand Reinhold. N.Y. pp. 97 - 98.

Passchier, C.W., and Simpson, C., 1986. Porphyroclast systems as Kinematic indicators: J. of Structural Geology, Vol. 8, No. 8, pp. 831-843.

Pearce, J.A., 1982. Trace element characteristics of lavas from destructive plate boundaries. In: Thorpe, R.S. (ed.), Andesites, Orogenic Andesites and Related Rocks. Wiley, New York, pp. 525-548.

Pearce, J.A., and Cann, J.R., 1973. Tectonic setting of basic volcanic rocks determined using trace element analysis. Earth and Planetary Science Letters, 19, pp. 290-300.

Pearce, J.A. and Gale, G.H., 1977. Identification of ore-deposition environments from trace - element geochemistry of associated igneous host rocks. In: Volcnic processes in ore genesis. Geol. Soc. Lond. Publ., 7, pp. 14 - 24.

Pearce, T., Gorman, B., and Birkett, T., 1975. The $TiO_2-K_2O-P_2O_5$ Diagram: a method of discriminating between oceanic and non-oceanic basalts. Earth and Planetary Sci. Lett., 24, 419-426.

Pearce, J.A., Harris, N.B.W., and Tindle, A.G., 1984. Trace element discriminiation diagrams for the tectonic interpretation of granitic rocks. Journal of Petrology, 25, pp. 956-983.

Pearce, J.A. and Norry, M.J. 1979. Petrogenetic implications of Ti, Zr, Y and Nb variations in volcanic rocks. Contrib. Mineral, Petrol. 69, 33-47.

Perchuk, L.L. and Lavrent'eva, I.V., 1983. Experimental investigation of exchange equilibria in the System Corderite-garnet-biotite. In: Saxena, S.K. (ed.), Advances in physical geochemistry, 3, Heidelberg:Springer - Verlag, 199-239.

Petro, W.L., Vogel, T.A., and Wilband, J.T., 1979. Major-element chemistry of plutonic rock suites from compressional plate boundaries. Chemical Geology, 26, 217-235.

Piper, J.D.A., 1982. The Precambrian paleomagnetic record: the case for the Proterozoic supercontinent. Earth Planet. Sci. Lett., 59, 61 - 89.

Pitcher, W.S., 1983. Granite type and tectonic environment. In: Hsu, K. (ed.), Mountain Building Processes, Academic Press, pp. 19-40.

Pohl, W., 1981. Is the Kashebib Group older basement to the Greenschist assemblage? In: Al-Shanti, A.M. (ed.), Newsletter, IGCP - Project 164. Institute of Applied Geology, Jeddah, 4, pp. 44-48.

Porada, H., 1979. The Damara-Riberia orogen of the Pan-African/Braziliano cycle in Namibia (South West Africa) and Brazil as interpreted in terms of Continental Collision. Tectonophysics, 57: 237-265.

Porada, H., 1989. Pan-African Rifting and Orogenesis in southern to Equatorial Africa and Eastern Brazil. Precambrian Res., 44, 103-136.

Powell, C.M. and Conaghan, P.J., 1975. Tectonic models for the Tibetan Plateau. Geology, 3, 723-731.

Prochaska, W., and Pohl, W., 1984. Petrochemistry of some mafic and Ultramafic rocks from the Mozambique belt, Northern Tanzania, J. Afr. Earth Sci., 1:183-191.

Rameshwar Rao, D. and Narayana, B.I., 1989. Chemical mobility of elements in the granulite facies environments: Dharmapori area, Tamil Nadu, India. Indian J. of Earth Sci., V. 16, No. 2, pp. 119-125.

Ramsay, C.R., Stoeser, D.B. and Drysdall, A.R. 1986. Guidelines to classification and nomenclature of Arabian felsic plutonic rocks. J. Afr. Earth Sci. 4, 13-20.

Ramsay, J., 1967. Folding and fracturing of rocks. Mc Graw-Hill book co., NY. 560p.
Richardson, S.W. and England, P.C. 1979. Metamorphic consequences of crustal eclogite production in overthrust orogenic zones. Earth Planet. Sci. Lett. 42, 183 - 190.
Ries, A.C., Shackleton, R.M., and Dawoud, A.S., 1985. Geochronology, geochemistry and tectonics of the NE Bayuda Desert, N. Sudan: implications for the Western Margin of the Late Proterozoic fold belt of NE Africa. Precambrian Research, 30, pp. 43-62.
Ries, A.C., Shackleton, R.M., Graham, R.H., and Fitches, W.F., 1983. Pan-African structures, ophiolites and melanges in the Eastern Desert of Egypt. Journal of the Geological Society of London.
Rogers, A.S., Miller, J.A., and Mohr, P.A., 1965. Age determinations on some Ethiopian basement rocks. Nature, 206, pp. 1021-1023.
Rogers, J.J.W. and Greenberg, J.K. 1981. Trace elements in Continental margin magmatism: Part III. Alkali granites and their relationship to cratonization: Summary Geol. Soc. Am. Bull., Part I. V. 52, p. 6-9.
Rogers, J.J.W. and Greenberg, J.K. 1990. Late-orogenic, post-orogenic, and anorogenic granites: distinction by major-element and trace-element chemistry and possible origins. J. of Geol., V. 98, No. 3, p. 231-309.
Rollinson, H.R. and Windley, B.F., 1980. Selective elemental depletion during metamorphism of Archean granulites, Scourie, N.W. Scotland. Contrib. Mineral Petrol., 72, 257-263.
Ronov, A., 1964. Common tendencies in the Chemical evolution of the Earth's crust, ocean and atmosphere Geochem. Int., 1, 713-737.
Roobol M.J., Ramsay, C.R., Jackson, N.J., and Darbyshire, D.P.F., 1983. Late Proterozoic lavas of the central Arabian Shield-evolution of an ancient volcanic arc system. Journal of the Geological Society of London, 140, pp. 185-202.
Sanders, L., 1965. Geology of the contact between the Nyanza Shield and the Mozambique belt in Western Kenya. Bull. Geol. Surv. Nairobi, Kenya, 7.
Sawkins, F.J., 1976. Widespread continental rifting: some considerations of timing and mechanism. Geology, 4: 427-430.
Schmidt, D.L. Hadlay, D.G. and Stoeser, D.B. 1979. Late Proterozoic crustal history of the Arabian Shield, southern Najd province, Kingdom of Saudi Arabia. In: Evolution and mineralization of the Arabian-Nubian Shield, 2, 41-58.
Shackleton, R.M., 1976. Pan-African structures. Royal Society of London, Philosophical Transactions, A280, pp. 491.
Shackleton, R.M., 1977. Possible late-Precambrian ophiolites in Africa and Brazil. 20th Annual Report, Research Institute of African Geology, Leeds University, pp. 3-7.
Shackleton, R.M., 1979. Precambrian tectonics of northeast Africa. In: Al Shanti, A.M.S., (ed.). Evolution and mineralization of the Arabian-Nubian Shield, V. 2. pp. 1-6, Pergamon Press, Oxford.
Shackleton, R.M., 1986. Precambrian collision tectonics in Africa. In: Coward, M.P., and Ries, A.C. (eds.), Collision Tectonics. Geological Society Special Publication, 19. Blackwell Scientific Publications, London, pp. 329-352.
Shackleton, R.M., Ries, A.C., Graham, R.H., and Fitches, W.R., 1980. Late Precambrian ophiolitic melange in the eastern desert of Egypt. Nature, 285, pp. 472-474.
Shandelmeier, H., and Darbyshire, F., 1984. Metamorphic and magmatic events in the Uweinat - Bir Safsaf Uplift (Western Desert/Egypt). Geologische Rundshau, V. 73, p. 819-831.
Shiferaw, A., 1981. Basement rocks and mineralization in southwestern Ethiopia. In. Chewaka, S. and deWit, M. (eds.): Plate tectonics and metallogenesis, some guidelines to Ethiopian mineral deposits. Bull. No. 2., Ethiopian Institute of Geological Surveys, pp. 93-96.
Simpson, C. and Schmid, S.M., 1983. An evalution criteria to deduce the sense of movement in sheared rocks: Geol. Soc. Am. Bull. V. 94, pp. 1281-1288.
Spooner, C.M., Hepworth, J.V. and Fairbairn, H.W. 1970. Whole-rock Rb-Sr isotopic investigation of some east African granulites. Geol. Mag., 107, 511-521.
Stacey, J. and Hedge, C., 1984. Geochronologic and isotopic evidence for early Proterozoic continental crust in the eastern Arabian Shield. Geology, 12, 310-313.
Stern, R.J., 1985. The Najd fault system, Saudi Arabia and Egypt: a Late Precambrian rift-related transform

system?: Tectonics, V. 4, p. 497-511.
Stern, R.J., Gottfried, D., and Hedge, C.E. 1984. Late Precambrian rifting and crustal evolution in the Northeastern desert of Egypt: Geology, V. 12, p. 168-172.
Stoeser, D., 1986. Distribution and tectonic setting of plutonic rocks of the Arabian Shield. J. Afr. Earth Sci., V. 4, pp. 21-46.
Stoeser, D.B., and Camp, V.E., 1985. Pan African microplate accretion of the Arabian Shield. Geological Society of America Bulletin.
St-Onge, M.R., 1987. Zoned Poikilioblastic garnets: P-T paths and synmetamorphic uplift through 30 km of structural depth, Wopmay Orogen, Canada: Jour. Petrol. V. 28, p. 1-21.
Streckeisen, A., 1976. To each plutonic rock its proper name. Earth Science Reviews, 12, pp. 1-33.
Strong, D.F., and Hanmer, S.K., 1981. The leucogranites of Southern Brittany, Origin by faulting, frictional heating, fluid flux and fractional melting: Canadian mineralogist, V. 19, p. 163-176.
Suppe, J., 1983. Mechanics of mountain building and metamorphism in Taiwan. Memoir of the Geol. Soc. of China. 4, pp. 67 - 89.
Sylvester, P.J. 1989. Post-collisional Alkaline granites. J. of Geology, Vol. 97, p. 261-280.
Taddese, A., 1987. Preliminary report on the geology of Subsheets T and U of map sheet NB 37-10 (the Agere Mariam sheet). Unpublished report, Ethiopian Institute of Geological Surveys. Addis Ababa, Ethiopia.
Tarney and Windely, B.F., 1977. Chemistry, thermal gradients and evolution of the lower continental crust. Jour. Geol. Soc. Lond., 134, 153 - 172.
Taylor, S.R., and McLennan, S.M., 1985. The Continental Crust: its Composition and Evolution. blackwell Scientific Publications, Oxford, 312p.
Taylor, S., Rundick, R., McLennan, S., and Eriksson, K. 1986. Rare earth element patterns in Archean high-grade metasediments and their tectonic significance. Geochimica et Cosmochimica Acta Vol. 50, pp. 2267-2279.
Thompson, A.B., 1976. Mineral reactions in pelitic rocks. II. Calculation of some P-T-X (Fe-Mg) phase relations. American Journal of Science, 276, 425-454.
Thompson, A.B., 1983. Fluid-abscent metamorphism. J. Geol. Soc. London, V. 140, pp. 533-547.
Thompson, J.B. and Norton, S.A., 1968. Paleozoic regional metamorphism in New England and adjacent areas. In: Zen, E-an, White, W.S., Hardley, J.B. (eds.), Studies of Appalachian geology - Northern and Maritime: New York, John wiley and Sons, p. 319 - 327.
Tracy, R.J., 1982. Compositional zoning and inclusions in metamorphic minerals. In: Characterization of metamorphism through mineral equilibria. T.M. Ferry (ed.). Mineralogical Society of America. Reviews in Mineralogy. Vol. 10, pp. 355-397.
Turner, F.J., 1981. Metamorphic Petrology, Mineralogical, field and tectonic aspects. New York: McGraw-Hill.
Turner, F.J. and Weiss, L.E., 1963. Structural analysis of metamorphic tectonites. N.Y., McGraw-Hill,545 p.
Vail, J.R., 1976. Outline of the geochronology and tectonic units of the basement complex of northeast Africa. Proceedings of the Royal Society of London, A350, pp. 127-141.
Vail, J.R, 1979. Outline of geology and mineralization of the Nubian Shield east of the Nile Valley, Sudan. In: A.M. Al Shanti (ed.), Evolution and Mineralization of the Arabian-Nubian Shield, V. 1, pp. 97-107.
Vail, J.R., 1983. Pan-African crustal accretion in north-east Africa. Journal of African Earth Sciences, 1, pp. 285-294.
Vail, J.R, 1985. Pan-African (late Precambrian) tectonic terrains and the reconstruction of the Arabian-Nubian Shield. Geology, V. 13, p. 839-842.
Vail, J.R. and Hughes, D. 1987. The contact between the Continental Sudan Shield and the Orogenic Nubian Shield in Blue Nile province, Sudan. In: Current research in African earth sciences, Matheis and Shandelmeier (ed.), Balkema, Rotterdam.
Valley, J.W., Bohlen, S.R., Essene, E.J. and Lamb, W., 1990. Metamorphism in the Adriondacks: II. The role of fluids. J. of Petrol., V. 31, part 3, pp. 555-596.
Vearncombe, J.R., 1981. Possible ophiolites from the Pan-African of west Pokot, Kenya. 11th Colloquium

of African Geology, Milton Keynes, Abstracts, pp. 9.
Vearncombe, J.R., 1983a. A proposed continental margin in the Precambrian of Western Kenya. Geol. Runschao, 72(2): 663-670.
Vearncombe, J.R., 1983b. A dismembered aphiolite from the Mozambique belt, West Pokot, Kenya. J. Afr. E. Sciences 1(2): 133-143.
Veizer, J., 1976. $^{87}Sr/^{86}Sr$ Evolution of Seawater during geologic history and its significance as an index of crustal evolution. In. B.F. Windley, 1976. Ed: The Early History of the Earth, p. 569-578.
Vernon, R.H. and Flood, R.H., 1988. Contrasting deformation of S- and I-type granitoids in the Lacklan fold belt eastern Australia. Tectonophysics, V. 147, pp. 127-143.
Vidal, P., Cocherie, A., and LeFort, P., 1982. Geochemical investigations of the Origin of the Mansalu leucogranite (Himalaya, Nepal): Geochimica et Cosmochimica Acta, V. 46, p. 2279-2292.
Wager, L.R., Brown, G.M., and Wadsworth, W.J., 1960. Types of igneous comulates, J. Petrol. 1, 73-85.
Warden, A.J., 1976. Catalogue of Precambrian rocks of Ethiopia, Unpublished manuscript, Ethiopian Institute of Geological surveys. Addis Ababa, Ethiopia.
Warden, A.J., and Horkel, A.d., 1984. The geological evolution of the northeast branch of the Mozambique Belt (Kenya, Somalia, Ethiopia). Mitteilungen Osterreich Geologische Gesellschaft, 77, pp. 161-184.
Whalen, J.B., Currie, K.L., and Chappell, B.W., 1987. A-type granites: geochemical characteristics, discrimination, and petrogenesis: Contrib. Mineral. Petrol., V. 95, p. 407-419.
White, A.J.R. 1979. Sources of granite magmas. Abstract, Geol. Soc. Am. Abstract with Program 11, 539.
White, A.J.R. and Chappell, B.W., 1977. Ultrametamorphism and granitoid genesis. In: D.H. Green (ed.), Experimental Petrology related to extreme metamorphism. Tectonophysics, 43: 7-22.
White, A.J.R., and Chappell, B.W., 1983. Granitoid types and their distribution in the Lachlan Fold Belt, southeastern Australia. Geological Society of America, Memoir 159, pp. 21-34.
Windley, B.R., 1977. Timing of crustal growth and emergence. Nature, 270, 425-428.
Windley, B.R., 1979. Tectonic evolution of the continents in the Precambrian. Episodes, pp. 12-16.
Windley, B.R., 1984. The Evolving Continents, 2nd edition. John Wiley and Sons, 399 pp.
Winchester, J.A., and Floyd, P.A., 1977. Geochemical discrimination of different magma series and their differentiation products using immobile elements. Chem. Geol. 20, 325-43.
Winkler, H.G.F., 1979. Petrogenesis of metamorphic rocks, 4th edition. Berlin: Springer-Verlag.
Witt, .K. and Swager, C.P. 1989. Structural setting and geochemistry of Archean I-type granites in the Bardoe-Coolgardie area of the Norseman-Wiluna belt, Western Australia Precambrian Res., 44, 323-351.
WoldeGabriel, G., White, T., Asfaw, B., and Suva, G., (in press, Journal of African Earth Sciences and the Middle East). Age of volcanism and fossils in the Burji-Soyoma area, Amaro horst, Southern Main Ethiopian rift.

APPENDIX I

Estimate of proportions of minerals in thin sections of selected specimens from the main map units within the Sagan-Afelata area.

Table 3.2 from mafic granulites (unit SD 1).

Sample No.	Qtz	Pl	Kfs	Opx	Cpx	Hbl	Mag	Grt	Bt	Sil
GS 535	-	15	70	tr	7	3	2	1	-	-
== 536a	15	45	tr	15	20	3	2	-	-	-
== 538	-	15	50	tr	25	5	1	3	-	-
NG 77a	-	45	30	5	5	5	2	1	1	tr
== 77b	-	15	70	5	5	5	5	2	1	tr

Note: All abbreviations of mineral names in this table and other similar tables are according to Kretz (1983).

All numbers are visual estimates (in volume %).

tr = trace (i.e. <1% by volume)

Table 3.3 from layered biotite gneiss and associated units (unit FD 2).

Sample No.	Qtz	Kfs	Pl	Hbl	Bt	Mag	Ms	Chl	Grt	Act	Ep	Ttn	Rt
GS 556	5	5	65	15	5	-	-	-	-	-	-	-	2
== 367	15	5	40	20	15	2	-	-	-	-	-	-	-
== 413	10	-	35	50	5	tr	-	-	-	-	-	-	-
== 425	10	-	35	50	5	tr	-	-	-	-	-	-	-
== 531	20	5	50	20	5	tr	-	-	-	-	-	-	-
== 264	5	5	20	70	-	2	s	-	-	-	-	1	-
== 532b	10	-	60	-	-	1	-	s	15	10s	2s	-	-
== 418	10	5	35	15	20	2	-	-	-	-	-	1	-

s secondary

Table 3.4 from different rock types in the "Paragneiss" (unit FD 3).

Sample No.	Qtz	Kfs	Hbl	Pl	Ep	Ttn	Act	Bt	Mag	Sil	Ms	Di	Cal	Fo	Tur	Chl	Grt
SG 136	35	25	18	15	3	3	2	-	-	-	-	-	-	-	-	-	-
== 154	23	tr	2	60	-	-	-	15	tr	-	-	-	-	-	-	-	-
== 174a	15	50	-	10	-	-	-	-	-	10	15	-	-	-	tr	-	-
== 176	-	-	62	30	2	-	-	-	6	-	-	-	-	-	-	-	-
== 176b	25	-	40	30	-	2	-	-	3	-	-	-	-	-	-	-	-
== 181	47	20	10	12	3	2	2	-	tr	-	-	-	4	-	tr	-	-
== 189b	27	35	20	10	-	-	-	-	tr	-	8	-	-	-	-	-	-
== 256a	35	-	-	30	-	1	-	-	-	-	-	15	-	20	-	-	-
== 256b	3	-	40	35	tr	-	-	-	-	-	-	20	-	-	-	-	-
== 137a	20	40	-	35	-	-	-	5	tr	-	3	-	-	-	-	-	-
== 137b	20	45	-	30	-	-	-	5	tr	-	2	-	-	-	-	-	-
== 152a	15	tr	35	40	10	tr	-	-	tr	-	s	-	-	-	-	-	-
== 152b	20	tr	30	45	-	tr	5	-	1	-	-	-	-	-	-	-	tr

Note: Trace amounts of Apatite and Zircon are present in almost all of the thin sections.

Table 3.5 from the Fincha (quartzofeldspathic) gneiss (unit FD 4).

Sample No.	Qtz	kfs	Pl	Mag	Bi	Hbl	Di	Hem	Zrn	Ap	Ttn	Ms	Sil
SG 197	15	70	7	3	-	tr	5	tr	tr	tr	tr	-	-
== 408b	15	70	5	tr	2	-	-	-	-	-	-	-	-
== 400	35	55	5	3	-	-	-	-	-	-	-	-	-
== 418	20	70	3	1	3	tr	-	tr	-	-	tr	-	-
== 421	25	65	2	8	-	-	-	-	-	-	-	-	-
== 424a	20	75	2	1	tr	-	-	-	tr	-	-	tr	-
== 438	30	10	57	tr	3	-	-	-	-	-	-	tr	-
== 449	25	65	5	1	3	tr	-	-	-	-	-	-	-
== 454	20	70	5	1	3	tr	-	-	-	-	-	-	-

Note: Kfs is approximately 90% microcline.

Table 3.6 from the megacrystic granite (unit FD 5).

Sample No.	Pl	Kfs	Bt	Qtz	Hbl	Ttn	Mag	Zrn	Ms	Chl	Ep	Abt
SG 148a	50	15	10	15	5	4	tr	tr	-	-	tr	tr
== 148c*	7	75	2	15	-	-	tr	tr	s	s	-	tr
== 150*	50	15	7	15	4	3	1	tr	-	-	-	tr
== 257a	15	50	10	20	-	1	-	tr	s	tr	-	tr
== 257c	40	5	10	20	20	1	-	tr	-	tr	2	tr
== B01	55	5	10	5	20	4	1	tr	-	-	-	tr
== TA2*	50	25	1	25	-	-	tr	tr	-	-	-	tr
== TA1	50	10	15	15	5	2	tr	tr	-	s	-	tr
== 242	10	70	2	15	-	-	tr	tr	s	s	-	tr
== K01	70	5	1	25	-	tr	tr	tr	-	-	-	tr

* are from late dykes (see text)

Table 3.7 from deformed agerine-bearing leuco-granite (unit FD 7).

Sample No.	Qtz	Kfs	Pl	Bt	Agt	Mag	Ttn	rm	Zrn
SG T32	20	50	10	-	15	5	-	1	tr
== T24	20	65	10	-	4	1	-	tr	tr
== 486	15	70	10	-	5	1	-	-	tr
== 487	20	60	15	-	2	1	tr	-	tr
KM 048	15	75	5	-	5	2	-	-	tr
KM 012	20	75	2	tr	1	1	-	-	tr
TA 028	20	70	5	-	1	1	tr	-	tr
== 014	10	75	5	2	tr	1	1	-	tr

Note: In samples KM 012 and KM 048, Kfs and Pl are predominantly perthitic and antiperthitic respectively.

Table 3.8 from the Bergudda pyroxene-hornblende granitoid complex (FD 8).

Sample No.	Qtz	Kfs	Pl	Hbl	Opx	Ol	Mgt	Di	Bt	Ep	Ttn	Zrn
TA 037	10	20	50	12	3	-	1	2	-	-	-	-
== 051	20	15	45	10	2	tr	3	5	-	-	-	-
== 059a	10	45	47	15	1	-	3	2	1	-	-	-
== 059b	20	4	50	10	2	-	10	1	2	-	-	-
== 064b	20	45	25	-	-	-	tr	-	10	-	-	-
SG 456	15	35	30	10	tr	-	2	10	-	s	2	1
== 457	15	40	35	5	2	-	2	-	-	-	-	-
== 458	10	10	40	10	-	5	4	20	-	-	1	-

Note: In this unit most Kfs and Pl are perthitic and antiperthitic respectively.

Table 3.9 from the meta-tonalite (unit AD1).

Sample No.	Pl	Qtz	Bt	Hbl	Ep	Ttn	Ap	Kfs	Opq	Hm	Chl	Zrn	Di
SG 222a	70	20	7	tr	tr	tr	tr	-	tr	-	-	tr	-
== 228	70	20	7	-	-	-	tr	tr	tr	tr	tr	tr	-
== 231	30	20	10	30	-	-	tr	-	tr	-	-	tr	-
== 312	50	15	15	20	-	1	tr	-	tr	-	-	tr	-
== 314	70	15	7	5	tr	1	tr	-	tr	-	-	tr	-
== 317b	52	18	18	10	-	2	tr	-	tr	-	-	tr	-
== 328	53	22	15	10	tr	tr	tr	tr	tr	-	-	tr	tr
== 334	65	15	10	5	tr	2	tr	tr	1	-	tr	tr	-
== 335	60	20	5	3	tr	tr	tr	10	tr	-	-	tr	-

Table 3.10 from different lithologies in the Hiddi Asasu amphibolite (unit AD 2).

Sample No.	Qtz	Ky	Kfs	Sil	Pl	Di	Mag	Ep	Hbl	Ttn	Ap	Bt	Ms	Zrn	Act	Ath	Tr	Chl	Tlc
SG 126	5	-	tr	-	47	-	tr	tr	45	tr	tr	-	-	tr	-	-	-	-	-
== 127	10	-	-	-	15	30	1	25	-	3	12	-	-	tr	-	-	-	-	-
== 207	30	-	10	-	50	-	3	-	4	2	-	tr	-	tr	-	-	-	-	-
== 209b	7	-	-	-	35	25	-	1	30	tr	tr	-	tr	tr	-	-	-	-	-
== 211a	2	-	1	-	25	10	-	3	60	-	tr	-	-	tr	-	-	-	-	-
== 211b	-	-	-	-	-	-	3	-	-	-	tr	-	-	tr	77	-	-	20	-
== 340	-	-	-	-	-	-	3	-	-	-	tr	-	-	tr	-	-	62	35	-
== 343	-	-	-	-	-	-	2	-	-	-	-	-	-	tr	-	-	-	-	98
== 355	5	-	-	-	30	4	tr	3	60	-	tr	-	1	tr	-	-	-	-	-
== 356a	34	-	tr	-	50	-	-	5	6	1	tr	-	-	tr	4	-	-	-	-
== 357	20	-	-	-	16	50	-	-	3	6	1	-	-	tr	-	-	-	-	-
== 360	-	-	-	-	8	2	-	s	90	-	tr	-	-	tr	-	-	-	-	-
== 362	50	10	-	15	30	-	-	-	-	-	-	-	-	tr	-	-	-	-	-
== 364	25	-	55	-	-	-	1	-	-	-	-	tr	-	19	tr	-	-	-	-

APPENDIX II

Bulk chemistry of magmatic rocks studied from the Sagan - Afelata area.

Table 6.2 Major oxide analyses and normative mineral proportions from the Seeb... tonalite (Unit AD 1).

	G317B	G 4561	G 4932	G 4971	G 4954	G 4931	SG527	MEAN
SI02	62.08	61.35	69.20	69.15	60.69	61.37	67.14	64.43
TI02	0.67	0.57	0.26	0.67	0.59	0.50	0.18	0.49
AL203	16.39	18.95	15.89	16.65	18.52	18.18	13.23	16.83
FE203	1.95	1.72	0.91	0.87	1.84	1.53	1.54	1.34
FEO	4.58	4.04	2.12	2.04	4.28	3.58	0.66	3.16
MNO	0.11	0.10	0.08	0.04	0.13	0.07	nd	0.09
MGO	2.68	1.59	0.83	0.67	1.96	1.76	2.40	1.70
CAO	5.69	6.02	3.83	4.55	5.92	6.10	6.79	5.56
NA20	3.86	4.62	4.53	4.52	4.69	4.71	2.56	4.21
K20	1.72	1.14	1.16	0.70	1.07	1.47	0.51	1.11
S	0.03	0.03	0.02	0.04	0.05	nd	nd	0.03
P205	0.18	0.27	0.14	0.09	0.26	0.39	0.04	0.20
TOTAL	99.94	100.40	98.97	99.99	100.00	99.66	100.23	99.93
Ap	0.39	0.59	0.31	0.20	0.57	0.85	0.09	0.41
Il	1.27	1.08	0.49	1.27	1.12	0.95	0.34	0.90
Mt	2.82	2.49	1.31	1.26	2.64	2.21	3.20	6.29
Or	10.11	6.71	6.84	4.12	6.29	8.65	3.01	6.29
Ab	32.50	38.92	38.23	38.15	39.50	39.71	21.65	34.12
An	22.20	27.48	18.04	21.93	26.20	24.03	23.09	22.72
Di	3.91	0.42			1.12	2.99	8.61	2.04
Hy	11.50	9.77	5.36	4.07	10.78	8.22	9.07	7.94
C			0.55	0.40				
Q	15.21	12.91	27.81	28.54	11.72	12.06	31.16	19.16
Total	99.91	100.37	98.95	99.95	99.95	99.66	100.23	99.85
A	35.96	41.89	57.55	57.21	39.67	45.38	23.44	30.90
M	17.27	11.56	8.39	7.34	13.50	12.92	18.33	9.86
F	46.77	46.55	34.06	35.44	46.84	41.70	58.23	59.24
Q	53.23	52.61	56.54	56.51	52.28	52.54	57.80	53.48
M	11.66	8.49	4.17	4.24	9.58	8.62	12.38	12.05
L	35.12	38.90	39.29	39.26	38.14	38.84	29.82	34.46

Table 6.2 Cont'd. Trace element analyses from the Sebbeto tonalite (Unit AD 1).

	G317B	G 4561	G 4932	G 4971	G 4954	G 4931	SG527	MEAN
BA	462	522	536	371	485	511	155	440
CR	127	11.00	19.00	18.00	14.00	23.00	106.00	45.43
ZR	191	104.00	71.00	122	84.00	52.00	7.00	90.14
SR	485	870	618	827	771	814	116	643
RB	43.00	20.00	16.00	nd	8.00	20.00	nd	21.40
Y	21.00	10.00	3.00	3.00	12.00	10.00	6.00	9.29
NB	nd	nd	nd	nd	nd	nd	nd	nd
ZN	107.00	128	120	95.00	129	78.00	63.00	102.86
NI	215	nd	nd	16.00	nd	35.00	135	100.25
V	150	85.00	34.00	25.00	125	147	242	115
GTOTAL	100.18	100.62	99.12	99.75	100.20	99.89	100.49	100.03
K/RB(W)	333	474	604	1000	100.05	610	100.49	460
RB/SR	.09000	.02000	.03000	nd	.01000	.02000	nd	.03400
BA/SR	.95000	.60000	.87000	.45000	.49000	.68000	1.34	.76357
K/RB(M)	728	1037	1320	1000	2008	1333	1000	1204
RB/SR	.09000	.02000	.03000	nd	.01000	.03000	nd	.03600
BA/SR	.61000	1.44	.55000	.29000	.31000	.43000	.85000	.64000

Table 6.3 Major element compositions and normative mineral proportions of the Altuntu granite (Unit FD 5).

	SGTK01	SGTA2	SGBD01	SGTA1	MNALT
SI02	75.65	73.40	73.82	66.54	72.35
TI02	0.21	0.05	0.13	0.62	0.25
AL203	12.37	13.85	13.41	15.37	13.75
FE203	0.26	0.67	0.18	0.71	0.33
FEO	0.92	0.19	0.63	2.51	1.19
MNO	0.04	0.02	0.02	0.06	0.04
MGO	0.40	0.28	0.36	1.54	0.65
CAO	0.80	1.14	0.88	2.88	1.43
NA20	3.51	3.67	3.66	4.38	3.81
K20	4.42	5.12	5.23	3.54	4.58
S	nd	0.01	nd	nd	0.01
P205	0.06	0.01	0.02	0.18	0.07
TOTAL	98.64	98.43	98.33	98.33	98.43
Ap	.13189	.02199	.04397	.39533	.14835
Il	.39948	.09513	.24736	1.18	.48024
Mt	.86353	.64412	.58560	2.35	1.11
Or	26.09	30.23	30.88	20.88	27.01
Ab	29.67	31.03	30.95	37.00	32.16
An	3.57	5.59	4.23	11.80	6.62
Di	nd	nd	nd	1.03	nd
Hy	1.42	1.17	1.19	4.34	2.15
C	.50067	.22180	.17583	nd	.10636
Q	35.99	29.42	30.03	19.36	29.63
Total	98.64	98.42	98.33	98.33	98.42
A	82.25	87.48	87.68	60.74	78.22
M	4.15	2.79	3.55	11.81	6.02
F	13.60	9.73	8.77	27.44	15.76
Q	57.94	56.55	56.68	54.26	56.46
M	1.74	1.18	1.27	5.99	2.43
L	40.32	42.27	42.05	39.75	41.11

Table 6.3 cont'd. Trace element analyses from the Altuntu granite (Unit FD 5).

	SGTK01	SGTA2	SGBD01	SGTA1	MEAN
BA	216	517	355	939	507
CR	23.00	51.00	41.00	37.00	38.00
ZR	118	85.00	74.00	220	124
SR	126	166	156	786	309
RB	125	115	84.00	72.00	99.00
Y	5.00	8.00	8.00	21.00	10.50
NB	8.00	nd	nd	7.00	7.50
ZN	nd	nd	nd	37.00	37.00
NI	13.00	31.00	30.00	20.00	23.50
V	nd	nd	nd	42.00	42.00
GTOTAL	98.72	98.55	98.40	98.60	98.57
K/RB(W)	293	369	517	409	397
RB/SR	.99000	.69000	.54000	.09000	.57750
BA/SR	1.71	3.11	2.28	1.19	2.07
K/RB(M)	641	807	1129	893	868
RB/SR	1.02	.71000	.55000	0.9000	.59250
BA/SR	1.09	1.98	1.45	.76000	1.32

Table 6.4 Major oxide analyses and normative mineral proportions in the Kinsho granite (Unit FD 7).

	SG 487	SG 486	GT 32	SG467a	SG D02	PK 01	KM 012	SG467b	MEAN
SI02	76.16	74.68	73.42	74.11	75.52	74.49	74.87	74.90	74.77
TI02	0.18	0.20	0.43	0.38	0.32	0.18	0.11	0.34	0.27
AL203	10.85	11.30	8.17	11.33	10.14	11.58	11.43	11.71	10.91
FE203	2.92	2.60	6.75	2.91	3.60	2.69	1.35	2.81	3.21
FEO	0.71	0.64	1.65	0.71	0.88	0.66	0.33	0.69	0.78
MNO	0.09	0.12	0.24	0.09	0.14	0.10	0.09	0.08	0.12
MGO	0.10	0.02	0.36	0.23	0.11	0.10	0.23	0.23	0.17
CAO	0.20	0.33	0.82	1.00	0.44	0.25	0.30	0.93	0.63
NA20	4.21	4.75	3.01	2.95	3.04	4.51	4.52	3.59	3.82
K2O	3.99	4.04	4.02	4.78	4.45	4.29	3.27	3.98	4.10
S	0.03	0.03	0.04	0.04	0.04	0.04	0.03	0.03	0.04
P205	.. nd	0.01	nd	nd	nd	0.05	0.02	0.01	0.02
TOTAL	99.44	98.72	98.91	98.53	98.69	98.94	96.55	99.30	98.63
Ap		0.02				0.11	0.04	0.02	0.05
Il	0.34	0.38	0.82	0.72	0.61	0.34	0.21	0.65	0.51
Mt	2.32	1.76	5.43	1.74	2.68	2.16	1.16	1.73	2.41
Or	23.54	23.84	23.69	28.20	26.25	25.32	19.30	23.48	24.20
Ab	33.55	35.59	19.59	24.93	25.68	35.64	38.22	30.34	32.30
An	0.00			3.55	0.88		1.24	4.08	0.23
Di	0.54	0.45	1.93	1.10	0.59	0.54	0.09	0.36	0.33
Hy				0.07			0.53	0.40	
Ac	1.79	4.02	5.13			2.19			
Q	36.50	32.18	40.39	36.47	39.97	32.06	35.17	36.58	35.97
Hm	0.70		1.23	1.72	1.76	0.45	0.56	1.62	1.55
Wo	0.13	0.44	0.66		0.23	0.09			0.45
Tot.	99.41	98.69	98.87	98.49	98.65	98.90	96.52	99.27	98.60
A	66.48	70.83	42.03	64.51	59.48	69.72	78.79	64.76	63.25
M	0.81	0.16	2.15	1.92	0.87	0.79	2.33	1.97	1.38
F	32.71	29.01	55.81	33.57	39.63	29.49	18.88	33.27	35.38
Q	58.16	57.48	59.28	58.04	58.81	57.22	57.74	58.00	57.94
M	4.21	4.24	11.46	4.39	5.08	4.02	1.99	4.01	4.79
L	37.63	38.28	29.26	37.57	36.12	38.77	40.27	37.99	37.28

Table 6.4 cont'd. Trace element analyses from the Kinsho granite (Unit FD 7).

	SG 487	SG 486	GT 32	SG467a	SG D02	PK 01	KM 012	SG457b	MEAN
BA	278	119	198	522	141	123	187	429	250
CR	19.00	9.00	nd	nd	nd	nd	nd	nd	14.00
ZR	417	470	2391	1019	657	587	346	1062	869
SR	28.00	16.00	57.00	119	35.00	8.00	13.00	112	48.50
RB	87.00	99.00	134	96.00	101.00	111	60.00	77.00	95.63
Y	12.00	50.00	141	177	67.00	49.00	32.00	153	85.13
NB	3.00	10.00	164	44.00	16.00	16.00	8.00	42.00	37.88
ZN	77.00	134	245	75.00	156	142	52.00	108.00	124
NI	nd	nd	nd	11.00	nd	nd	nd	nd	11.00
V	nd	nd	nd	19.00	nd	nd	2.00	nd	10.50
GT	99.55	99.84	99.35	98.79	99.04	99.06	96.63	99.55	98.98
WK/RB	381	339	249	414	366	321	452	429	369
RB/SR	3.11	6.19	2.35	.81000	2.89	13.88	4.62	.09000	4.24
BA/SR	9.93	7.44	3.47	4.39	4.03	15.38	14.38	3.83	7.86
MK/RB	832	741	544	904	799	701	988	938	806
RB/SR	3.18	6.34	2.41	.83000	2.96	14.22	4.73	.70000	4.42
BA/SR	6.32	4.74	2.21	2.79	2.57	9.79	9.16	2.44	5.00

Table 6.5a Major oxide compositions and normative mineral proportions in the dark core of the Bergudda complex (Unit FD 8)

	SG5631	SG5651	SG5572	MEAN
SI02	62.47	61.49	59.59	61.18
TI02	0.66	1.15	0.88	0.90
AL203	16.84	14.73	15.96	15.84
FE203	1.33	1.70	1.92	1.65
F_O	4.99	6.40	7.23	6.21
MNO	0.15	0.18	0.18	0.17
MGO	0.45	1.10	0.55	0.70
CAO	2.30	2.74	2.68	2.57
NA20	5.82	4.99	5.19	5.33
K20	4.94	4.54	5.26	4.91
S	0.06	0.05	0.04	0.05
P205	0.18	0.33	0.21	0.24
TOTAL	100.19	99.40	99.69	99.76
Ap	.39388	.72102	.45836	.52447
Il	1.25	2.17	1.66	1.70
Mt	1.92	2.45	2.77	2.38
Or	29.03	26.63	30.83	28.83
Ab	48.98	41.93	43.57	44.82
An	5.21	4.35	4.68	4.75
Di	4.35	6.04	6.28	5.56
Hy	7.08	9.63	7.38	8.92
Ol	nd	nd	nd	nd
Q	1.92	5.41	nd	2.23
Total	100.13	99.35	99.65	99.71
A	59.01	48.54	49.37	52.07
M	2.47	5.60	2.60	3.56
F	38.52	45.85	48.04	44.37
Q	49.65	50.30	48.85	49.49
M	8.92	12.51	12.67	11.38
L	41.43	37.19	38.48	39.13

Table 6.5a Contd. Trace element analyses from the dark core of the Bergudda complex (Unit FD 8).

	SG5631	SG5651	SG5572	MEAN
BA	1183	1048	1177	1136
CR	22.00	nd	2.00	12.00
ZR	396	1105	1491	997
SR	203	210	191	201
RB	48.00	47.00	42.00	45.67
Y	42.00	73.00	52.00	55.67
NB	38.00	65.00	85.00	62.57
ZN	144	239	209	197
NI	133	nd	nd	133
V	nd	10.00	nd	10.00
GTOTAL	100.45	99.73	100.08	100.09
K/RB	855	803	nd	829
RB/SR	.24000	.22000	.22000	.22667
BA/SR	5.83	4.99	6.16	5.66
MK/RB	1869	1754	2270	1965
RB/SR	.24000	.23000	.23000	.23333
BA/SR	3.71	3.18	3.93	3.61

Table 6.5b Major oxide compositions and normative mineral proportions in the intermediate zone of the Bergudda complex (Unit FD 8).

	SG5812	SG5781	SG5791	MEAN
SI02	63.44	64.76	64.26	65.15
TI02	1.25	1.28	1.13	1.22
AL203	14.00	13.61	13.52	13.71
FE203	2.67	2.77	2.57	2.66
FEO	4.14	4.33	4.01	4.17
MNO	0.12	0.12	0.11	0.12
MGO	1.17	1.16	1.31	1.21
CAO	3.03	2.75	3.18	2.99
NA20	4.05	3.86	3.80	3.90
K20	4.20	4.15	3.96	4.10
S	0.04	0.03	0.04	0.04
P205	0.38	0.39	0.32	0.36
TOTAL	98.49	99.21	98.21	98.64
Ap	0.83	0.85	0.70	0.80
Il	2.37	2.43	2.14	2.31
Mt	3.86	4.03	3.73	3.87
Or	24.70	24.40	23.29	24.13
Ab	34.11	32.51	32.01	32.88
An	7.58	7.52	8.10	7.73
Di	4.13	2.97	4.62	3.91
Hy	5.21	5.98	5.29	5.49
Q	15.65	18.50	18.28	17.48
Tot.	98.45	99.18	98.17	98.60
A	48.56	46.95	47.37	47.63
M	6.89	6.80	8.00	7.22
F	44.55	46.25	44.64	45.15
Q	52.82	53.52	53.57	53.34
M	10.84	10.81	10.75	10.80
L	36.34	35.67	35.59	35.86

Table 6.5b Cont'd. Trace element analyses from the intermediate zone of the Bergudda complex (Unit FD 8).

	SG5612	SG5781	SG5791	MEAN
BA	888	827	684	800
CR	nd	nd	3.00	3.00
ZR	653	786	635	691
SR	276	232	220	243
RB	74.00	97.00	107.00	92.67
Y	68.00	86.00	78.00	77.33
NB	43.00	49.00	35.00	42.33
ZN	134	127	149	137
NI	nd	3.00	nd	3.00
V	66.00	51.00	58.00	58.33
GT.	98.76	99.49	98.45	98.90
K/RB	472	355	307	378
RB/SR	.27000	.42000	.49000	.39333
BA/SR	3.22	3.56	3.11	3.30
MK/RB	1031	776	672	826
RB/SR	.27000	.43000	.50000	.40000
BA/SR	2.05	2.27	1.98	2.10

Table 6.5c Major oxide compositions and normative mineral proportions in the pink rim of the Bergudda complex (Unit FD 8).

	PG 78A	SG 543	MEAN
SI02	69.32	57.92	63.62
TI02	0.57	2.07	1.32
AL203	14.12	13.47	13.80
FE203	1.89	6.58	4.63
FEO	2.68	4.65	3.27
MNO	0.08	0.19	0.14
MGO	0.35	1.93	1.14
CAO	1.50	4.11	2.81
NA20	4.15	4.25	4.20
K20	5.11	3.45	4.28
S	0.04	0.07	0.06
P205	0.10	0.73	0.42
TOTAL	99.91	99 42	99.67
Ap	.21933	1.60	.90852
Il	1.08	3.91	2.50
Mt	2.74	6.71	4.73
Or	30.09	20.24	25.16
Ab	35.01	35.72	35.36
An	4.79	7.44	6.12
Di	1.70	6.76	4.24
Hy	3.09	7.87	5.48
Q	21.14	9.10	15.11
Total	99.87	99.35	99.61
A	63.04	34.83	46.09
M	2.38	8.73	6.20
F	34.57	56.44	47.71
Q	54.57	49.66	52.36
M	5.95	18.14	12.03
L	39.48	32.20	35.61

Table 6.5c cont'd. Trace element analyses from the pink outer rim of the Bergudda Complex (Unit FD8).

	PG 78A	SG 543	MEAN
BA	803	777	790
CR	nd	nd	3.00
ZR	720	583	652
SR	160	344	252
RB	127	25.00	76.00
Y	72.00	71.00	71.50
NB	50.00	76.00	63.00
ZN	124	129	127
NI	nd	nd	nd
V	nd	70.00	70.00
GTOTAL	100.16	99.67	99.92
K/RB	344	1145	739
RB/SR	.79000	.07000	.43000
BA/SR	5.02	2.26	3.64
MK/RB	730	2503	1616
RB/SR	.81000	.07000	.44000
BA/SR	3.20	1.44	2.32

Table 6.6 Major oxide compositions and normative mineral proportions from the Hiddi-Asasu amphibolite (Unit AD 2).

	SGC522	SG5241	SGC511	GS221	SG516	SG5201	MEAN
SI02	48.34	48.21	47.08	45.62	49.55	48.17	47.83
TI02	0.87	0.62	1.49	0.81	1.35	1.41	1.09
AL203	14.09	11.75	16.24	15.36	15.73	14.58	14.63
FE203	1.92	1.51	2.27	1.76	1.97	2.16	1.93
FEO	9.62	7.60	11.41	8.82	9.87	10.88	9.70
MNO	0.19	0.15	0.22	0.17	0.19	0.22	0.19
MGO	7.92	10.69	5.98	6.67	7.04	7.06	7.56
CAO	13.25	15.80	12.15	15.39	11.32	11.54	13.24
NA20	3.43	2.16	2.42	2.23	3.13	3.38	2.79
K20	0.81	0.99	0.67	0.73	0.50	0.72	0.74
S	nd	0.01	nd	nd	nd	0.01	0.01
P205	0.22	0.12	0.17	0.19	0.14	0.19	0.17
TOTAL	100.66	99.61	100.10	97.75	100.79	100.32	99.87
Ap	0.48	0.26	0.37	0.42	0.31	0.42	0.38
Il	1.66	1.18	2.83	1.54	2.57	2.68	2.08
Mt	2.79	2.19	3.30	2.56	2.86	3.14	2.81
Or	4.78	5.84	3.96	4.31	2.95	4.25	4.35
Ab	13.54	5.02	19.46	6.24	26.46	20.32	15.17
An	20.64	19.42	31.45	29.72	27.37	22.47	25.18
Di	35.82	46.99	23.04	37.33	22.93	27.69	32.30
Ol	12.58	11.53	15.15	8.80	15.34	14.87	13.04
Ne	8.37	7.17	0.54	6.83	0.00	4.47	4.56
Total	100.66	99.60	100.10	97.75	100.79	100.31	99.87
A	17.73	13.63	13.43	14.51	15.97	16.78	15.34
M	33.12	46.24	26.00	32.69	30.97	28.89	32.98
F	49.15	40.13	60.57	52.81	53.06	54.34	51.68
Q	47.68	48.28	48.98	48.00	49.28	48.24	48.41
M	28.89	32.58	26.11	27.85	25.44	27.71	28.10
L	23.42	19.14	24.91	24.15	25.28	24.05	23.49

Table 6.6 Cont'd. Trace element analyses from the Hiddi-Asasu amphibolite (Unit A2).

	SGC522	SG5241	SGC511	G5221	SG516	SG5201	MEAN
BA	198	224	93.00	178	73.00	123	148
CR	246	586	53.00	212	256	186	257
ZR	44.00	21.00	43.00	32.00	83.00	64.00	47.83
SR	302	455	352	403	155	325	322
RB	nd	30.00	9.00	nd	3.00	3.00	11.25
Y	17.00	13.00	20.00	17.00	38.00	31.00	22.67
NB	nd	nd	nd	nd	nd	nd	32.30
ZN	64.00	45.00	75.00	67.00	96.00	99.00	74.33
NI	99.00	214	60.00	81.00	94.00	100.00	108.00
V	377	299	804	349	309	404	424
GTOT.	100.83	99.87	100.35	97.97	100.94	100.49	100.07
K/RB(W)	1000	275	618	1000	1386	1979	1043
RB/SR	nd	.07000	.03000	nd	.02000	.01000	.03250
BA/SR	.66000	.49000	.26000	.44000	.47000	.38000	.45000
K/RB(M)	1000	601	1350	1000	3030	4326	1885
RB/SR	nd	.07000	.03000	nd	.02000	.01000	.03250
BA/SR	.42000	.31000	.17000	.28000	.30000	.24000	.29667

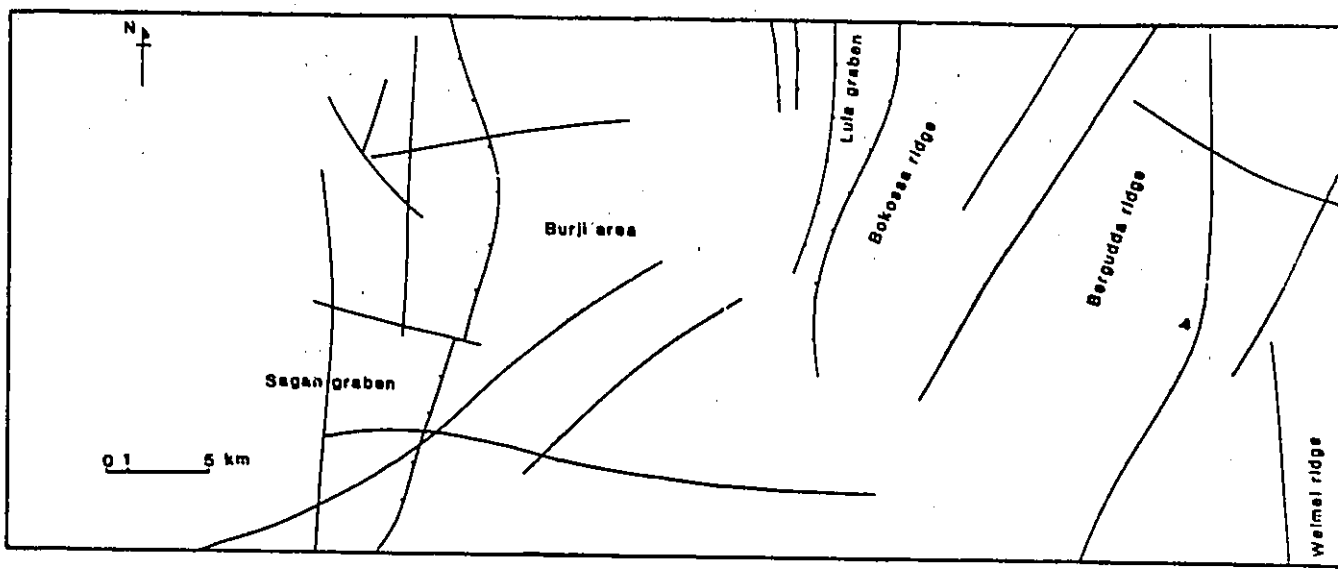
N
Luia graben
Bokosea ridge
Burji area
Bergudda ridge
Sagan graben
0 1 5 km
Welmel ridge

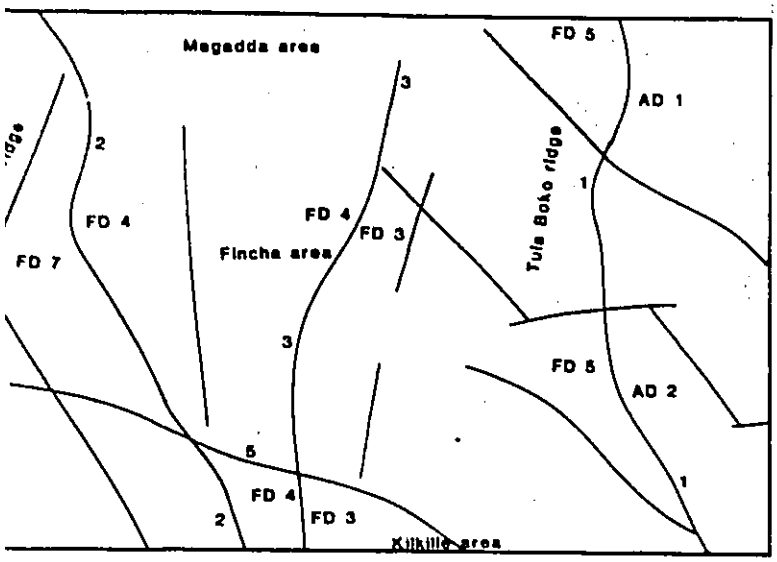

Fig. 4. Map showing the spatial distribution of major lineaments in the Sagan - Afdata area.

SYMBOLS

Lineaments — Rift related faults

Numbers refer to some lineaments which have been referred to in the text and Gichile et al (1986).

(1) The Kolie-Altunta lineament
(2) The Doga-Diddiga lineament
(3) The Dima-Surruppitti lineament
(4) The Godolle lineament
(5) The Kilkille lineament

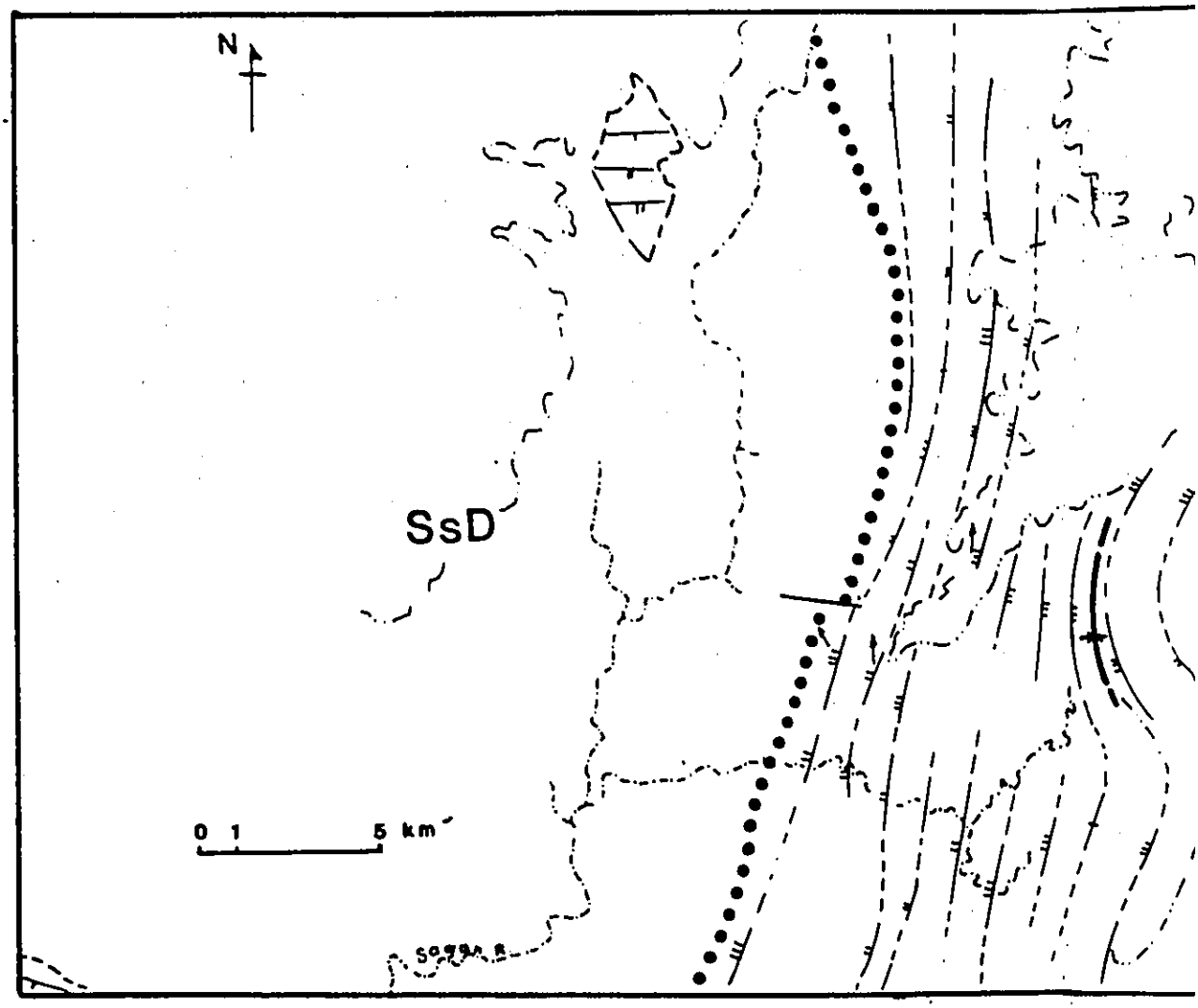

Fig. 4.1 Simplified structural map of the Sagan-Afelata area

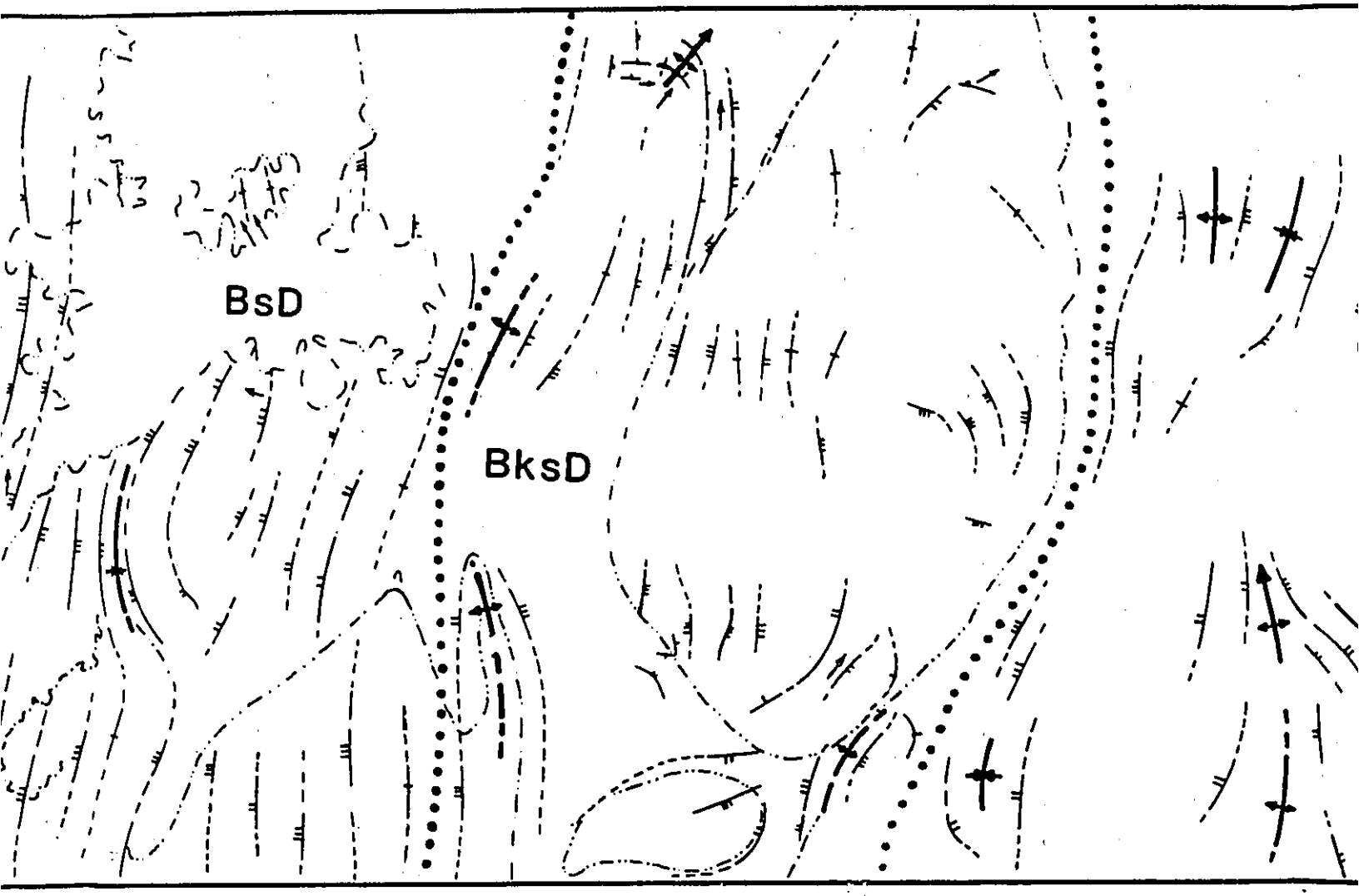

ıta area

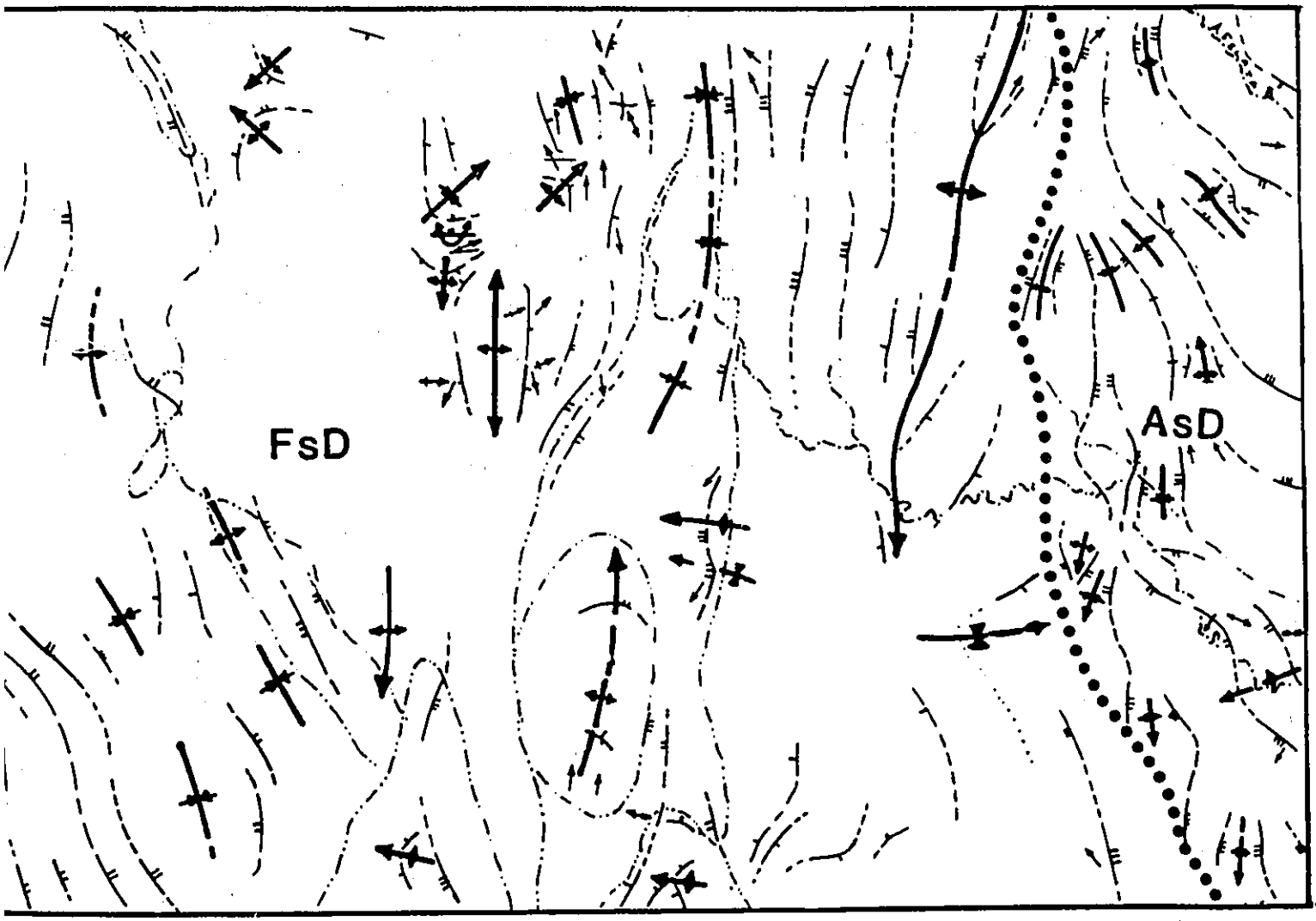

Samuel Gichile (1990)

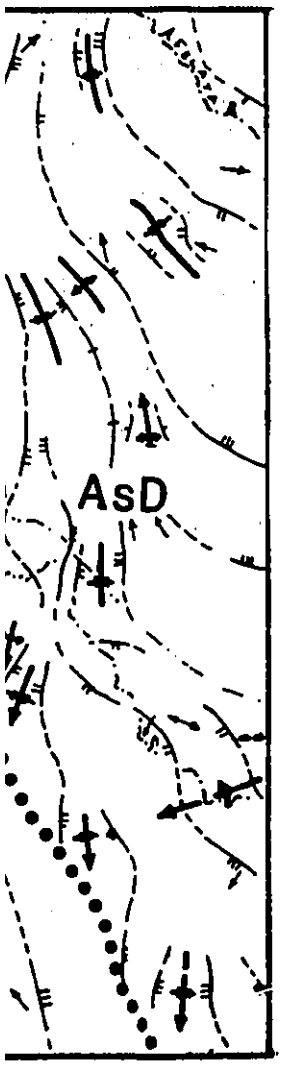

SYMBOLS

Trace of foliation

- Observed
- Inferred
- extrapolated
- horizontal
- 0 -30° dip
- 31-60° dip
- 61- 89° dip
- vertical
- **representative lineation**

Axial surface trace of major folds

- F_1 antiform overturned
- F_2 antiform /synform
- F_3 antiform/ synform

Other Symbols

- main stream
- main lithologic boundary (simplified)
- domain boundary

SsD	Sagan structural domain
BsD	Burji structural domain
BksD	Bokossa structural domain
AsD	Afelata structural domain
FsD	Fincha structural domain

al Gichile (1990)

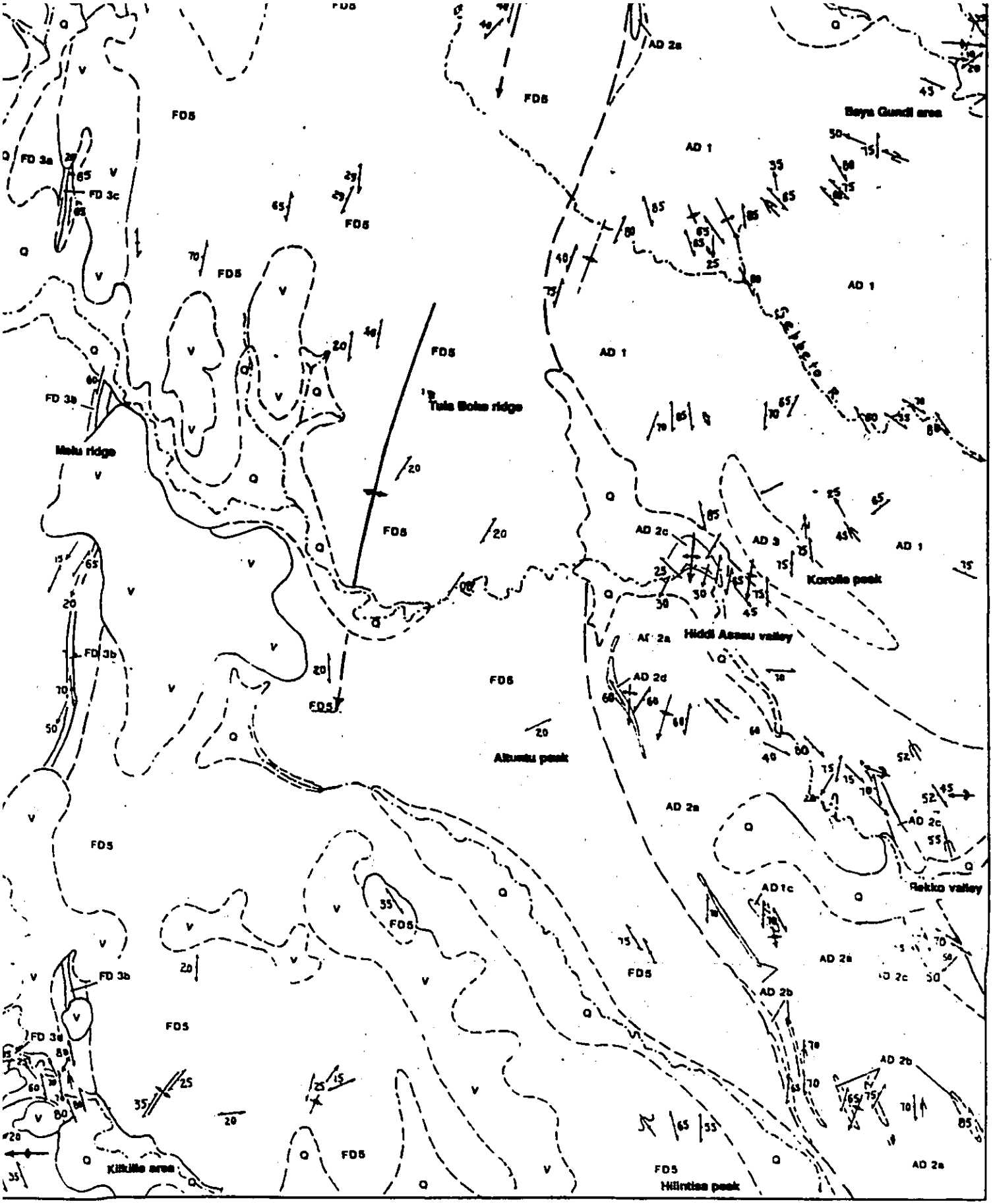
Baya Gundi area
Tula Bolse ridge
Melu ridge
Korolle peak
Hiddi Assau valley
Albuetu peak
Rekko valley
Kikilla area
Hilintisa peak
FDS
AD 1
AD 2a
AD 2b
AD 2c
AD 2d
AD 3
AD 1c
FD 3a
FD 3b
FD 3c
5°15' N
38°30'E

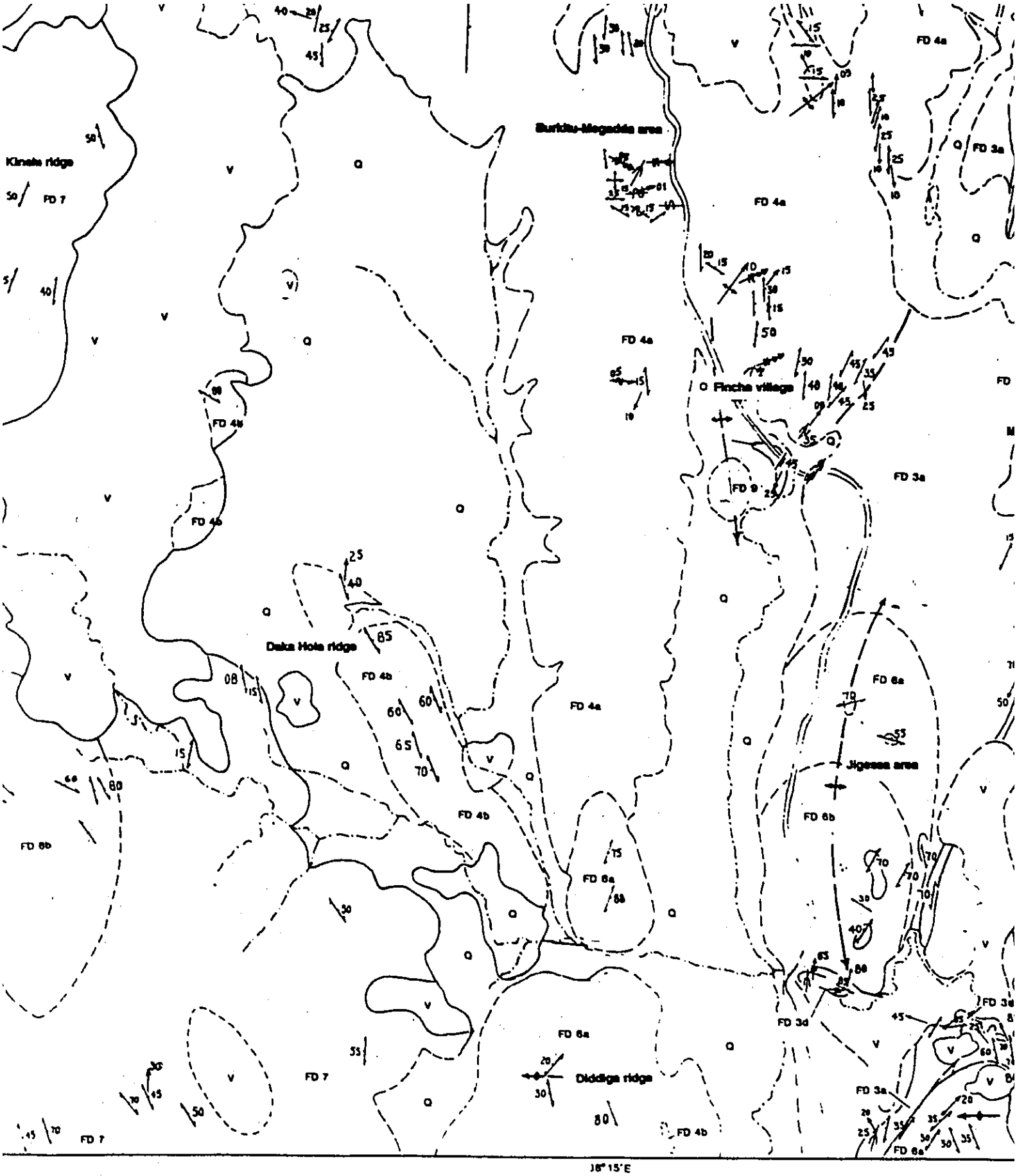
Kinete ridge
Buridu-Megadda area
Finche village
Deka Hole ridge
Jigessa area
Diddiga ridge
FD 7
FD 4a
FD 4b
FD 3a
FD 3d
FD 6a
FD 6b
FD 9
38°15'E

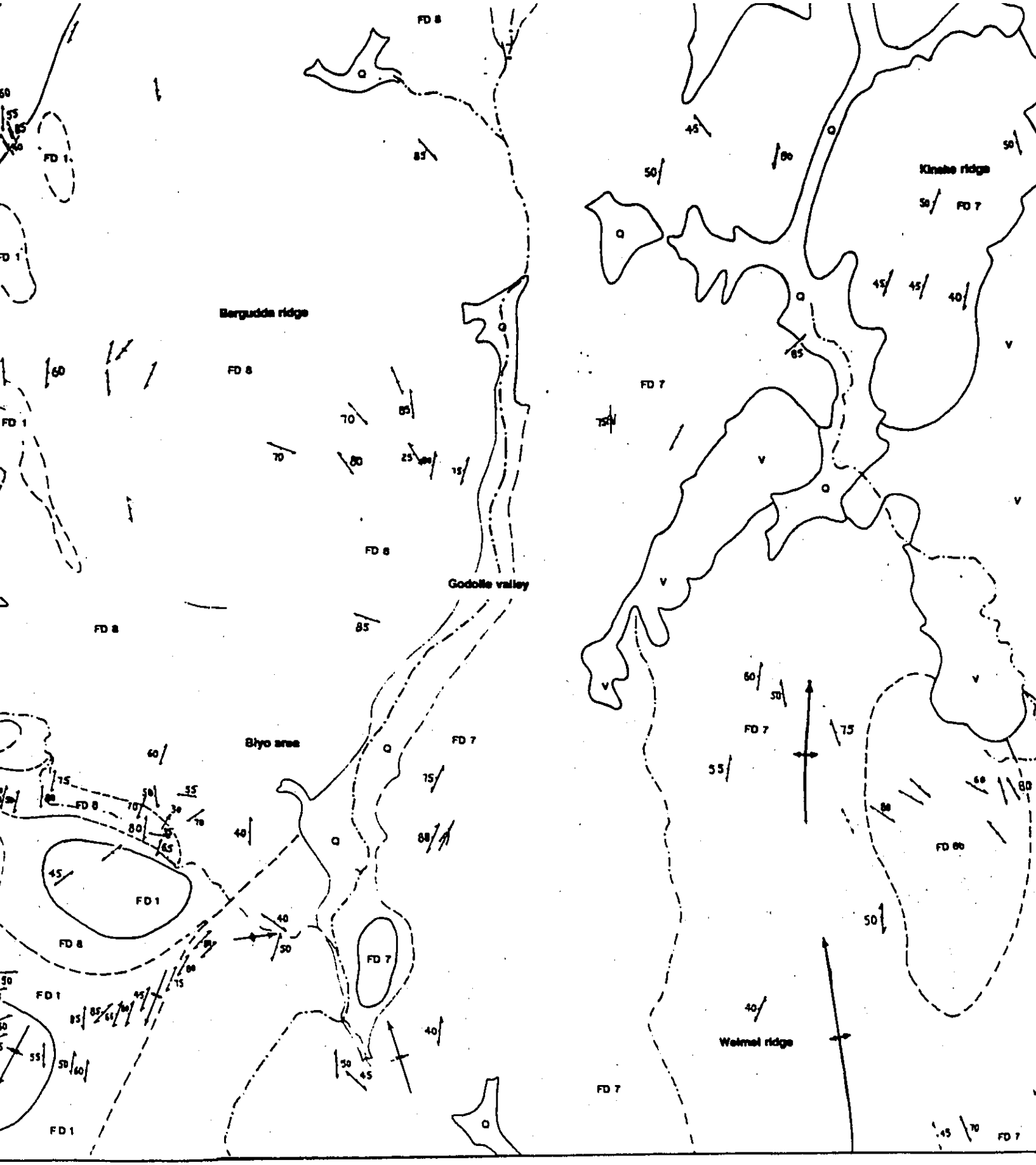
Bergudda ridge
Godolle valley
Biyo area
Kinake ridge
Waimei ridge
FD 1
FD 6
FD 7
FD 8
Q
V
38°00'E

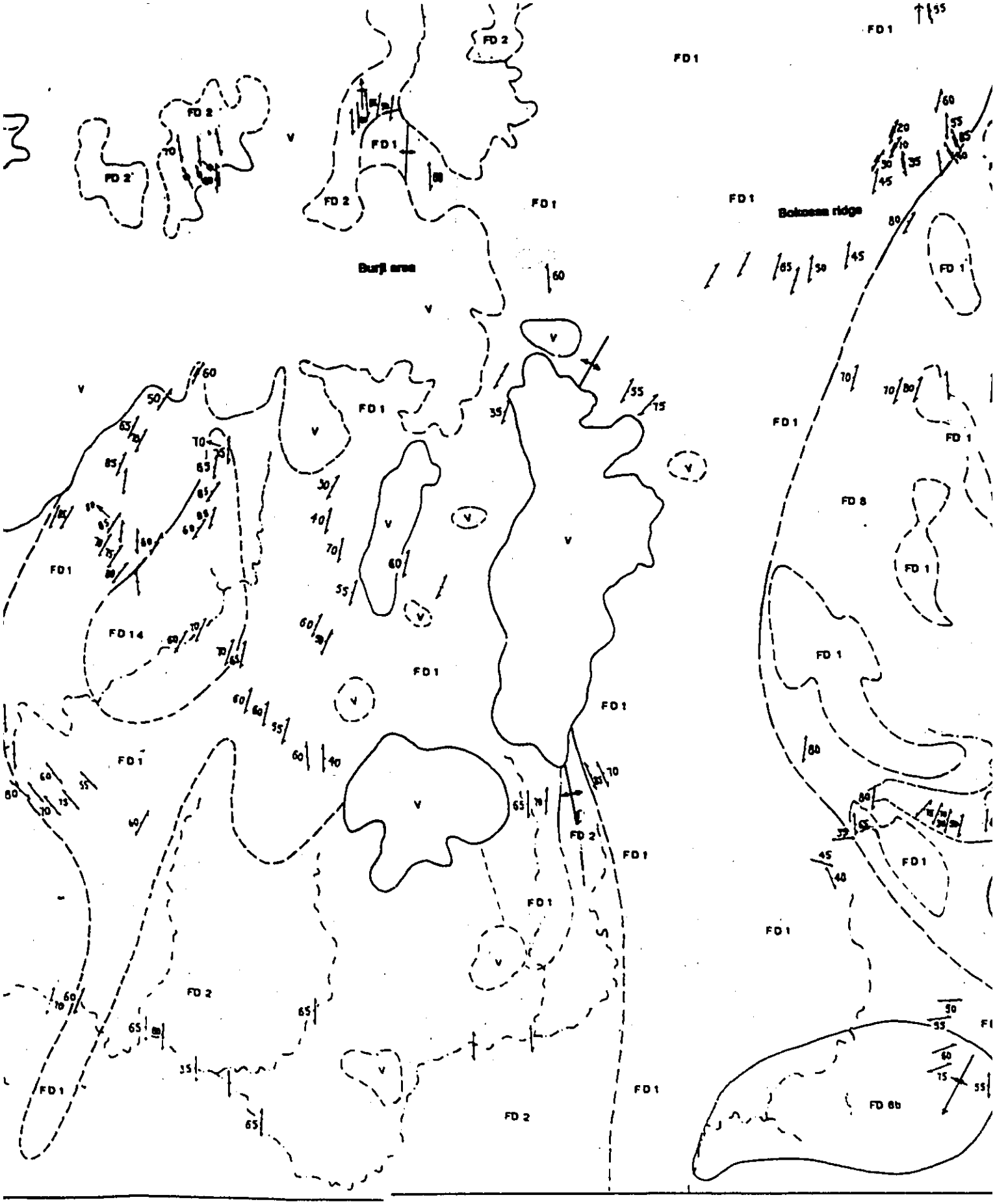
Burji area
Bokoona ridge
FD 1
FD 2
FD 8
FD 14
FD 8b
V

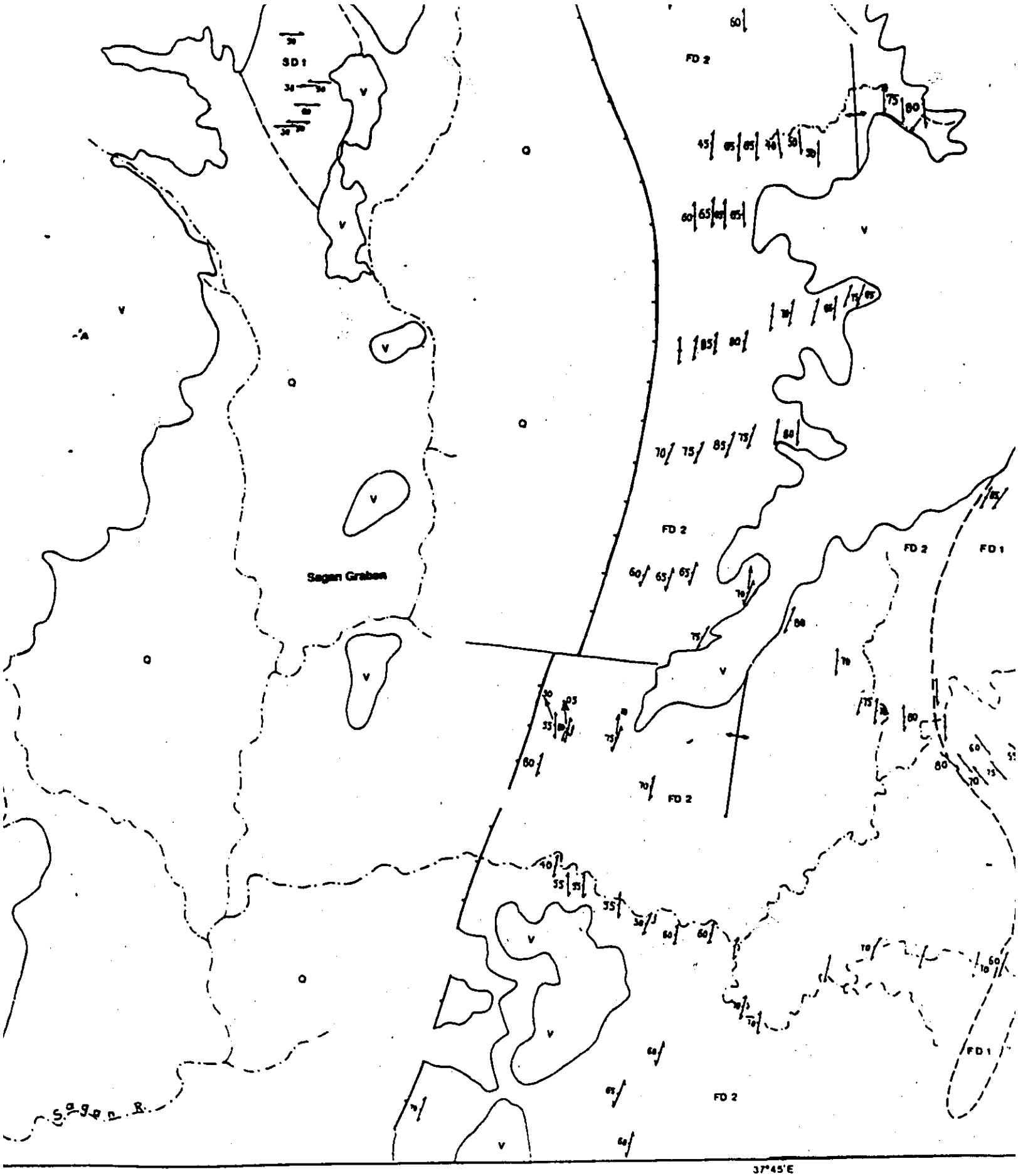
SD 1
FD 2
FD 1
Sagan Graben
37°45'E

Location map

TERTIARY AND QUATERNARY

V / G	Volcanics / Granite	Q	sediments

PRECAMBRIAN - PALEOZOIC

AFELATA DOMAIN

AD 3	Meta pyroxenite	AD 2	Amphibolite (a), talc schist (b), biotite (c) and calcsilicate (d) gneiss
AD 1	Meta tonalite		

FINCHA DOMAIN

FD 9	Massive granite

FD 8	Meta-Pyroxene - Hbl plutonic complex	FD 7	Foliated agerine bearing leucogranite
FD 6	Foliated small (a) granite (b) quartzdiorite bodies	FD 5	Meta- mega crystic granite
FD 4	(a) Quartzofeldspathic gneiss,(b) Quartzite and ultramafic schist	FD 3	Paragneisses (a) Bt., (b) Calc-sil.,(c) Sil-Ms (d) Amphibolite
FD 2	Layered Biotite gneiss	FD 1	Granitic gneiss

SAGAN DOMAIN

SD 1	Mafic granulite

Note: Rock units not necessarily in stratigraphic order.
Western Quarter of map modified from Gottchun and Abas (1987) with additional traversing.

STRUCTURAL SYMBOLS

- Foliation (includes gneissosity) (a) dip indicated (b) vertical (c) horizontal (d) layer parallel
- L_1 Lineation (a) Plunging (b) horizontal (c) fold axis
- L_2 Lineation (a) Plunging (b) horizontal (c) minor fold axis
- Profile of minor fold (a) F_1 (b) F_2 (c) F_3
- Axial trace of major [1] F_2, [2] F_3 folds (a) antiform (b) synform
- Minor shear zone (sense indicated)
- Major faults (a) observed (b) inferred (c) rift fault with teeth on downthrown block
- Lithologic boundary (a) observed (b) inferred

OTHER SYMBOLS

- Village
- Major highway (Addis Ababa - Nairobi)
- Stream

Scale
1 0 2 5 km

Samuel Gichile (1989)

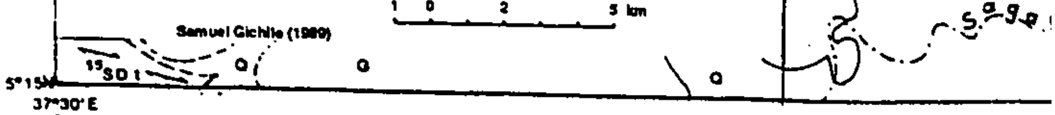

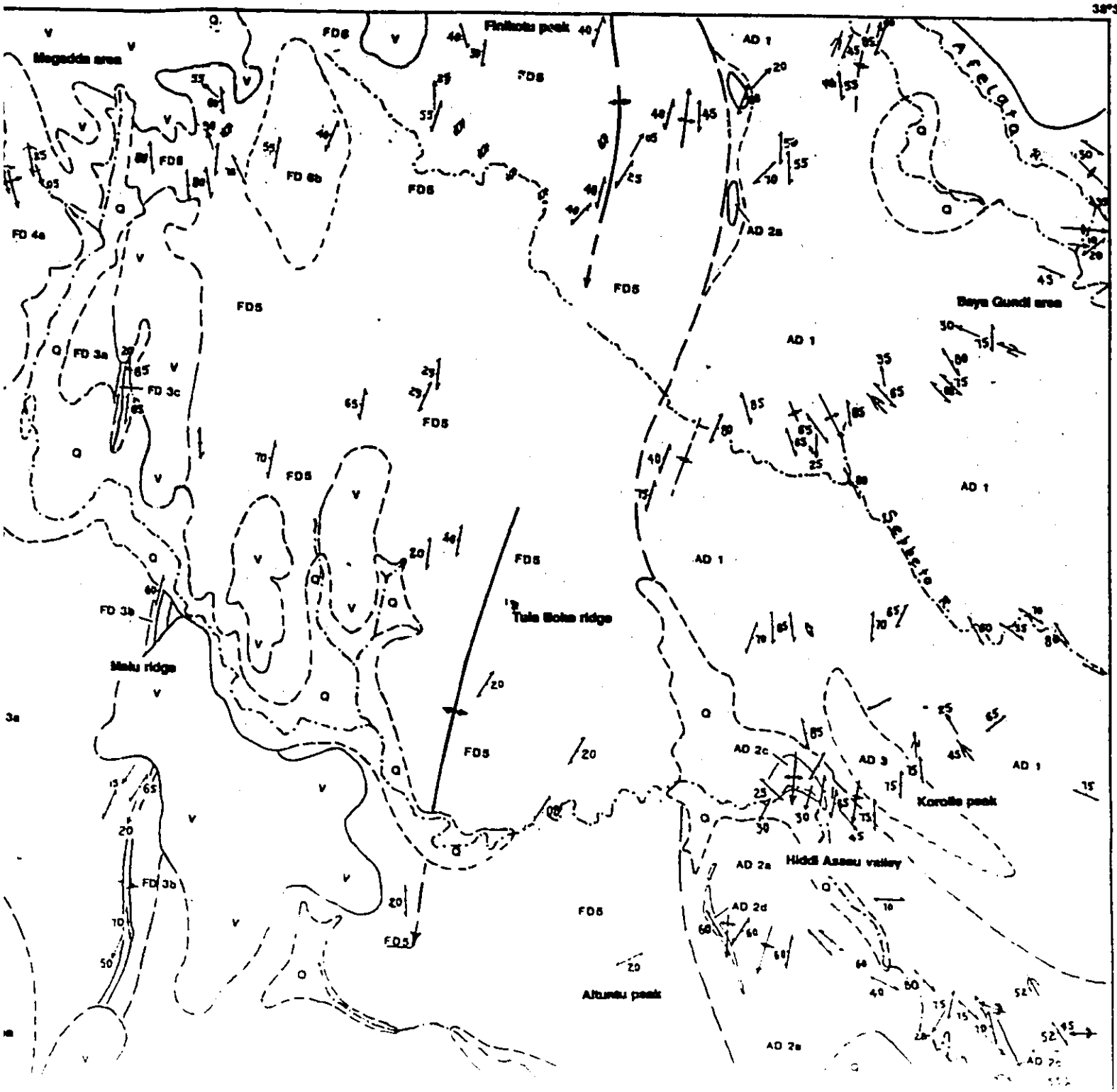
38°30'E
9°30'
Megadda area
Finiktota peak
Beya Gundi area
Tula Bolse ridge
Mielu ridge
Korolle peak
Hiddi Assau valley
Altunau peak
FDS
AD 1
AD 2a
AD 2c
AD 2d
AD 3
FD 3a
FD 3b
FD 3c
FD 4a
FD 6b
Q
V

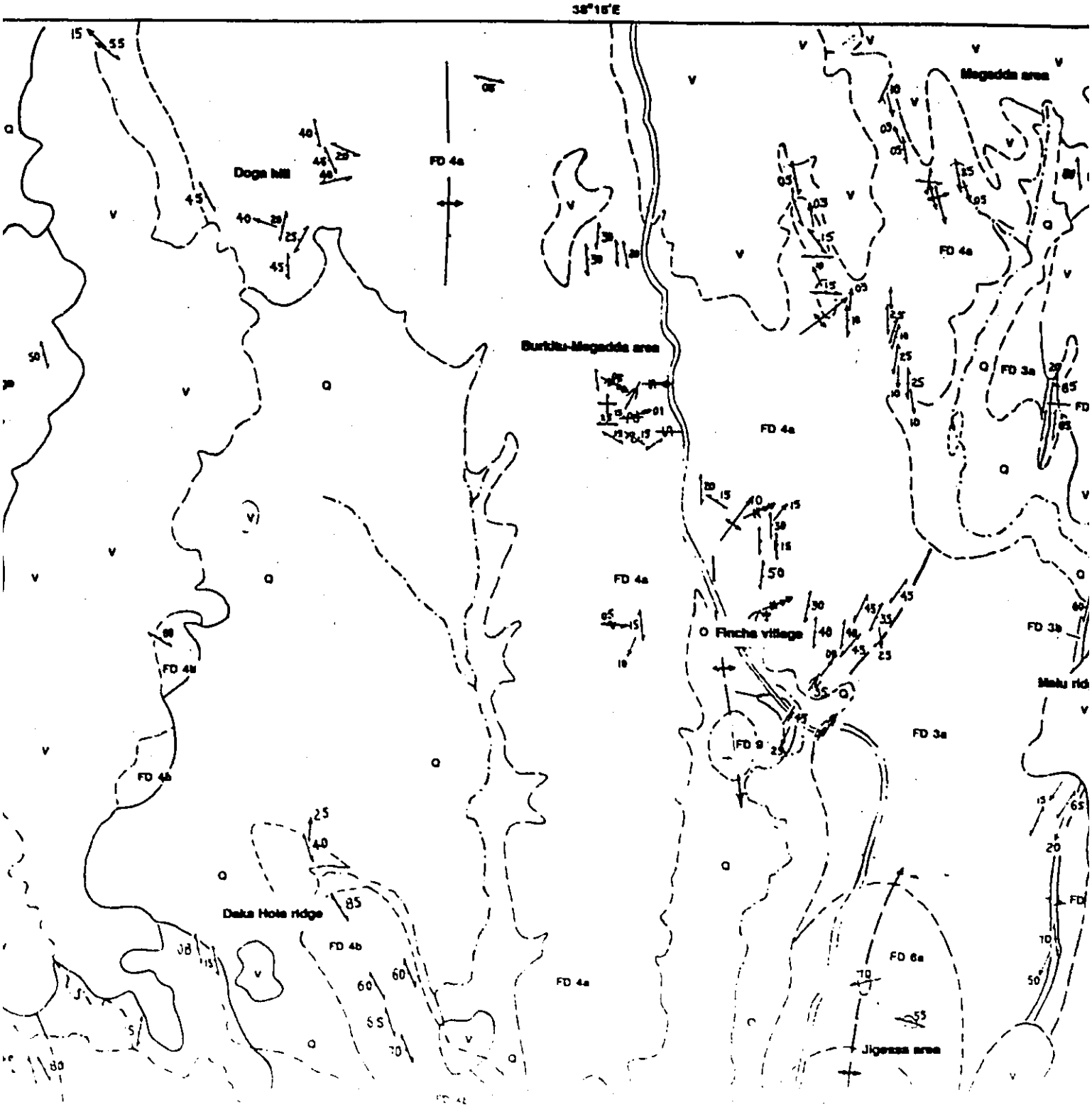
38°15'E
Doga hill
FD 4a
Burkitu-Megadda area
Megadda area
FD 4a
FD 3a
FD 4a
FD 4a
Finche village
FD 3b
FD 4a
FD 4b
FD 9
FD 3a
FD 4b
Daka Hola ridge
FD 4b
FD 4a
FD 6a
Jigessa area

IAN ROCKS, SAGAN – AFELATA AREA

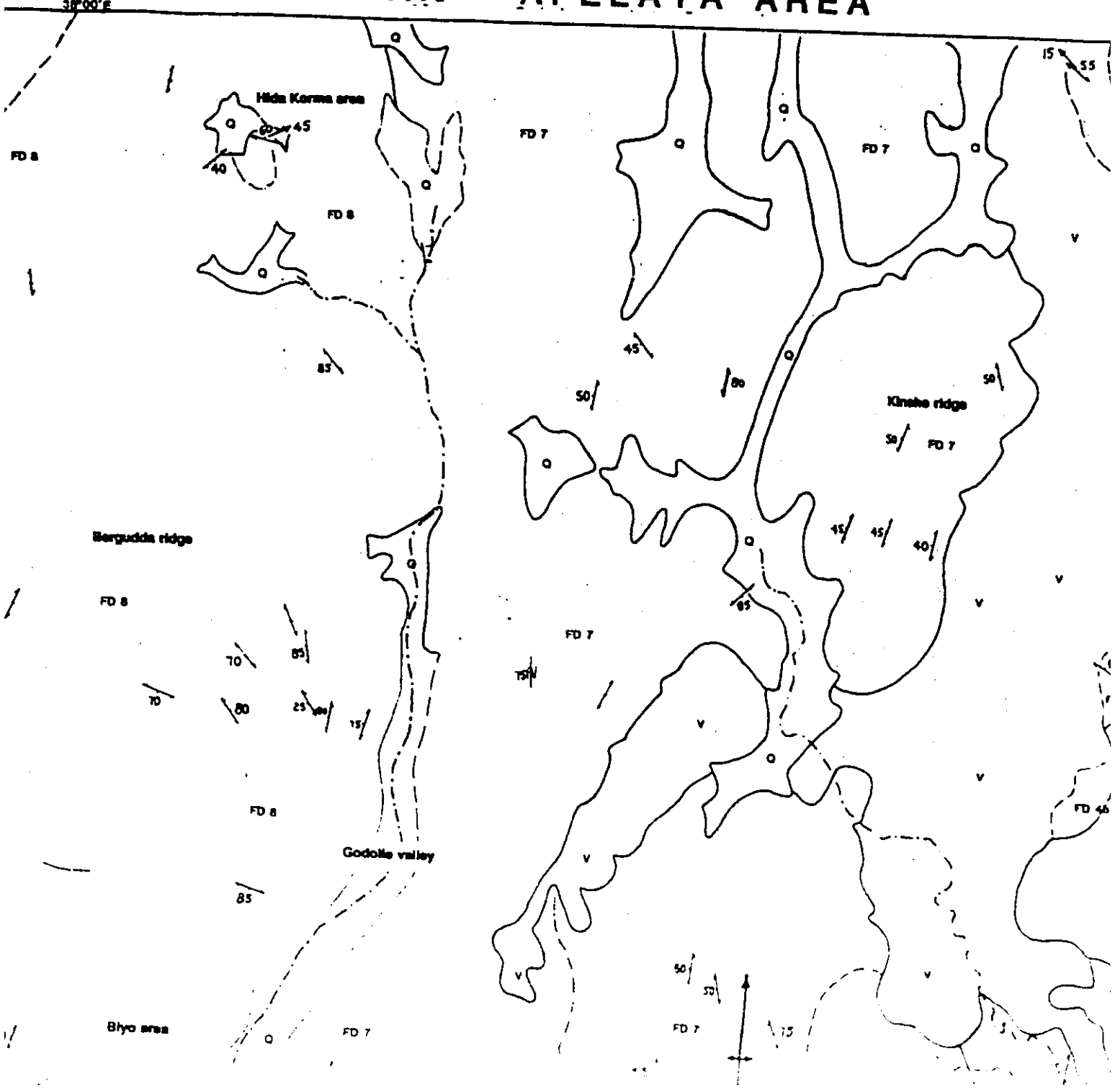

GEOLOGICAL MAP OF PRECAMBRIAN ROCKS, SA

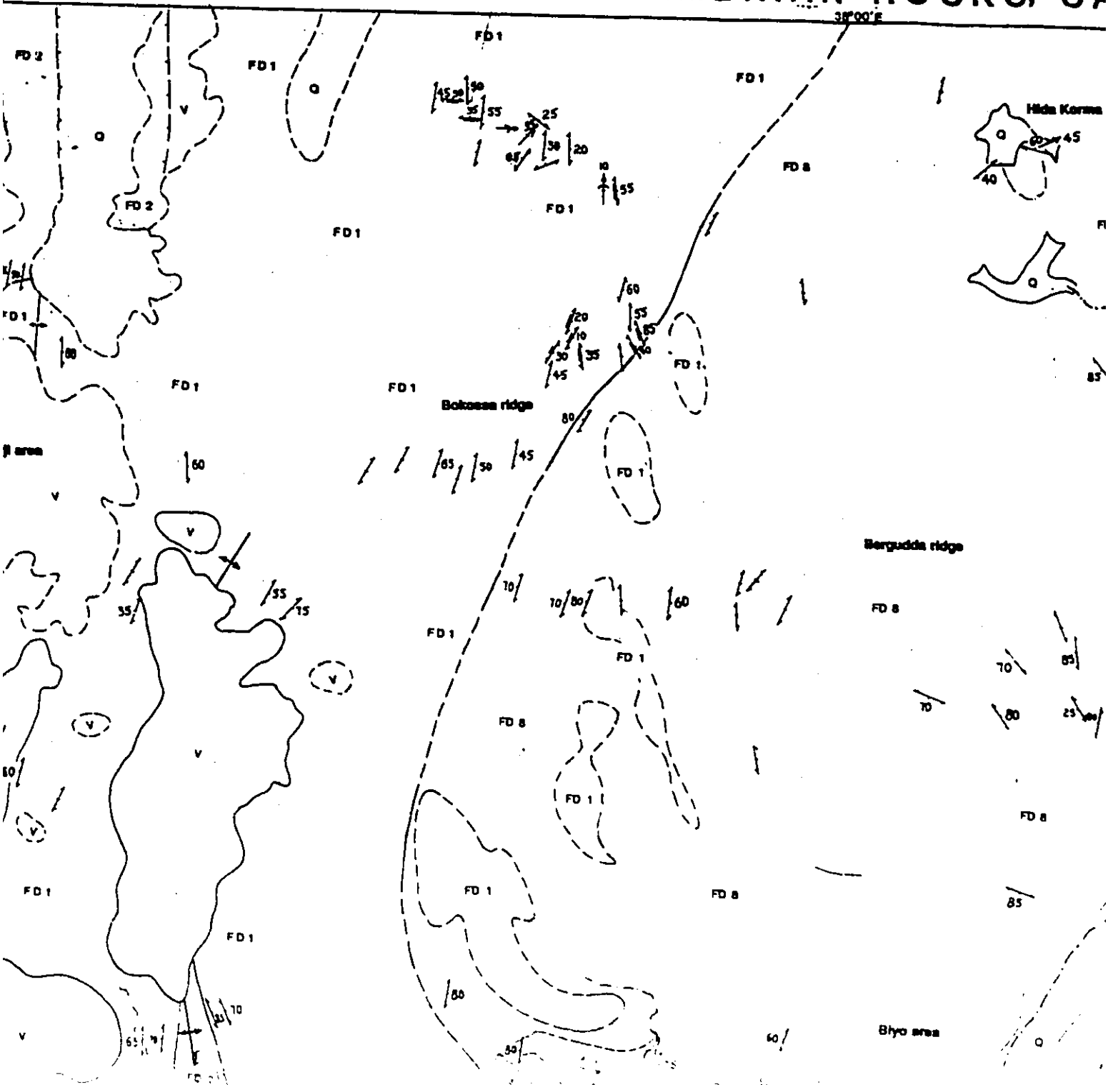

37°45'E

GEOLOGICAL MAP C

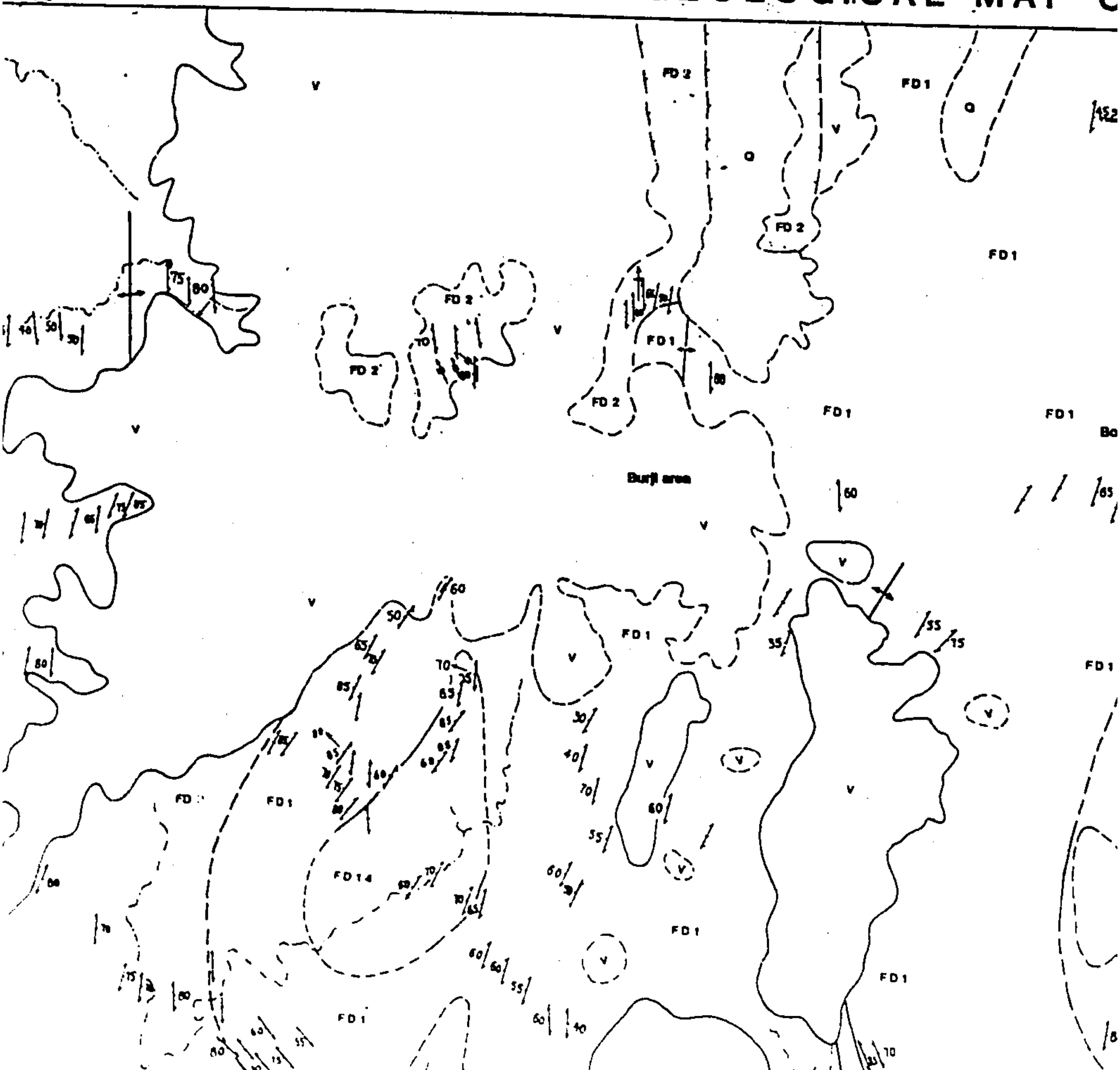

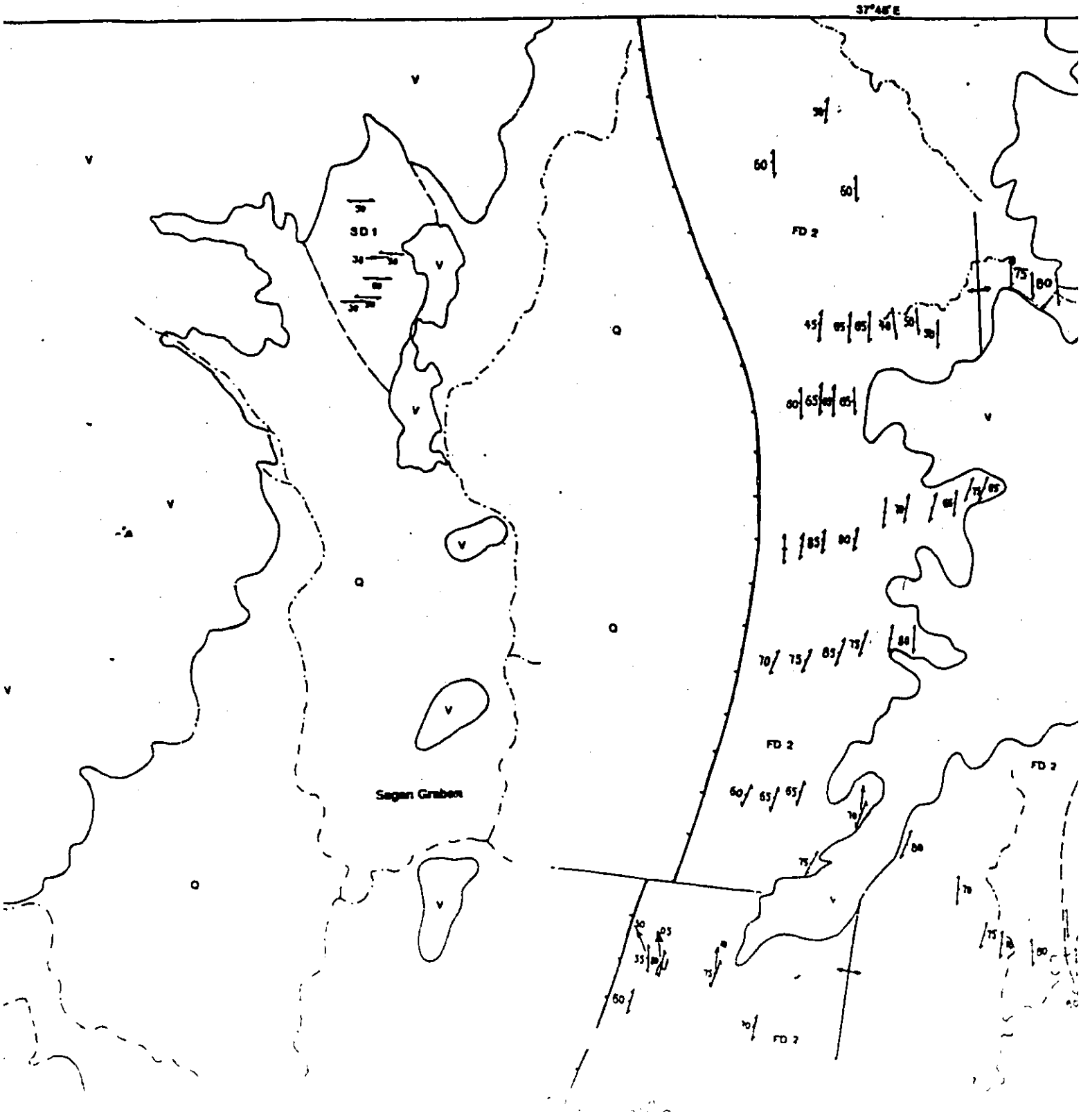
37°45'E
SD 1
FD 2
FD 2
FD 2
FD 2
Sagan Graben

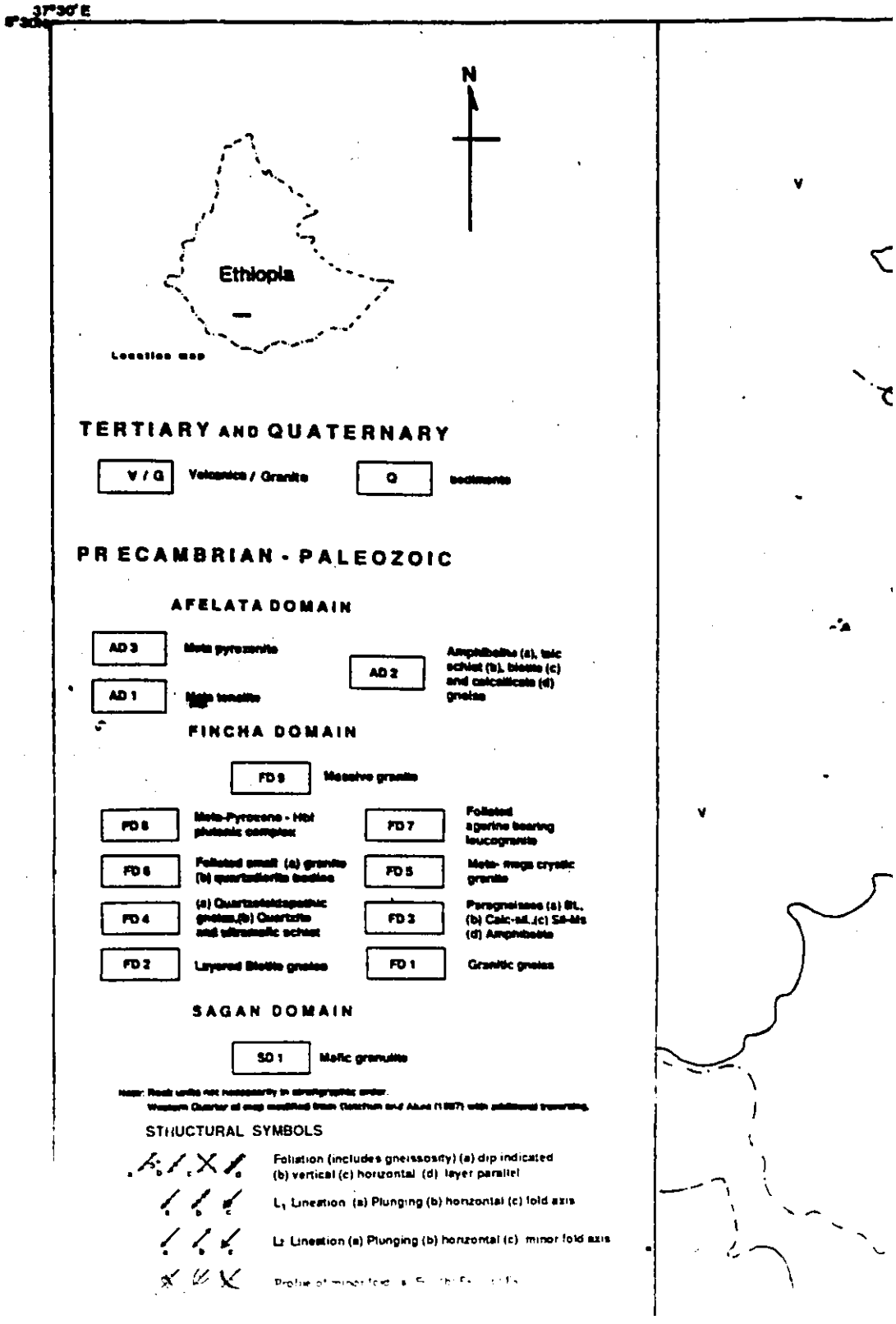
37°30'E
N
Ethiopia
Location map
TERTIARY AND QUATERNARY
V / G
Volcanics / Granite
Q
sediments
PRECAMBRIAN - PALEOZOIC
AFELATA DOMAIN
AD 3
Meta pyroxenite
AD 2
Amphibolite (a), talc schist (b), biotite (c) and calcsilicate (d) gneiss
AD 1
Meta tonalite
FINCHA DOMAIN
FD 8
Massive granite
FD 7
Foliated agpirine bearing leucogranite
FD 6
Meta-Pyroxene - Hbl phyllonitic complex
FD 5
Foliated small (a) granite (b) quartzdiorite bodies
FD 4
Meta- mega crystic granite
FD 3
(a) Quartzofeldspathic gneiss,(b) Quartzite and ultramafic schist
FD 2
Paragneisses (a) Bt, (b) Calc-sil.,(c) Sil-Mis (d) Amphibolite
FD 1
Layered Biotite gneiss
Granitic gneiss
SAGAN DOMAIN
SD 1
Mafic granulite
STRUCTURAL SYMBOLS
Foliation (includes gneissosity) (a) dip indicated (b) vertical (c) horizontal (d) layer parallel
L1 Lineation (a) Plunging (b) horizontal (c) fold axis
L2 Lineation (a) Plunging (b) horizontal (c) minor fold axis